PRODUCTS AND PROCESSES OF CONE-BUILDING ERUPTIONS FROM NORTH CRATER, TONGARIRO

A thesis
submitted in partial fulfilment
of the requirements for the Degree

of

Masters of Science

in Earth and Ocean Sciences

At the University of Waikato
By

Anna M. Griffin

THE UNIVERSITY OF
WAIKATO
Te Whare Wānanga o Waikato

University of Waikato
2007

“Most volcanologists die in bed”

- **volcanologist Maurice Krafft**
- **killed by a pyroclastic flow at Mt Unzen, Japan, 1991**

Abstract

North Crater occupies the north-western quadrant of the Tongariro Volcanic Centre and represents one of at least eleven vents which have been active on Tongariro since the last glacial maximum. The most recent cone-forming activity at North Crater is thought to have occurred between 14-12 ka ago to produce the distinct, wide, flat-topped andesite cone. This project focused mainly on the cone-building eruptions at North Crater, including stratigraphic correlations with distal tephra, interpreting eruptive processes, and establishing the sequence of events during cone construction.

Detailed field work identified key stratigraphic sections and facies in the proximal, medial and distal environments. These sections allowed stratigraphic correlations to be made between proximal cone-building facies and distal sheet-forming facies at North Crater, and established a complete North Crater eruption stratigraphy. In the proximal environment, welded and non to poorly welded facies formed from fallout of a lava-fountain, pyroclastic flow or as fallout from a convecting plume. In the medial and distal environment, the lithofacies consist of fallout from a convecting plume and minor pyroclastic flow. Convective fall and non to poorly welded pyroclastic flow deposits dominate the lower eruption stratigraphy suggesting explosive eruptions involving a gas-rich magma. A change to welded deposits produced from lava-fountaining occurs later in the cone-building sequence and suggest a change to lower explosively and eruption of gas-poor magma.

Grain size, componentry data, density, petrography and SEM analysis were carried out on representative samples to characterise the different facies, and reveal information about eruption processes. The non to poorly welded deposits are typically made up of vesicular pumice, scoria and mingled clasts of sub-rounded bombs and lapilli. The welded facies are relatively dense and clast outlines are often difficult to distinguish. The eruptives are porphyritic with abundant plagioclase>clinopyroxene> orthopyroxene>opaques. Quartzofeldspathic crustal xenoliths are common and indicate crustal assimilation. Mingled clasts of light and dark glass were found to have microlites present in the dark glass, but were absent in the light glass. Electron microprobe analyses found that the dark and light glass components in a single clast had similar compositions, showing that the contrasting physical appearance of the glass is not due to a different chemical composition.

Forty three whole rock XRF analyses showed that the magmas ranged from basaltic andesite to andesite, and Harker variation plots display linear trends typical of magma mixing. Magma mixing as the most important magmatic process is supported by disequilibrium of phenocryst compositions and phenocryst textures. Magma viscosity, bulk density and temperature was determined using MAGMA (Kware), and indicate that they fall into the range of typical andesites.

Eruptive activity involved vigorous lava-fountaining, minor convecting eruption plumes and dominant collapsing eruption plumes. This activity has produced welded and non-welded pyroclastic flow and fall deposits to form the large cone seen today. There are significant volcanic hazards associated with this style of activity at North Crater, characterised by lava-fountaining, eruption plume fallout, and widespread pyroclastic flows and lahars extending beyond the ring plain. These could all be potentially devastating to the central North Island of New Zealand.

Acknowledgments

The completion of this thesis has come at the end of five years of hard study, of which the last two years have been both challenging and exciting and I have loved every minute of completing my own research project!

I would firstly like to thank my chief supervisor Dr Richard Smith as without him I would not have found a project I have loved as much as this one. A huge thanks must also go to my secondary supervisor Dr. Roger Briggs as without his help and guidance I would have been lost during the time Richard was away. Thank you for all the expert help with XRF and all the many interesting and entertaining conversations we have had over the year! You have both encouraged and supported me during my years at Waikato and without your patience and knowledge during the past two years I would not be where I am today. Thanks for always having an open door and for putting up with the seemingly endless questions at times!

My second huge thanks goes to my dad, Allan 'isn't that fascinating!' Griffin. Without the help from this 'suitably' qualified (MBA, DipCM, ACIS) field assistant I would have not been able to undertake and complete the fieldwork component of this thesis. As this thesis revolved around weeks of fieldwork in a sometimes unforgiving alpine environment I really would not have been able to undertake this work at all without his help. Thanks for being the packhorse, encouraging me on the long and tiring days, providing 7 weeks of great conversation on the side of a mountain and "spending quality time with the baby". I know you now have as much of a passion for volcanoes as I do!

I would like to thank R. Simms for his expert knowledge and help with the electron microprobe at Auckland Uni, H. Turner for expert help with the SEM at Waikato Uni, S. Cooke for help with XRF at Waikato Uni, Xu and Renat for help with thin section preparation, and the other EOS technicians for providing help and support with field and laboratory equipment.

Without the support of the DoC my dad and I would not have been able to stay at the Ketetahi hut during the seven weeks of fieldwork. I would like to thank Jimmy, at Turangi DoC, for guaranteeing a bed at the hut, and all the hut wardens who provided many nights of entertainment and good conversation. I would also like to thank DoC for permitting me to collect samples from the National Park as part of my research.

I would like to thank all the EOS grad students for providing support, nights out and always distracting conversation at lunchtime! I'm sure we were all slowly going insane but it's been great to have an awesome bunch of likeminded EOS geeks to rely on! I would also like to thank my mum, Jen, Matt and Jason, without your support over this busy time and constant reminder that I have a life outside of the grad office I would have not have got through this!

Table of Contents

List of Figures

Chapter 1

Chapter 2

Chapter 3

Chapter 4

Chapter 5

List of Tables

Chapter One
Introduction

1.1 Introduction

North Crater cone is located in the northwest sector of Tongariro volcanic complex, within the Tongariro Volcanic Centre (TgVC, Fig. 1.1), and represents one of at least eleven vent systems that have been active on the Tongariro volcanic complex since the last glacial maximum (c. 25-15 ka, Newnham *et al.* 1999) (Hobden *et al.* 2002). Previous work has identified the majority of cone building at North Crater to have occurred around 14-12 ka.

This thesis is the first project to focus on the physical aspects of cone-building eruptions from North Crater. This chapter outlines the objectives of the thesis, the geological setting of North Crater and Tongariro Volcanic Centre, and previous work undertaken.

1.2 Study Objectives

This project aims to determine the nature and dynamics of North Crater's eruptions, and establish the sequence of events involved in the construction of the cone.

This will involve:

- Establishing the nature of the proximal, welded pyroclastics that make up the cone, and determining the mechanisms involved in pyroclastic

transport and deposition in the proximal environment. This project seeks to determine to what extent the welded sequences are the product of pyroclastic flow or hot avalanching, or from fallout, either from a low hot fountain or from a higher plinian-style convective plume.

- Establishing the relationship between proximal cone-forming facies and distal sheet-forming tephra fall. The deposits in these two areas are lithologically distinct but appear to be the product of the same eruption(s). This study will attempt to reconcile the disparate records of eruptive activity on the cone and on the ring-plain to derive a more accurate model of North Crater's eruptions.

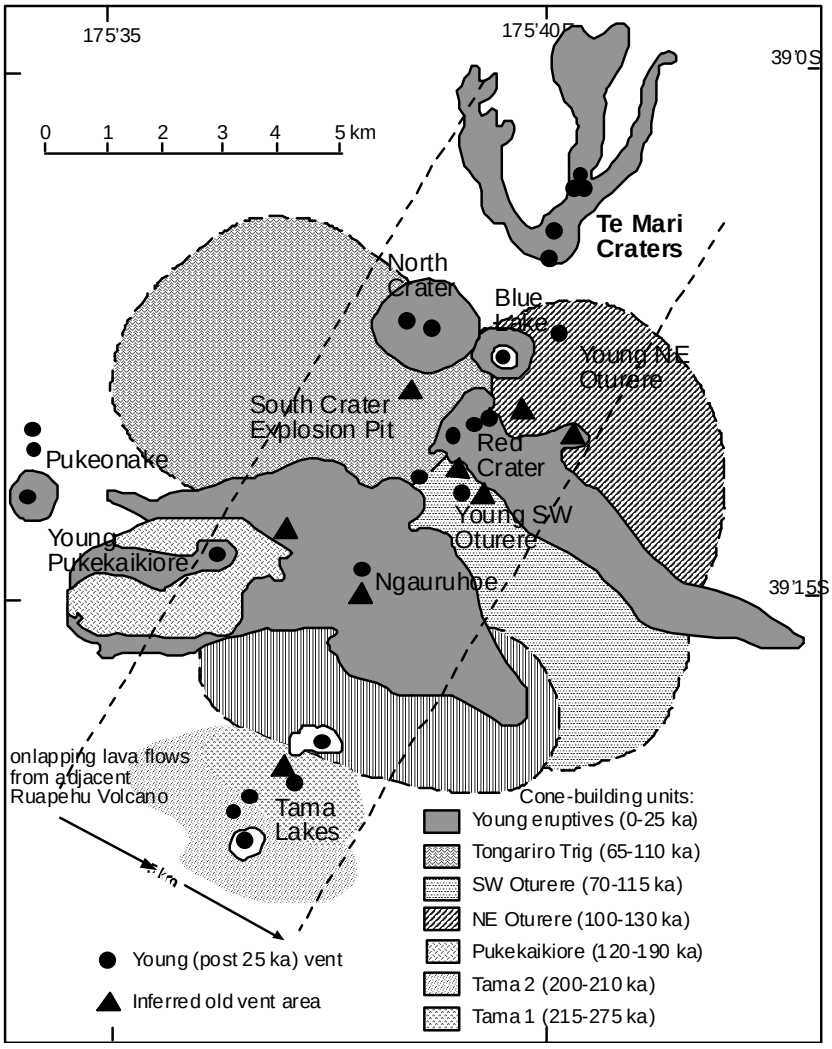

Figure 1.1: *Locality map of the Tongariro Volcanic Centre showing location of North Crater, from Hobden et al. (2002).*

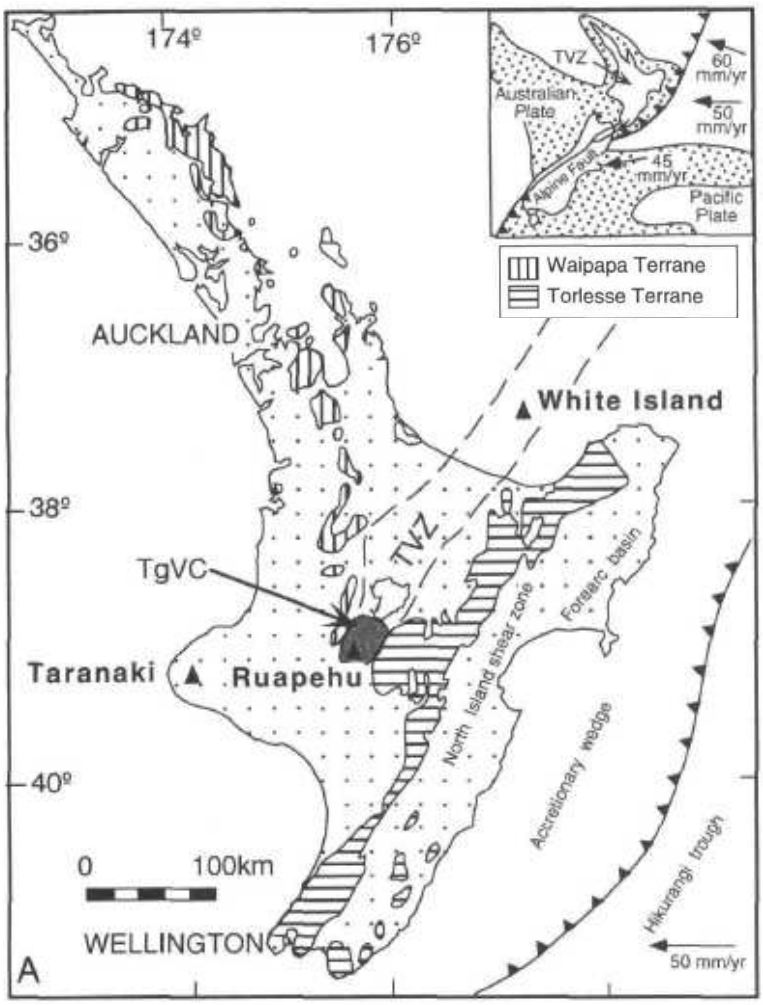

Figure 1.2: *Map of North Island New Zealand, showing the location of Taupo Volcanic Zone (TVZ) and Tongariro Volcanic Centre. After Waight and Price (1999).*

1.3 Geological Setting

North Crater lies in the north-west sector of the TgVC, which forms the southern-most centre of the Taupo Volcanic Zone (TVZ, Fig. 1.2). The TVZ is the focus for young volcanism in New Zealand, being the dominant region of activity from late Pliocene to the present, and results from the subduction of the Pacific Plate under the North Island. The TVZ also represents a region of crustal extension bounded to the east by the North Island Shear Zone (Waight and Price 1999). It is a NNE-SSW trending continental rifted arc c.300 km long and up to 60 km wide, and has produced at least 10,000 km^3 of magma since formation (Waight and Price 1999). Andesitic activity began at c. 2 Ma, joined by voluminous rhyolitic activity from c. 1.6 Ma in the central part of the modern TVZ (Wilson *et al.* 1995).

The TgVC forms a relatively young cluster of andesitic-dacitic volcanoes at the southern end of the dominantly rhyolitic TVZ. It includes the large massifs of Ruapehu, Tongariro, Pihanga and Kakaramea, and has been active since c. 275 ka (Hobden *et al.* 1996, Waight and Price 1999). Tongariro Volcano is a young cone complex within the TgVC, with the first significant cone-forming episode occurring between 275-215 ka at the southern end of the complex. Other major eruptive episodes followed at 210-200 ka and 130-65 ka followed by relative quiescence from 65 ka to the establishment of recent vents from 25 ka to the present (Hobden *et al.* 1996). Recent activity since the last glacial has occurred at Te Maari, Tama Lakes, Red Crater, Emerald Lakes, North Crater, Pukekaikiore and Blue Lake Crater, and dominated at Ngauruhoe since 2.5 ka (Hobden *et al.* 1996).

North Crater lies at the north-western edge of the Tongariro volcanic complex and forms a large flat-topped cone rising from the northern Tongariro ring plain. The flanks of the cone rise at an angle of about 30-35° to a height of 1830 m (Topping 1974). North Crater represents one of the eleven vent systems that have been active since the last glacial maximum, and activity at North Crater likely began soon after the peak of glaciation, but the largest and latest eruptions probably occurred after about 14 (Topping 1974).

The 1100 m wide crater is defined by large cliffs of lava, non-welded pyroclastic material and welded agglomerate to the north, south and north-east, and is filled by a large solidified lava lake or ponded flow. The lava lake forms a horizontal surface and appears to have overtopped the crater rim to the west flowing about 300 m and to the east flowing about 50 m. An explosion pit 300 m across and 70 m deep lies in the north-west sector of the crater which has exposed a series of irregular pancake jointing, massive units and columnar jointing present in the lava stratigraphy. Large andesite blocks 2-6 m across are found on the crater plateau and some distance down the flanks of the cone which display radial concentric fractures indicating they were ejected while solid but still hot (Mathews 1967, Topping 1974). Taupo Pumice blocks found on the crater plateau adjacent to the explosion pit indicate eruptions from North Crater had ceased by (^{14}C age) 1850 ± 10 yr B.P. (Froggatt and Lowe 1990)

1.4 Previous Work

Some of the earliest work undertaken in the TgVC was compiled by Gregg (1960) in a publication by the New Zealand Geological Survey. Here, early descriptions of North Crater are given including one which describes the two lengths of cliffs on the summit that mark the present rim of the crater, which previously was filled with lava (now solidified); and the centre of the plateau being occupied by an ephemeral shallow lake which frequently dries up and emits small amounts of steam during evaporation. Gregg (1960) also noted articles in the New Zealand Herald (5, 6 and 10 September, 1927) which reported an ash eruption from Tongariro. Gregg (1960) suggested this eruption may have been from the explosion pit in North Crater, although its location was never definitely determined. Gregg (1960) described the andesites from North Crater as distinctly richer in pyroxene than those from the lower flanks of Tongariro. The majority of samples were described as labradorite-pyroxene andesites and labradorite andesites, and show distinct petrographic resemblances to Ngauruhoe lavas.

Mathews (1967) described the proximal units near North Crater and Blue Lake as "welded agglomerate" and suggested this was formed by lava-fountaining from a nearby crater. Although this rock is common over all of Tongariro, it is particularly abundant on the slopes of North Crater. The moderately welded agglomerates in the Blue Lake and North Crater area show an assortment of monolithologic clasts 3-5 cm in diameter of non-vesicular to weakly-vesicular porphyritic andesite. Accumulations are also typically one colour, either reddish or greyish.

Mathews (1967) also noted the degree of welding within the agglomerate units varied from layer to layer and from location to location. However, strongly welded agglomerate is abundant near the North Crater lip. Where the welding is weaker, the outcropped agglomerate surface appears knobbly from the larger fragments and if the welding is weak enough, these clasts can be plucked from the outcrop. Where there is strong welding the rock may be broken along a bedding plane, or broken up by columnar jointing. Mathews (1967) described how on the

north slope of North Crater a clear example of lateral gradation from moderately to weakly welded pyroclastics rock can be seen. Here a single set of beds can be traced down a steep gully for about 280m, from the top end where virtually all of the beds are moderately welded, to the lower end where the deposits are weakly welded. The majority of agglomerate beds found on North Crater display similar characteristics. These agglomerate beds at North Crater drape the topography, but taper out with distance from source. Mathews (1967) suggested these agglomerates accumulated while hot as indicated by welding and appearance of cooling joints. The lava fragments may have been showered down from a considerably high lava-fountain, inferred by the lack of dependence on the underlying topography. Mathews (1967) stated that the distribution of the agglomerate and the obvious degree of welding variations suggested local sources for the unit, and the height and discharge rate of the fountains must have been large to account for the wide distribution of hot debris.

Mathews (1967) also tried to estimate an approximate age for the North Crater deposits when he described a thin lens of ash interbedded with breccias below the west rim of the cone. Mathews stated this ash bed has a unique and diagnostic mineral assemblage which can be compared with, but not unquestionably assigned, to the Waimihia Ash (part of the Taupo Sub-group) which has been given an age of ~3.5 ka. Mathews also describes blocks of Taupo Pumice unexpectedly found inside the SW rim of the crater. This indicates major eruptions at North Crater had ceased by about ~2 ka.

Mathews (1967) described massive lava on the eastern side of the plateau rim which is exposed inside and below the up-dip edges of the agglomerate bed. Crude prismatic jointing is exposed which define irregular stout columns. The explosion pit in the plateau exposes in its walls similar massive lava which lacks consistent columnar jointing. Mathews goes on to suggest the rocks exposed in the pit and along the edges of the plateau may be part of a single lava sheet which has been contained within the walls of the agglomerate beds at the crater rim. For the impounding walls not to have been broken down by the ponding lava, it must have been relatively viscous or exerted very low hydrostatic pressure.

The explosion pit within the plateau is also described as being about 300 m wide and ~70 m deep with a broad ring of debris which slopes gradually away to the main plateau. Debris close to the pit includes many angular broken lava blocks (possibly derived from the solid rock lower in the pit). Large lava blocks up to 2 m in diameter showing radial contraction fractures are also found in the debris. Thus they have been thrown into their present position when solid but still hot.

Mathews (1967) is unclear whether the development of the explosion pit and the surrounding debris was a late phase in the cooling of the mass of lava directly underlying the summit plateau, or if it is instead a product of some later magmatic activity. Either way Mathews stated this was the latest episode in the volcanic history of North Crater.

Mathews (1967) suggested landsliding along bedding planes in the agglomerate caused gaps to form high on the flanks of the cone. However he also stated no landslide debris has been identified below these gaps, and debris on the lower slopes may now be covered by younger deposits from Te Maari.

Topping (1973; 1974) was the first to study the eruption deposits thought to be associated with North Crater. His research of the Tongariro Sub-group from the TgVC, 13.8 ka to present, used distal outcrops to identify source vents for the various formations and members. Topping described six tephra formations within the sub-group including the Mangamate Tephra Formation and its 6 members. In the Mangamate Tephra Formation he suggested the Te Rato Lapilli Member source vent is North Crater, while the other member locations tended to be Tama Lakes – Ngauruhoe sourced. The Te Rato Lapilli conformably underlies the Oturere Lapilli and immediately overlies a rhyolitic tephra – the Papanetu Tephra (Topping 1973). Wood found in peat directly underlying the Te Rato Lapilli has been C14 dated at 9780 ± 170 years B.P. giving the oldest age for the member. The isopach map constructed by Topping (1974) for the Te Rato Lapilli (Fig. 1.3) alone does not convincingly define a particular vent for the member, especially as the dispersal axis coincides with a number of vents. With eruptions immediately following and prior to the deposition of the Te Rato Lapilli taking place from a number of vents in the TgVC it is possible for any of these vents to be the source

of this lapilli (Topping 1973; 1974). Topping (1973; 1974) suggested North Crater is the source vent as there is a lack of Te Rato Lapilli in sections to the west of Ngauruhoe. As Te Rato Lapilli is recognised in sites up to 1320 m elevation on the northern slopes of the cone this suggests the majority of the cone is older than 10 ka.

Topping (1974) also suggested that the informally named Pahoka Lapilli was erupted from a North Crater source, although sufficient data are lacking to make any definite conclusions. The unit underlies the Mangamate Fm and has an age range of 9.8-10 ka, with the andesitic and dacitic lapilli showing similar characteristics to those of the younger Te Rato Lapilli. However, an isopach map was unable to be constructed by Topping for this unit as too few sections were available, but available data did suggested mainly SE directed lobe with a possible North Crater source.

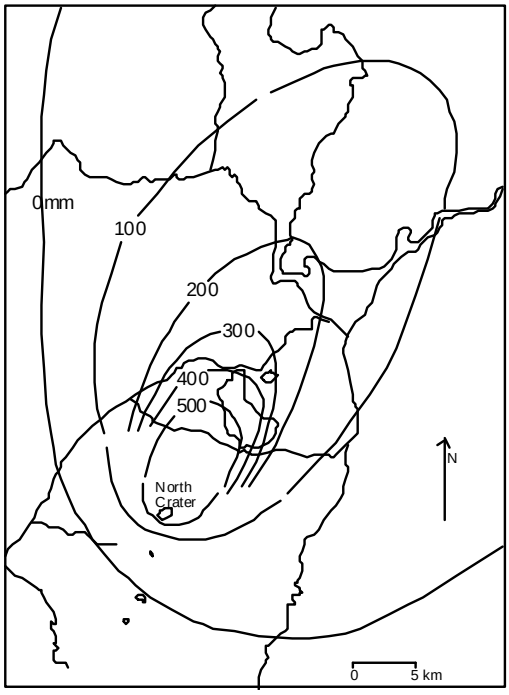

Figure 1.3: *Isopachs (mm) of Te Rato Lapilli, from Topping (1973).*

Topping (1973; 1974) also suggested that even though the majority of cone building activity at North Crater had ceased by 10 ka, the appearance of Papakai Tephra (3.4-9.7 ka) gave evidence for a considerably younger age for the upper section of the cone (Topping 1973). Although this tephra is largely associated

with one or more vents in the Ngauruhoe-Tama Lakes area, there is a notable component added from one or more northern Tongariro vents. An increase in the rate of Papakai Tephra deposition occurred after an initial slow deposition of the basal tephra, and this could have been associated with the initiation of cone building eruptions from Ngauruhoe. However, Topping (1974) suggested this increase is far more likely due to renewed cone building eruptions from North Crater. This younger age range is supported by the identification of a rhyolitic ash, which has been questionably assigned to the Waimihia Lapilli by Mathews (1967). The thin ash bed is found interbedded with breccias below the west rim and is given an approximate ^{14}C age of 3280 ± 20 yr B.P. (Froggatt and Lowe 1990).

Topping (1974) identified several meter thick, black pumiceous block and ash flows exposed in stream cuttings several km's north of North Crater. These were probably deposited as one or more flows from North Crater about 10 ka which have been overlain by a thin mud flow, a yellowish brown ash with minor brown lapilli and the Papanetu Tephra.

The Rotoaira Lapilli is suggested by Topping (1973, 1974) to have a lower Te Maari crater source but is not convincingly proved in his work. Lower Te Maari crater was proposed as the source vent for this lapilli based on chemical and titanomagnetite analyses which are similar to lavas found exposed in the lower crater wall. The Rotoaira Lapilli often lies on the eroded Oruanui Formation and is the oldest andesitic unit conformable with the present day topography to the south-east of Lake Rotoaira. The Rotoaira Lapilli is easily distinguishable by a black ash separating two lapilli horizons. The yellowish red colour of the upper lapilli horizon and brownish yellow of the lower lapilli horizon also make the unit recognisable. This unit has been dated from charcoal found directly below it, which is considered to have been carbonised by this eruption, giving an estimated age 13.8 ka ± 0.8 ka (Topping 1973; 1974). Incomplete isopach mapping (Fig. 1.4) of the unit suggested a northern Tongariro source, and because of the similar chemical characteristics to the lava flows exposed at Te Maari craters, Topping (1973; 1974) suggested the likely source vent is at Te Maari craters.

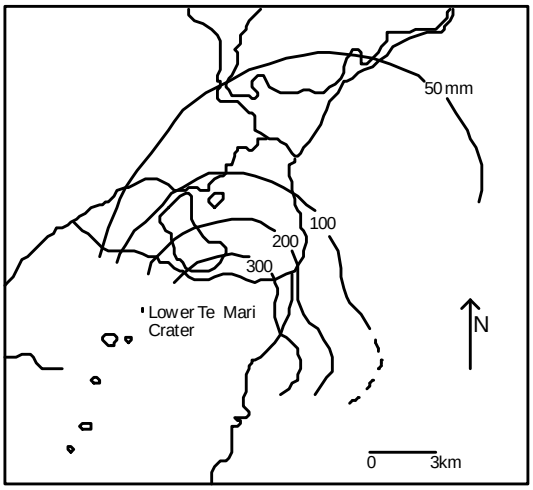

***Figure 1.4**: Isopachs (mm) of Rotoaira Lapilli Formation, from Topping (1973).*

Little work was carried out on the Tongariro complex during the 1980s and early 1990s, with most research focused on Mt Ruapehu during this time. It was not until the mid to late 1990s when in-depth research on the Tongariro complex continued with a doctoral thesis by Hobden (1997) and research papers by Hobden *et al.* (1996), Donoghue *et al.* (1995a) and two conjunction papers by Nairn *et al*. (1998) and Nakagawa *et al*. (1998). These conjunction papers focus primarily on the eruptions since ~10 ka and not specifically on eruptions from North Crater, while Hobden (1997) looks at all Tongariro Volcano vents including North Crater.

Hobden (1997) described the stratigraphy at North Crater, stating the spatter cone was built up at a similar time to the one at Blue Lake. Hobden (1997) suggested the activity culminated with sub-plinian eruptions around 9.8-10 ka producing the Pahoka Tephra and Te Rato Lapilli. Hobden described the crater rim to be composed of 1-10 m thick welded agglutinates and rheomorphic tuffs formed during Hawaiian and Strombolian style lava-fountaining. Eruptions from the young cone probably produced the lava flows on the north-west flanks of North Crater, and approximately 25 exposed lavas and pyroclastic units are exposed.

Work by Nairn *et al.* (1998) used new tephra mapping to considerably revise the vent locations suggested by Topping (1973; 1974), which were based on partial isopach maps. Nairn *et al.* (1998) compiled new and more complete isopach maps by adding new proximal data to the distal data of earlier works.

Pahoka Tephra previously suggested by Topping (1973; 1974) to be from a North Crater source, is revised by Nairn *et al.* (1998) to be from a vent in the Saddle Cone area. From mapping and identification of proximal facies ejecta they were able to establish the Pahoka Tephra vent location more accurately, and although there is no vent here today it is inferred to have been buried by the Saddle Cone lavas.

The Te Rato Lapilli, also suggested by Topping (1973; 1974) to have a North Crater source, is revised by Nairn *et al.* (1998) to be from a vent now buried under Ngauruhoe cone. This vent was also able to be more accurately located from the new mapping of dispersal patterns and facies distribution, and a possible vent site at North Crater is excluded by the absence of proximal Te Rato facies ejecta in nearby exposures (Nairn *et al.* 1998).

Topping (1973; 1974) suggested young lava flows from North Crater which extend north-west from the cone relate to the Papakai Tephra eruptions; however Nairn *et al.* (1998) found Te Rato Lapilli overlying these lavas to 250 m below North Crater rim. They consider these young North Crater lavas are most likely related to the Rotoaira eruptive episode (Nairn *et al.* 1998).

Recent work by Basher (2005) on Te Maari craters notes the absence of any pyroclastic deposits which suggests Te Maari craters were not significantly explosive (sub-plinian). This implies the Rotoaira Lapilli described by Topping does not originate from Te Maari. This is supported by unpublished mapping by T. Kobayashi (pers. comm. 2006) which correlates the agglutinates of North Crater with the sub-plinian Rotoaira Lapilli.

Since the late 1990s studies on Tongariro have mainly been focused on the young eruptions at Ngauruhoe, Red Crater, Te Maari craters, Tama Lakes and Ruapehu. Little formal work has been carried out on North Crater and distal deposits in recent years, although informal mapping and field studies by Tetsuo Kobayashi (Univ. of Kuyoshima) and the recent completion of a MSc. thesis on the geochemistry of the Rotoaira eruptive sequence (Doyle 2006) marks the continued

interest in the cone-building processes of North Crater and the correlation with distal tephra deposits.

Chapter 2

Stratigraphy and Facies Characteristics

2.1 Introduction

This chapter describes the field characteristics of North Crater eruptives, including geomorphology, stratigraphy, field correlations and facies characteristics. Stratigraphy, correlations and facies data have been compiled from field stratigraphic logging and mapping of 80 outcrops in proximal (0-2 km), medial (2-6 km) and distal (>6 km) environments around North Crater (Fig. 2.1). Often the medial to distal localities will hold a more complete record of a volcano's history compared with the proximal stratigraphy, as non-welded or consolidated units may not be preserved on the steep gradients of the upper slopes. However, this study focuses on the cone-forming eruptions of North Crater and products of these events are observed mainly at proximal localities. Possible correlation of distal ash and lapilli beds (Rotoaira Lapilli) with proximal units on the cone has meant stratigraphic sections through the medial and distal environments are also important. However with the last glacial maximum, transition to interglacial period, and sustained warming from about 15 ka (Newnham *et al.* 1999), there is some loss of the tephra record by erosion, hence there is sometimes a discontinuous nature of medial and distal deposits.

Mathews (1967), Topping (1973, 1974) and Hobden (1997) have previously studied the stratigraphy of deposits associated with North Crater along with

Fig 2.1

unpublished mapping by Nairn (pers. comm. 2005) and Kobayashi (pers. comm. 2006) but only as part of more general volcanological research on the TgVC. Recent work by Doyle (2006) has identified the possible correlation of distal Rotoaira Lapilli with units on the upper slopes of North Crater through geochemical data, and in this chapter an attempt will be made to correlate these distal and proximal units stratigraphically to confirm the work of Nairn and Kobayashi and assess Doyle's findings.

Figure 2.2: *Photo looking south showing North Crater geomorphology and neighbouring vents at TgVC.*

2.1.1 Terminology

It is important to define the terms commonly used which are associated with hot lava-fountaining style eruptions and their relevance to North Crater deposits. The term agglutination is the instantaneous or syn-depositional flattening and adhesion of hot, soft pyroclasts upon landing, with the resultant deposit forming an agglutinate or spatter pile and particle outline is in part retained. Welding is defined as the post-depositional compaction of a hot pyroclastic deposit under its own weight into a coherent rock; clast accumulation rate influences the degree of welding, as a slow rate allows clasts to cool before being buried (Wolff and

Fig 2.3-2.5

Sumner 2000). These two processes form a continuum and often form deposits similar in appearance (Wolff and Sumner 2000).

2.2 Geomorphology of North Crater

North Crater is a large, distinct, flat-topped cone rising to 1820 m above sea level, (c. 1100 m above the surrounding ring plain) that marks the north-western edge of the TgVC. To the east the cone is bounded by the young (c. 10-20 ka) Blue Lake vent (Fig. 2.2) which was probably built up around the same time, although North Crater is possibly not quite as old (Hobden *et al.* 2001). To the south the cone is bounded by the older (c.65-110 ka, Hobden *et al.* 2001) Tongariro Trig and it is assumed that North Crater deposits onlap onto this cone. These cones may have applied some topographical control on the dispersal of both hot and cool flows associated with the sub-plinian and fire-fountaining eruptions during cone formation at North Crater.

The present volume of North Crater cone is estimated to be 0.5 km^3 with probably very little change from its original volume since eruptive activity ceased (Hobden *et al.* 2001). This implies the cone flanks and slope angle has remained relatively similar since formation. The cone flanks comprise welded flows and agglutinates, scoria and pumiceous flow and fall deposits, talus and scattered ballistic blocks. These lithologies are described in detail in the following sections. The flanks of the cone have a varying slope angle of 27-30° and up to 35-37° on the upper welded cone (Fig. 2.3) and rise to a flat top about 1 km wide (Fig. 2.2). This level surface is a solidified lava 'lake', or ponded lava flow, infilling the crater. A section through this ponded lava is exposed in a 350 m wide and 70 m deep explosion pit in the north-western sector (Fig. 2.2). Large and small blocks of this lava are scattered around the explosion pit, with debris forming a slight rise of about 5 m from the cone plateau to the lip of the pit. These blocks have also been found part way down the flanks of the cone. On the upper slopes of the cone only a few gullies are present which cut into the cone stratigraphy. During the fieldwork period (summer) these gullies were dry, but during winter they may drain any amount of water off the cone from snow and ice melt. On the lower slopes to the north some of these gullies form small streams where groundwater enters them and the cone-forming material becomes softer, less welded and more

easily erodable. A small splay fault from the main fault to the west is also seen to cross the summit crater from the southwest to northeast and has helped form the amphitheatre notch in the NE crater rim. Little physical evidence remains from this fault and it is unclear the amount and direction of movement it has undergone.

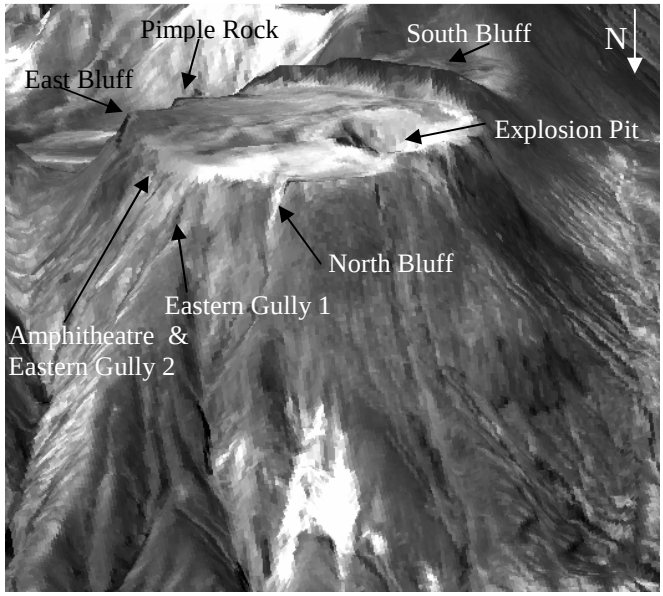

Figure 2.4: *North Crater DEM showing main features discussed in text.*

Near the crater rim several main features can be seen which will be referred to in later sections (Fig. 2.4). The large bluff rising above the summit plateau to the south (T19 384280) is herein termed "South Bluff", the smaller knob on the edge of the crater rim to the south east (T19 391278) is here in termed "Pimple Rock", the lower bluff rising above the summit plateau to the east (T19 393282) is herein termed "East Bluff", the large horseshoe shaped bluffs cutting into the lava lake (T19 392284) at the eastern rim is herein termed "the Amphitheatre" and the large bluffs tracing down the northern slope from the crater rim is herein termed "North Bluff".

Ketetahi Hot Springs are located on the northern slopes of North Crater (Fig. 2.2) at an elevation of 1340 m and are thought to be fed by a vapour-dominated system (area of 15-20 km^2) underlying the TgVC. It is formed by a combination of magmatic steam mixed with circulating meteoric water with inferred equilibrium temperatures of 230-290°C (Hobden *et al.* 2001). Ketetahi Springs contain hot springs, mud pools, fumaroles (some superheated) and thermally altered ground,

with the hot springs discharging acid-sulphate waters. No evidence for major eruptions has been found at Ketetahi, although a lahar was generated down the Mangatipua Stream in about 1895 with deposits found at site 67 (Hobden *et al.* 2001).

Neighbouring vents and the proto-North Crater morphology may have played a significant role in the construction of the young North Crater cone. The southern Tongariro Trig grew between 115 and 65 ka involving andesitic-dacitic autobrecciated lavas, agglutinates and pyroclastic and epiclastic deposits, to form a cone 12 km^3 (Hobden *et al.* 2001). Unpublished mapping by Nairn (pers. comm. 2005) and Kobayashi (pers. comm. 2006) suggests lavas from Tongariro Trig flowed predominantly to the west and northwest, and may partially underlie the proto-North Crater vent. This mapping has also identified lavas associated with a proto-North Crater vent which flow predominantly to the north and have been dated as pre-Oruanui and pre-Rotoaira (Nairn pers. comm. 2005). It is unclear what form the underlying vent had built during eruption of these lavas, however due to the lava composition being andesitic in nature it may be possible to assume a similar, but smaller cone to the present had been built. Due to the presence of Tongariro Trig and proto-North Crater lavas, eruptions from the young North Crater may have only formed the prominent upper cone seen today, while the surrounding sloping ring plain consists predominantly of the older lavas from Tongariro Trig and proto-North Crater.

When comparing the shape of North Crater to other composite volcanoes the broad flat topped summit is distinct and is rarely seen at other composite cones. For example Ngauruhoe (New Zealand), Stromboli (Italy) and Mt Mayon (Philippines) all exhibit the typical conical shape associated with andesite cones formed at subduction margins (Fig. 2.5). They all rise with slopes of about 30-35° and have lavas in the range of basaltic to andesitic. However, they differ from North Crater in that the flanks rise up to meet at a relatively sharp summit, with only a small crater present indicating a sole vent with no to very minor vent migration. The distinctive flat topped morphology of North Crater may reflect a) an eruption style involving a high, spreading fountain of fluid magma, b)

structural controls on vent dimensions or) continuous eruption of a collapsing eruption column.

Cross-sectional profiles across North Crater and the surrounding landscape (Fig. 2.6 and 2.7) show the varying slope angles with distance from the vent. Two main slope segments can be identified and correspond to a) the upper steep cone dominated by welded eruptive products (~30-35°), b) the lower cone dominated by non to poorly welded eruptive products (~25-30°) and c) the lower surrounding ring plain (<25°) (Fig. 2.7). The cross-sectional profiles show North Crater to be relatively symmetrical, with the varying slope angles insufficient to disrupt the symmetrical cone building of North Crater, and indicate no large scale collapses have occurred. The E-W profile shows the greatest variation from the others, with lower slope angles and less elevation change with distance. This could be due to the presence of underlying deposits from the older Tongariro Trig which lie to the west of North Crater. The crater summit also appears to be symmetrical with minor variations between profiles. The symmetry of the cone and summit crater suggests limited vent migration during the eruption episodes and a summit focus for activity throughout. Intense fountaining of fluid magma with high gas content may also contribute to the broad structure, due to a high, spreading fountain.

Ngauruhoe is a symmetrical composite volcano in the TgVC showing similar magmatic processes and but contrasting eruption style and morphology to North Crater (Fig. 2.5c). It is a young cone which has grown over the last 2,500 years (Hobden *et al.* 2002) involving alternation between effusive, vulcanian, strombolian and sub-plinian eruptions of andesitic magma (Hobden *et al.* 2002). The slopes rise at ~32-35° to an elevation of 2,287 m, and the summit crater is 400 m wide undergoing frequent modification due to minor vent migration over the last 150 years (Hobden 1997). Growth of the cone has followed a sectorial pattern which reflects constant modification of summit morphology. The geometry and morphology of the summit and vent influence the direction of deposition of new lava flows, with small geometric changes in the vent having a major influence on the pattern of cone growth (Hobden *et al.* 2002). Spatter has occasionally overtopped higher parts of the crater rim forming detached flows down the less favoured side of the cone. With no overall even radial distribution

Fig 2.6

Fig 2.7

of lava flows from Ngauruhoe, and concentration in the N, NW and SW sectors the cone has been able to maintain its overall symmetry and peaked summit (Hobden 1997). This symmetry may be maintained by deposition of associate pyroclastic avalanches, pyroclastic fall material and formation of scoria cones at the vent. The differing eruption styles occurring at Ngauruhoe compared to North Crater may account for the different summit morphologies. Eruptions at Ngauruhoe involved vulcanian, strombolian and effusive eruptions building up the flanks and summit with lava flows and scoria pyroclasts. Eruptions at North Crater may have involved intense fountaining of gas-rich fluid magma and collapsing eruption plumes resulting in subsequent deposition of pyroclasts further from the vent due to a spreading fountain, thus allowing formation of a broad crater.

2.3 Proximal Stratigraphy

In the following sections the stratigraphy of eruptive units from North Crater is described for the proximal (<2 km from vent) and medial-distal (2-8 km from vent) environments. A number of lithofacies are recognised within the stratigraphy and the nature of these is discussed in section 2.6.

A distinct but broad range of deposits and thus facies types are observed in proximal localities at North Crater. Sixty eight sites (Fig. 2.1) were logged in proximal localities to North Crater (<2 km from vent) revealing these distinct eruptive units. Key stratigraphic columns are given in Appendix B.

North Bluff (Fig. 2.4), the main bluff on the northern slopes of the upper cone, is 300-350 m in length, reaches a maximum height of ~35-40 m, and exposes a large section through the upper cone stratigraphy. Logging seven sections (sites 9, 10, 8, 44, 45, 15 and 7, see Appendix B for complete stratigraphic columns) at various intervals down this bluff identifies a broad range of eruptive products. This includes a basal grey, medium ash with dense angular wall rock lithics and sequences of non-welded scoria and pumice deposits along with moderately to strongly welded fall and flow deposits. From these seven logged sections a

Fig 2.8

Fig 2.9

composite stratigraphy may be compiled of near vent eruptives seen at North Bluff (Fig. 2.8).

South Bluff, on the southern rim of the cone (Fig. 2.4) displays strong to intensely welded units through most of the exposed thickness (~30 m). Three sections were logged along the northern face of the bluff (Fig. 2.9), and one at the most southern tip of the bluff. Although from a distance it appears the bluff is mainly bedded, and strongly welded, there is also a minor component of moderately welded units which grade up into each strongly welded unit and therefore, probably represent the cool base of each depositional unit.

Eastern Gully 1 (Fig. 2.4) is a narrow stream gully which exposes cone deposits from the crater rim down to the Tongariro Crossing track at 1670 m, and includes logged sections at sites 20, 14, 19, 13, 12, 11 and 1 (see Appendix B for complete stratigraphic columns). The upper section of this gully forms the Amphitheatre at the crater rim, where stream erosion and slope failure has exposed the highly jointed ponded lava infilling the crater. Visible at the edges of the Amphitheatre is the original crater rim and the down-slope dipping beds; these are seen to butt up against the solidified ponded lava. Down-slope the gully cuts into the cone and a series of non to moderately welded scoria and pumiceous units can be seen, with some of the more pumiceous units containing mingled clasts. Midway down-slope (at site 1) an orange red bomb/block unit is seen below the scoria and pumice deposits. This unit is not seen at any other outcrops on the cone and is thought to be a localised flow.

Eastern Gully 2 (Fig. 2.4) is also a small stream cutting which extends from just below the crater rim down to just below the Tongariro Crossing track and includes logged sections at sites 28, 27, 26, 25, 24 and 36 (see Appendix B for complete stratigraphic columns). The upper portion of the stratigraphy is a red scoria welded unit overlying a sequence of non-welded scoria and pumice deposits. The more pumiceous deposits contain mingled clasts similar to that seen in Eastern Gully 1. From these six logged sections a composite stratigraphy for Eastern Gully 2 can be established (Fig. 2.10).

Fig 2.10

Fig 2.11

Sites 58-60 (Fig. 2.1), inside the explosion pit, reveal the internal columnar and platy jointed stratigraphy of the solidified ponded lava, which matches the stratigraphy seen in the Amphitheatre. Ponding of the lava within the summit crater is likely to have occurred in the final stages of the North Crater eruptions, as the lava is largely impounded by the original upper cone deposits.

In the field it is evident the stratigraphy changes both vertically at individual sites (Fig. 2.8b), and horizontally between sites to the north, south and east (Fig. 2.11). Many of the intensely welded units occur predominantly to the north and south of the vent, while moderately to poorly welded units are predominantly found to the east and underlying the intensely welded units in the north (Fig. 2.11). A few of the units are only seen in one or two outcrops suggesting localised emplacement by flows. Some of the non-welded units also have a lensed appearance with beds thickening and thinning down-slope. These features indicate varying eruption intensity, fountain heights and plume heights resulting from the tapping of various magma batches with varying compositions, volatile contents, pressures and temperatures. These eruptive processes will be discussed in detail in chapter 5.

2.4 Distal and Medial Stratigraphy

A limited number of sections were logged at distal and medial localities during this study due to the nature of some of the outcrops and limited accessibility in the medial environment. The location of these sections is shown in Fig. 2.1.

Medial units thought to be associated with North Crater and not products from younger vents are characterised by scoria and pumiceous lapilli and ash deposits overlying block and ash pyroclastic flow deposits (Fig. 2.12). It appears these pyroclastic flow deposits overlie a grey andesitic lava flow which is seen in the nearby stream; however the contact between these two units is not seen at any medial locality. It is possible these pyroclastic flow deposits may be related to some of the welded flow deposits seen higher on the cone which have cooled and become less welded with distance from vent. The pumiceous and scoriaceous units are thought to match stratigraphically with non-welded units close to the

Fig 2.12

vent as they display similar features such as clast vesicularity, componentry and sorting.

Figure 2.13: *Distal units associated with North Crater (Rotoaira Lapilli) at site 74. This unit consists of alternating yellow orange pumice lapilli beds and dark grey/black ash. Tool handle measures 30cm.*

Distal units thought to be associated with North Crater eruptions include the lapilli and ash-rich Rotoaira Lapilli. This unit consists of 2-3 yellow orange pumice lapilli beds alternating with dark grey fine ash (Fig. 2.13). As described in Chapter 1, many authors have debated the source vent for the Rotoaira Lapilli. This study will attempt to correlate the distal Rotoaira Lapilli logged at sections 70, 72, 74 and 75 with medial and proximal sections on North Crater proving the source vent is North Crater (suggested by Basher 2005; Doyle 2006 and Kobayashi, pers. comm., 2006) and not Te Maari craters as suggested by earlier authors.

2.5 Stratigraphic Correlations

Section 2.3 described several of the main outcrops on North Crater and the units seen at each. It was possible to make stratigraphic correlations along the outcrops, especially where they have extended tens to hundreds of meters down slope and units could be traced out, and often a composite stratigraphy for the outcrop could be produced.

Fig 2.14

Fig 2.15

Fig 2.16

Key stratigraphic sections logged in proximal localities around the vent are able to be correlated using fence diagrams (Fig. 2.14). This correlation around the cone allows us to compile a complete stratigraphic section of youngest to oldest deposits (Fig. 2.15), and infers eruption history. These round the cone correlations are made based on many of the contacts being able to be sighted/walked out between sites. Where units could not be sighted between sites correlation was made based on unit characteristics such as unit geometry, grain size, sorting, componentry and stratigraphic location above/below certain marker beds.

Proximal to distal stratigraphic correlations were made (Fig. 2.16) for units from the cone trending northward towards the Rotoaira Highway. Correlations suggest a possible relationship with the lower non-welded units on North Crater cone, seen at site 15, indicating North Crater as the source vent for this distal Rotoaira Lapilli unit. Correlations between proximal, medial and distal sites were made based on units overlying certain marker beds, and units with similar characteristics.

From these correlations and field logging several main facies types at proximal and distal localities have been identified. Each facies will be described separately in the following sections.

2.6 Proximal Facies Characteristics

2.6.1 Welded Lithofacies

Intensely Welded Facies

These are massive, dense, intensely welded (2.22 - 2.6 g cm^{-3}) units where no clast outlines are visible. This facies is crystal-rich, medium to coarse grained and ranges in colour from medium grey to dark grey. Rare wall rock lithics and crustal xenoliths can be distinguished in some rock faces as 2-5 cm, lighter grey and cream, undeformed, sub-round inclusions indicating a probable pyroclastic origin to the unit. Often these units contain irregular, columnar and platy jointing. An example of this type of facies is seen in the walls of the explosion pit at T19 385283 (Fig. 2.17), where the exposed thickness is ~70 m. This facies occurs

Fig 2.17, 2.18, 2.19

predominantly as the solidified ponded lava infilling the crater, but is also seen in minor amounts in the upper-most units of North and South Bluffs. The possible mode of origin for this facies is by rapid spatter accumulation from dense lava-fountains within or near the vent with post-deposition shear movement (Table 2.1).

Table 2.1: *Summary of proximal lithofacies characteristics seen at North Crater.*

Proximal Facies	Unit Density	Clast Size	Type Section	Mode of Emplacement
Welded Lithofacies				
Intensely Welded Facies	2.22 - 2.6 g cm^{-3}	Not visible	Site 58	Rapid spatter accumulation near vent with post-depositional shear movement
Strongly Welded Facies	1.3 - 2.46 g cm^{-3}	Faint stretched ribbons	Site 53	Spatter accumulation, agglutination and welding, some post-depositional movement in areas
Moderately Welded Facies	1.11 - 2.01 g cm^{-3}	5-20 cm	Site 17	Slower spatter accumulation, cool base to hot units.
Non-Poorly Welded Lithofacies				
Massive Bomb/Block Facies		5-10 cm	Site 28	Concentrated density current
Reverse Graded Bomb/Block Facies		12-20 cm	Site 25	Low energy, granular pyroclastic flows
Massive Mingled Bomb Facies		6-9 cm	Site 23	Concentrated pyroclastic flow
Massive Lapilli Facies		2-4 cm	Site 45	Pyroclastic fallout, sub-plinian plume
Reverse Graded Lapilli Facies		3-7 cm	Site 25	Low energy granular pyroclastic flows
Massive Ash Facies		<2 mm	Site 15	Pyroclastic fallout
Bedded Ash Facies		<2 mm	Site 24	Pyroclastic fallout or ash cloud surge

Strongly Welded Lithofacies

These are massive to cm-bedded dense, strongly welded (1.3 - 2.46 g cm^{-3}) units where some clast outlines are visible. Clast outlines that are seen are typically faint and often distinguished in the massive face by their slightly different colour. They are often seen as pinkish or greyish ribbons stretched out to <2 cm thick and often up to 30 cm long (Fig. 2.18). The clast ribbons lie parallel to the slope/unit dip indicating possible deposition while hot and subsequent attenuation after lava-fountain deposition. Some units in this facies show bedding on the 30-40 cm

scale, and are planar to weakly bedded and with some beds pinching out down slope indicating a change to lateral transport is occurring. No grain size variations can be easily distinguished, but are defined by sharp bedding planes and minor changes in welding. The facies is crystal rich, medium to coarse grained and range in colour from dark pinkish grey to light pinkish grey. Rare wall rock lithics can be distinguished in some rock faces as 2-5 cm or 15-30 cm, medium grey to black porphyritic andesite, sub-angular to sub-round inclusions. Often units in this facies contain irregular to columnar jointing. A good example of this facies is seen in South Bluff at site 53 (Fig. 2.18) where this facies is most abundant. However it also occurs through North Bluff, East Bluff, Pimple Rock and minor occurrences on the eastern upper flanks of the cone. Some units, i.e. South Bluff (Fig. 2.19), display features which indicate welding of hot pyroclasts, but has undergone little or no post-depositional lateral transport.

Moderately Welded Lithofacies

These are massive, moderately welded (1.11 - 2.01 g cm^{-3}) units with moderate density where clast outlines are more visible than the previous facies. Clast shapes are more easily distinguished in the face and typically appear as scoriaceous, 5-20 cm, sub-round, well sorted, elongate to cowpat-like shapes which appear poor to moderately vesicular. These elongated clasts are typically compacted together but show no imbrication, but instead lie flat and are stacked to near parallel to the slope. These units are thought to have formed by pyroclastic fall from a high lava fountain. Some units have clasts which are typically sub-round and poorly sorted and the unit appears massive with no to very minor bedding features defined by subtle changes in grain size. These units are interpreted as the cooler base of hot flows. The units of this facies are typically 0.4-1.0 m thick, but in a few localities they reach 2-2.5 m thick. This facies is typically crystal rich, fine to medium grained, reddish brown to black in colour and scoriaceous. Some dense wall rock lithics can be seen in faces and are medium grey to black porphyritic andesite, 5-10 cm, and angular. A good example of this facies is seen at site 17 (Fig. 2.20), and it is typically found as thin units capping the eastern slopes, and sometimes associated with the strongly welded facies.

Fig 2.20, 2.21, 2.22

2.6.2 Non to Poorly Welded Lithofacies

Massive Bomb/Block Facies

This is a non to poorly welded massive, poorly sorted, bomb or block facies where clasts are round to sub-round, 2-10 cm, moderate to highly vesicular, crystal rich and reddish brown or black scoria. Units in this facies are either clast supported or contain minor matrix. Matrix consists of coarse black ash and small red and black lapilli. Some pockets within the units of this facies appear to be poorly welded, but density of these pockets has not been determined. Units are typically 0.5-1.5 m thick and are seen to thin rapidly with distance from vent in extensive outcrops. Dense wall rock lithics are also common, and are medium grey to black porphyritic andesite, 2-5 cm and angular. Rare crustal xenoliths are also found in the form of <2 cm sugar-like quartz lumps. These crumble under pressure and are often rounded with orange surface staining. Clast rounding in this facies suggests emplacement involving lateral transport, possibly as a concentrated density current. Some of the units are seen to grade into the moderately to strongly welded facies overlying them and therefore may represent the cool base of hot pyroclastic flows, or are separate pyroclastic flows where no overlying welded deposits exist. A good example of this facies is seen at site 28 (Fig. 2.21).

Reverse Graded Bomb/Block Facies

This is a non to poorly welded, compacted, moderate to poorly sorted, graded bomb or block facies very similar to the previous facies. Clasts are round to sub-round, 4-20 cm, moderately to highly vesicular, crystal rich and reddish brown or black scoria. Units are reverse graded with large bombs (12-20 cm) found in the upper portions, grading down to smaller bombs (4-8 cm) in the lower portions of a unit. Units are either clast supported or with minor matrix support, with the matrix consisting of coarse black ash and small lapilli. Some pockets within the units of this facies are poorly welded; the density of these has not been determined. Units in this facies are typically 0.5 to 1.5 m thick and are seen to thin down slope with distance from the vent. A few of the units show minor gradational contacts over centimetre scale suggesting minor entrainment of clasts into the upper flow units. Dense andesite wall rock lithics are also common and are medium grey to black, 4-7 cm and angular, and are often concentrated toward the bottom of the unit. A

good example of this facies is at site 25 (Fig. 2.22). Clast rounding and graded nature suggests this facies formed from relatively low energy granular pyroclastic flow.

Massive Mingled Bomb Facies

This is a non-welded, but compacted, massive small bomb facies. Units in this facies are made up of a mixture of black scoria clasts, yellow brown pumice clasts and clasts showing a mingled, streaky texture of both the black scoria and yellow brown pumice. Clasts show varying degrees of mingling with little to none in scoriaceous clasts to moderate and intensely mingled pumiceous clasts. Both end member clasts are always present. Clasts in these units are either 2-4 cm or 6-9 cm, sub-round to round, poorly to moderately vesicular, crystal rich and are typically clast supported with minor matrix and poorly sorted. Matrix consists of black and yellow brown coarse ash and small lapilli, with minor pinkish red small lapilli also present. Some dense wall rock lithics are also found and are dark grey/black porphyritic andesite, 1-5 cm, crystal rich and angular. A good example of this facies is at site 23 (Fig. 2.23). Clast rounding in this facies suggests emplacement involving lateral transport, possibly as a concentrated pyroclastic flow.

Massive Lapilli Facies

This is a non to poorly welded, compacted, massive lapilli facies. Units in this facies are either black or reddish brown scoriaceous or yellow brown pumiceous, with pumiceous clasts finely vesicular and scoria clasts poor-moderately vesicular. Most are 2-4 cm (with a few units <2 cm), sub-round, crystal rich, moderately to well sorted and clast supported. Very minor matrix consists of medium to coarse yellow brown or black ash. Some dense wall rock lithics are seen, being dark grey to black porphyritic andesite, 1-3 cm and angular. The units in this facies are typically 0.3-1.0 m thick and are seen to have a relatively consistent thickness away from vent in the proximal zone. A good example of this facies is seen at site 45 (Fig. 2.24a). The massive bedding and relatively well sorted character suggests this facies is the product of pyroclastic fallout from a sub-plinian plume.

Fig 2.23

Reverse Graded Lapilli Facies

This is a non to poorly welded, compacted, graded lapilli facies. Units are typically reverse graded with larger (5-7 cm), sub-rounded clasts in the upper portion, and smaller (3-5 cm), sub-round clasts in the lower portion of the units. Clasts are either yellow brown pumiceous or black/red scoriaceous and are clast supported with minor matrix. Matrix consists of coarse yellow brown and black ash and very small lapilli. Units in this facies are typically 0.4-1.0 m thick with some having irregular thicknesses as they lens in and out away from vent. Some dense wall rock lithics are also seen, and are 1-3 cm, angular, dark grey/black porphyritic andesite. A good example of this facies is at site 25 (Fig. 2.22) where a graded pumice unit can be seen which lenses in and out downslope. Clast rounding and the graded nature suggest emplacement of this facies involved lateral transport possibly as a lower energy, granular pyroclastic flow.

Massive Ash Facies

This is a very fine to fine, massive, very well sorted ash facies. It appears to be the lower most unit in the 14-10 ka North Crater eruptive sequence, and is a light to medium grey colour. It contains a number of dense wall rock lithics (~ 25%) which are angular, 4-8 cm, medium grey andesite. The exposed thickness of this facies is 1.5-2 m as the base of the unit is not seen anywhere on the volcano. A good example of this facies is at site 15 (Fig. 2.24b) where it is exposed at the base of the stratigraphy. It is possible this facies formed during vent clearing at the start of the eruption sequence.

Bedded Ash Facies

This is a very fine to medium, bedded, well sorted ash facies. This facies consists of purplish or bluish grey medium ash bedded with brown or grey very fine ash beds. Bottom beds contain few pumice lapilli, but no dense wall rock lithics are seen. A good example of this facies is at site 24 (Fig. 2.24c). It is possible this facies formed during small phreatomagmatic eruptions, deposition of an ash cloud or co-ignimbrite surge, or as fallout during waning stages of activity.

Fig 2.24a,b,c,d

2.7 Distal Facies Characteristics

2.7.1 Non to Poorly Welded Lithofacies

Massive Lapilli Facies

This is a massive, loose, pumice lapilli facies. Lapilli clasts are orange to yellow, poorly to moderately vesicular with minor matrix of dark grey coarse ash, sub-round to round, well sorted, 1-3 cm and crystal rich. The thickness of this facies ranges from 10-40 cm and with rapid thickness variations along lengthy outcrops. These variations indicate erosion of the unit may have taken place during the last glacial, and original thickness may no longer be represented at some sites. A good example of this facies is at site 74 (Fig. 2.24d) on the Rotoaira Highway. The grain size and sorting characteristics of this facies indicate emplacement as a widespread pyroclastic fall.

Massive to Bedded Ash Facies

This is a massive to bedded, dark grey/black, fine ash. It is distinctive in the field and is found bedded with the previous facies with a thickness ranging from 8-12 cm. However like the massive lapilli facies described above, the thickness is seen to change rapidly over short distances. The units of this facies are seen to grade between massive and bedded along an outcrop. It has been suggested that the ash has been redeposited, and the appearance of cross bedding and pinched bedding dispersed with sections of more massive ash may confirm this. Bedding is seen on the millimetre scale and is distinguished by slightly different coloured and size ash. A good example is found at site 74 (Fig. 2.24d). It is possible this ash was originally deposited as fallout from a co-ignimbrite ash cloud surge or phreatomagmatic ash, and has since undergone lateral reworking.

Table 2.2: *Summary of distal lithofacies characteristics of North Crater eruptives*

Distal Facies	Clast Size	Type Section	Mode of Emplacement
Non-Poorly Welded Lithofacies			
Massive Lapilli Facies	1-3 cm	Site 74	Pyroclastic fall, sub-plinian plume
Massive to Bedded Ash Facies	<2 mm	Site 74	Pyroclastic fall or ash cloud surge and lateral reworking

2.8 Summary

North Crater is a relatively young andesite cone made up of a complex suite of non- welded and welded pyroclastic deposits. Good exposures around the cone provide a detailed record of the eruption stratigraphy. North Crater has slope angles typical of subduction related andesite cones but has a large flat plateau at the summit created by ponded lava infilling the vent crater. It is unsure why North Crater displays such a large summit crater, but multiple closely-spaced vents or a collapsing eruption plume during the eruption episode are likely causes. The solidified ponded lava has then been locally excavated by a possible steam driven eruption sometime after the main eruptions ceased, forming the explosion pit in the northwest sector. The eruptive products and thus the formation of North Crater may have been topographically influenced by the similar age Blue Lake vent, and the older Tongariro Trig vent, directing the majority of ground-hugging pyroclastic flows to the north and west.

By compiling stratigraphic logs in the field, correlation of proximal, medial and distal deposits on North Crater has been possible. Correlations can be made along large outcrops showing the changing nature of units away from the vent, especially those of strongly welded near-vent units. Round the cone correlations shows how outcrops fit spatially and has allowed a complete eruptive sequence for North Crater to be produced. However, as the stratigraphy changes rapidly over small distances with units lensing in and out or disappearing completely, absolute correlations cannot be made. These lateral variations suggest many units in the proximal cone deposits have lateral equivalents in the medial and distal environment.

Correlations from proximal vent locations to distal Rotoaira Lapilli units have also been possible. From these correlations we can establish Rotoaira Lapilli has a source vent at North Crater; however correlation between more medial sites is needed to firmly establish the stratigraphic correlation of individual beds.

From these correlations a number of lithofacies are identified. These facies show the variability of products of the North Crater eruptions indicating rapid changes of complex eruption processes at North Crater.

These lithofacies and stratigraphic correlations make it possible to define several phases of activity at North Crater, starting with onset of eruptions, cool pyroclastic falls and collapsing columns producing hot pyroclastic flows, along with high intensity lava-fountaining forming the hot intensely to moderately welded fall and flow units on the upper cone. It is possible there were several breaks in the eruption sequence of days, weeks, months or years as intensely to moderately welded units are found to overlie other welded units with sharp contacts between. The lack of major unconformities in the North Crater sequence suggests no significant time breaks in the eruption have occurred, indicating the main eruption activity may have taken place over a few months or years. These eruption mechanisms and history will be discussed in detail in chapter 5.

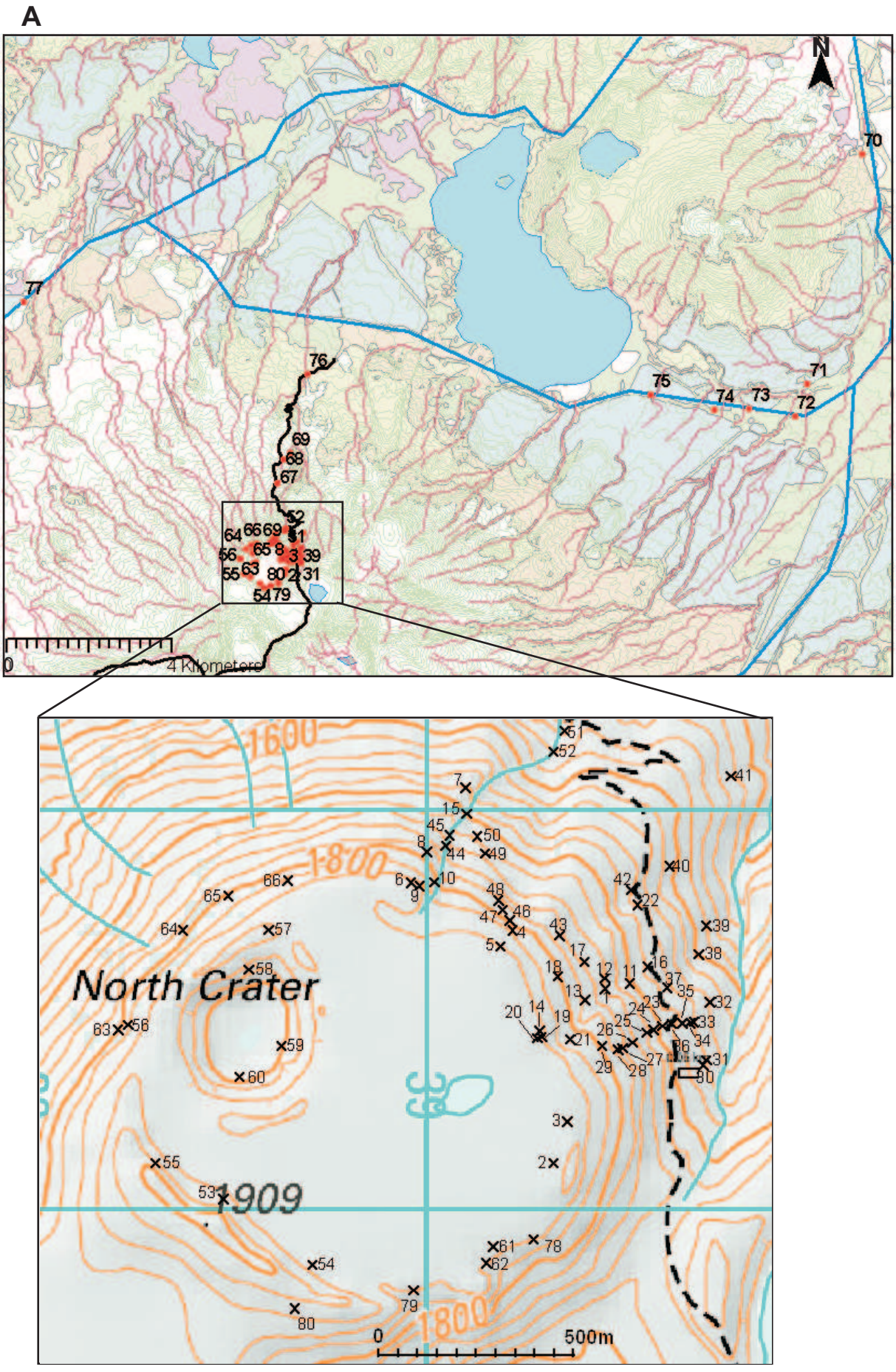

Figure 2.1: *A) Map showing numbered field sites in proximal and distal localities relative to North Crater. B) Detailed map showing numbered proximal localities around North Crater. Grid references given in Appendix A*

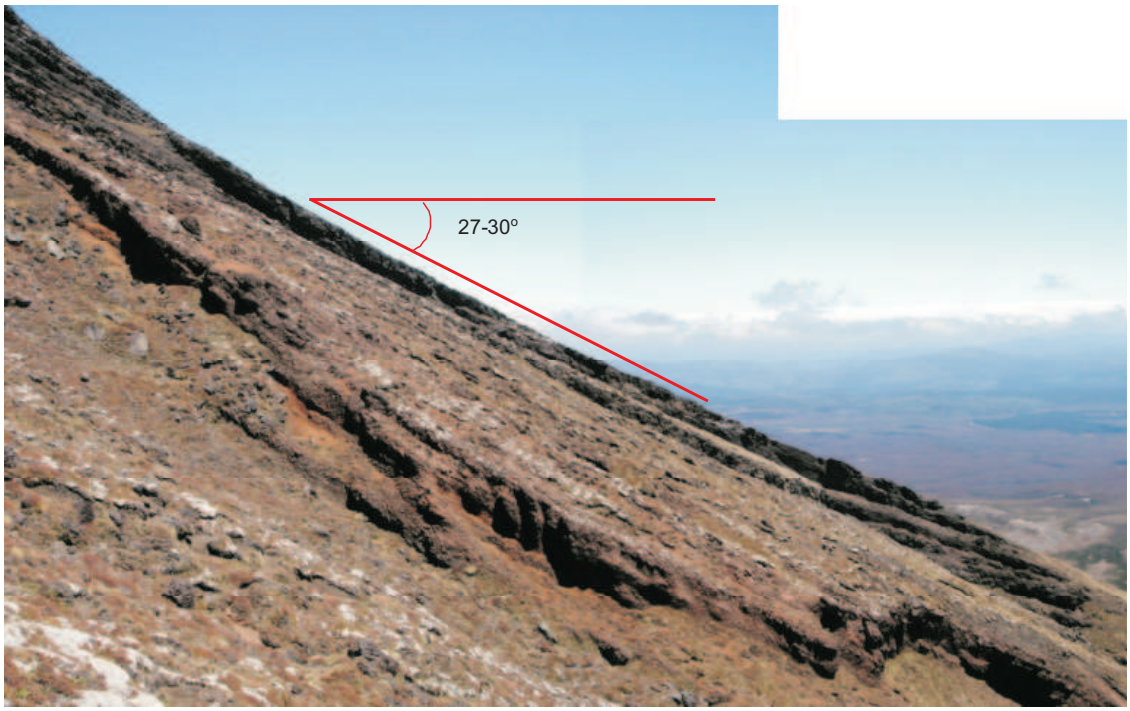

Figure 2.3: *Photo of the lower portion of North Bluff on North Crater showing slope angles on the upper cone.*

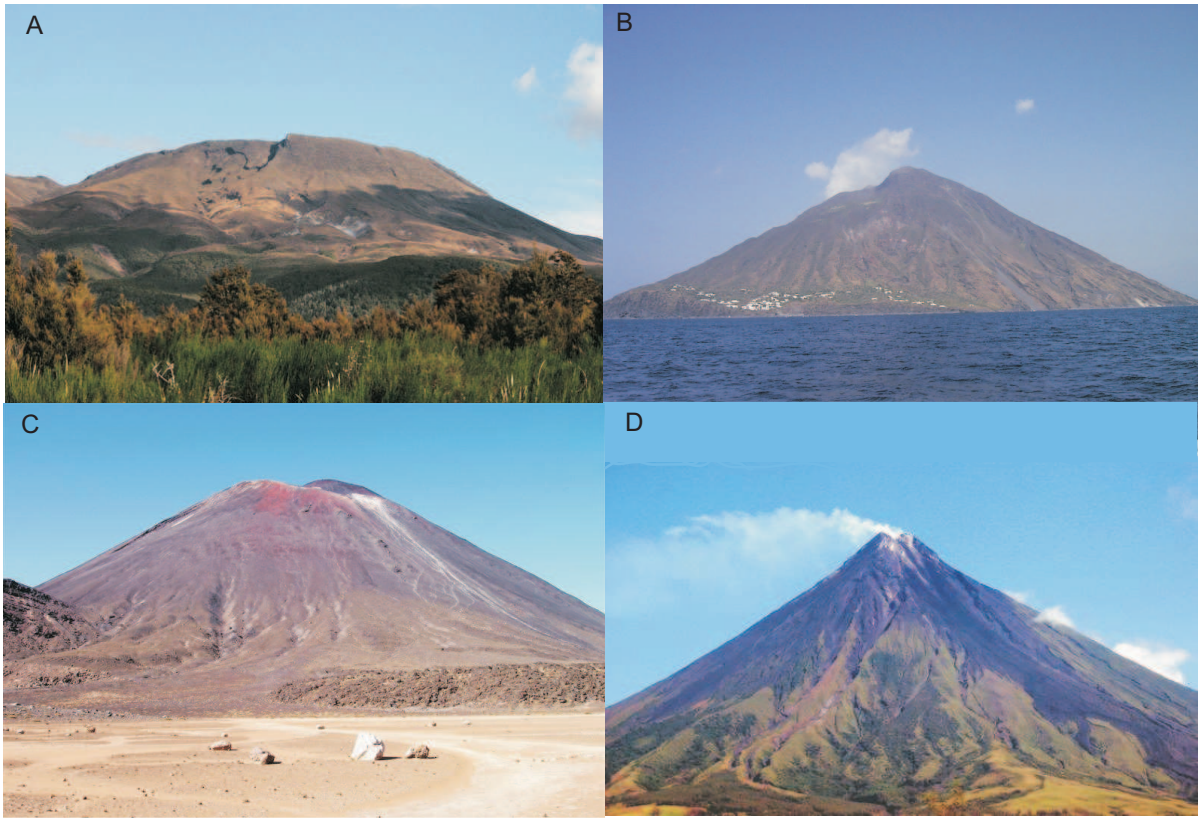

Figure 2.5: *Geomorphology of North Crater (A) and typical subduction zone cones, (B) Stromboli - Italy, (C) Ngauruhoe - New Zealand and (D) Mt Mayon - Phillippines.*

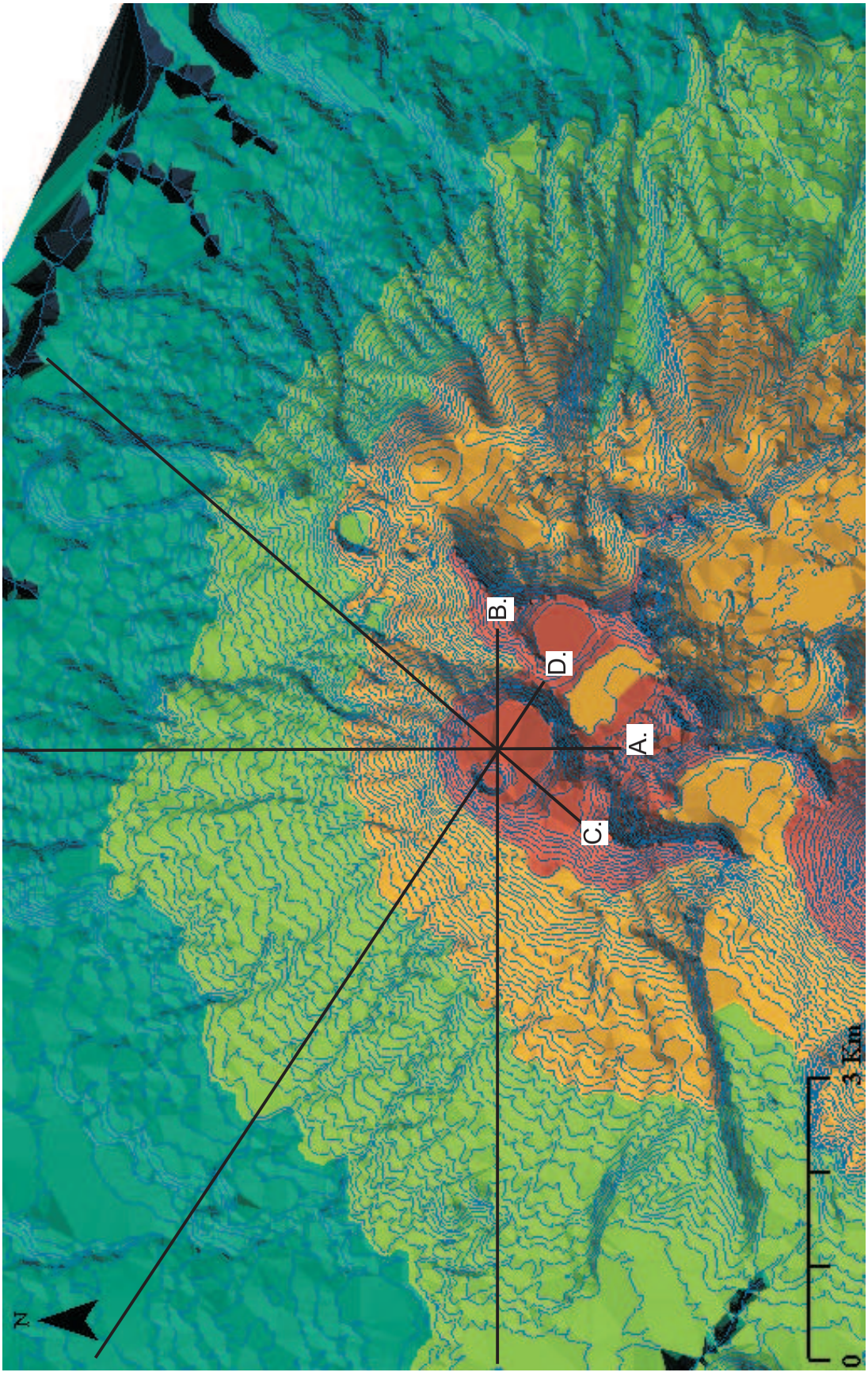

Figure 2.6: *Elevation model for a section of Tongariro National Park, North Crater centred. Line showing where topographical cross-section profiles taken from, A) S-N, B) E-W, C) SW-NE, D) SE-NW.*

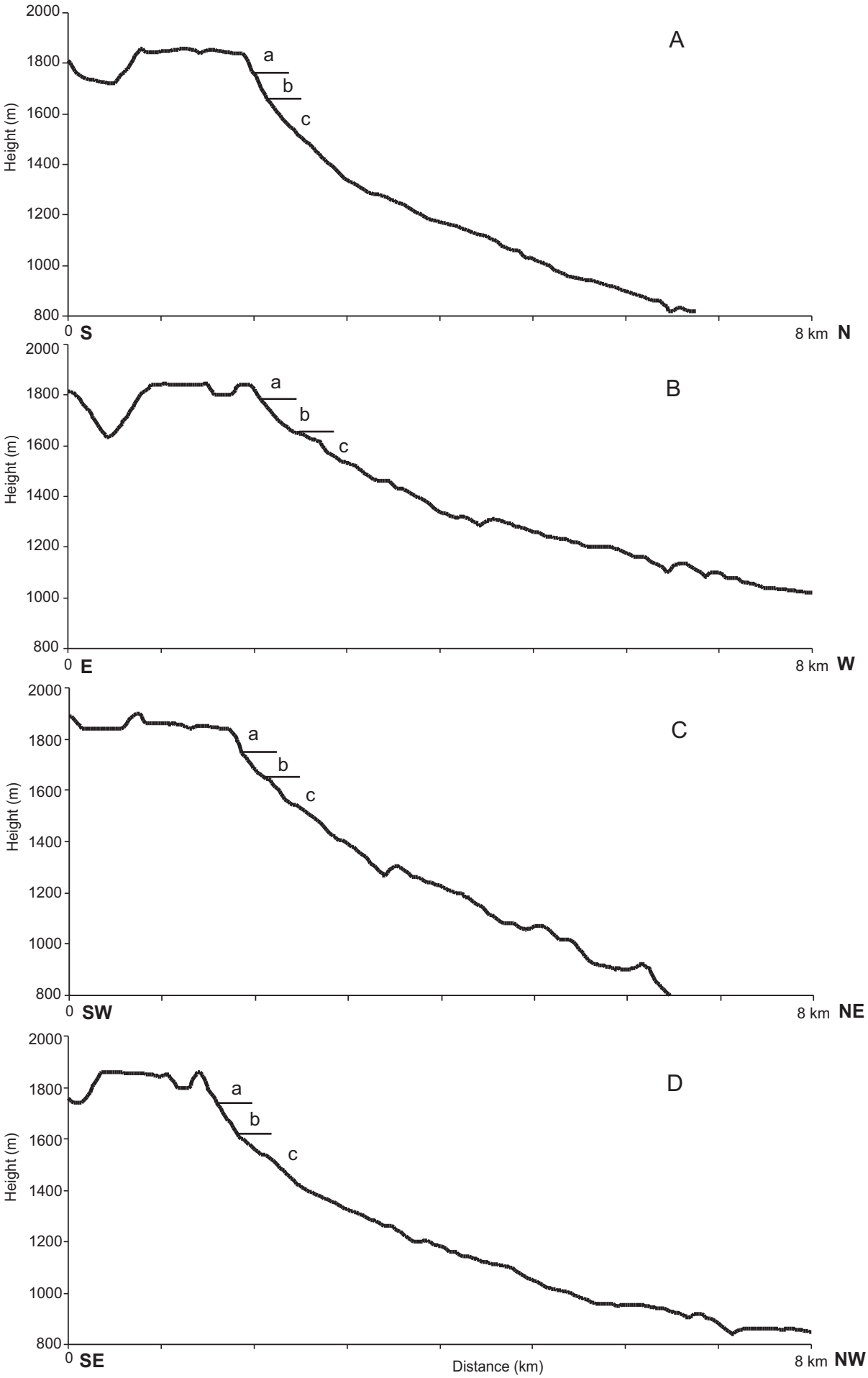

Figure 2.7: *Cross-sectional profiles across North Crater and surrounding landscape. a) S-N, b) E-W, c) SW-NE and d) SE-NW. Slope segments a & b show where there is greatest slope angle change on the cone.*

A

North Bluff Composite Stratigraphy and Facies Descriptions

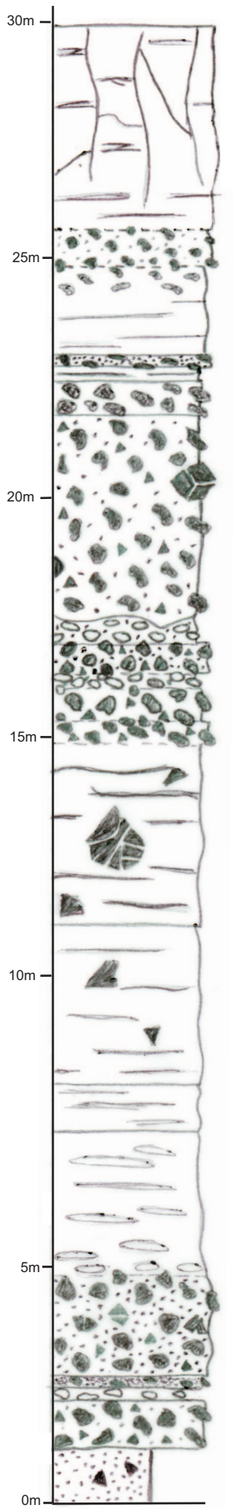

Strongly welded facies, with minor intensely welded facies on very top. Irregular to columnar jointing.

Non-welded massive bomb facies, black scoria.

Non-welded massive bomb facies, black scoria.

Non-welded massive lapilli facies, yellow brown pumice with minor black scoria.

Non-welded massive bomb facies, black scoria.

Non-welded bomb/lapilli mingled facies, black scoria and yellow brown pumice.

Non-welded massive bomb facies, black scoria.

Strongly welded facies, red vesicular, scoriaceous, material with few clast outlines. Dense juvenile bombs with surface breadcrust cracking.

Strongly welded facies, red vesicular, scoriaceous, material with few clast outlines. Dense juvenile bombs with surface breadcrust cracking.

Strongly welded facies, red vesicular, scoriaceous, material with few clast outlines. Dense juvenile bombs with surface breadcrust cracking.

Moderately welded facies, red vesicular, scoriaceous, material with few clast outlines.

Non-welded massive bomb facies, black scoria.

Non-welded bomb/lapilli mingled facies, black scoria and yellow brown pumice..

Non-welded massive bomb facies, black scoria.

Massive ash facies

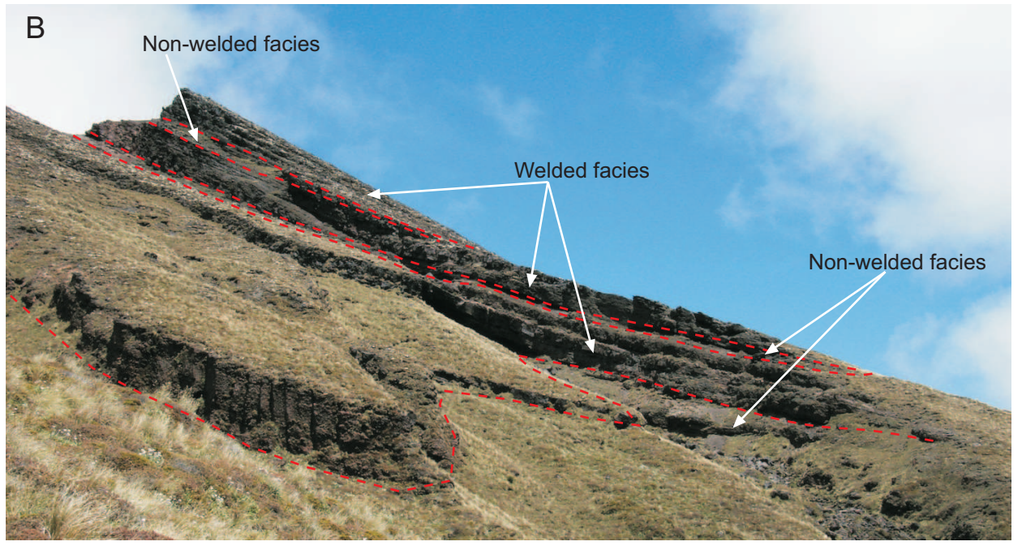

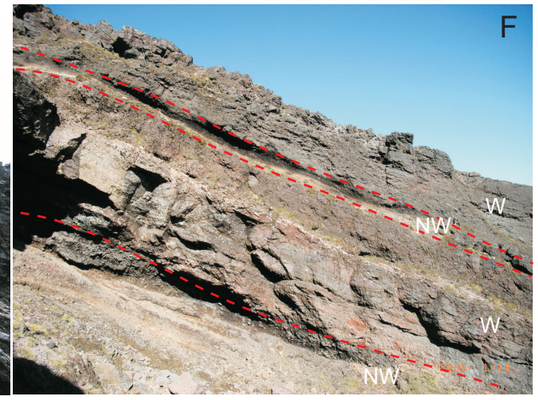

Figure 2.8: *A) Column of North Bluff composite stratigraphy, North Crater, with general facies descriptions. B) the total length of the North Bluff, C) the units of North Bluff closest to the vent, main bluff height 25 m (NW=non-welded facies, W=welded facies), D) site 44 lower non-welded pumice and scoria units, prominant black scoria unit 3.2 m, E) the varying structures just below site 44, full height of bluff 35 m, F) all the units at site 15, height of bluff 22 m.*

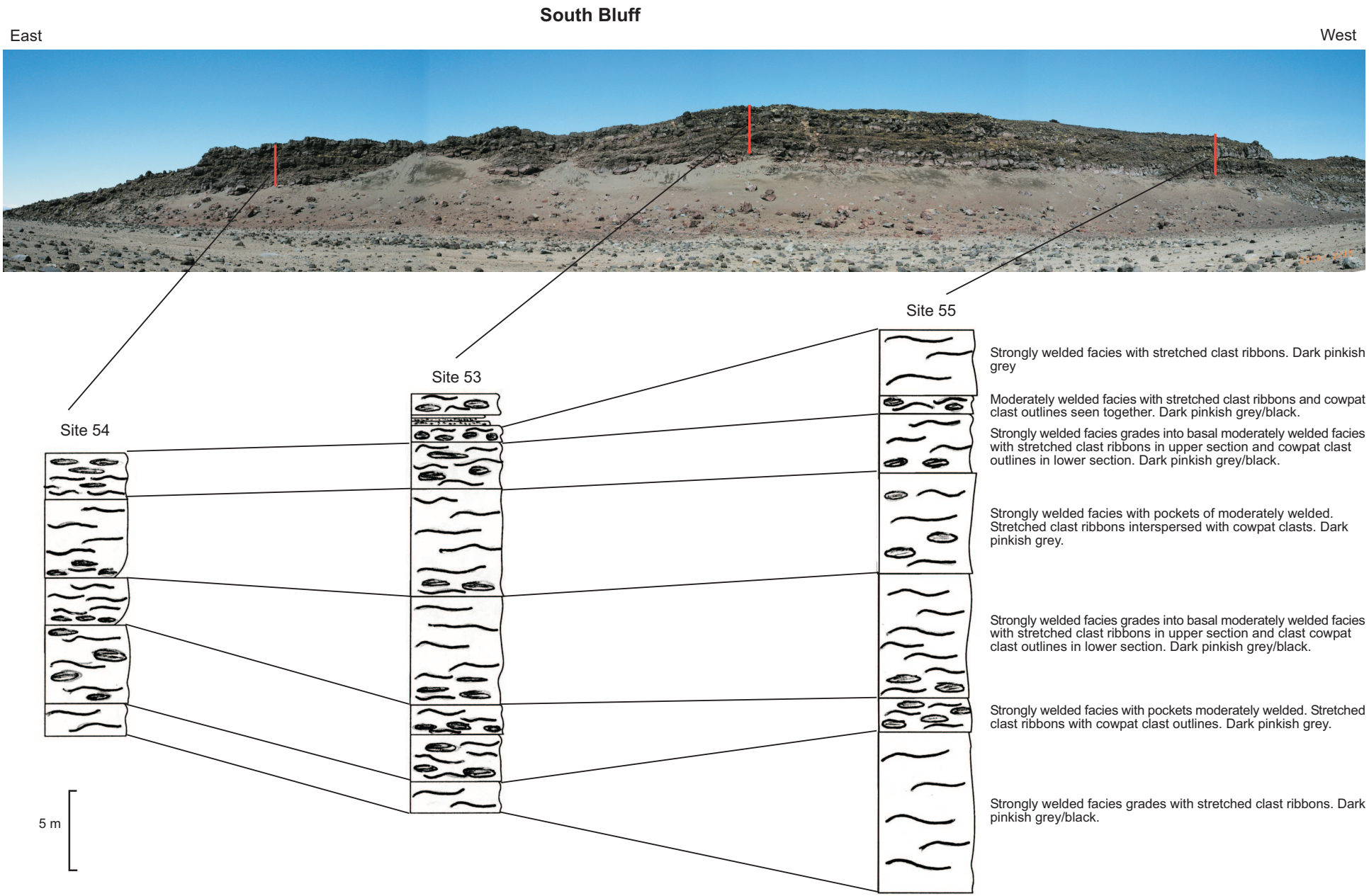

Figure 2.9: *South Bluff stratigraphy and correlation, with general facies descriptions. See Appendix B for full stratigraphic columns.*

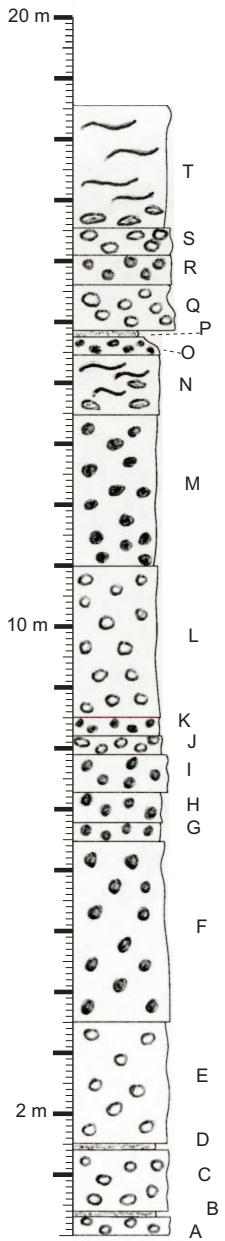

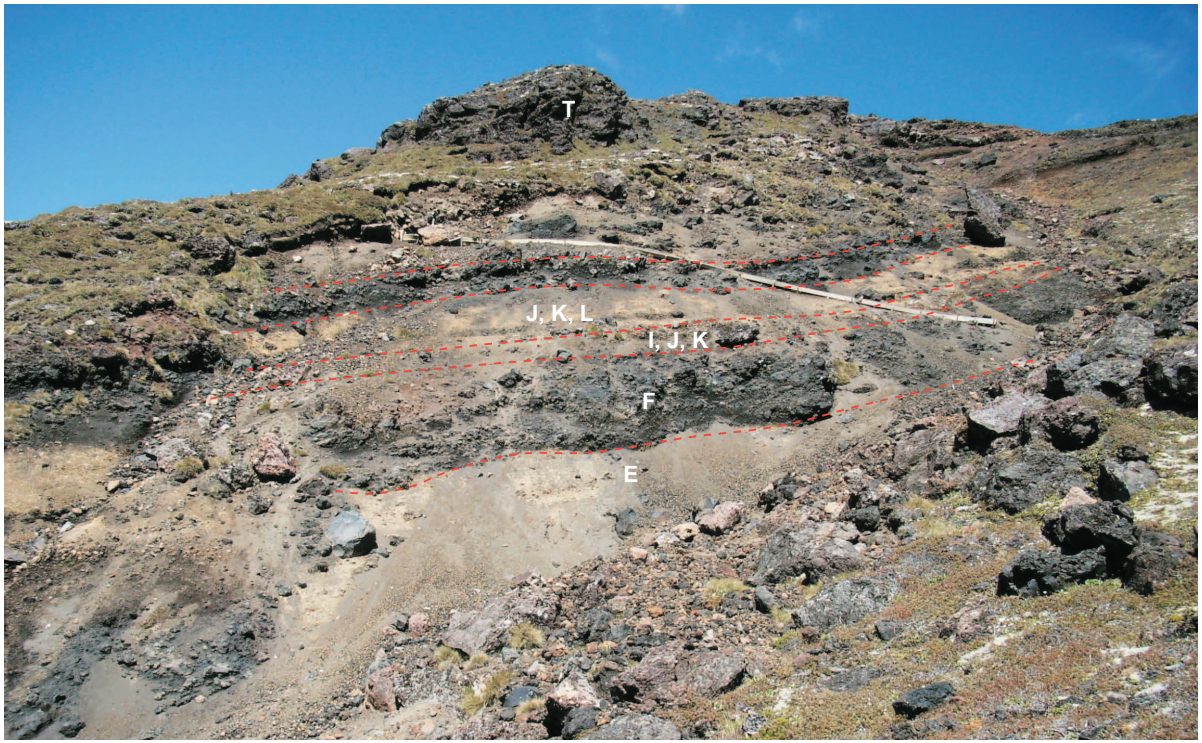

Units O to T seen here.
Note the lensed appearance
to the pumice lapilli bed.

Figure 2.10: *Composite stratigraphy of Eastern Gully 2, sites 36, 24-28, North Crater. Unfilled circles represent mingled lapilli facies, and black filled circles represent black scoria bomb facies. Complete stratigraphic logs for each site are found in Appendix B. Letters in stratigraphic log refer to sections outlined in the photographs.*

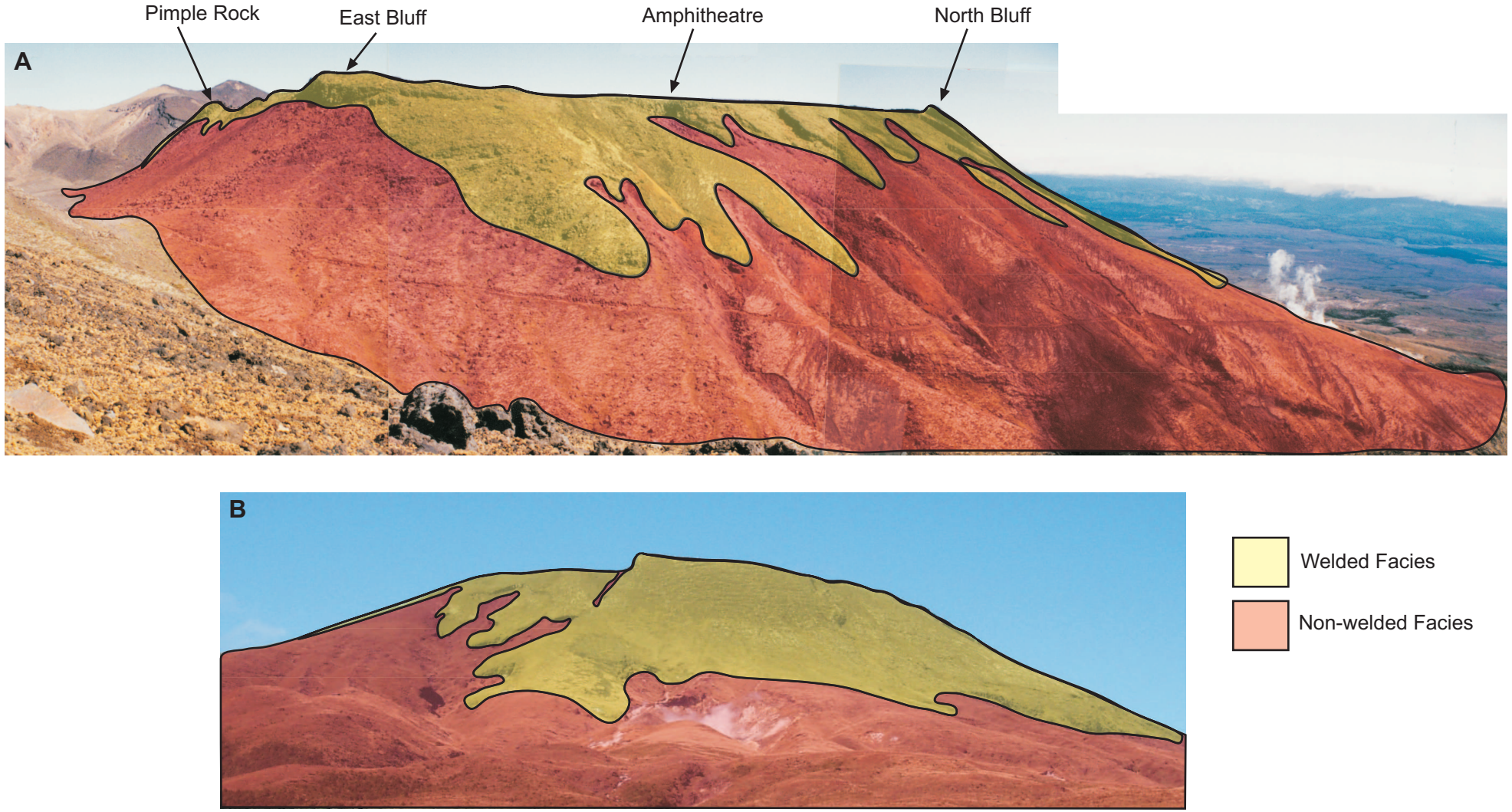

Figure 2.11: *A) Photo from Te Maari Craters looking west towards the eastern flank of North Crater, showing areas non-welded and welded facies (Photo provided by T. Kobayashi). B) Photo looking south towards the northern flank of North Crater, showing areas of non-welded and welded facies.*

Figure 2.12: *Photo of medial site 69 with block and ash flow (seen below dashed red line) and overlying pumice, ash and scoria deposits sourced from North Crater and later deposits from younger Tongariro vents . See Appendix B for complete stratigraphic column. Person for scale (1.6m).*

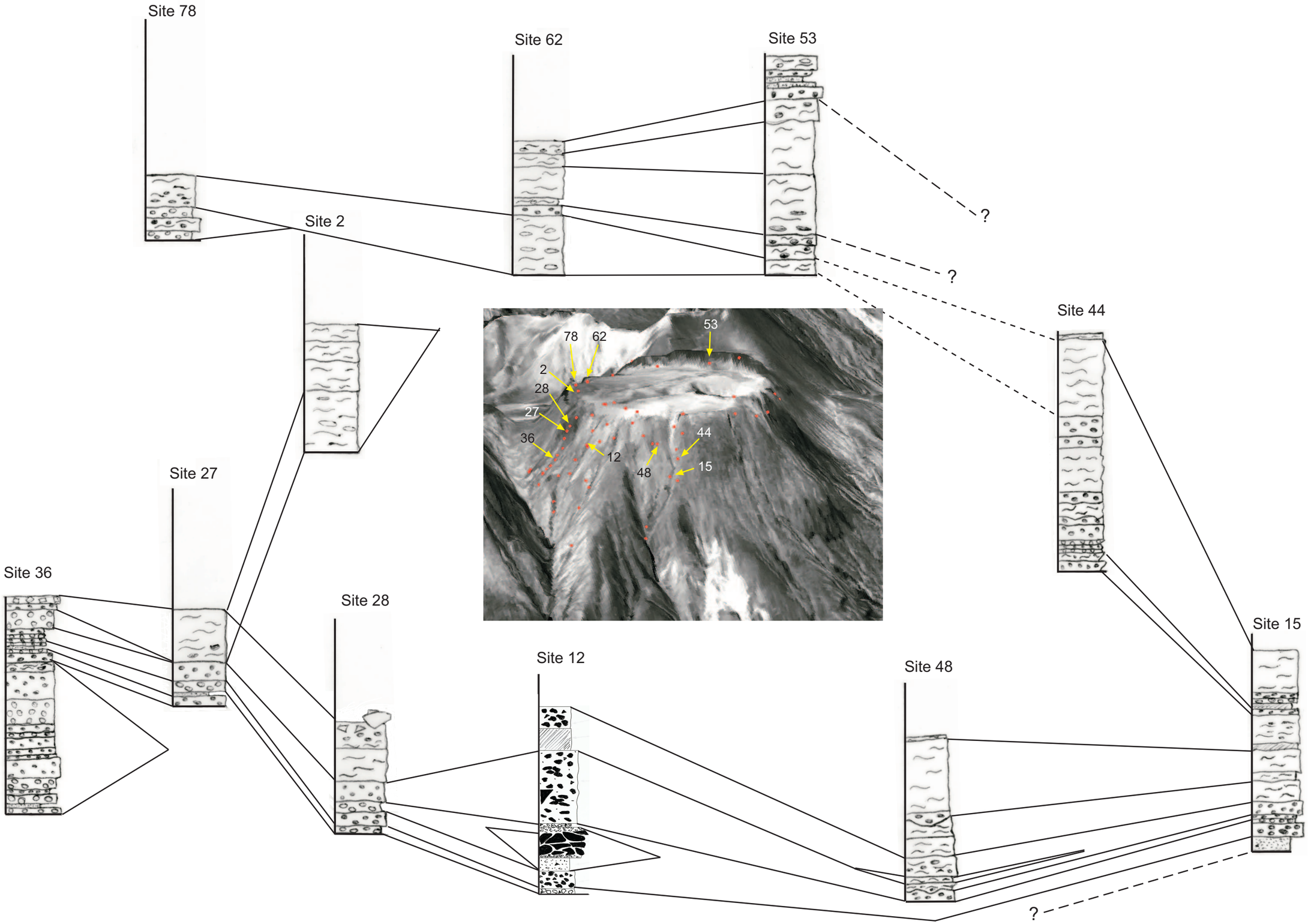

Figure 2.14: *Fence diagram showing stratigraphic correlations between key proximal sites on North Crater. See Appendix A for detailed stratigraphic columns of these sites. Red dots on insert DEM denote other field sites. Dashed lines indicate possible correlations.*

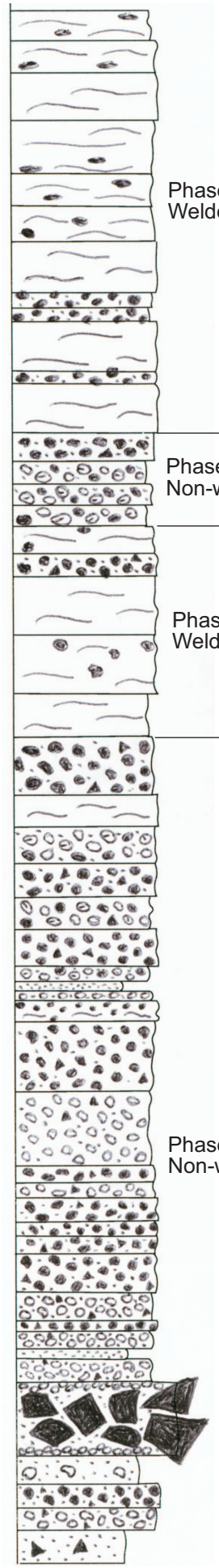

Phase 4 eruptives are predominantly strongly welded with basal moderately welded zones, minor intensely welded units are also present.
In the early stages of this phase base flows where cooler resulting in more poorly welded deposits underlying strongly welded facies. Later in the phase, base flows had little cooling and formed moderately welded zones at the base of strongly welded facies. These units are localised primarily to the south (South Bluff) and to a lesser extent to the west and capping North Bluff.

Phase 3 eruptives are predominantly non to poorly welded units. This phase consists of predominantly mingled facies, with each unit containing varying amounts of pumice and scoria. This phase occurs predominantly at North Bluff.

Phase 2 eruptives are predominantly moderately to strongly welded facies. Some units show mixed clasts and strong welding, while others have basal moderately welded flows.
This phase can be traced from North Bluff around the northern and eastern slopes to East Bluff.

Phase 1 eruptives are predominantly non to poorly welded facies. The units range from massive/graded scoria bomb and pumice lapilli to mingled lapilli and ash.
Many of the units in this facies are localised at various sites around the northern and eastern slopes of North Crater. The unit found lowest in the stratigraphy appears to be a fine light grey ash possibly produced during vent clearing at the start of the eruption sequence. No units were found at the lower contact to this grey ash.

Figure 2.15: *Column of complete North Crater eruptive products and general facies descriptions. Entire sequence 40-60 m thick.*

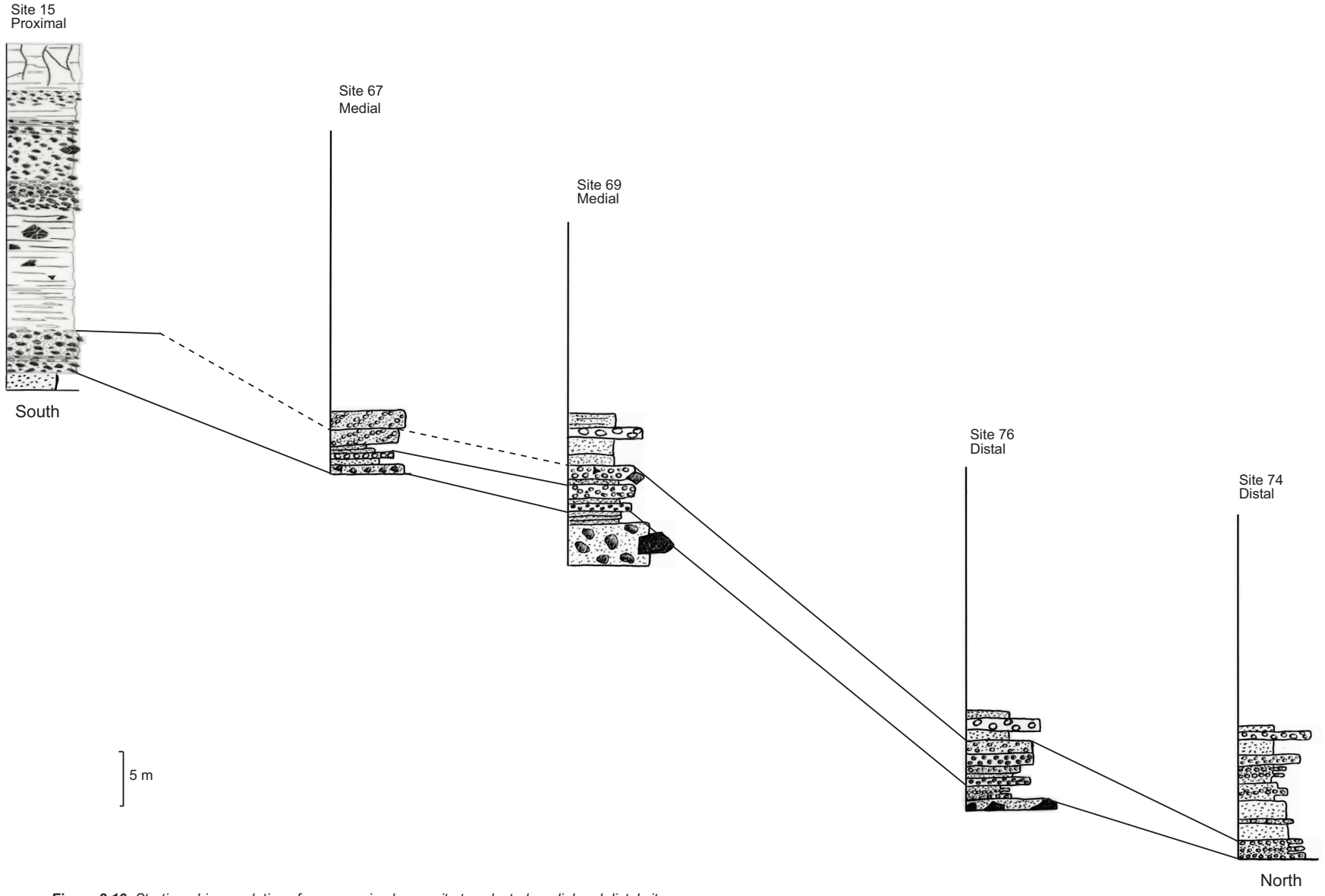

Figure 2.16: *Stratigraphic correlations from a proximal cone site to selected medial and distal sites.*

Site 75
Distal

Site 72
Distal

Figure 2.17: *Intensely welded facies at the Amphitheatre with platy fracturing and massive units visible. Note the folded structures in the platy jointed zone. Person for scale (1.6 m height).*

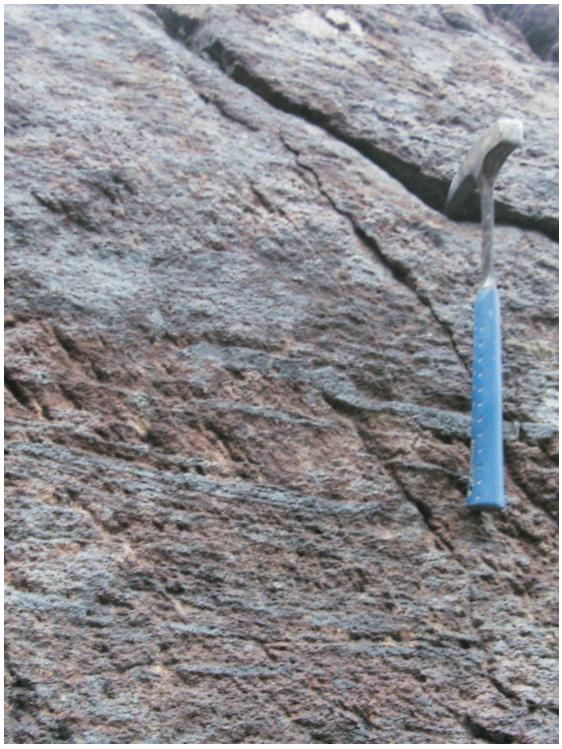

Figure 2.18: *Strongly welded facies at site 20. Faint clast outlines are visible in the face as stretched ribbons. Hammer handle measures 30cm.*

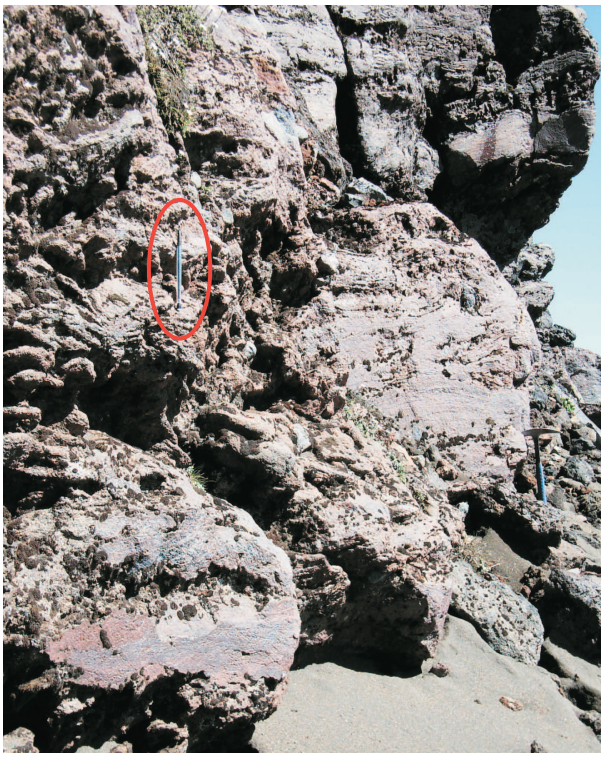

Figure 2.19: *Stongly welded facies at South Bluff, areas of stretched clast seen next to areas of cowpat-like clasts. Pen 15cm long.*

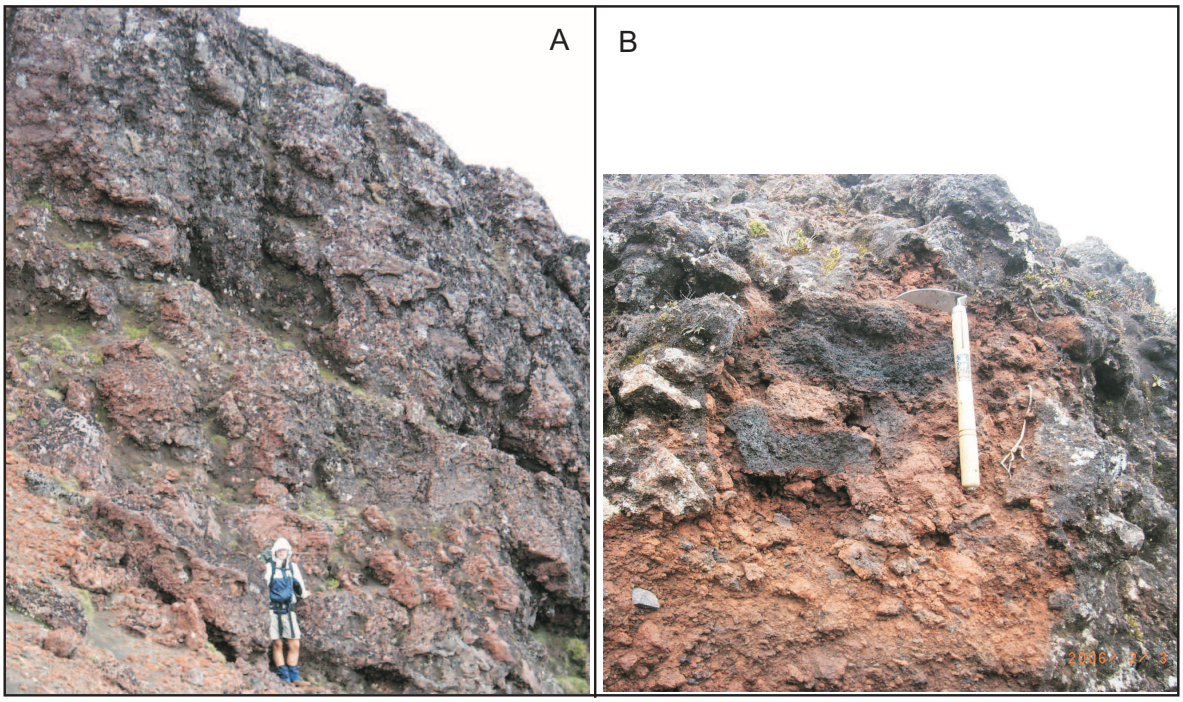

Figure 2.20: *A) Moderately welded facies at site18 (person for scale 1.6 m), B) black scoria clasts seen in reddish brown moderately welded facies site 18 (tool handle 30 cm).*

Figure 2.21: Massive *non to poorly welded bomb/block facies site 29. Hammer handle 30 cm long.*

Figure 2.22: *Graded non to poorly welded bomb/block facies (a) and graded non to poorly welded lapilli facies (b) site 27. Tape measure set at 1 m.*

Figure 2.23: *Massive mingled bomb facies seen in units a and b, site 23/36. Insert shows typical mingled clast found in this facies. Person height for scale 1.6 m.*

A) *Massive non to poorly welded lapilli facies (a), site 45. Tool handle 30 cm long.*

B) *Massive non to poorly welded ash facies (unit next to drink bottle), site 15. Drink bottle 30 cm.*

C) *Bedded ash facies, site 24. Tool head 10 cm long.*

D) *Massive non to poorly welded distal lapilli facies and massive to bedded distal ash facies, site 74. Tool handle 30 cm long.*

Figure 2.24: *A) massive to poorly welded lapilli, B) massive non to poorly welded ash facies, C) bedded ash facies and D) distal non-welded facies*

Chapter 3

Textural and Petrographic Characteristics

3.1 Introduction

This chapter details laboratory analyses which were carried out on a number of pyroclastic samples from North Crater eruptives collected in proximal, medial, and distal environments. Laboratory work included grain size, componentry, petrographic, SEM and clast density and vesicularity to determine spatial and temporal differences in the deposits. Figure 2.1 shows site localities, and a catalogue of samples is given in Appendix A. Appendix B describes stratigraphic columns and shows position of samples collected at each field site.

3.2 Grain Size Analysis

Many bulk samples of non-welded pyroclastic units were collected in the field at proximal, medial and distal localities which were able to be sieved for grain size analysis. Grain size analyses were carried out in order to determine grain size distribution variations stratigraphically in proximal sections, and grain size distribution variations between facies. The data contain samples from all over the field area (Fig. 2.1) and full results for grain size analysis undertaken in this study are given in Appendix D.

3.2.1 Methods

Non-welded ash, lapilli and block samples were collected from various proximal, medial and distal sites around the vent. All samples were oven dried at 50°C for 48 hours prior to dry-sieving. Sieving was carried out using Endecott sieves ranging from -6.0 phi to 4.0 phi at 0.5 phi intervals using the mechanical shaker. Hand shaking was used for softer, more pumiceous samples in order to minimise clast degradation. Samples were shaken at moderate amplitude for 5-10 minutes on the mechanical shaker, or 5 minutes by hand. Each size fraction was weighed and separately retained for further analysis.

3.2.2 Results and Discussion

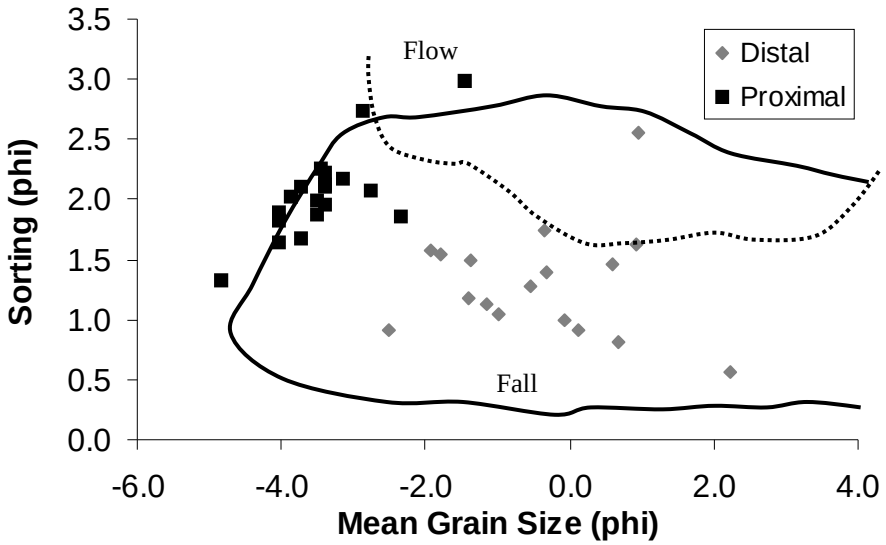

Figure 3.1: *Graph of mean grain size versus sorting for all sieved North Crater samples with typical fall and flow fields from Freundt et al. 2000. All grain size data are presented in Appendix D.*

A plot of mean grain size versus sorting (Fig. 3.1) shows a clear distinction between the grain size character of proximal cone building units and distal deposits. The majority of proximal samples fall into a clustered group exhibiting relatively constrained coarse mean grain size (-2.0 phi to -4.0 phi) and sorting (1.5 phi to 2.25 phi). They are of significantly coarser mean grain size and less well sorted than the medial and distal samples. The medial to distal samples show a wider range of values, and have mean grain sizes in the -2.0 phi to 2.0 phi range and sorting of 0.7 phi to 1.7 phi (Fig. 3.1). These data are likely to underestimate

Fig 3.2

the coarsest grain sizes because of technical constraints on sampling very coarse deposits in the field.

Proximal Relationships

Figure 3.2 shows the mean grain size, sorting and maximum clast size for samples collected from the North Bluff composite stratigraphy. The mean grain size and sorting data was compiled from laboratory analysis, while maximum clast size data are taken from measurements collected in the field. Figure 3.3 shows the typical grain size distributions for selected main proximal facies. Figure 3.16 shows how mean grain size varies up through the complete sequence of North Crater cone-building eruptives.

The mean grain size for individual units sampled from North Bluff ranges from -5 to -3 phi (Fig. 3.2). All units sampled have coarse mean grain size (bomb/blocks) and are relatively poorly sorted (1 - 2.5 phi, Fig. 3.2). The maximum grain size observed in the field was often not represented in the sieved samples, but was recognised in the field as being a discrete population in many of the units. This implies many of the units in North Bluff, and thus around the cone, have bimodal grain size distributions. The maximum clast size data indicates the presence of this coarser fraction, and density determinations on chips off larger bombs from the sampling zone allows inferred grain size data of this discrete population to be added to the sieved data sets.

Some samples from North Bluff have clasts larger than about -5.5 phi measured in the field. These clasts were measured with dimensions of height, width and length recorded as well as a brief description of their shape. Small chips were broken off these outsize clasts and numbered. In the lab density of these chips was determined using the methods described in section 3.4.1. Maximum volume of the original clast was then determined by using the formula for the volume of an ellipsoid (Eqn. 3.1) which best approximated the shape of the majority of the clasts measured.

$$Volume\ of\ \ ellipsoid\,(cm^3) = \frac{1}{6}\pi\ lwh \qquad \text{Eqn. 3.1}$$

Total mass of the original clast could then be determined using the volume and density (Eqn. 3.2). Results are given in Appendix D.

$$Mass = density\ (gcm^{-3}) \times volume\ (cm^{3}) \qquad \text{Eqn. 3.2}$$

The mass and grain sizes determined for the outsize fraction was then added to the sieved grain size distribution (Appendix D).

Many of the maximum size measurements at North Bluff and around the cone included dense juveniles and lithics and may represent ballistic bomb/blocks which have been deposited simultaneously with the pyroclastic convective fall and flow deposits.

Proximal Facies Grain Size Variations

The massive bomb/block facies, previously described in chapter 2, typically displays a coarsely skewed size distribution (Fig. 3.3a) with very little fine material (<2 phi) and ranges from very poorly to poorly sorted with a typical range of -2 phi to -4 phi. Grain size data for the coarsest size fractions were added from measurements from clast chips described earlier and with this data distributions are typically bimodal. There was clear evidence for this in the field where there was a distinctly coarser population (-6 to -8 phi) with a more uniform finer population (-2 to -5 phi). The mean grain size for this facies derived from sieved fractions is typically -5 to -3.5 phi, however with the addition of the coarser population the mean grain size is -6.5 to -7 phi.

The mingled lapilli/bomb facies, previously described in chapter 2, typically displays a distinct bimodal distribution, with slight coarse skew (Fig. 3.3b) and very poorly sorted (-3 - -2 phi). Some units which are bomb rich display a stronger coarse skew than those which are lapilli rich. The mean grain size for this facies ranges from -2.5 phi to -4.5 phi, which attests to the broad range of grain sizes seen in the field for these units, and are typically of finer mean grain size than the massive bomb facies.

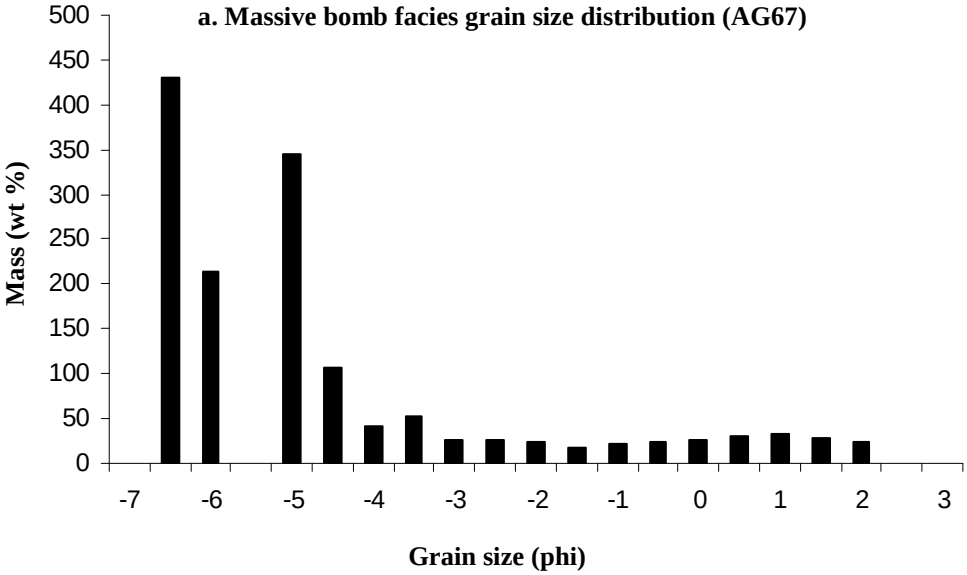

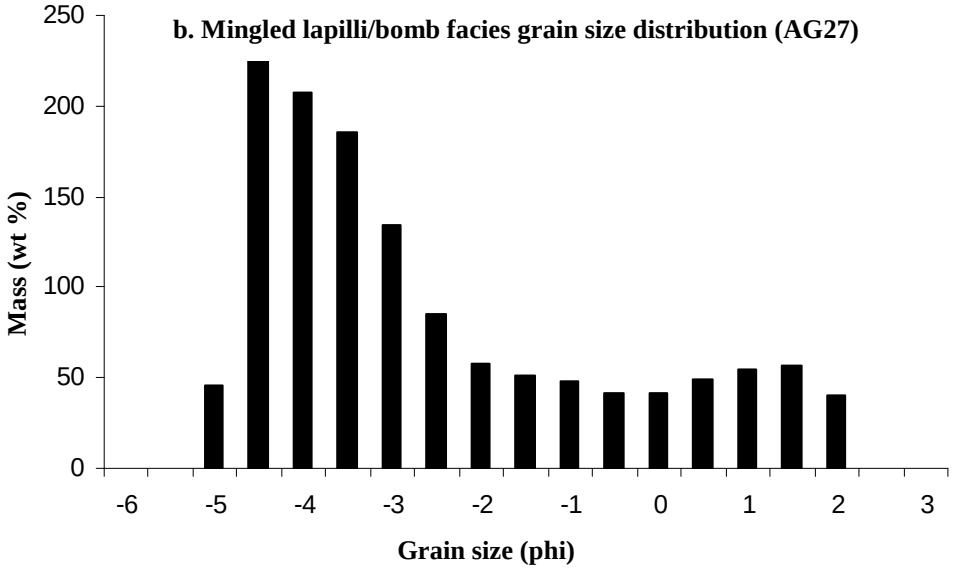

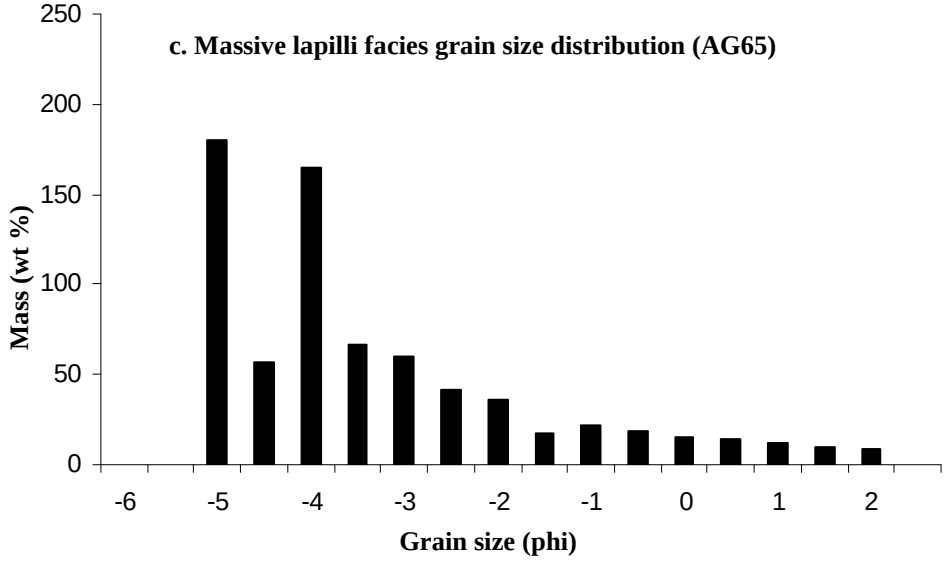

Figure 3.3: *Typical proximal grain size distributions for the main non-welded proximal facies. Full grain size results are given for all samples in Appendix D.*

Grain size distributions of the massive lapilli facies are typically coarsely skewed and weakly polymodal to bimodal (Fig. 3.3c). The mean grain size is finer than the massive bomb (-3 to -4.5 phi), poorly to very poorly sorted ranging (1 phi to 2.5 phi). Rare outsize clasts (> -6 phi) were found at some field sites consisting of dense juveniles and wallrock lithics, thought to represent ballistic fallout during deposition of these units. A few of these are represented in the grain size data (Appendix D).

Medial/Distal Grain Size Distribution

The majority of lapilli units in the distal environment show normal to finely skewed grain size distributions and range from -2 – 1 phi and are moderate to well sorted (1.7-0.8 phi). Only a few of the units display polymodal grain size distributions, with all the others displaying bimodal distributions. The ash units in the distal environment typically range from 0 to 4 phi and are well sorted (1.6-2.5 phi). They show slight polymodal distributions and this could be due to the reworked nature of these deposits. In the medial environment grain size typically ranges from -3 to 1 phi (mean -2.5 - -1 phi) and is well sorted (0.9 – 1.05 phi) and typically displays a normal, bimodal distribution.

3.3 Componentry

Hand specimen componentry was conducted on the majority of sieved bulk samples collected in the field. The aim of this was to characterise various field units and determine the average componentry of major facies described in chapter 2. Componentry analysis was carried out on all size fractions above -3.5 phi, however where samples were predominantly lapilli, samples down to -3 phi were taken. This componentry analysis was undertaken in conjunction with density and vesicularity analysis, thus only samples/clasts chosen for density analysis were analysed for detailed componentry. The material was separated into groups of similar texture/lithology (Fig. 3.4) and described, weighed and recorded (see Appendix C). The five main clast types identified are:

- Type 1 – scoria, black or reddish brown, moderately to highly vesicular
- Type 2 - black scoria with small mingled amounts of yellow brown pumice bands, moderate to highly vesicular
- Type 3 – clasts with intense mingling, containing near equal amounts of black scoria and yellow brown pumice, moderately to highly vesicular
- Type 4 – pumice, yellow brown, moderately vesicular
- Type 5 – a) wall rock lithics, dense, angular, dark grey to black and b) xenoliths, white sugary quartz with outside orange staining.

3.3.1 Results and Discussion

Figures 3.5, 3.6 and 3.7 show the componentry of proximal samples AG25, AG26 and AG27 respectively in the five to seven coarsest grain size fractions. These samples are from successive units at site 25 (AG25 at the bottom, AG27, and AG26 at the top) and used to characterise the stratigraphic variation in componentry. The average distribution of the combined fractions tends to approximate that of individual size fractions, except for the coarsest fraction. The size fractions in the -4 phi to -3 phi range tend to show the average range of componentry found in each sample.

This relationship is consistent with all samples which were analysed and therefore a weight percent average of all the size fractions analysed is used to compare samples. Componentry details are included in Appendix C. From this averaged componentry data it is then possible to give average componentry descriptions for several main facies types (Fig. 3.8), described in chapter 2.

Fig 3.4

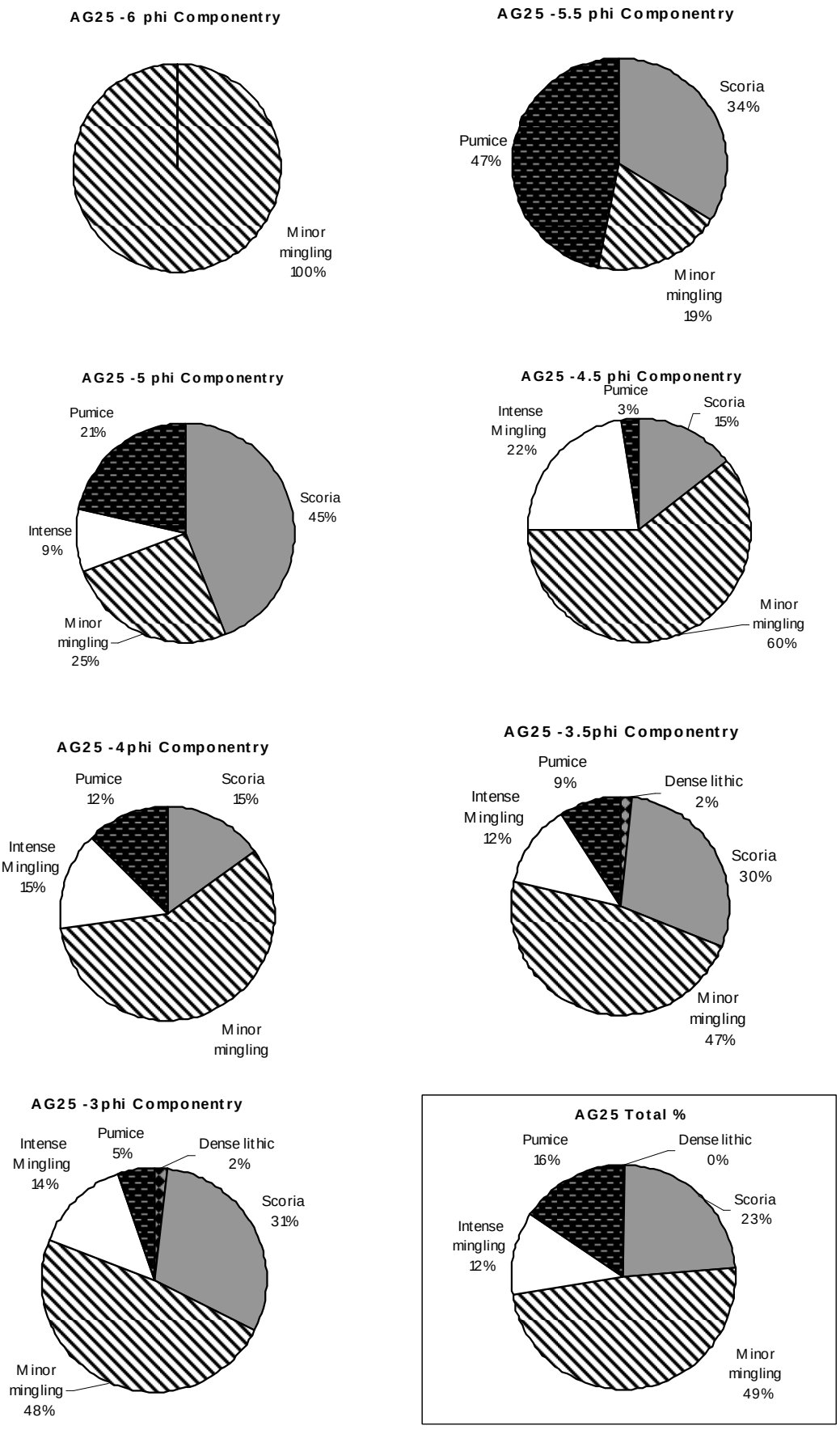

Figure 3.5: *Componentry data for sample AG25 for the seven coarsest size fractions. Total % (in box) appears to approximate those size fractions.*

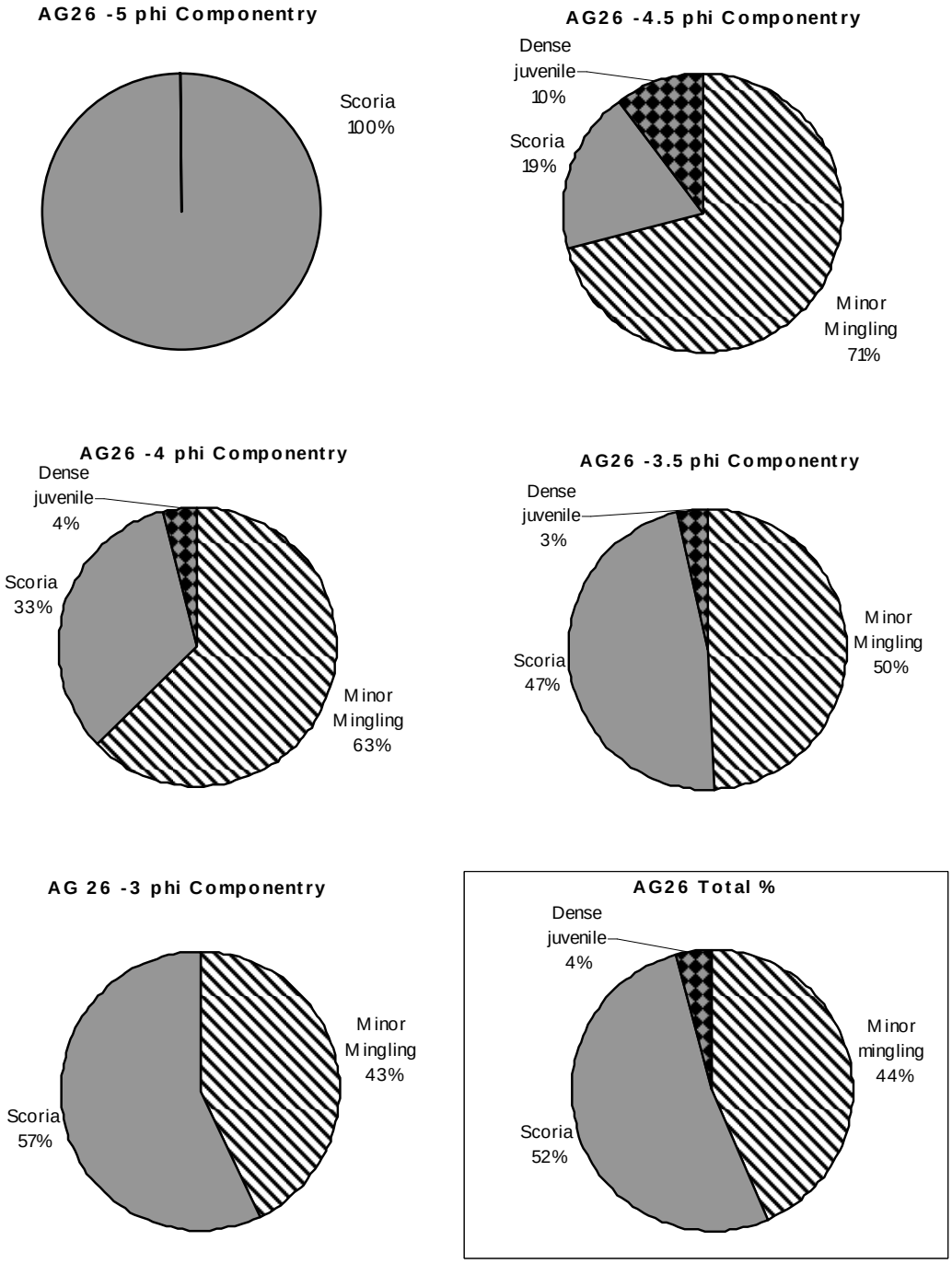

Figure 3.6: *Componentry data for AG26 for the five coarsest size fractions. Total % (in box) appears to approximate those size fractions.*

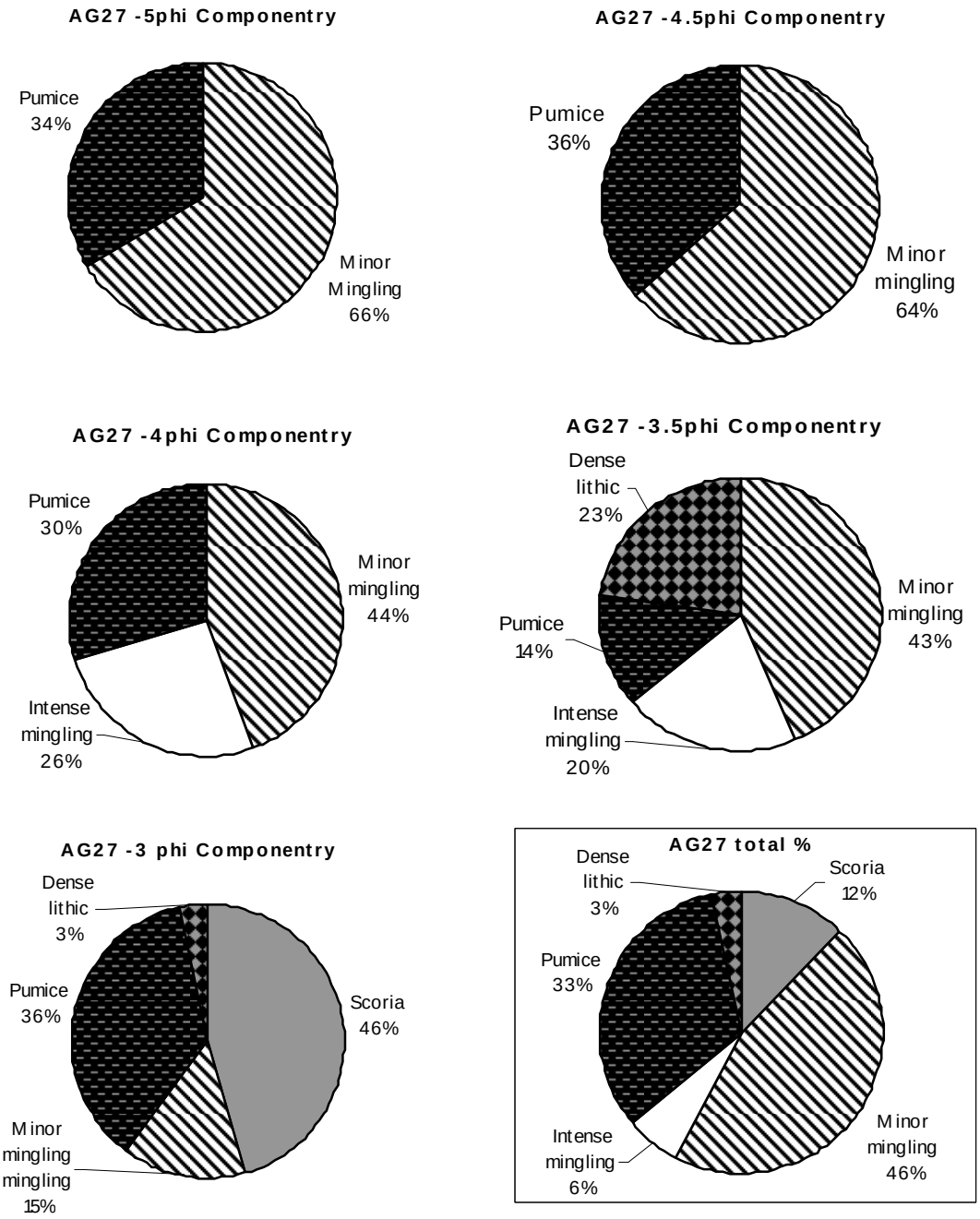

Figure 3.7: *Componentry data for AG27 for the five coarsest size fractions. Total % (in box) appears to approximate those size fractions.*

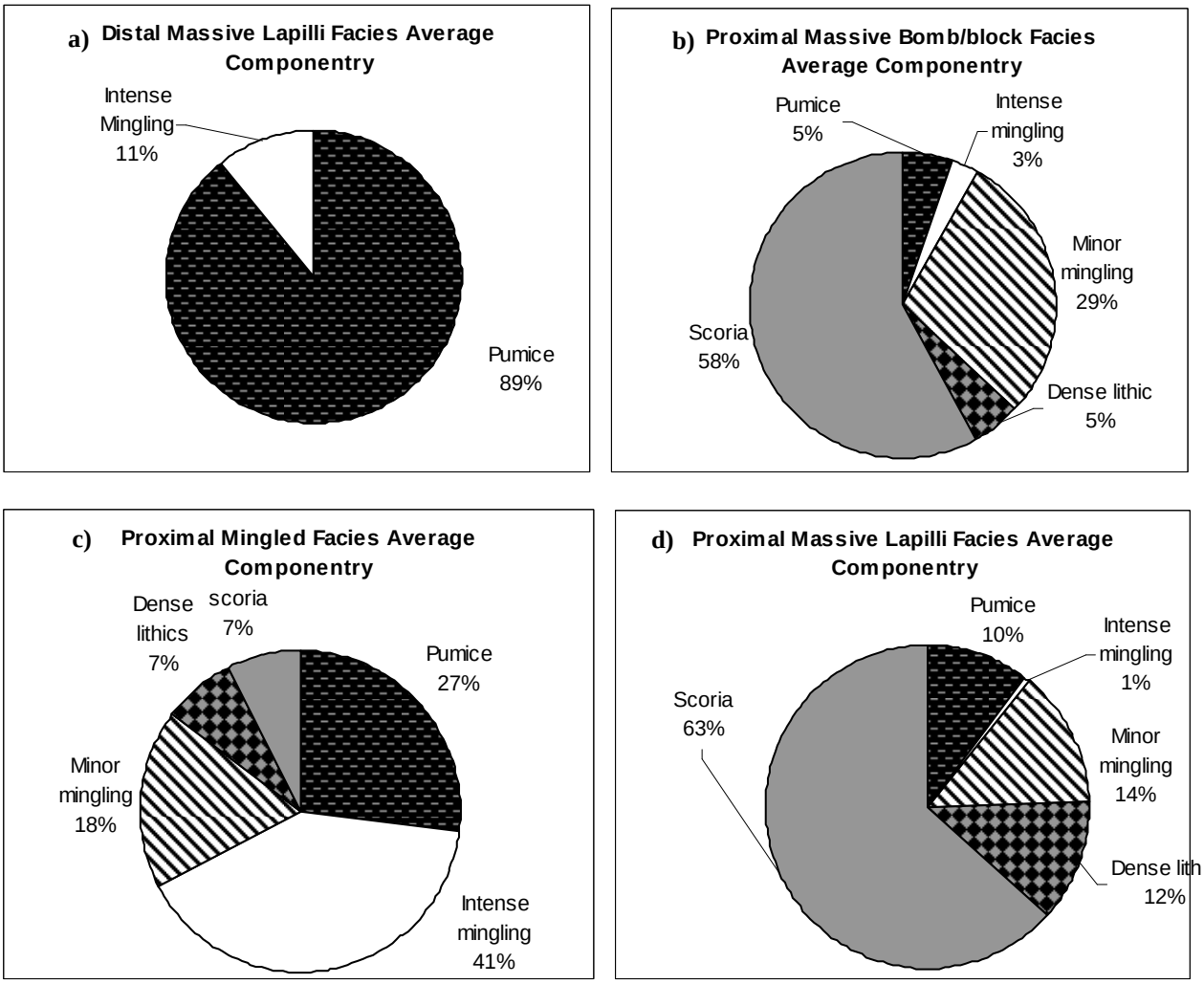

Figure 3.8: *Componentry of main facies seen on North Crater. Data are compiled from averaged totals of units within each facies.*

Proximal massive bomb/block facies assemblage

The massive bomb/block deposits are dominated by juvenile scoriaceous material. The average componentry of this facies is show in Fig. 3.8b with Type 1 clasts making up 58% of the average sample by weight, with lesser amounts of Type 2, Type 4, and Type 5 clasts also making up a significant portion of the facies. Type 5 clasts are predominantly wall rock lithics (Type 5a), with trace amounts of quartzofeldspathic metasedimentary xenoliths (Type 5b). The metasedimentary fragments represent basement rock brought to the surface by the rising magma column. Similar fragments have been found at other Tongariro and Ngauruhoe sites (e.g. Graham *et al.* 1988, Hobden 1997). There are also a small proportion of

intensely mingled clasts found in one sample which may record erosion of underlying beds during transportation and emplacement of this unit, or reflect clast recycling in the vent (Houghton and Smith 1993). The proximal graded bomb/block facies average assemblage is very similar to this facies assemblage, thus is not given a separate description in this chapter.

Proximal massive lapilli facies assemblage

The massive lapilli deposits analysed are dominated by juvenile scoriaceous and pumiceous material. The average componentry of this facies is shown in Fig. 3.8d with Type 1 clasts making up 63% of the average sample by weight. Type 2, Type 4 and Type 5 clasts also make up significant proportions of the facies. An insignificant amount of Type 3 (1%) material is found in one sample, possibly entrained by the same mechanism described in the previous section. The dense lithics (Type 5) found in this facies are similar to those described in the previous section, with both dense wall rock lithics and quartzofeldspathic metasedimentary xenoliths identified. The proximal graded lapilli facies average assemblage is very similar to this facies assemblage, and is not separately described.

Proximal mingled lapilli and bomb/block facies assemblage

The mingled deposits are dominated by juvenile mingled pumiceous and scoriaceous material. The average componentry of this facies is shown in Fig. 3.8c with Type 3 clasts making up 41% of the average sample by weight. Also making up significant proportions of the average assemblage are Type 3 (27%) and Type 2 (18%) clasts, with lesser amounts of Type 1 and Type 5 material. From individual samples the mingled lapilli and bomb/block facies can be defined as having more than 15% Type 3 and a significant proportion of Type 2 clasts. Type 5 clasts consist solely of dense wall rock lithics.

Distal massive lapilli facies assemblage

The distal lapilli deposits analysed are dominated by pumiceous juvenile material. The average componentry for this facies is shown in Fig. 3.8a, with Type 4 clasts making up 89% of the average sample by weight. Type 3 clasts are also found in one unit, but not in sufficient amounts to define the unit as a mingled facies variant. This facies contains no Type 5 clasts, as at a distance of <6 km from the vent we would assume dense wall rock lithics have already fallen from the plume.

This facies contains no scoriaceous material in the lapilli fraction (present in small amounts in the matrix ash) suggesting these units may have formed from fallout of a buoyant sub-plinian plume. Denser scoriaceous material (compared to the pumice lapilli, Table 3.1) may not have been entrained into the high buoyant plume and has been dispersed on a different trajectory compared to the pumiceous component.

3.4 Vesicularity and Density

A selection of clasts from proximal and distal localities were measured for density and vesicularity to assess the vesiculation state of the magma during the eruption. Dry magmatic eruptions (driven by exsolution of magmatic gas) typically yield clasts of vesicularity 70-80% regardless of magma viscosity (Francis 1993). Clast vesicularity can also indicate if external water was an important factor in the eruption mechanism.

3.4.1 Methods

Density and vesicularity measurements were obtained from juvenile clasts using the wax coating method developed by Houghton *et al.* (1988). Clasts were taken from the -5.0 to -3.0 phi fractions for most samples, although with some lapilli samples from distal sites clasts from the -2 to -3.5 phi had to be analysed for lack of larger fractions. Each clast was oven dried, weighed, coated in a known volume of wax paper and weighed again immersed in water. When the density of a clast was less than 1, the clast floated and was weighed down with a lead ballast. The density of each clast was calculated using equation 3.3 below.

$$Density = \frac{weight\ in\ air}{wt\ in\ air - \left(wt\ in\ water - ballast\ wt + \left(0.02\ x\ no.\ wax\ sheets\right)\right)} \quad \text{Eqn. 3.3}$$

Vesicularity of clasts was calculated (equation 3.4) using a Dense Rock Equivalent (DRE) of 2.6 g cm^{-3}, typical of most andesitic rocks (Houghton *et al.* 1988).

$$\text{Vesicularity} = 1 - (\text{density} / \text{DRE}) \times 100 \quad \text{Eqn. 3.4}$$

3.4.2 Results and Discussion

Full results for density and vesicularity analysis are given in Appendix C. The important results, trends and relationships of these data are discussed in this section.

Table 3.1: *Minimum, maximum and mean density and vesicularity values for the five main clast types identified in section 3.3. Density values given in g cm^{-3}, vesicularity values given as a percentage. Mean values are an average of the mean values for that clast type in each sample.*

	Minimum Density	Maximum Density	Mean Density	Mean Vesicularity	Minimum Vesicularity	Maximum Vesicularity
Type 1 - Scoria	0.06	2.43	1.12	56.7	6.6	80.9
Type 2 - Minor Mingling	0.61	1.56	1.00	61.6	39.9	76.4
Type 3 - Intense Mingling	0.65	1.42	0.89	65.8	45.2	74.9
Type 4 - Pumice	0.38	2.51	0.93	64.0	3.4	85.4
Type 5a –Lithics	2.08	2.59	2.42	6.9	0.3	20.1

There is a wide range of density and vesicularity values in proximal and distal environments at North Crater (Table 3.1). Results show that Type 4 clasts have the largest vesicularity range (3.4 - 85.4%) but have one of the highest mean vesicularites (64%) of all the clast types. Type 3 clasts have the smallest vesicularity range (45.2 - 74.9%), and the highest mean vesicularity (65.8%) of all the clast types. We would expect Type 5a clasts to have the lowest range and mean vesicularity. Although the maximum vesicularity (20.1%) is unexpected for a dense lithic and it is possible some dense juveniles may have been mistaken for wall rock lithics. The mean vesicularity of Type 5a clasts (6.9%) may be a better representation of the typical wall rock population. The degree of mingling is also reflected in the vesicularity of a clast. Type 3 clasts have a higher mean vesicularity (65.8%) than Type 2 clasts (61.6%), indicating the more a clast is mingled with pumiceous magma the higher the vesicularity. Type 1 clasts have the lowest mean vesicularity (56.7%). Clasts of Type 1 and Type 4 also display relatively high density (2.2 - 2.5 g cm^{-3}) and low vesicularity (3.4 - 15.4%); this indicates dense juvenile clasts are also present in North Crater deposits.

Whole-Unit In-Situ Density

The density of depositional facies types reflects the density and vesicularity of constituent clasts as well as the concentration and compaction of clasts within the deposit. Facies which are dominated by Type 1 and Type 2 clasts, (typically the non to poorly welded, massive and graded bomb/block facies) will have the lowest mean vesicularity (56.7 - 61.6%) and highest mean density (1.0 - 1.12 g cm^{-3}). Facies which are dominated by Type 2, Type 3 and Type 4, (typically the non-welded, mingled massive bomb/block and lapilli and massive or graded lapilli facies) will have a moderate mean vesicularity (61.6 - 65.8%) and density (0.89 - 1.0 g cm^{-3}). Those facies which are predominantly Type 4 and/or Type 3, (typically non-welded, distal massive lapilli and massive or graded lapilli) will have the highest mean vesicularity (64 - 65.8%) and lowest mean density (0.89 - 0.93 g cm^{-3}).

Table 3.2: *Mean, minimum and maximum density of the three welded facies. All density values are given in g cm^{-3}.*

	Minimum Density	Maximum Density	Mean Density
Intensely welded facies	2.22	2.60	2.47
Strongly welded facies	1.30	2.46	2.11
Moderate welded facies	1.11	2.01	1.54

Whole rock density (Table 3.2) was determined for rocks from the welded facies at selected proximal locations around the vent. By comparing visual observations and facies descriptions a relationship between the visibility of spatter clasts in each facies and the whole rock density becomes apparent. The intensely welded facies has no visible clast outlines and shows the highest mean whole rock density (2.47 g cm^{-3}) and narrow density range (2.22 - 2.6 g cm^{-3}). The high mean density of the facies could reflect rapid compaction of hot plastic spatter during emplacement. Rocks in the strongly welded facies contain some visible clast outlines, often as thin stretched out ribbons. This facies has a relatively high mean whole rock density (2.11 g cm^{-3}) with a large range (1.3-2.46 g cm^{-3}) indicating the rocks in this facies may have originated from magmas with varying gas content, and rates of emplacement and compaction were variable. The moderately welded facies contains visible clast outlines with often clast sizes (bombs) and

shapes (sub-rounded to elongated) easily distinguished by a low mean density (1.54 g cm^{-3}). The low mean density of this facies probably reflects the relatively lower intensity activity and lower rates of spatter accumulation compared to the other welded facies.

Due to the small size of clasts in many distal deposits a comprehensive analysis of density and vesicularity changes within the distal units was not obtainable. Also due to field and transportation constraints only a few samples from the medial area were collected.

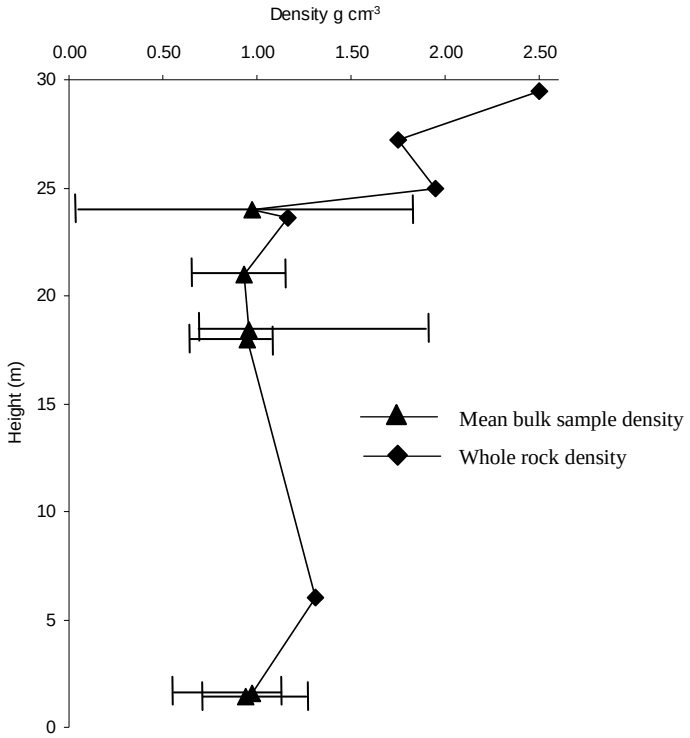

Figure 3.9: *Mean density of samples from complete North Bluff composite stratigraphy, contains both bulk sample densities and whole rock densities. Range of densities is shown for bulk samples.*

Proximal Temporal Relationships

Mean density of proximal samples varies with height up through the North Bluff composite stratigraphy (Fig. 3.9). Density is initially low but variable reflecting dominantly non-welded deposition but with fluctuations in eruption intensity or style of pyroclastic deposition. An abrupt shift is evident in the upper 5 m marking the dominance of strong welding and agglutination. A complete record of North Crater deposits (Fig. 3.16) shows the mean density and vesicularity changes

during each phase of eruptions at North Crater. It appears the final climactic phase of activity at North Crater involved magma erupted at a high intensity allowing deposition and rapid accumulation of hot plastic spatter, with the formation of predominantly strongly to intensely welded facies (Fig. 3.16).

3.5 Petrography

Petrographic analysis was carried out on selected whole rock welded pyroclastic samples as well as individual clasts selected from sieved samples. The aims of this analysis were to describe phenocryst textures and assemblages and groundmass texture of whole rock and clasts. Selection of individual clasts from bulk samples was based on vesicularity and density features as well as clast type (i.e. mingled, scoria etc). Full petrographic descriptions are given in Appendix E. Groundmass textures and vesicle morphology was carried out using the SEM (section 3.6).

3.5.1 Methods

Bulk rock and clast samples were cleaned, trimmed and cut into small blocks (~4.7 x 3.7 x 2.5 cm). Vesicular samples were dried on a hot plate overnight at ~50°C then impregnated with araldite K142 and dried again overnight at ~50°C. All samples had one side ground flat using the diamond lap wheel and #600 polish powder, then dried overnight before being mounted on frosted glass slides with Hillquist glue. Impregnated samples were cured overnight on a cool bench, while other samples were cured on the hotplate overnight at ~50°C. Samples were then trimmed to ~1mm and ground to ~30 µm using first a Struers Discoplan-TS and then #600 polish powder on a glass plate. Thin sections being used for electron microprobe and SEM analysis were then polished on the lap wheel using #800 polish paper and finally cloth with fine alumina powder. Sections not being used for microprobe or SEM were sealed with a glass coverslip.

3.5.2 Results and Discussion

The main mineral phases present in products of North Crater eruptions include plagioclase, orthopyroxene (hypersthene), clinopyroxene (augite), opaque minerals and rare olivine. The rocks also have a wide range in abundance of vesicles, lithics and groundmass textures.

Plagioclase

Plagioclase (13-35% modal abundance) is typically subhedral, displaying a range of shapes including tabular, lath and lozenge ranging typically from 0.8 to 2 mm, but up to 2.8 mm. These crystals display a wide range of textures with the majority showing some degree of disequilibrium sieve, resorption or dissolution textures. Sieve textures show a wide variety and examples include small round sieves concentrated in the centre, or in a ring at some distance from the edge (Fig. 3.10g). Some also have long needle like sieves or irregular large sieves concentrated in the centre. A small number of crystals display intense sieve coverage. Some crystals also display normal or reverse zoning, or oscillatory zoning, and often crystals will display a combination of zoning and sieve textures. Some phenocrysts are poikilitic with inclusions of opaque minerals, pyroxenes and glass. Crystals occur predominantly as discrete grains, but are often seen on clumps of 2-3 or in glomeroporphyritic groups with other mineral phases pyroxene and opaques.

Clinopyroxene and Orthopyroxene

Both of these phases (5-15%) are typically subhedral, rarely euhedral and anhedral, with shapes ranging from prismatic, tabular, lath to irregular. They are typically smaller than plagioclase crystals (0.4 to 0.9 mm, max 1.5 mm), although some orthopyroxenes occur as long tabular crystals (2-3 mm). A small number of clinopyroxene crystals are twinned (Fig. 3.10b), and many of the clino and ortho-pyroxenes occur in groups of 2-3 or in glomeroporphyritic groups (Fig. 3.10k) with other mineral phases (plagioclase and opaques). These mineral phases rarely show sieve or other disequilibrium features, as well as inclusions of opaque minerals or other pyroxenes.

Opaque Minerals

Opaque minerals (1-5%) are typically euhedral, rarely anhedral, and occur as sub-rounded to cubic crystals, or irregular skeletal growths in glomeroporphyritic clumps. They range in size from 0.1 to 0.5 mm, with some irregular shapes being up to 1 mm. Under reflected light the phases present include ilmenite (15-25%), titanomagnetite (65-70%), titanomagnetite with ilmenite exsolution lamellae (5-10%), and rare inclusions of pyrrhotite and chalcopyrite.

Fig 3.10

Olivine

Olivine is rare (c. 1%) in North Crater deposits, occurring as irregular, anhedral crystals, 0.8-1 mm, and were always ringed by fine-grained augite crystals (Fig. 3.10h) indicating disequilibrium with the enclosing magma.

Xenoliths and Lithics

Xenoliths (1-15% xenolith and lithic modal abundance) occur in the majority of thin sections. They are typically sub-rounded to elongate quartzofeldspathic metasedimentary xenoliths and range in size from 1 to 4 mm and are extremely fine-grained (<0.1 mm) (Fig. 3.10i). Quartz xenoliths contain quartz, plagioclase and often opaque minerals. The source of these quartzofeldspathic xenoliths is most likely the basement greywacke directly below the TgVC (Graham *et al.* 1988, Hobden 1997). Rarely these xenoliths have minor sieve textures where crystals may have been out of equilibrium with the melt. Fine-grained pyroxene xenocrysts are also found in a few thin sections. These are finer grained than the augite glomeroporphyritic clumps and may originate from a deeper magma source, and may represent olivine crystals which have completely reacted to clinopyroxene. Wallrock lithics derived from the volcanic structure occur within sections of welded pyroclasts. They are identified by their high density and sharp boundaries with the surrounding groundmass (Fig. 3.10j). Wallrock lithics are of andesitic composition and contain phenocrysts previously described, but have a fresh glass groundmass compared to the partially devitrified host groundmass.

Groundmass

A wide range of groundmass (22-50% modal abundance) types were seen throughout the North Crater deposits (Figs. 3.10 & 3.11). The textures ranged from hyalopilitic and intersertal to intergranular, and those which were intergranular were trachytic with minor areas being felted with mottled microlites. The hyalopilitic and intersertal textures ranged from fresh glass, partially/strongly devitrified glass, to completely devitrified glass. Often microlites show a sub-parallel alignment around phenocrysts, suggesting flowage and late-stage deformation. Microlites were predominantly of plagioclase, pyroxene and opaque minerals. Some groundmass plagioclase display rapid quenching features such as swallow-tail terminations.

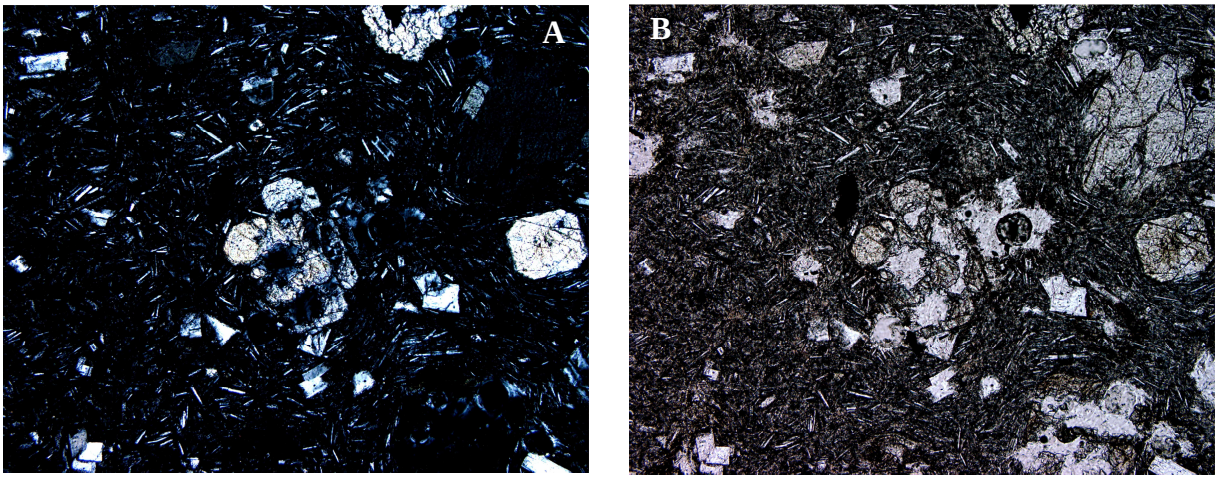

Figure 3.11: *Groundmass glass seen in a) crossed polarised light and b) plain-polarised, for whole rock sample AG03.*

A small number of welded bulk rock thin sections appear to have clast outlines distinguished as different coloured glass under the microscope (Fig. 3.10a, d, l). These are thought to be from accumulation and extreme plastic deformation of hot agglutinate. Clast outlines are irregular and thin or stretched out, and often are more devitrified than the surrounding groundmass. Some display sharp to slightly mingled boundaries and are often a darker colour compared with the surrounding groundmass. Where crystals are present they display similar features to the phenocrysts described previously.

Banded or mingled clasts (Fig. 3.10e) appear to have no differences in fresh glass other than colour at 20x magnification, but have been further analysed under the SEM to determine the basis for differences between glass colourings.

3.6 Scanning Electron Microscope (SEM) Analysis

SEM analysis was carried out on ash and matrix material of the 1 or 1.5 phi fraction from selected samples using a Hitachi S-4100 Field Emission Scanning Electron Microscope. Analysis was also carried out on polished thin sections to produce images of clast/rock groundmass and microlite textures within the glass. Rock and clast vesicle morphology analysis was also undertaken using binary images produced from original SEM images.

Fig 3.12

3.6.1 Ash Clast Morphology

A range of ash morphologies can be distinguished in samples from selected proximal, medial and distal localities (Fig. 3.12) (see Fig. 2.1 for site locations and Appendix B for sampled units in stratigraphic columns). Ash matrix, taken from non-welded units at proximal and distal sites, show a range of morphological features which can be broadly classified as group 1: moderate to highly vesicular, delicate bubble wall ash; group 2: poorly vesicular, sub-rounded ash; or group 3: blocky to prismatic or angular crystals with adhesions of vesicular glass.

Group 1 is found in samples AG26, AG25, AG27, AG69, AG71, AG52 and AG67 (Fig. 3.12). This group of ash generally represents ash that has been deposited from a pyroclastic fall as they have sharp and delicate edges which have suffered little abrasive action and are angular to sub-angular (Heiken and Wohletz 1985). The moderate to highly vesicular nature of these clasts infers they were produced from magma which was actively vesiculating (Heiken and Wohletz 1985). Vesicles range from long stretched tubes, to elongated and ovoid shapes, with often many different shapes seen in the same clast. The shapes of the clasts reflect the nature of the vesicles, i.e. elongate parallel vesicles form elongate, sub-angular ash clasts. In some units mixed populations of highly vesicular and poorly vesicular delicate ash occur together, suggesting fragmentation of slower moving, partially crystallised, degassed magma from the conduit walls along with the more gas-rich, less crystalline magma near the conduit axis (Sable *et al.* 2006). This group of ash is associated with the proximal massive bomb/block and lapilli facies.

Group 2 is found in samples AG28, AG34, AG42 and AG70 (Fig. 3.12). This group of ash generally represents ash that has been deposited by a pyroclastic flow as they have high degrees of edge modification, display very few delicate glass structures and are rounded and chipped indicating abrasion during lateral transport (Heiken and Wohletz 1985). The poorly vesicular nature of these ash clasts indicates they were produced either from magma which had partially degassed prior to eruption, or have undergone post fragmentation bubble collapse (Sable *et al.* 2006). This group of ash is associated with the proximal graded

bomb/block and lapilli facies. It is important to note here that sample AG34 (Fig. 3.12e) is a fine black ash from the Rotoaira Lapilli unit, however it shows strong rounding and edge modification suggesting it has been deposited by lateral transport (Heiken and Wohletz 1985).

Group 3 is found in samples AG27, AG34 and AG69 (Fig. 3.12), and represents free crystals, dense juvenile or wall rock lithics found in ash beds or matrix. Some of these show vesicular areas where glass has adhered to them during eruption (Fig. 3.12, group 3). The identification of individual crystals in the matrix and ash indicates the eruption was sufficiently intense to separate crystals from the magma at fragmentation, or is associated with emplacement processes.

3.6.2 Juvenile Clast and Whole Rock Vesicle Morphology

Images were taken of polished thin sections at high magnification under the SEM in order to characterise vesicle morphology from welded whole rock and individual juvenile clast samples from several of the main facies.

Whole rock thin sections of welded facies displayed very few vesicles and were typically irregular, elongate shapes (Fig. 3.13c). At higher magnification these vesicles have irregular walls bounded by randomly orientated microlites and vesicle spaces (Fig. 3.13d). Vesicles in these welded facies typically occur in small groups, and rarely as individual vesicles.

Vesicles in pyroclastic clasts with moderate to highly vesicular textures show a range of vesicle shapes. The majority of vesicles show irregular shapes indicating bubble coalescence, as the majority of bubbles are deformed with some ruptured walls (Gurioli *et al.* 2005). Clasts with high vesicularity (c. 80%) typically display larger (500-750 µm) more complex and contorted vesicle shapes with a few smooth, spherical vesicles distributed between (Fig. 3.13e,f). Clasts with lower vesicularity (64-67%) typically display medium (50-80 µm) to small (15-30 µm) vesicles with smoother elongate to ovoid shapes in a denser packing arrangement (Fig. 3.13g,h,i). The change from lowest to highest vesicularity may be accomplished principally by an increase in the abundance and size of the largest vesicles (Gurioli *et al.* 2005). Complex vesiculation histories are important and

Fig. 3.13

suggested in North Crater samples by the interactions between bubbles, with complex shapes resulting from bubble coalescence, deformation and minor collapse. Large vesicles in the North Crater samples also suggest significant vesiculation time to allow growth and maturation of the bubble population (Gurioli *et al.* 2005). Stretched and elongate vesicle shapes are identified in clasts of lower vesicularity (Fig 3.13a, b), and are interpreted to result from extensional shear at the conduit margins. Bubble size and strain rate also control the degree to which bubbles are elongated in the conduit (Klug and Cashman 1996).

Vesicle distribution in intensely mingled clasts varies from vesicle distribution in end member scoria and pumice clasts. The presence of microlites in the 'dark' glass of mingled clasts limits bubble expansion and coalescence. Thus, clasts with mingled dark (microlite-bearing) and light (microlite-free) glass of similar composition (discussed in chapter 4) have varying vesicle densities in a single clast and result in varying clast densities in a single unit (Klug and Cashman 1996).

3.6.3 Groundmass and Microlite Textures

The various clast types identified in componentry analysis have been analysed using polished thin sections under the SEM to characterise the range of groundmass types and microlite textures identified in petrographic analysis.

Microlites in samples from North Crater display the mineral phases previously identified in petrographic analysis and include plagioclase + orthopyroxene + clinopyroxene + titanomagnetite + ilmenite (+ glass). Type 1 clasts analysed by SEM display little to no microlite textures (Fig. 3.14a), and tend to be fresh glass (non-devitrified). Where rare microlites are present in these clasts they occur as individual plagioclase laths of ~ 2 µm. Type 2 and 3 clasts are discussed in the following section (Mingled Clasts). Type 4 clasts show a small degree of microlite abundance (Fig. 3.14b). The microlites range in size from 2-4 µm and form single crystals, with plagioclase morphologies typically tabular to acicular with very few skeletal, hopper and swale shapes. Pyroxene crystals are typically tabular to lath 2-3 µm, and Fe-Ti oxides are typically cubic and <2 µm. The

Fig 3.14

microlite density is low in group 4 clasts with some areas being microlite free. Microlites show random orientation over the cm scale

Mingled Clasts Groundmass

One of the aims of SEM analysis was to determine the nature of any physical differences between the light and dark glass seen in mingled clasts. Several clast samples were selected from Type 2 and 3 samples which displayed minor to intense mingling between light and dark glass. Areas of light and dark glass were mapped out on the glass slide in order to determine areas of different colouring once viewed under the SEM. These selected samples were also used later in glass geochemistry and microprobe analysis (chapter 4) to determine the nature of any chemical differences between the light and dark glass in a single clast.

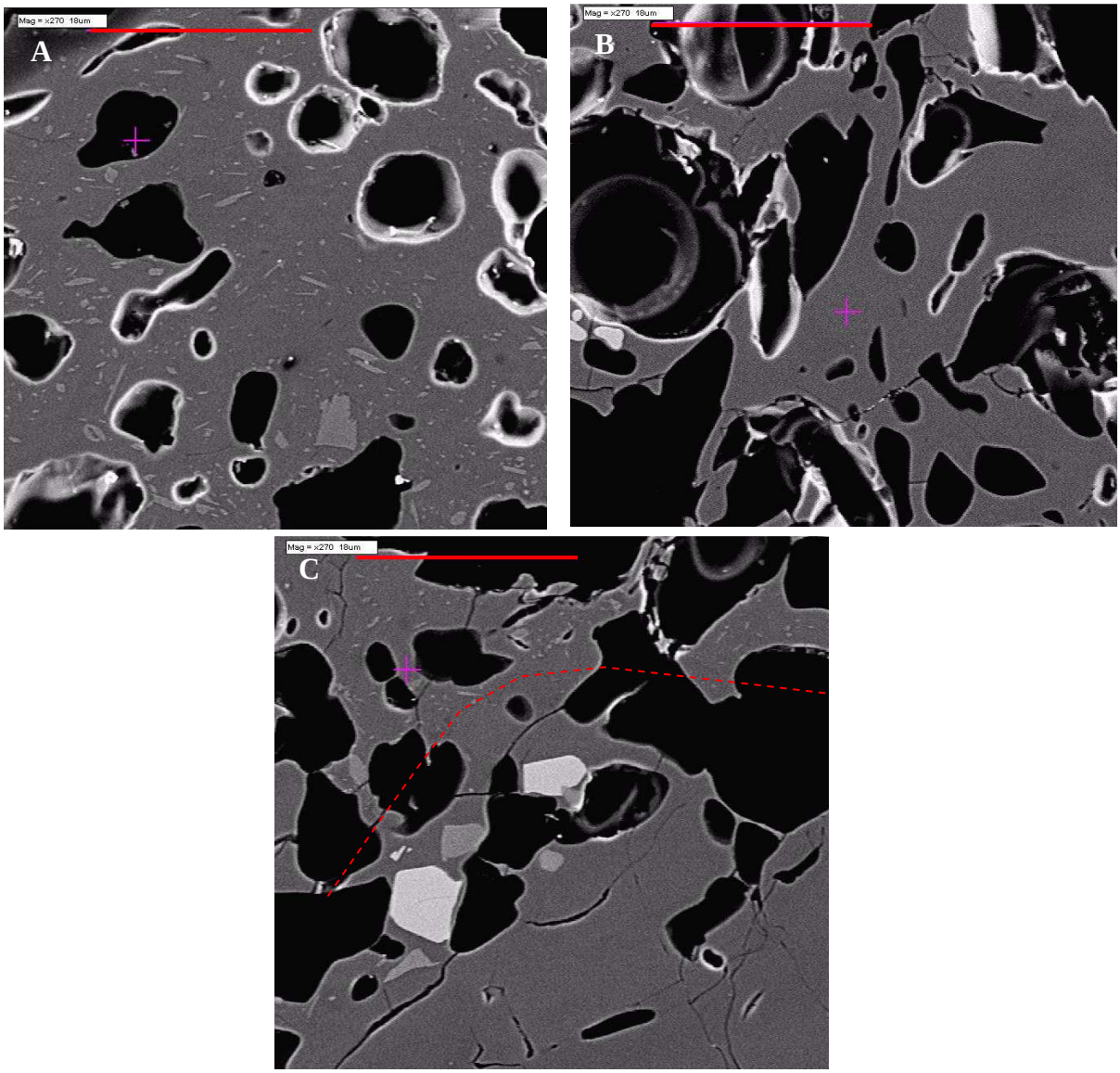

***Figure 3.15*:** *SEM images of glass seen in mingled clast AG25. a) dark glass showing microlites, b) light glass free of microlites, c) area where boundary (red dashed line) between microlite-free 'light' and microlite-bearing ' dark' glass can be seen. Red scale bar 18 µm and photos taken at 270x magnification.*

Images of polished thin sections revealed interesting physical features in the glass of mingled clasts (Fig. 3.15). 'Dark' glass textures display fine microlites in moderate abundance of predominantly plagioclase and pyroxenes (Fig. 3.15a), while 'light' glass is entirely microlite free (Fig. 3.15b). The microlites in the dark glass are predominantly plagioclase with pyroxenes and Fe-Ti oxides and have a relatively high proportion of crystals (c. 40%). Microlite morphologies include tabular, acicular, lath and cubic to rare swallow-tail, hopper and skeletal and have typical size range of 2-5 µm. In greyscale SEM images the sharp boundary between 'dark' and 'light' glass can be seen in the microlite abundance (Fig. 3.15c). It is possible that the only difference between the glasses in mingled clasts may be physical, due to the abundance of microlites in dark glass. Geochemical analysis may determine the nature of any chemical differences (Chapter 4).

Welded Facies Groundmass

Several samples from the welded facies were analysed under the SEM to characterise the groundmass and microlite textures. All welded samples analysed showed a range of microlite abundance, with the proportion of crystals being extremely high (90-100%, Fig. 3.14c, d, e, f). The predominant mineral phase is plagioclase and morphology ranges from tabular, lath and acicular to rare swallow-tail with typical size ranges of 2-5 µm, and in some areas the plagioclase is so dispersed it appears as mottled glass. Lesser amounts of pyroxene and Fe-Ti oxides occur as crystals which are tabular, lath or cubic and typically 2-4 µm. The microlites are typically at random orientation with sub-parallel alignment seen in some areas alongside phenocrysts. One slide contained a large stretched clast inclusion with a partially melted boundary to the groundmass. The groundmass inside this clast was noticeably coarser (5-8 µm) than the surrounding groundmass (2-4 µm) and all microlites are displayed at a random orientation (Fig. 3.14f).

A few of the microlites in the welded units display minor swale features indicating possible pressure decrease and supercooling during crystal growth. Higher crystallinity in these welded rocks suggests rapid decompression and conditions of slow nucleation and growth (Hammer and Rutherford 2002). The sub-parallel orientation near phenocrysts might suggest crystallisation directly from the melt with orientation during emplacement, while the randomly orientated

microlites may have formed from devitrification of the remaining melt (Davies and McPhie 1996).

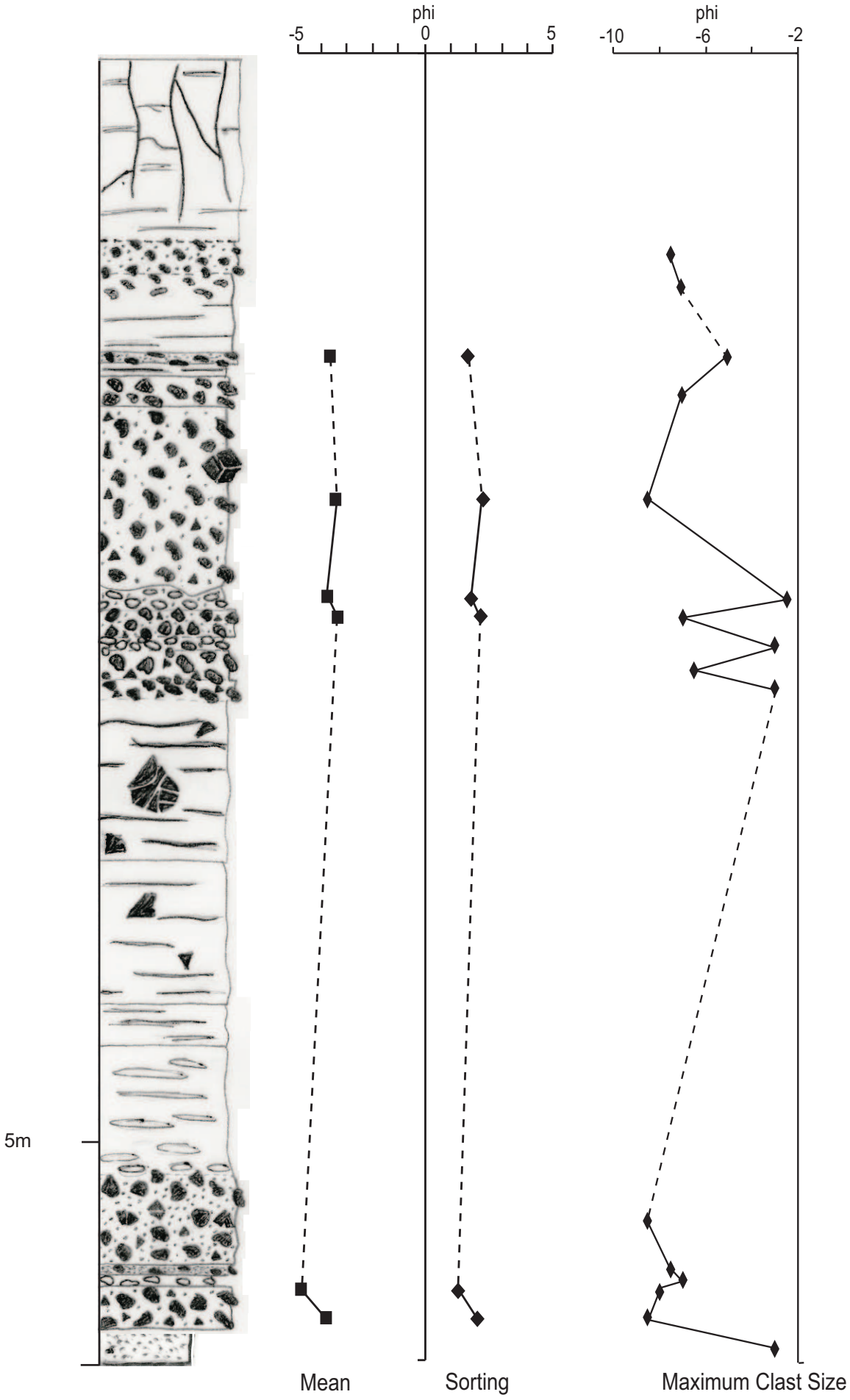

Figure 3.2: *North Bluff composite stratigraphy showing mean grainsize, sorting and maximum clast size variations.*

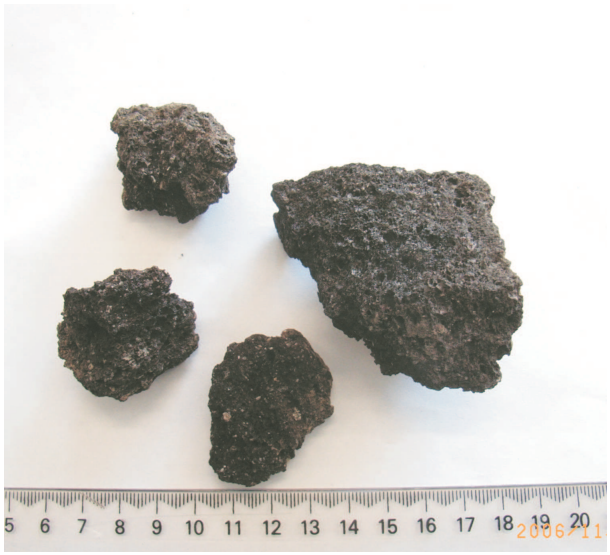

a. Type 1: scoria

b. Type 2: minor mingling

c. Type 3: intense mingling

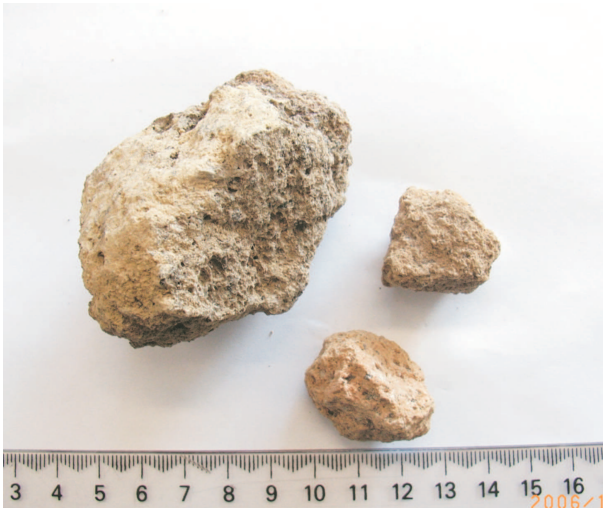

d. Type 4: pumice

e. Type 5a: dense lithic

f. Type 5b: quartz sugary xenoliths (upper 2 clasts)

Figure 3.4: *The main clast types identified in North Crater deposits from componentry analysis.* ***a****) scoria.* ***b****) minor mingling.* ***c****) intense mingling.* ***d****) pumice.* ***e****) wall rock lithics.* ***f****) quartz sugary xenolith, white scale measures 12cm.*

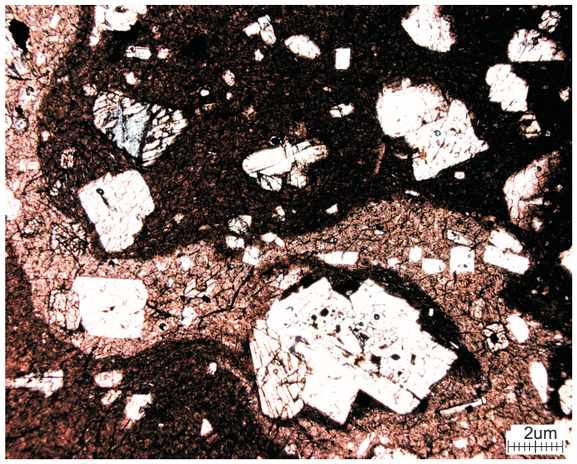

a. Dense wall rock lithic groundmass and phenocrysts, AG65.

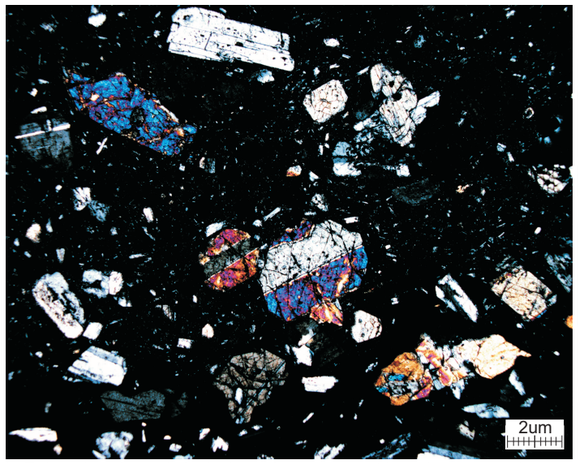

b. Twinned augite and plagioclase phenocrysts set in a glassy groundmass, AG63

c. General groundmass and phenocryst texture, AG62

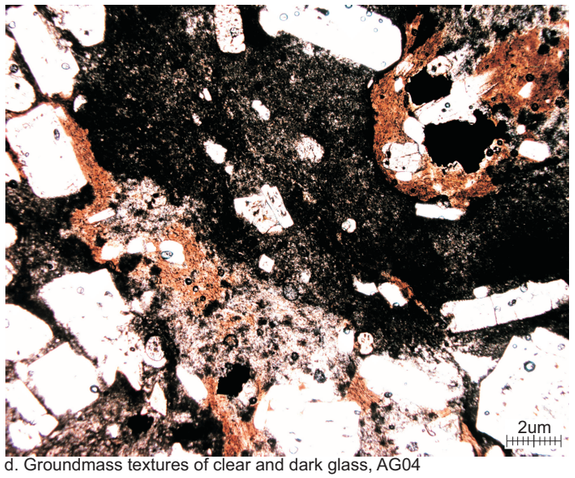

d. Groundmass textures of clear and dark glass, AG04

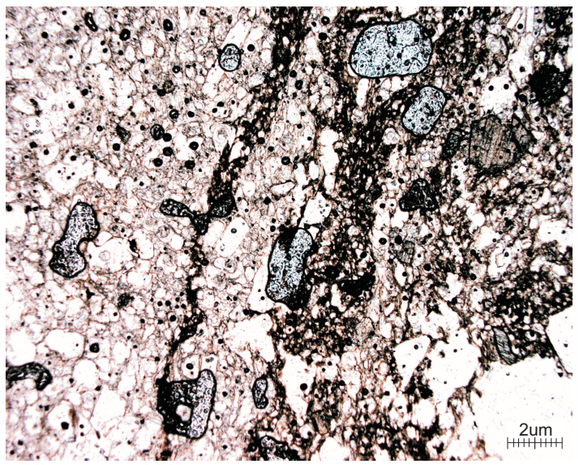

e. Mingled glass, AG29

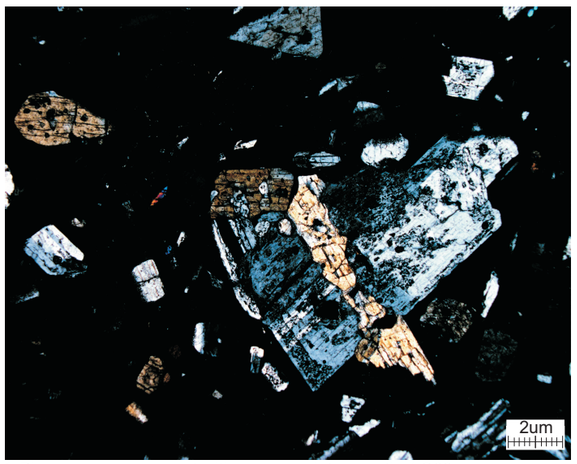

f. Plagioclase phenocryst with pyroxene intergrowth, AG62

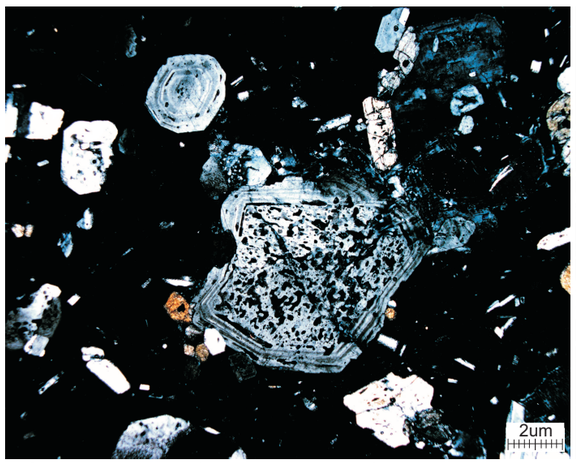

g. Plagioclase phenocrysts, upper shows oscillatory zoning, lower large one shows heavy sieve texture and osc illatory zoning, AG14

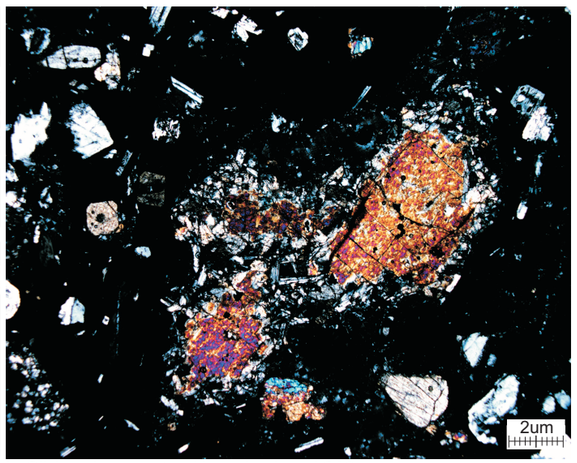

h. Olivine phenocrysts with augite rims, AG09

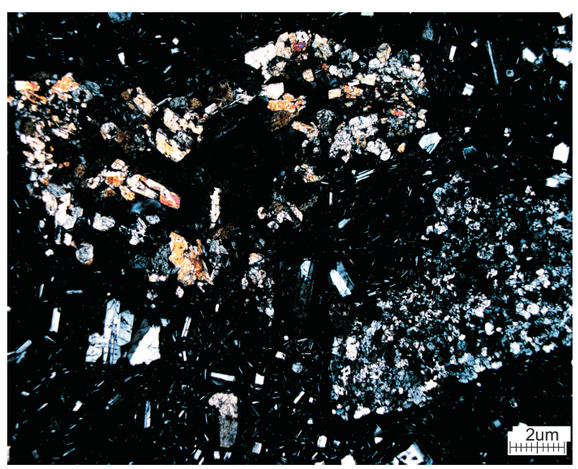

i. Xenoliths AG06

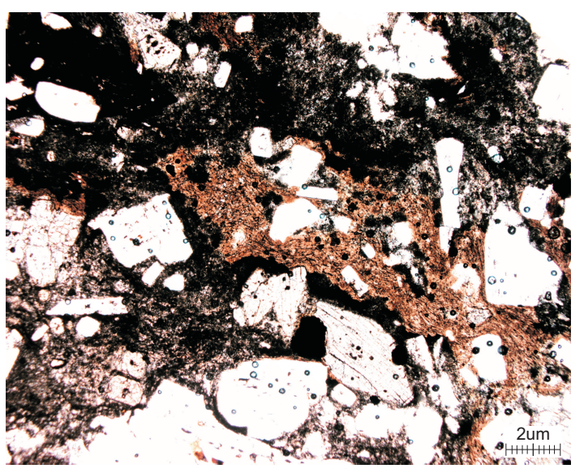

j. Lithic inclusions seen as reddish brown, AG04

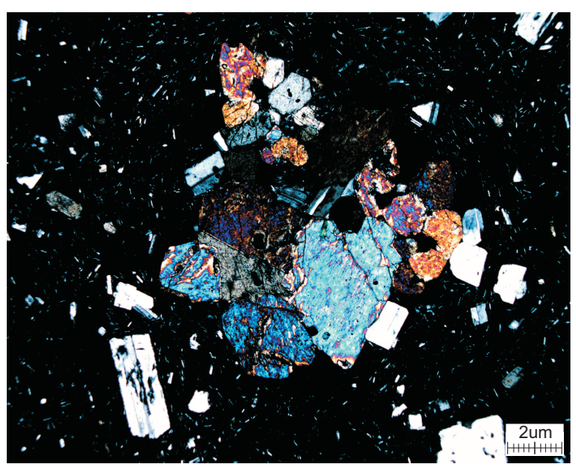

k. Glomeroporphyritic clump and groundmass texture, AG03

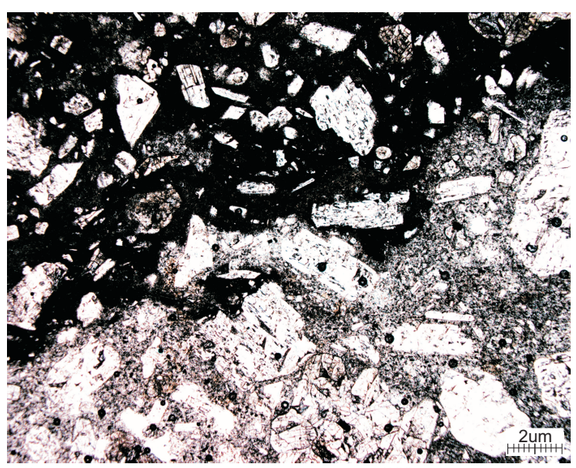

l. Groundmass textures of light and dark glass, AG63

Figure 3.10: *Photomicrographs of selected features seen in North Crater samples.*

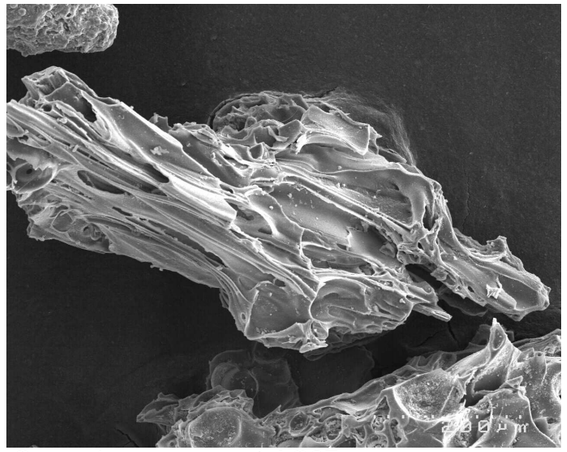

Group 1 a) AG27

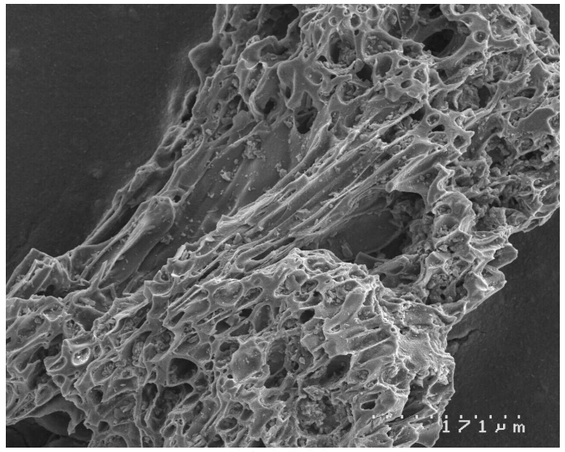

b) AG69

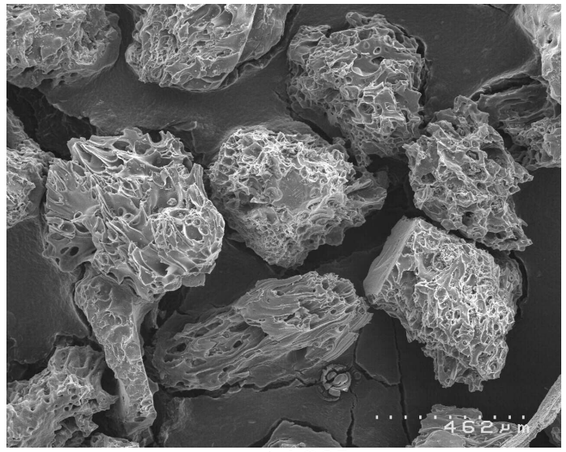

c) AG25

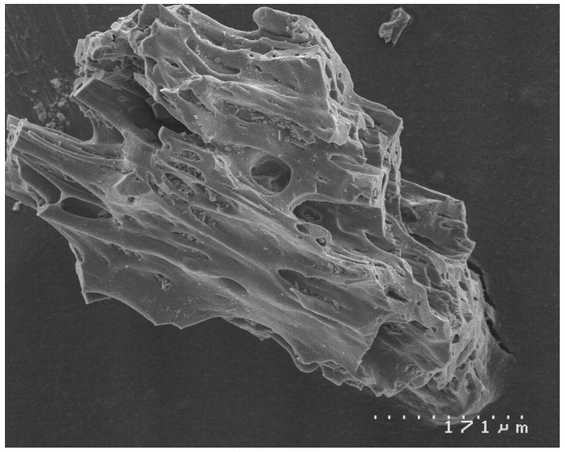

d) AG26

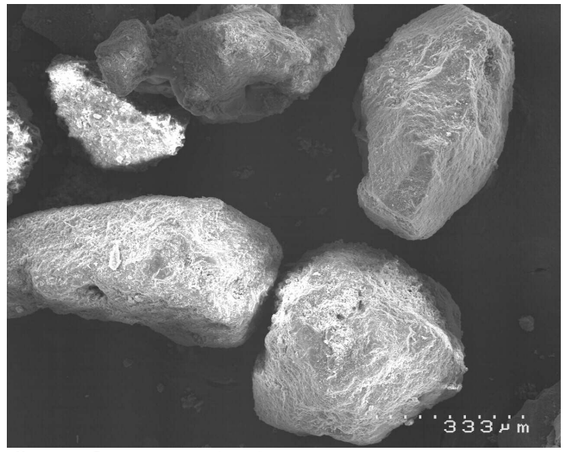

Group 2 e) AG34

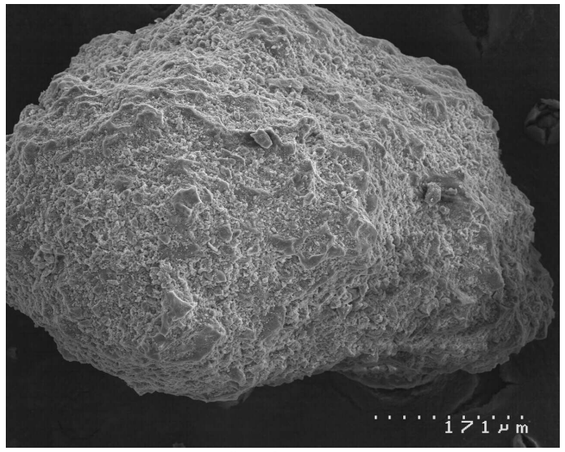

f) AG28

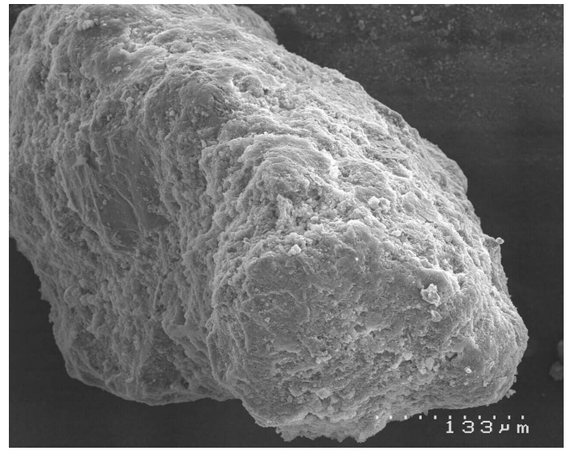

g) AG42

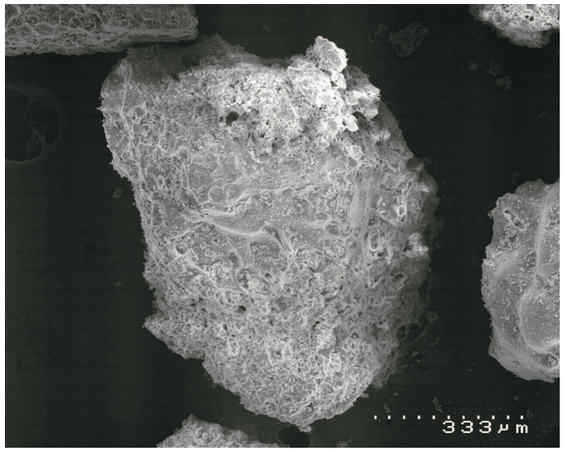

h) AG70

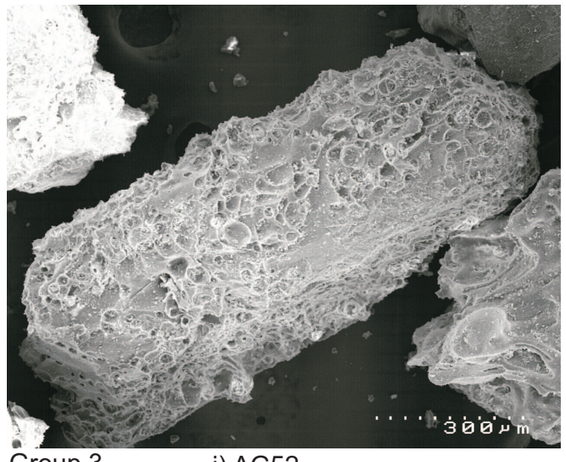

Group 3 i) AG52

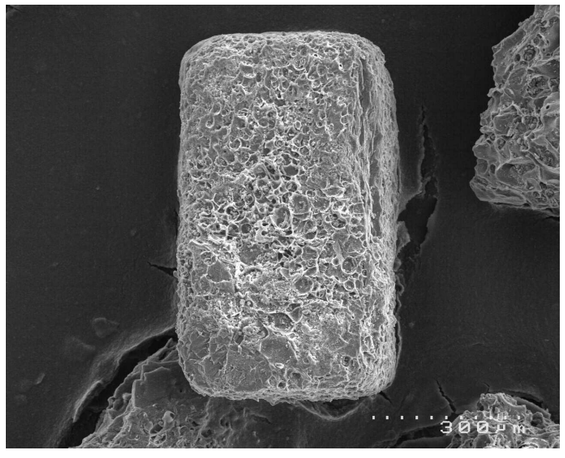

j) AG27

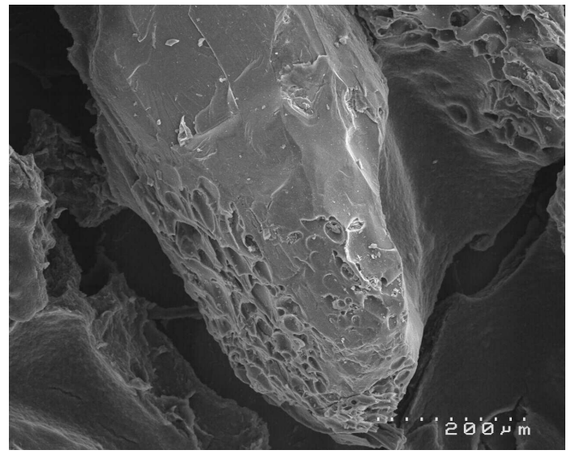

k) AG69

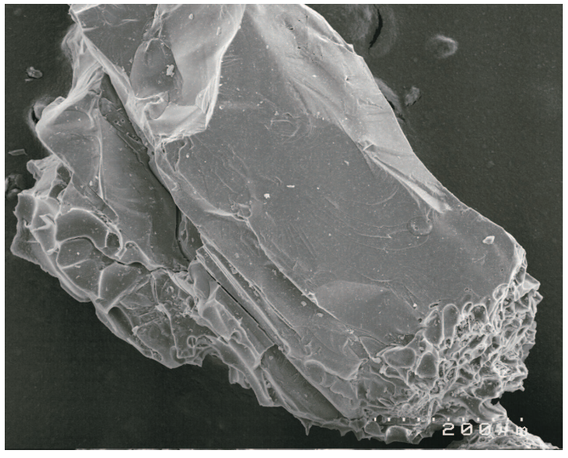

l) AG68

Figure 3.12: *SEM images of ash clasts from selected bulk samples. Group 1 (a-d) - brittle, high to moderately vesicular. Group 2 (e-h) - poorly vesicular, sub-rounded. Group 3 (i-l) - blocky, prismatic or angular.*

a. elongate vesicles AG25-12, 67% vesicularity

b. elongate vesicles AG29, 72% vesicularity

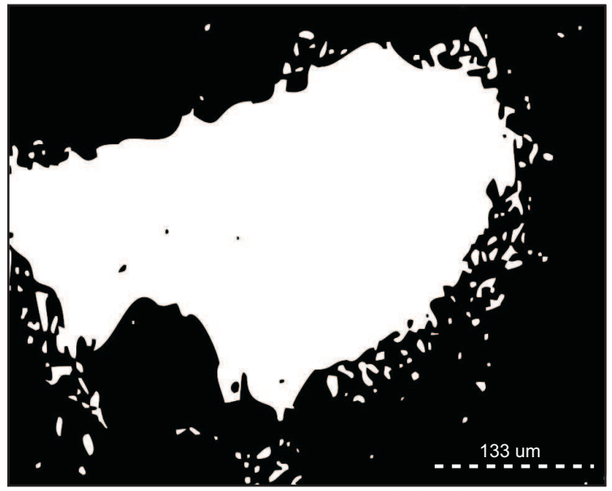

c. vesicle morphology in welded unit AG62, 4.8% vesicularity

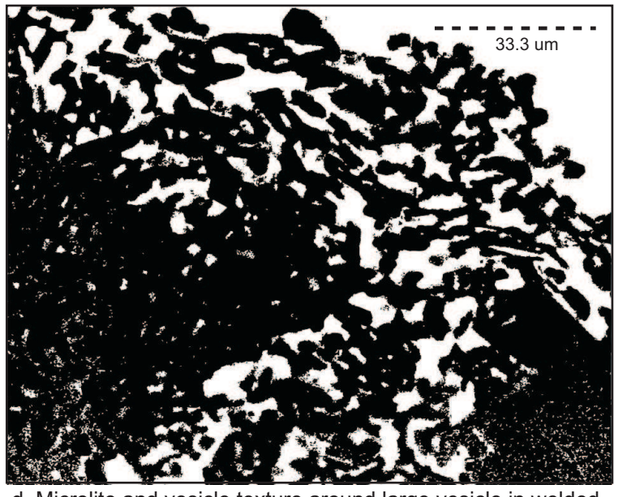

d. Microlite and vesicle texture around large vesicle in welded unit AG62, 4.8% vesicularity.

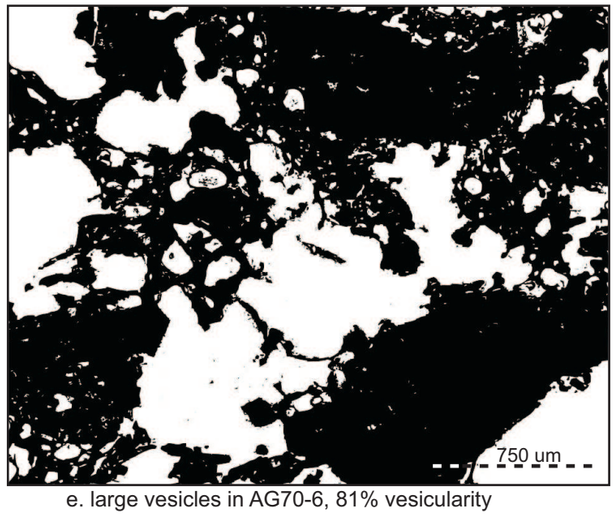

e. large vesicles in AG70-6, 81% vesicularity

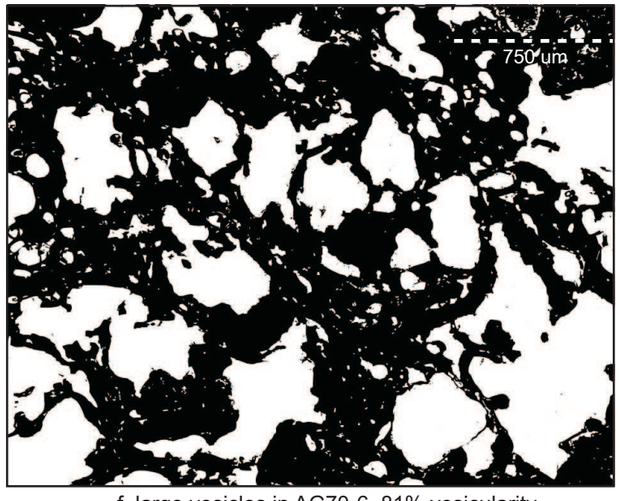

f. large vesicles in AG70-6, 81% vesicularity

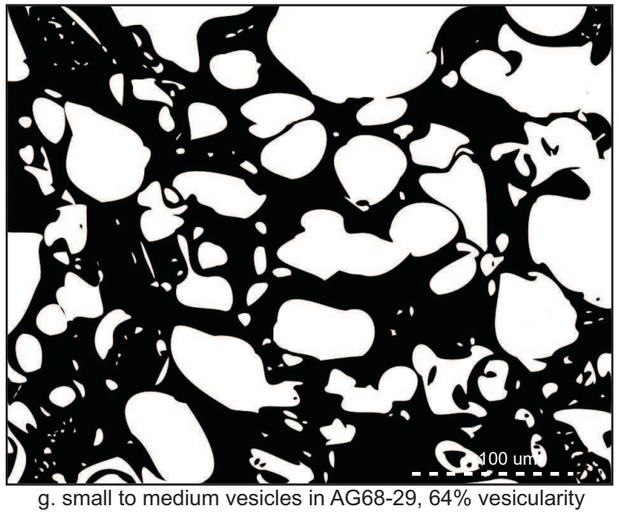

g. small to medium vesicles in AG68-29, 64% vesicularity

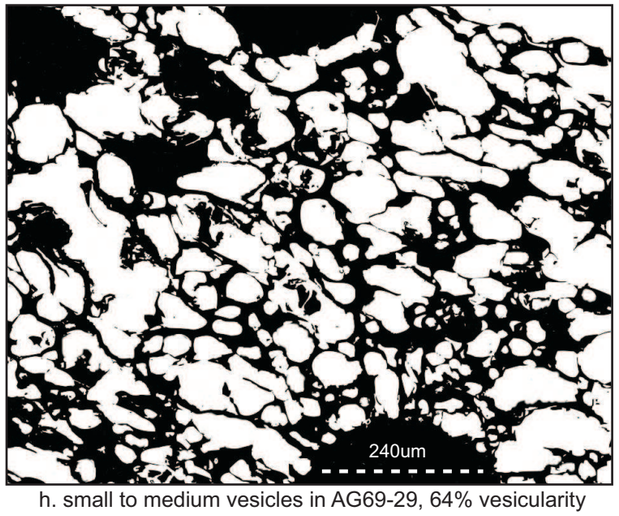

h. small to medium vesicles in AG69-29, 64% vesicularity

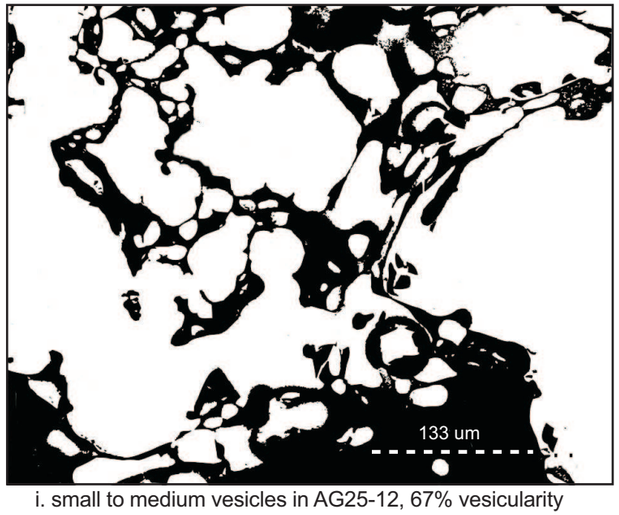

i. small to medium vesicles in AG25-12, 67% vesicularity

Figure 3.13: *Binary images of various vesicularities from SEM images for vesicle morphology analysis*

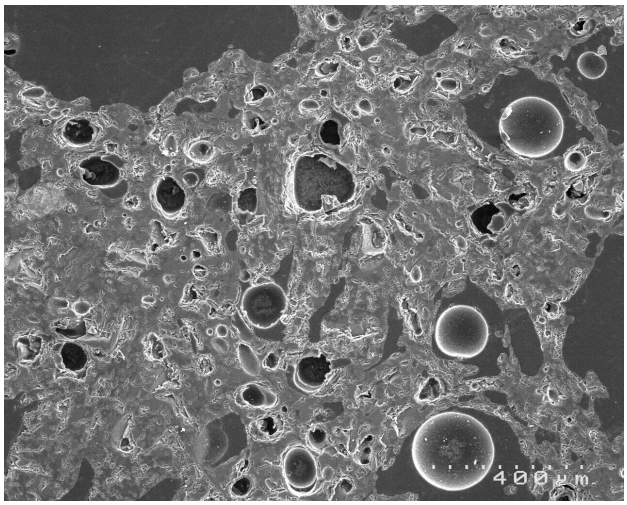

a. Black scoria microlite free AG72

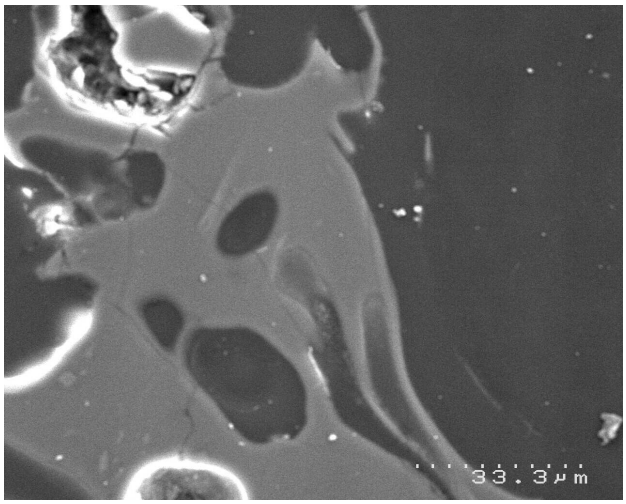

b. Faint microlites (lighter gray) seen in pumice clast AG68-28

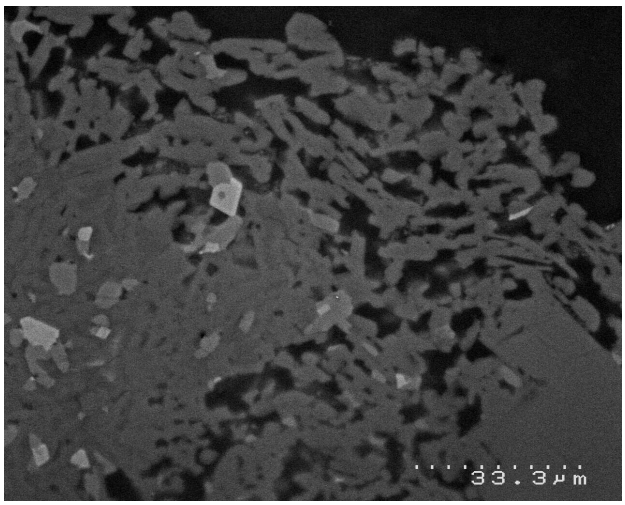

c. Microlites surrounding vesicle in welded unit AG62

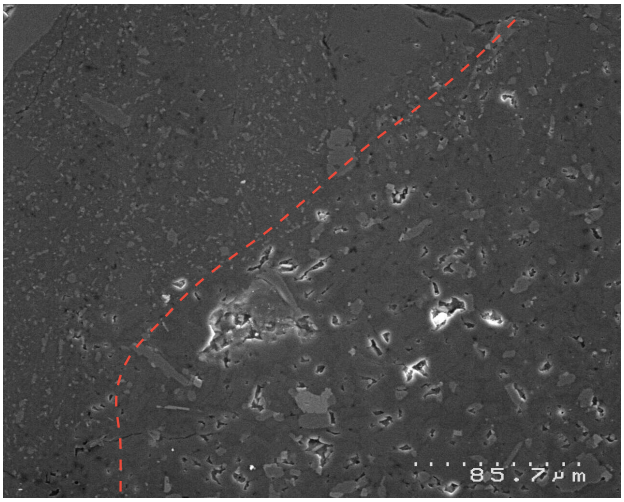

d. Boundary (dashed red line) between clast inclusion, smaller microlites in groundmass and larger microlites in clast inclusion of AG63

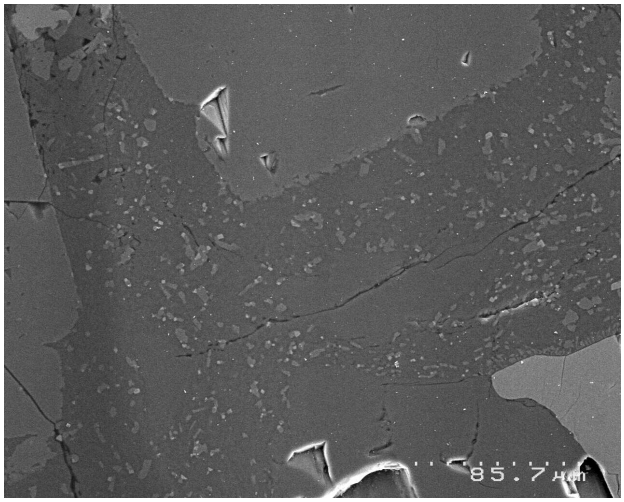

e. microlites surrounding phenocrysts in welded unit AG62

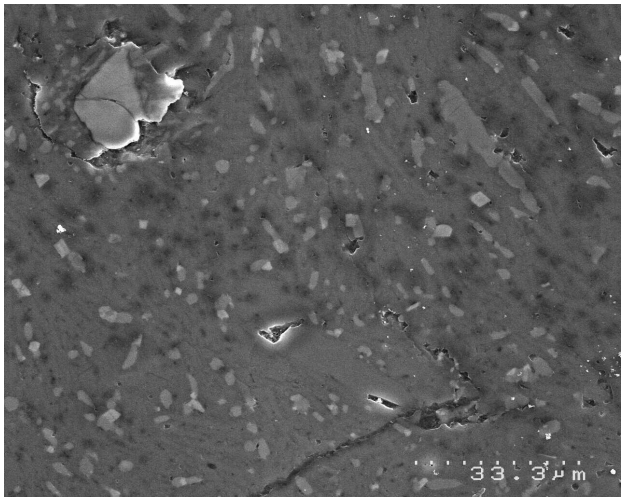

f. Microlites at random orientation with mottled appearance AG63

Figure 3.14: *SEM images of groundmass and microlite textures in welded rocks and individual clasts.*

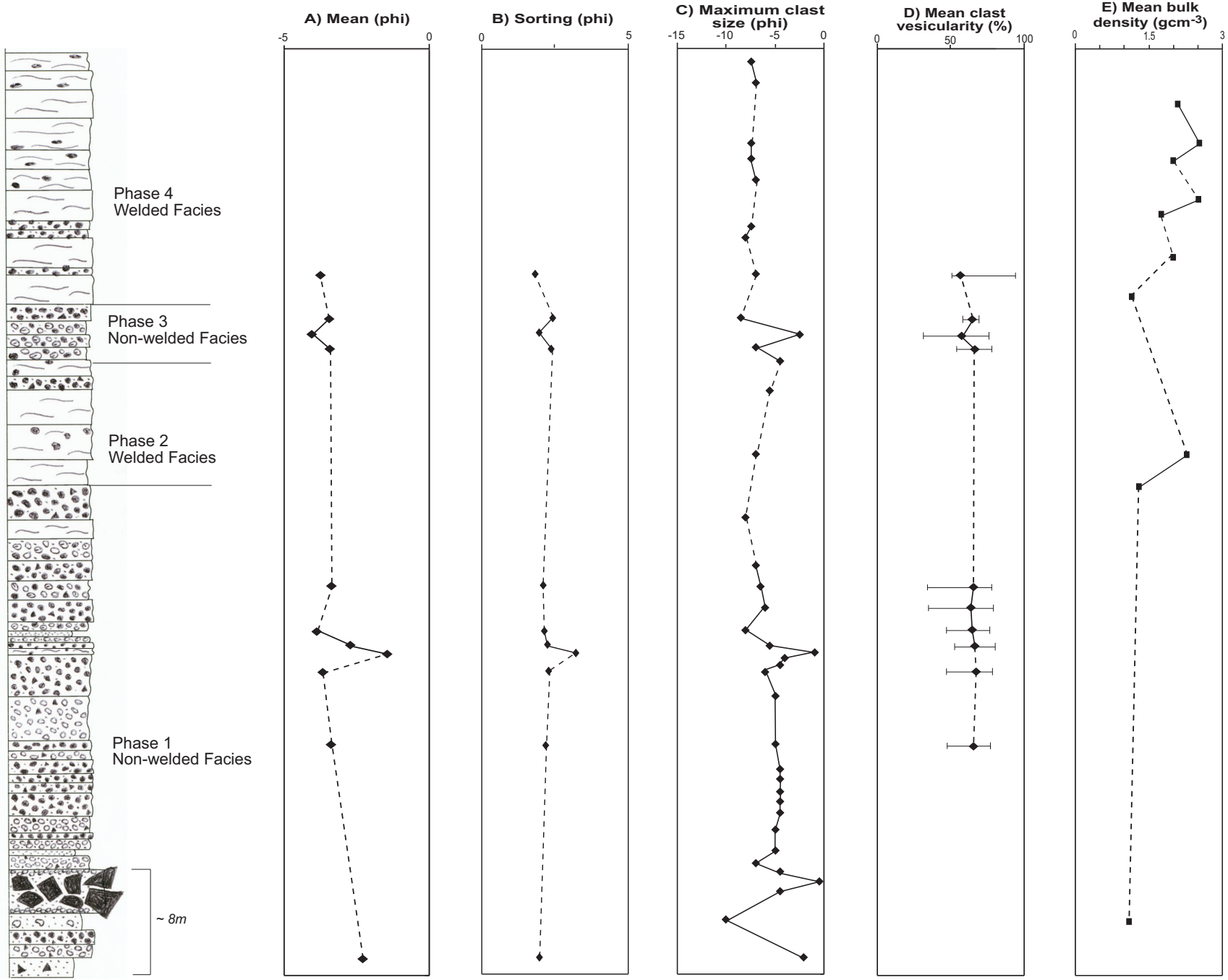

Figure 3.16: *Complete stratigraphy of North Crater eruptives with a) mean grain size, b) sorting, c) maximum clast size, d) mean clast vesicularity and e) mean bulk density.*

Chapter 4

Geochemistry and Mineralogy

4.1 Introduction

Eruptives from many of the vents on Tongariro and Ruapehu have been analysed for glass and whole rock geochemistry to determine magma composition and magmatic processes. However, little work has been carried out on North Crater deposits. Recent studies by Doyle (2006) on glass and whole rock geochemistry of the Rotoaira Subgroup includes analysis of both distal and proximal deposits that may possibly be related to North Crater.

In this chapter, whole rock XRF geochemistry is examined for a suite of samples through the stratigraphic succession at North Crater. Also glass microprobe analyses of mingled and homogeneous clasts will be used to determine phenocryst composition, any differences between light and dark types of glass, and the nature of magma mingling and mixing prior to eruption. A complete set of whole rock, phenocryst and glass geochemical data are given in Appendix F.

4.2 Background and Previous Work in the TgVC

Recent studies have shown that during magmatism associated with subduction zones many deep and/or shallow processes occur which control the chemical composition of eruptives. Deep processes can include varying degrees of partial melting, volatile fluxing and slab-mantle interactions. Shallow processes can include magma mixing, assimilation and fractional crystallisation. However, it is

possible for some of these processes to occur together to variable extents, thus limiting the ability to clearly interpret geochemical data (e.g. Waight and Price 1999).

At TgVC the young eruptive vents have been the main focus for geochemical analysis with many published papers by several authors. However, very little analytical work has been carried out on the lavas from older Tongariro vents. The 1954 eruption of Ngauruhoe renewed interest for more analytical work to be carried out on other Tongariro vents (Hobden 1997). Authors of early work (pre-1980, e.g. Greg 1960; Mathews 1967; Topping 1973, 1974) favoured crustal contamination of a parent basaltic magma, along with limited fractional crystallisation as the main processes producing andesite magmas at Tongariro (Hobden 1997).

Early work by Cole (1978) on the young eruptives at Tongariro was the first published study solely devoted to TgVC lavas. He classified the lavas as calc-alkaline andesites dominated by phenocryst-rich pyroxene and olivine andesites. Cole (1978) also noted that the NE alignment of eruptive vents at Tongariro suggested a magma source from the NE-striking subduction zone, although the lavas differed chemically from typical island arc andesites possibly by crustal contamination. He also recorded that the most voluminous lava types at TgVC were labradorite and labradorite-pyroxene andesite with phenocrysts of plagioclase (An_{65-48}), orthopyroxene and clinopyroxene, in a fine to medium grained groundmass.

Work by Graham and Hackett (1987) focused on Mt Ruapehu, and found the majority of lavas were calc-alkaline, medium-K basic and acid andesites with phenocrysts of plagioclase, clinopyroxene, orthopyroxene, olivine and titanomagnetite. They were able to divide the lavas into 6 distinct groups that were each petrographically, geochemically and isotopically distinct. Three other types have since been added to this scheme and now most andesites in the TgVC fit into a group within the scheme (Graham *et al.* 1995). Graham and Hackett (1987) recognised assimilation concurrent with fractional crystallisation (AFC) as

the dominant magmatic process at Ruapehu, with some lavas also showing evidence of crystal accumulation or magma mixing.

Tongariro andesite crystallisation temperatures were able to be derived from co-existing clino- and orthopyroxenes and found to range between 1200°C (basalt) and 1050°C (dacite), with relatively low crystallisation pressures (<10 kbar) implied by the mineralogy and metamorphic inclusions (Graham *et al.* 1995). Graham *et al.* suggested andesitic magmas could be generated by a combination of AFC of a primitive mantle-derived basaltic magma and magma mixing, but they noted that the geochemical characteristics cannot be convincingly explained by any single magmatic process.

Hobden (1997) produced a comprehensive whole rock (370 samples) and electron microprobe (phenocrysts only) geochemical data set for the TgVC which encompassed all volcano-stratigraphic units. Hobden (1997) found that some volcano-stratigraphic units had similar geochemistry and suggested an origin from a common deep magma reservoir. Other units, however, show patterns which indicate a common high level differentiation history involving magma mixing, fractional crystallisation and crustal contamination. Hobden (1997) suggested that a relatively complex history may have existed for the plumbing system of the TgVC where combinations of both deep and shallow processes, operating independently or interconnected, may have existed during different periods of Tongariro's development. She also noted that no eruptives from Tongariro had the primitive characteristics of direct mantle melts with no true basalts erupted, and that low pressure crystallisation with delayed ascent, or stalling of magma in high level chambers was an important process. Earlier crystallisation in an intermediate-level 'parent' chamber may also have occurred (Hobden 1997).

Donoghue *et al.* (1995a) identified a magma mingling episode at Ruapehu (the Pourahu Member) between two andesitic magmas. They recorded non-mingled clasts of 'end-member' predominantly pale yellow-brown andesite and dark brown andesite, that also contained rare clasts of streaky mingled pumice of the two colours. Through electron microprobe analysis for adjoining glasses they found the light and dark glass to have different compositions, with the dark glass

having 60-68 wt% SiO_2, and the light glass 71-73 wt% SiO_2. Donoghue *et al.* (1995a) suggested the light coloured andesitic magma was contained in a high-level chamber beneath the vent, and the dark hotter and denser magma was injected into the bottom of the chamber which triggered the eruption (Donoghue *et al.* 1995a).

Studies of the young eruptives on Tongariro (<10 ka Pahoka-Mangamate (PM) eruption sequence) by Nakagawa *et al.* (1998) suggested that prior to ~10 ka, magmas ascended slowly and stagnated at shallow depths (<5km) before eruption. However, around 10 ka regional rifting episodes began in the southern TVZ involving the andesitic TgVC and the rhyolitic Taupo Volcanic Centre. This rifting opened fissures to some depth and allowed rapid ascent of underlying magma bodies resulting in the eruption of ~10 ka PM eruptives from multiple fissure vents at TgVC. Nakagawa *et al.* (1998) recognised three magma types within the PM sequence, each the mixing product of two end-member magmas, but found that products from each vent had varying compositions. They suggested that separate storage and transport systems from a deeper level magma chamber must have existed beneath each vent, allowing some fractional crystallisation and/or magma mixing to occur.

Short-term variability in whole rock geochemistry in Ruapehu andesitic lavas was identified by Price *et al.* (2005). This is also the case at Tongariro (Hobden *et al.* 1999) and indicates that a complex andesitic magma plumbing system is present beneath the active vents. Eruptions are not fed from a classical simple magma chamber, but rather through a complex interconnecting dike, sill and chamber network, leading to fractional crystallisation, magma mixing and assimilation (Price *et al.* 2005).

4.3 Methods

4.3.1 Electron Microprobe Analysis

Polished thin sections of nine selected rocks from North Crater were prepared using the methods outlined in section 3.4.1. and analysed for glass and mineral

chemistry using a JEOL-JXA(5A) electron probe micro-analyser, at the Department of Geology, University of Auckland, New Zealand, under the direction of R. Sims. All analyses were made using an electron gun accelerating voltage of 15 kV, with 1.8 nA electron beam current. An electron spot diameter of ~3 µm was used, with the beam defocused for glass analyses to ~20 µm. The standard deviations associated with the glass analysis are: SiO_2 <±4.7 %, TiO_2 <±0.21 %, Al_2O_3 <±4.05 % FeO* <±1.09%, MnO <±0.08 %, MgO <±0.39 %, CaO <±2.5%, Na_2O <±0.90 %, K_2O <±0.96 %, Cl <±0.05% and NiO <±0.12 %.

4.3.2 X-ray Fluorescence Analysis

Selected samples were analysed for major and trace elements by a Spectro X-Lab 2000 fully automated X-ray fluorescence (XRF) spectrometer housed in the Department of Earth and Ocean Sciences at the University of Waikato.

Samples were taken from whole rock blocks and whole individual pyroclastic clasts, and broken into small fragments using a heavy hammer; heavy paper was used around the sample to prevent contamination. Fragments were selected based on their freshness and any which showed contamination from paper, hammer or xenoliths were discarded. Rock fragments were ground in a tungsten carbide ring mill, which was thoroughly cleaned between each sample. Rock powders were then prepared for major and trace element analysis following the sample preparation techniques similar to Norrish and Hutton (1977) and Chappell (1992). Glass fusion disks were prepared with 0.3300-0.3500 g of sample powder and 2.5000-2.5500 g of 1.2:2.2 flux, and trace element briquettes were prepared with 5g of dried rock powder with 10-20 drops of liquid PVA binder.

4.4 Whole Rock Geochemistry

4.4.1 Magma Classification

The whole rock composition of North Crater samples is displayed in a TAS classification diagram (Fig. 4.1) which shows the majority of rocks fall in the calc-alkaline andesite field (57-63 SiO_2 wt%), with a few samples of basaltic-andesite to basalt composition. From the TAS classification we can broadly define

three groups: Group 1: the majority of samples ranging from 58.17-61.92 SiO_2 wt%; Group 2: four clustered samples ranging from 56.41-56.89 SiO_2 wt% which are in the lower stratigraphic level of North Crater deposits; and Group 3: two samples ranging from 50.74-53.97 SiO_2 wt%, which are samples from the Rotoaira Lapilli. The most evolved compositions occur in the stratigraphic middle of the North Crater sequence, indicating that a simple systematic geochemical progression with time does not occur.

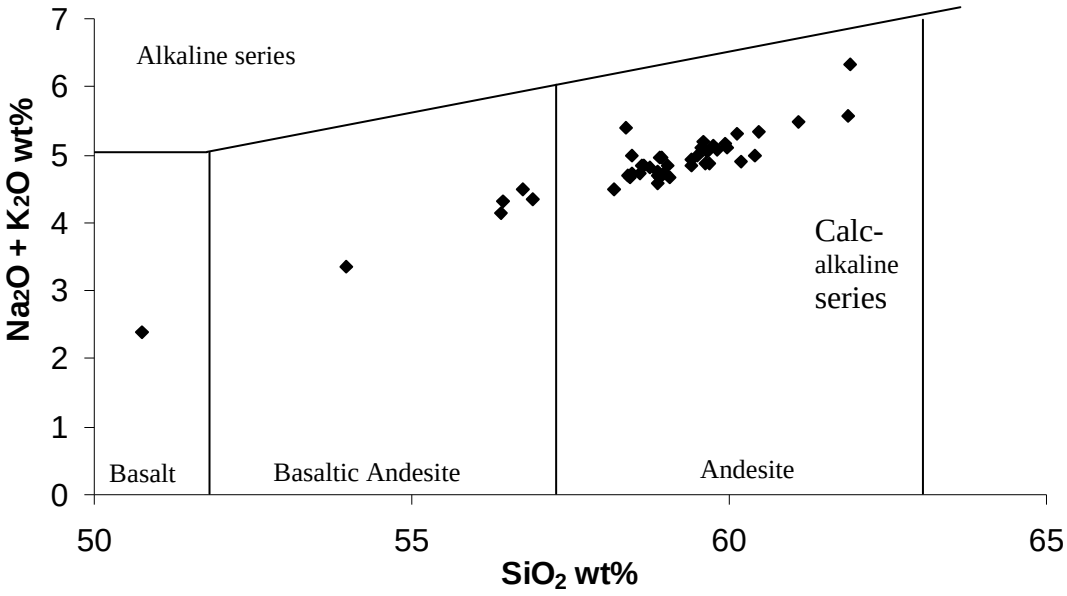

Figure 4.1: *Graph showing TAS whole rock magma classification of North Crater eruptives.*

4.4.2 Major Oxides – variation diagrams

For North Crater the major oxides of CaO, TiO_2, Fe_2O_3, MnO and MgO decrease with increasing SiO_2, while Na_2O and K_2O increase with increasing SiO_2. These trends would be expected for fractional crystallisation involving the mineral phases observed at North Crater (Fig. 4.2). Trends of decreasing CaO versus SiO_2 are consistent with fractional crystallisation of plagioclase and clinopyroxene, and the tightly clustered decreasing Fe_2O_3 trend is consistent with the removal of pyroxenes and Fe-Ti oxides by fractional crystallisation. However, the variation diagrams show more straight lines than curved trends and often scattered points in some elements, e.g. P_2O_5, which suggests processes other than closed system

fractional crystallisation could be occurring at North Crater with eruptives not derived from a single parent magma. Plots of Al_2O_3, TiO_2, CaO and MgO show the main group of North Crater samples to lie on a similar trend line, although the samples analysed from the Rotoaira Lapilli appear to lie on different trend lines from this main group in some oxide variation diagrams (Fig. 4.2b). The presence of crystal xenoliths in the majority of samples indicates that some crustal assimilation is occurring.

In comparison with other eruptive deposits from Tongariro (Ngauruhoe, Red Crater, Tongariro Trig, Pukekaikiore and NE Oturere from Hobden *et al.* 2001 and Tama Lakes and Half Cone from Nakagawa *et al.* 1998), North Crater samples appear slightly more enriched in K_2O, MgO, TiO_2 and Na_2O, more depleted in MnO, while Fe_2O_3, CaO, and Al_2O_3 are similar (Fig. 4.2). When comparing North Crater samples to the Rotoaira Subgroup (Doyle 2006), similar trends are apparent, although North Crater samples are enriched in Al_2O_3, MgO, Na_2O and CaO and indistinguishable in Fe_2O_3, MnO, TiO_2 and K_2O (Fig. 4.2). This could be due to the more complete sampling regime undertaken on the entire sequence of North Crater proximal eruptives compared with Doyle's (2006) samples which were restricted to basal proximal and distal ring-plain deposits.

SiO_2 wt% varies significantly in phase one of the North Crater sequence (Fig. 4.3). It appears the lower-most units of North Crater eruptives show a progressive increase in SiO_2 content, which is inconsistent with the eruption of a typical closed system, normally zoned magma chamber. The magma chamber may have been completely overturned prior to eruption, caused by the injection of hotter or more mafic magma, which has then lead to the eruption. The presence of mingled units in the lower part of phase one would also suggest injection and mingling of magmas prior to or during the initial phase of the eruption. About half way through phase one there appears to be some event which has caused the SiO_2 content to change relatively quickly and begin to decrease. Other major oxides and trace elements also show these variations (Fig. 4.3). The injection of fresh magma into the erupting magma chamber could have caused this to occur. In the following phases of the eruption, SiO_2 wt% and other oxides and trace elements tend to show steady patterns with any fluctuations mostly within analytical error.

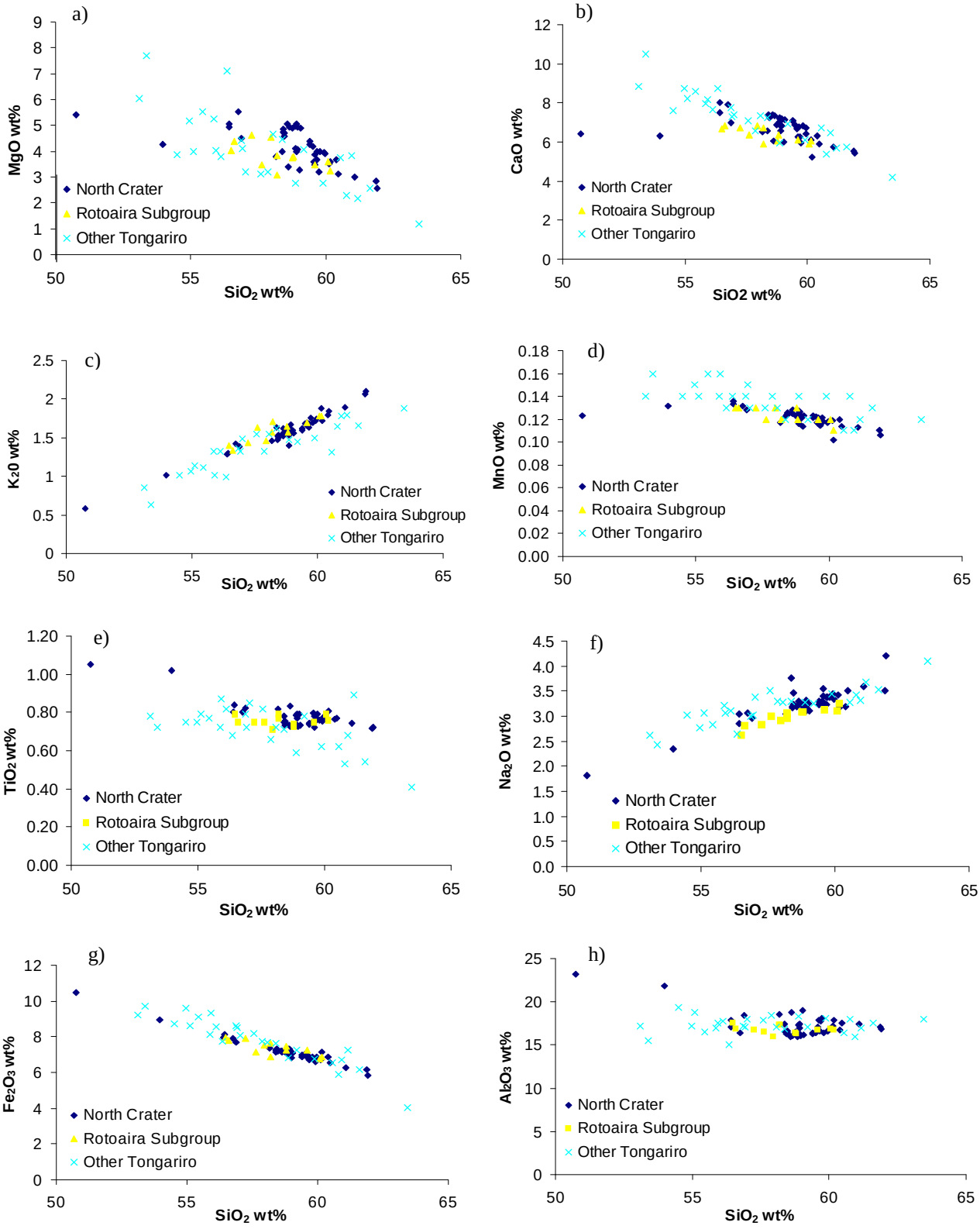

Figure 4.2: *Harker variation diagrams for selected whole rock major oxides of North Crater, Rotoaira Subgroup and other Tongariro eruptives a)MgO, b) CaO, c) K_2O, d) MnO, e) TiO_2, f) Na_2O, g)Fe_2O_3 and h) Al_2O_3.*

Fig 4.3

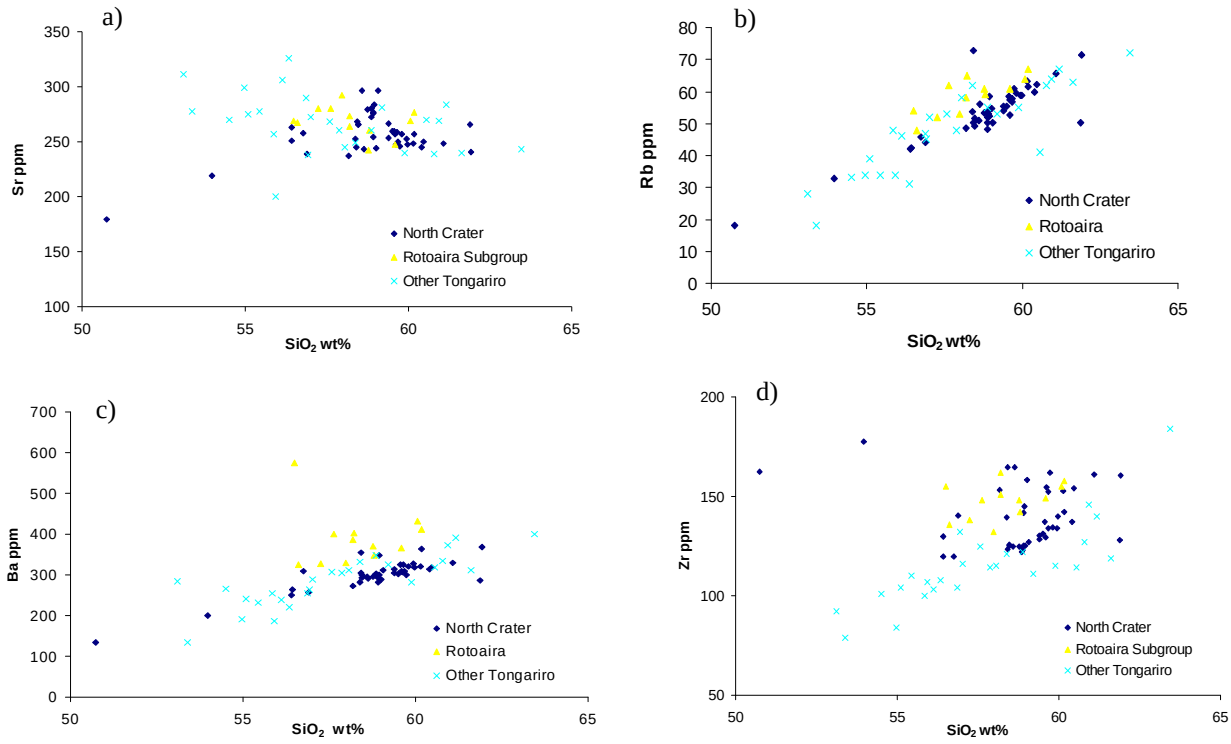

Figure 4.4: *Harker variation diagrams for selected whole rock trace elements, a) Sr, b) Rb, c) Ba and d) Zr.*

4.4.3 Trace Elements – variation diagrams

In Harker variation diagrams for North Crater eruptives the trace elements Rb, U, Th and Ba behave incompatibly and increase in abundance with increasing SiO_2 wt%, while V, Zr, Sc and Cu behave compatibly and decrease in abundance with increasing SiO_2. Other trace elements display no apparent trends with increasing SiO_2 (Fig. 4.4).

In comparison with other Tongariro eruptive deposits (from Nakagawa *et al.* 1998 and Hobden *et al.* 2001), Rb, Th, Ni, Cr and Zr show slight enrichment, Cu appears slightly depleted, and elements Sr and Ba are indistinguishable. Compared with Rotoaira Subgroup (Doyle 2006), North Crater trace elements Ni, Th and Cr appear slightly enriched, Rb, Ba and Cu are slightly depleted, while Zr and Sr show no trends. The relatively low levels of Ni indicate the magma at North Crater has undergone considerable crystal fractionation of early olivine, which is now reacted with pyroxene.

There also appears to be no systematic geochemical change in trace elements through the vertical succession of North Crater eruptives. Harker variation plots of key stratigraphic sections around North Crater show no patterns of increasing or decreasing element abundance with stratigraphic height (Fig. 4.5).

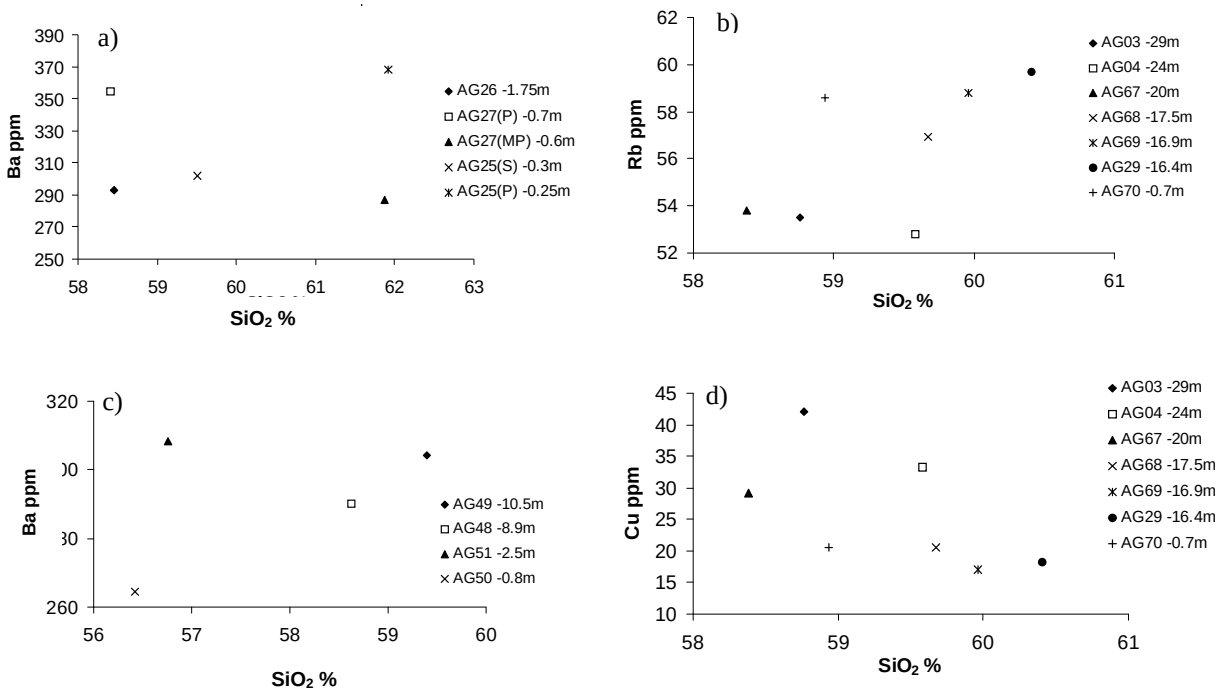

Figure 4.5: *Harker variation plots of selected whole rock trace elements in key stratigraphic sections around North Crater (see Fig 2.1 for locations) a) Rb at North Bluff, b) Ba at Eastern Gully 1, c) Ba at Eastern Gully 2, and d) Cu at North Bluff.*

4.5 Phenocryst Composition

4.5.1 Plagioclase Feldspar

Plagioclase feldspar is the most abundant mineral phase in North Crater deposits and phenocrysts range from andesine to bytownite An_{48-77}. Analysis of phenocryst cores and rims revealed that some crystals were not always homogenous, with cores ranging from An_{57-69} and rims ranging from An_{48-73}, with typically 4-10 mol% An variation within one crystal. Some phenocrysts display reverse zoning (An-poor core and An-rich rim) and sieve textures, indicating disequilibrium, typical of magmas which have been mixed or undergone decompression. Compared with samples from the Rotoaira Subgroup (An_{48-85}, Doyle 2006), North

Crater samples are indistinguishable, and fall into the same range as other TgVC eruptives (An_{45-90}, Hobden 1997) (Fig. 4.6).

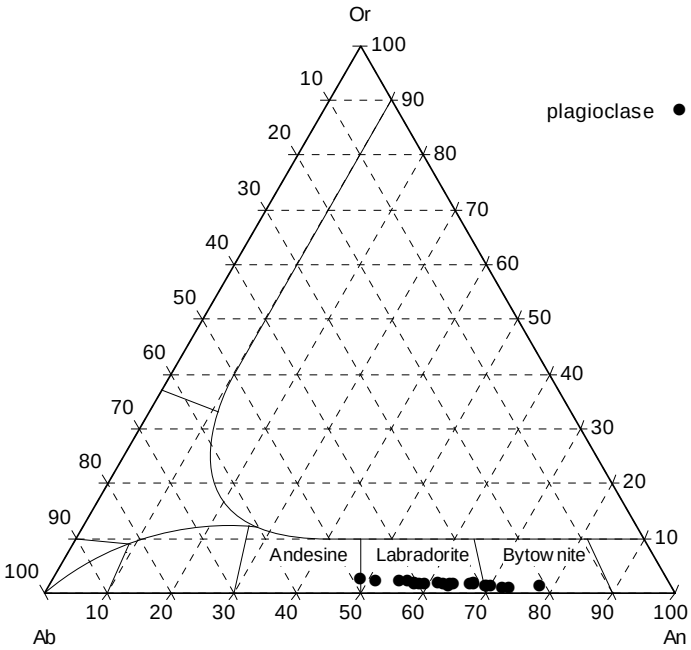

Figure 4.6: *Triplot of plagioclase feldspar phenocryst compositions in North Crater deposits.*

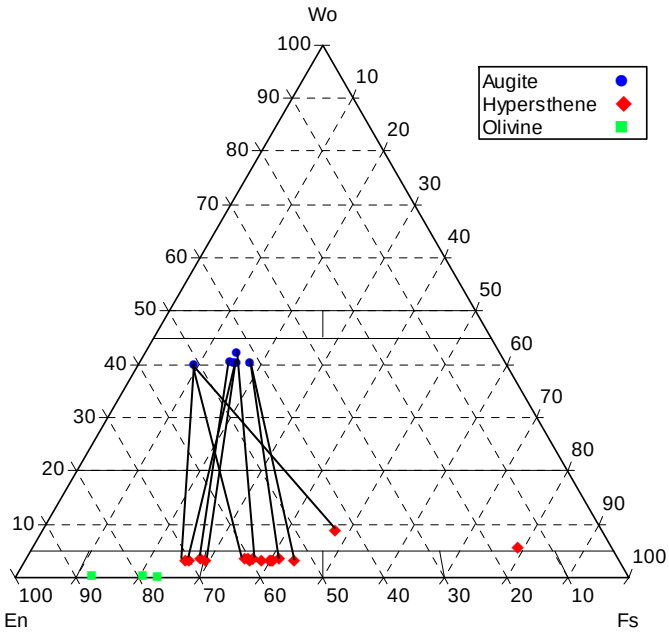

Figure 4.7: *Triplot of clinopyroxene, orthopyroxene and olivine phenocryst compositions in North Crater deposits, tie lines connect phenocryst compositions in the same rock to show equilibrium (parallel tie lines) or disequilibrium (crossed tie lines).*

4.5.2 Pyroxene

Pyroxene is the dominant mafic phase in North Crater deposits, with both orthopyroxene and clinopyroxene phenocrysts occurring in all eruptives (section 3.5). Orthopyroxene has a compositional range (En_{41-70}), and clinopyroxenes vary from $Ca_{39-42}Mg_{41-50}Fe_{9-18}$, which is similar to clinopyroxene compositions from other TgVC deposits ($Ca_{35-46}Mg_{35-52}Fe_{7-24}$, Hobden 1997) and the Rotoaira Subgroup ($Ca_{38-43}Mg_{38-52}Fe_{5-23}$, Doyle 2006). Orthopyroxenes range in composition from $Ca_{3-8}Mg_{41-70}Fe_{26-47,}$ which is similar to other TgVC eruptives ($Ca_{1-5}Mg_{55-86}Fe_{11-42}$, Hobden 1997) and the Rotoaira Subgroup (En_{55-75}, Doyle 2006). Tie lines connecting clino- and ortho-pyroxene phenocrysts in the same rock show some phenocrysts to be in equilibrium with each other, while others are slightly out of equilibrium indicating mixing of magmas (Fig. 4.7).

4.5.3 Olivine

Olivine phenocrysts are rare and found in only a few samples from North Crater eruptives, occurring as small (0.8-1 mm, section 3.5) anhedral crystals rimmed with fine-grained clino- or orthopyroxene. The composition of North Crater olivine ranges from Fo_{87-76} and falls into the range for other TgVC eruptives (Fo_{96-67}, Hobden 1997), but are generally more forsteritic than (distal) Rotoaira Subgroup (Fo_{72-77}, Doyle 2006) (Fig. 4.7).

4.5.4 Fe-Ti Oxides

Fe-Ti oxides are found as phenocrysts and inclusions in plagioclase, orthopyroxene and clinopyroxene and as skeletal growths in glomeroporphyritic clumps (section 3.5). The spinel phase is much more abundant than the rhombohedral phase (ilmenite), which is often absent in many North Crater eruptives. The composition of titanomagnetite ranges from 10.33-18.33 TiO_2 wt% and ilmenite from 46.29-48.55 TiO_2 wt%, with titanomagnetite varying by 18.07 TiO_2 wt% within a single clast. In comparison with Doyle's (2006) Rotoaira Subgroup, the titanomagnetite phase of North Crater has a similar composition of ~7-20 TiO_2 wt%, and also compares to other TgVC eruptives (~10-20 TiO_2 wt%, Hobden 1997). Fe-Ti oxides are sensitive to changes in magma composition, so large variations in Fe-Ti oxide composition within a single clast could indicate

complex mixing involving several magma batches in North Crater eruptions (e.g. Carmichael 1967).

4.6 Glass Geochemistry

Matrix glass analyses were carried out on 8 polished thin sections of individual clasts from pyroclastic samples. Microprobe analyses of glass from North Crater eruptive deposits show glass compositions range widely from andesite to rhyolite (SiO_2 = 57.7-73.7 wt% and K_2O = 0.93-4.57 wt%) (Fig. 4.8). In one clast, SiO_2 ranged from 57-71 wt% indicating large magma heterogeneity. This will be discussed further in section 4.6.

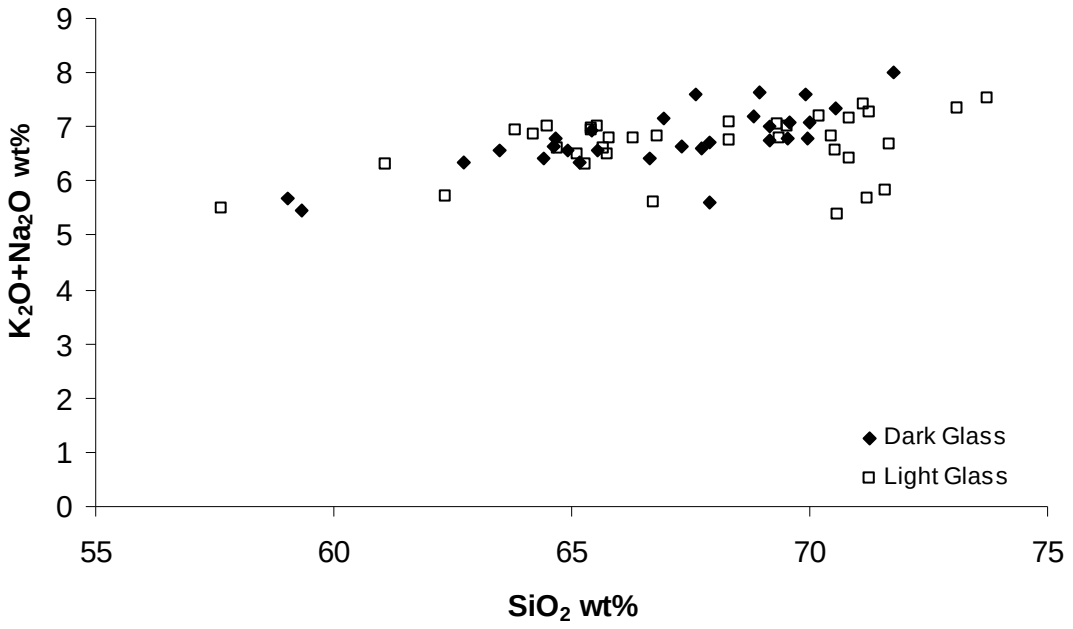

Figure 4.8: *TAS classification plot of North Crater glass from electron microprobe analyses.*

In comparison with distal Rotoaira Subgroup (Doyle 2006), North Crater deposits appear to be slightly more enriched in K_2O and cover a slightly broader range of values, although when compared with proximal Rotoaira Subgroup (Doyle 2006), North Crater deposits are nearly indistinguishable (Fig. 4.9). K_2O is only shown here as it is the best discriminator for identifying similarities and differences in matrix glass since it is the least likely element to be affected by undetected microlites in matrix glass (Doyle 2006).

Limited electron microprobe data exists for Tongariro glass, with only detailed whole rock XRF analysis carried out by recent workers (e.g. Donoghue *et al.* 1995a; Hobden 1997; Price *et al.* 2005). Glass analyses from the young Te Maari lava flow, Central Crater lava flow and agglutinate found west of Tongariro Trig (Doyle 2006) all show relatively constrained and separate groups on a K_2O versus SiO_2 plot (Fig. 4.9). The young lava flow from Te Maari is the most evolved of the group (SiO_2 = 72.7-76.5 wt%, K_2O = 3.37-4.39 wt%, Doyle 2006), which might be expected as it is one of the younger deposits on Tongariro. North Crater eruptives appear slightly more enriched in K_2O compared to the lava flow from Central Crater (SiO_2 = 57.3-60.1 wt%, K_2O = 0.95-1.81 wt%, Doyle 2006) and slightly depleted in K_2O compared with the agglutinate west of Tongariro Trig (SiO_2 = 63.9-67.1 wt%, K_2O = 3.04-3.68 wt%, Doyle 2006). Ruapehu glass analyses show similar trends to North Crater eruptives and fall within a similar compositional range (SiO_2 = 66.1-71.1 wt%, K_2O = 2.56-4.29 wt%, mean values, Donoghue *et al.* 1995a) (Fig. 4.9).

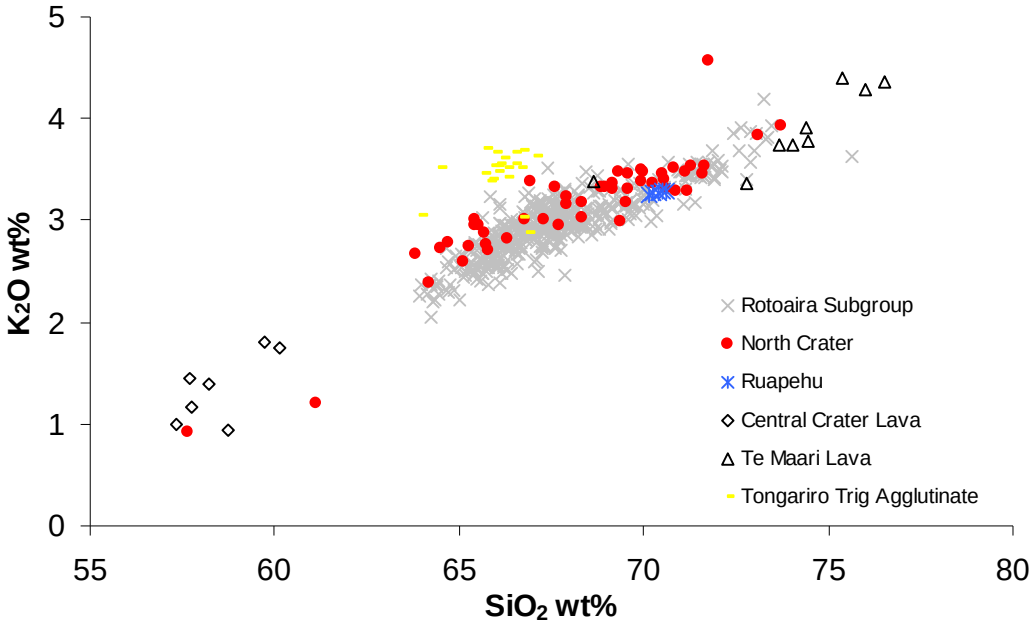

Figure 4.9: *K_2O vs. SiO_2 wt% plot showing composition of glass from North Crater, compared with proximal Rotoaira Subgroup (Doyle 2006), Ruapehu (Donoghue et al. 1995a), and other Tongariro sites (Doyle 2006).*

4.7 Evidence of Magma Mingling and Mixing

Evidence of clast heterogeneity was seen in the field (section 2.6) and in petrographic analysis of various pyroclastic units. Four clasts were selected which showed magma mingling, visible as streaky and banded 'light' pumice glass and 'dark' scoria glass, and analysed using the electron microprobe in order to determine the nature of any chemical differences (Table 4.1). Areas of 'light' and 'dark' glass were mapped out on the thin section to determine between different glass zones when under the microprobe. The dark and light glass components occur in varying amounts in each clast and unit, as previously described in section 3.3, and range from minor mingled to intensely mingled. The majority of clasts which show mingled textures have sharp contacts between the light and dark zones, indicating these two components did not mix efficiently before eruption (Donoghue *et al.* 1995a).

The glasses in the dark glass component range between 57.66-71.76 wt% SiO_2, and 0.93-4.57 wt% K_2O, and within an individual clast the largest range of SiO_2 is 57.66-69.31 wt%. The light glass component ranges between 59.04-73.72 wt% SiO_2 and 1.06-3.93 wt% K_2O, and within an individual clast the largest range of SiO_2 is 65.68-71.28 wt% (Fig. 4.10). Comparison of these two glass types (Fig. 4.10) shows they are not separated into two distinct groups, for example more felsic light glass and more mafic dark glass. However, the light glass appears to have several distinct compositional 'groups', but this may be the result of a small and incomplete data set.

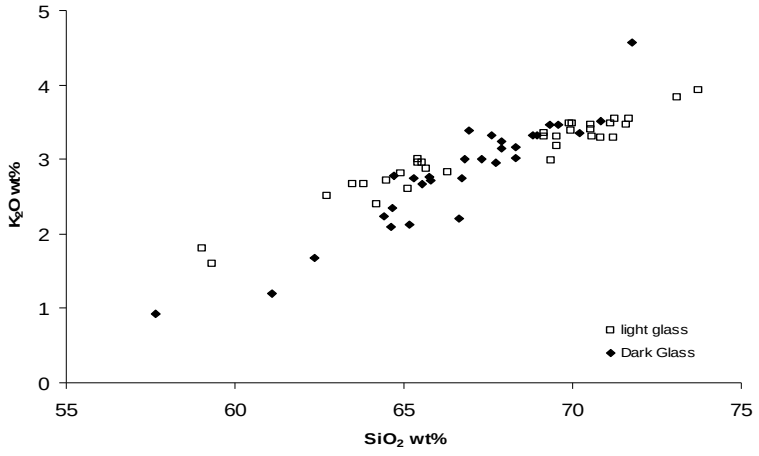

Figure 4.10: *Graph of K2O vs SiO2 wt% for light and dark glass compositions in North Crater eruptives.*

Table 4.1: *Electron microprobe analyses of light and dark glass in mingled clasts from North Crater, Tongariro.*

	Microprobe ID	SiO_2	TiO_2	Al_2O_3	FeO	MnO	MgO	CaO	Na_2O	K_2O	Cl	Total
AG68-29 glass light	6655	69.95	0.65	13.05	3.32	0	0.54	2.43	3.4	3.39	0.16	96.89
AG68-29 glass light	6656	69.17	0.71	12.88	3.15	0.11	0.52	2.43	3.43	3.31	0.19	95.9
AG68-29 glass light	6657	69.17	0.57	12.84	3.17	0.06	0.58	2.41	3.65	3.36	0.18	95.99
AG68-29 glass light	6658	69.55	0.71	12.97	3.27	0.1	0.57	2.28	3.46	3.31	0.21	96.43
AG68-29 glass dark	6661	67.73	0.73	14.04	3.96	0.1	0.7	3.29	3.63	2.96	0.17	97.31
AG68-29 glass dark	6662	67.91	0.84	13.47	4.56	0.1	0.59	3.11	2.46	3.15	0.22	96.41
AG68-29 glass dark	6663	67.3	0.81	13.75	4.43	0.08	1.01	3.51	3.64	3.01	0.11	97.65
AG68-29 glass dark	6664	67.92	0.81	13.36	3.99	0.09	0.82	2.82	3.46	3.24	0.16	96.67
AG68-29 glass dark	6665	69.59	0.64	13.1	3.52	0.16	0.56	2.28	3.62	3.46	0.17	97.1
AG29 glass dark	6573	66.74	0.97	14.38	4.27	-0.11	0.57	3.77	2.86	2.75	0.23	96.50
AG29 glass light	6578	71.67	0.67	13.01	3.28	0.07	0.55	1.9	3.15	3.54	0.21	98.05
AG29 glass light	6585	70.53	0.56	13.1	2.83	0.08	0.53	2.14	3.1	3.46	0.12	96.45
AG29 glass light	6891	70.6	0.76	13.07	2.89	0	0.55	2.1	2.08	3.31	0.14	95.5
AG29 glass dark	6592	68.34	0.74	14.55	3.93	-0.01	0.49	3.77	3.72	3.02	0.23	98.78
AG29 glass dark	6593	69.31	0.71	13.22	3.78	0.01	0.66	2.78	3.58	3.47	0.18	97.7
AG29 glass light	6594	71.2	0.6	13.13	3.16	0.08	0.51	2.23	2.38	3.29	0.15	96.73
AG29 glass light	6595	71.58	0.61	13.35	1.8	0.08	0.53	2.04	2.37	3.46	0.11	95.93
AG42-4 dark glass	6596	70.84	0.49	13.24	3.39	-0.06	0.55	2.42	3.63	3.51	0.12	98.13
AG42-4 dark glass	6597	68.34	0.81	13.63	4.09	0.05	0.79	3.09	3.9	3.17	0.14	98.01
AG42-4 glass light	6608	65.68	0.81	14.2	5.09	-0.01	0.95	3.71	3.74	2.88	0.18	97.23
AG42-4 glass light	6609	66.3	1.01	14.18	5.25	0.08	1.14	3.96	3.96	2.82	0.19	98.89
AG42-4 glass dark	6611	66.79	1.2	14.15	5.02	0.21	0.89	3.47	3.82	3	0.16	98.71
AG42-4 glass dark	6612	65.8	1.03	14.42	5.07	0.14	1.06	3.82	4.07	2.71	0.14	98.26
AG42-4 glass light	6613	71.28	0.63	13.22	3.25	0.03	0.52	2.44	3.72	3.54	0.15	98.78
AG42-4 glass light	6614	71.15	0.74	13.23	3.23	0.13	0.53	2.23	3.92	3.48	0.12	98.76
AG42-4 glass light	6615	69.54	0.81	13.35	4.12	0.06	0.8	2.9	3.82	3.18	0.16	98.74
AG25-12 glass light	6619	70.85	0.69	13.63	3.59	0.06	0.6	2.84	3.11	3.29	0.18	98.84
AG25-12 light glass	6621	73.12	0.52	12.67	2.61	0.21	0.28	1.72	3.5	3.83	0.24	98.7
AG25-12 light glass	6622	69.36	0.63	14.25	3.84	0.1	0.79	3.37	3.8	2.99	0.21	99.34
AG25-12 glass light	6626	73.72	0.52	12.54	2.49	0.07	0.34	1.7	3.59	3.93	0.2	99.1
AG25-12 dark glass	6632	65.74	0.87	14.62	5.12	0.03	1.34	4.02	3.72	2.76	0.12	98.34
AG25-12 dark glass	6633	64.71	0.81	15.35	4.02	0.01	1.08	3.87	3.81	2.78	0.13	96.57
AG25-12 dark glass	6634	65.29	0.97	14.24	5.58	0.16	1.21	4.19	3.55	2.74	0.16	98.09
AG25-12 dark glass	6635	70.23	0.69	13.63	3.57	0.08	0.65	2.73	3.85	3.36	0.22	99.01

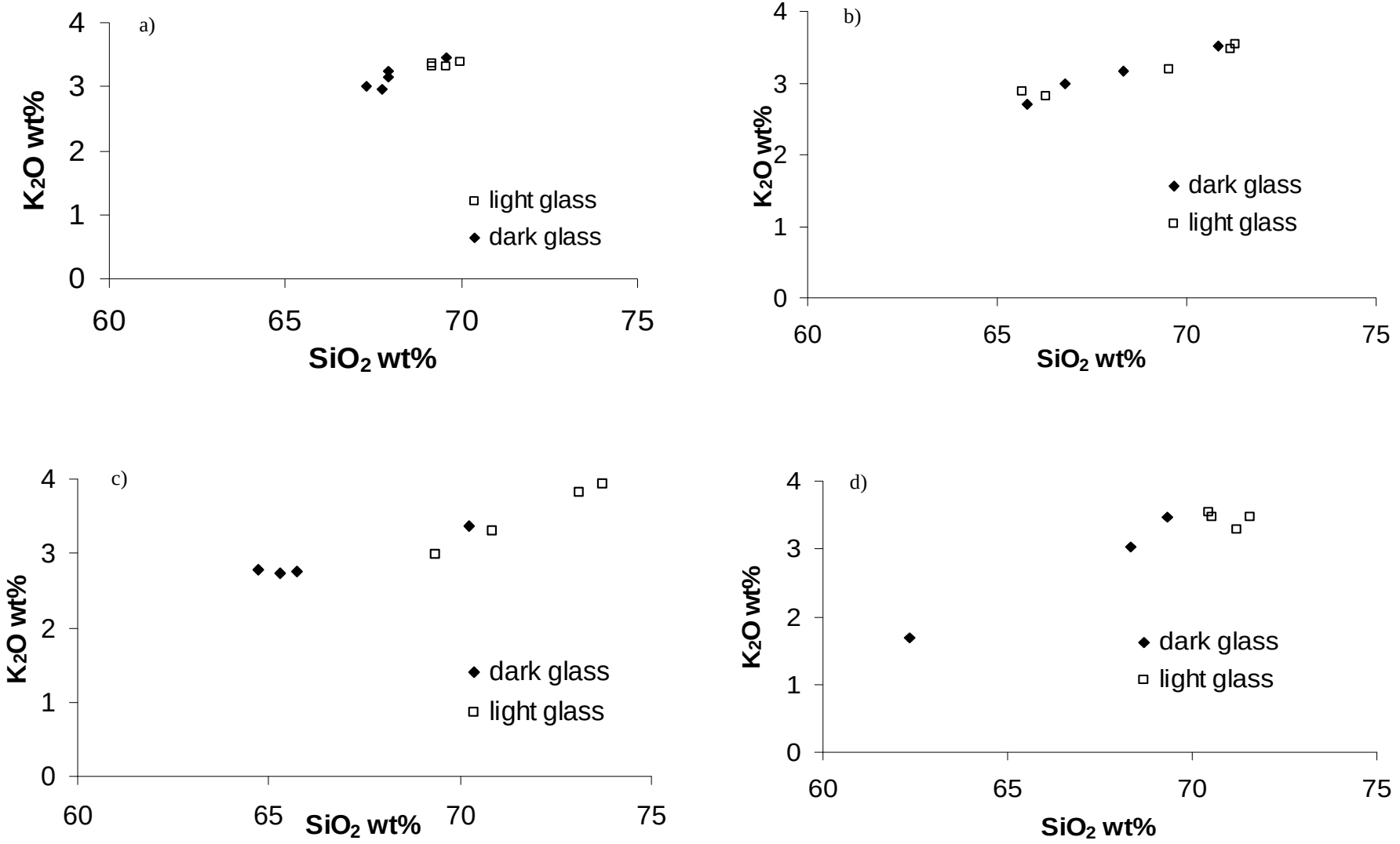

Figure 4.11: *K_2O vs. SiO_2 wt% compositions of light and dark glass in mingled clasts from North Crater. A) AG68-29, b) AG42-12, c) AG25-12 and d) AG29.*

The dark and light glass within three of the four clasts (AG25-12, AG29 and AG68-29) appear to have slightly different compositions, with only one or two data points plotting within the opposite group (Fig. 4.11 a,b,d). AG42-4 is the exception, with compositions for the light and dark glass showing no distinction (Fig. 4.11c).

As previously identified in section 3.6.3 the dark glass component in mingled clasts is microlite rich, while the light glass component is microlite free. It is possible the presence of microlites in the dark magma has caused the slight compositional and physical differences of the melt, and resulted in physically mixed units when erupted and emplaced. The microlites may have formed during cooler, slow ascent along the conduit margins, while the microlite free glass formed from the hot, rapidly ascending magma near the centre of the conduit (Castro *et al.* 2004; Sable *et al.* 2006). The two subtly contrasting andesitic magmas may not have been efficiently mixed prior to eruption because of other physical properties, such as viscosity, dissolved volatiles and temperature, resulting in a mingled magma. These processes will be discussed in chapter 5.

4.8 Magma Physical Properties

4.8.1 Geothermometry and Oxygen Fugacity

Co-existing ilmenite and titanomagnetite pairs from North Crater eruptives were analysed using the electron microprobe from polished thin sections in order to estimate mean temperature (T°C) and oxygen fugacity (fO_2). Ilmenite is scarce in North Crater eruptives compared to titanomagnetite and were often not found within the same thin section, limiting the number of geothermometry calculations. Ideally oxide pairs should show evidence of equilibrium, i.e. direct contact with each other, but this was generally not the case with North Crater Fe-Ti oxides. The Mg/Mn partitioning test for equilibrium between two pairs of co-existing oxides by Bacon and Hirschmann (1988) is used to identify possible equilibrated pairs in North Crater samples. The results (Fig. 4.12) show the majority of these titanomagnetite-ilmenite pairs from North Crater plot outside the error envelope,

which indicates the region of mineral-host-rock equilibrium. The reason the majority of the pairs may fall outside of the equilibrium envelope may be due to: a) small temperature and/or compositional dependence on Mg/Mn partitioning, b) electron microprobe analytical precision, c) post-equilibrium alteration, or d) crystal disequilibrium (Bacon and Hirschmann 1988).

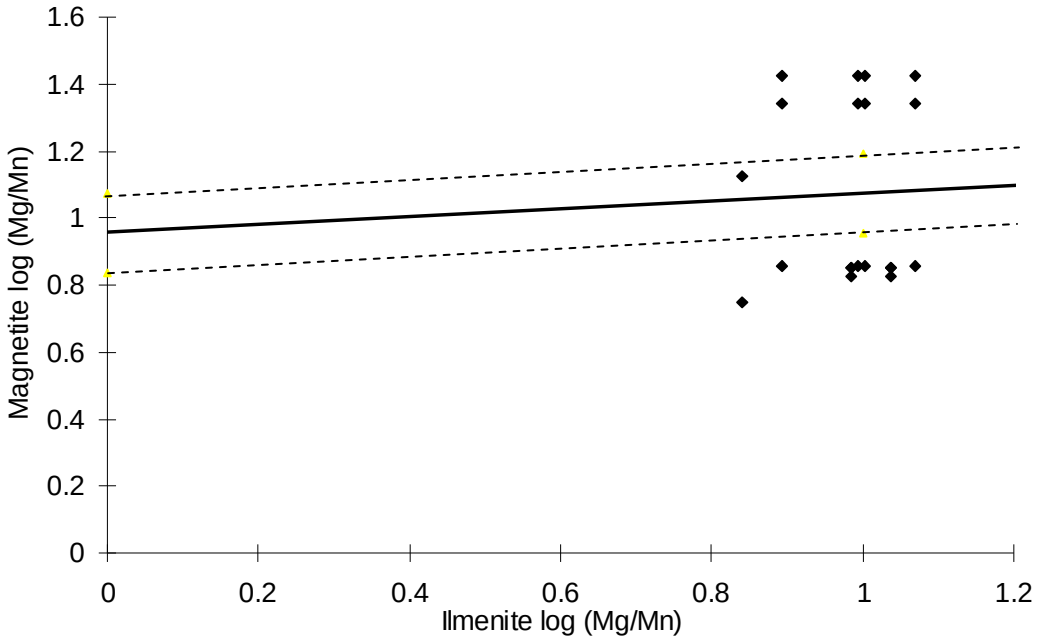

Figure 4.12 *Log Mg/Mn for 20 ilmenite-magnetite pairs in North Crater eruptives. Best fit equilibrium line (heavy solid line) is surrounded by error envelope (95% confidence limits, ±2 s.d., dashed lines) determined from Bacon and Hirschmann (1988).*

It is likely that crystal disequilibrium is the most important factor influencing North Crater Fe-Ti oxide pairs, due to the extensive mixing and mingling of multiple magma batches occurring through a complex network of sills, dikes and chambers beneath TgVC. Because of this disequilibrium between oxide pairs only one sample passed the equilibrium test, which gave a temperature of 898 °C and fO_2 of -11.71.

4.8.2 Magma Viscosity, Density and Temperature

Kware MAGMA (Wohletz 2005) geological software was used to calculate the effective viscosity, bulk density and liquidus temperatures for North Crater

eruptives. The program uses major oxide values from whole rock XRF analyses to calculate effective melt viscosity using Shaw (1972), melt bulk density using Bottinga and Weill (1972), and liquidus temperature using Sisson and Grove (1993).

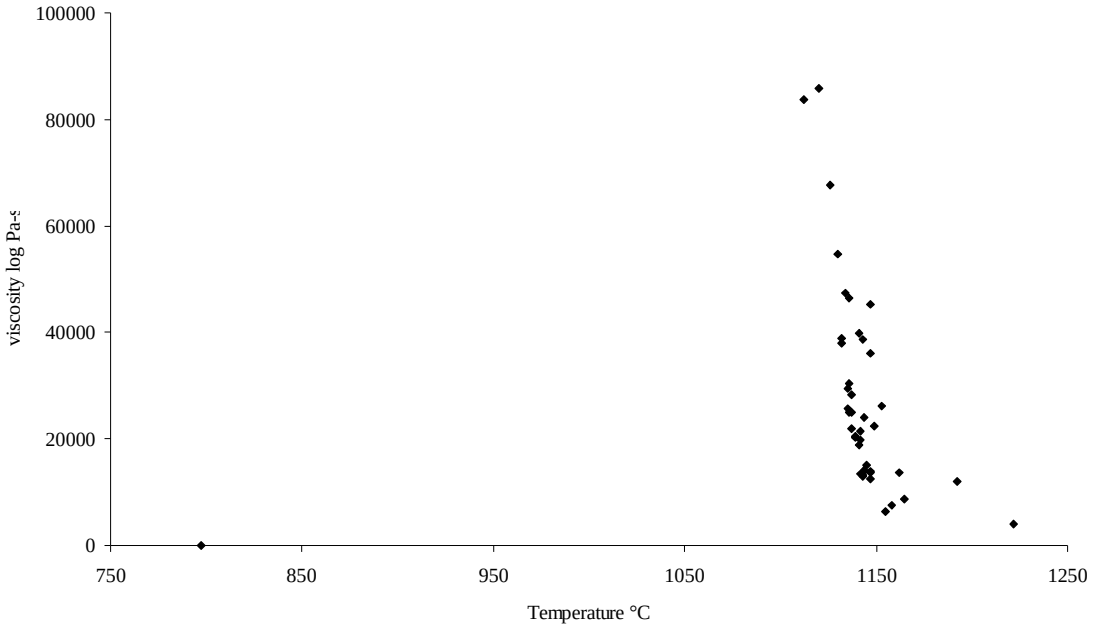

Figure 4.13: *Whole rock viscosity and temperatures for a range of North Crater eruptives, calculated from Magma model (Wohletz 2005).*

Variations in the viscosity exist in eruptions from North Crater (Fig. 4.13), with the average effective viscosity of the eruptives being 2.69 x 10^4 log Pa-s, with a range of 2.88 x 10^0 to 8.58 x 10^4 log Pa-s (Table 4.2). Differing magma viscosities in a single magma chamber is an effective barrier to efficient mixing between the contrasting magmas resulting in mingled and streaky eruptive deposits (Donoghue *et al.* 1995a). Where magma viscosity is higher at a similar temperature (Fig. 4.13), it is likely little dissolved water may be contained in the magma, as water acts to decrease the viscosity of the magma at the same temperature (Spera 2000). Andesite magma viscosities typically range from 10^4 to 10^1 log Pa-s at temperatures 1000 to 1300 °C, dacites range from 10^5 to 10^8 log Pa-s at temperatures 800-1100 °C, and rhyolites range from 10^{10} to 10^7 log Pa-s at temperatures 800 to 1000 °C (Spera 2000). When comparing North Crater effective viscosity to these viscosities, North Crater magmas fit into the typical

andesite range. There also appears to be a general trend of increasing viscosity with increasing SiO_2 content (Fig. 4.14). This trend is expected as more siliceous magmas (containing dissolved water) tend to have higher viscosities than less siliceous magmas (Spera 2000).

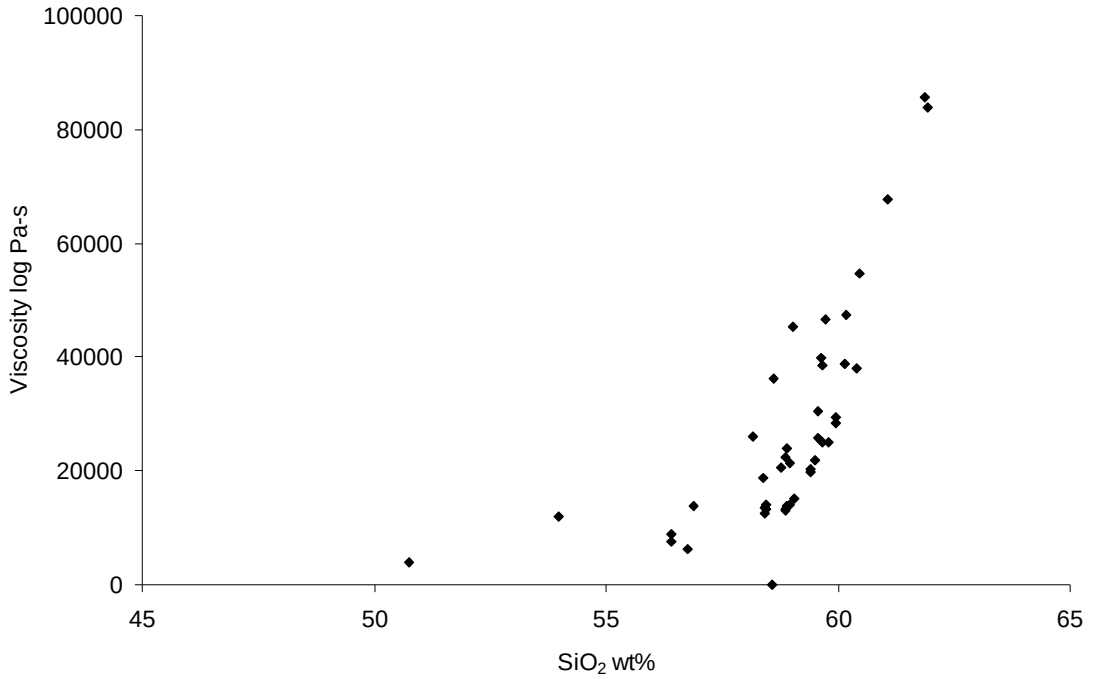

Figure 4.14: *Whole rock viscosity vs SiO_2 content for analysed North Crater deposits.*

North Crater magmas have an average temperature of 1136 °C calculated from whole rock composition (Fig. 4.13, Table 4.2), which is typical of andesitic magmas (1000-1300 °C, Spera 2000). The temperatures are relatively constrained, with the majority of points falling between 1112-1222 °C, with one outlier at 797 °C, however they are higher from the temperature calculated from Fe-Ti geothermometry and it is unclear why this occurs. The method defined by Sisson and Grove (1993) gives no equilibrium or error envelopes when calculating temperature, thus the temperatures calculated using this method may not be any more reliable than those determined using Fe-Ti oxide geothermometry (section 4.6.1). There no clearly defined patterns with varying viscosity and temperature (Fig. 4.13). Temperature, viscosity and SiO_2 wt% all show similar patterns with stratigraphic position in the North Crater sequence (Fig. 4.15). At the start of the eruption initially high temperature and low viscosity magma is erupted, evolving into lower temperature and higher viscosity magma. There is an abrupt change where temperature increases (with decreasing viscosity) in the middle of phase 1

Fig 4.15

(Fig. 4.15), and could indicate the injection of fresh magma into the magma chamber. During phases 2, 3 and 4, temperature and viscosity appears to stabilise, with only minor fluctuations as SiO_2 content varies in the magma. The presence of microlites, phenocrysts, dissolved water and other volatiles are important factors which can influence the viscosity of a magma and may be playing an important role in North Crater magmas.

Table 4.2: *Summary table of physical properties of North Crater melts. Complete data set in Appendix F.*

	Viscosity, log Pa-s (Shaw 1972)	Liquidus Temp, °C (Sisson and Grove 1993).	Melt Bulk Density, kg m-3 (Bottinga and Weill 1972)
Mean	2.69 x 104	1136	2669
Minimum	2.88 x 100	1112	2246
Maximum	8.58 x 104	1222	2831

Bulk density measurements (calculated by Kware MAGMA) determined North Crater magmas to range from 2246-2831 kg m^{-3}, with an average density of 2669 kg m^{-3} (Fig. 4.16, Table 4.2). These results are similar to results calculated in the laboratory (section 3.4.2) for the welded facies, however the calculated bulk densities are slightly higher. By adding FeO, Fe_2O_3, MgO, TiO_2 and CaO to a magma it typically increases its density, whereas adding alkalis typically decreases the magma density. Thus at North Crater with fractional crystallisation occurring and removing mineral phases from the melt containing MgO, TiO_2, Fe_2O_3 and CaO there should be an overall decrease in the melt bulk density with increasing SiO_2 wt% content. Also influencing the melt bulk density is the amount of dissolved water, as only small amounts of dissolved water will dramatically lower melt density and significantly affect other properties such as viscosity (Spera 2000). The production of bubbles in a cooling, crystallising volatile-saturated magma reservoir affects the density of the magma and has a key role in triggering eruptions. Typical magma bulk densities at 1 GPa range from 2720-2660 kg m^{-3} at 1000-1350 °C for andesite, 2620-2580 kg m^{-3} at 800-1180 °C for dacite, and 2550-2500 kg m^{-3} at 800-1000 °C for rhyolite (Spera 2000). North Crater magmas mainly fall within the range of typical andesite magmas. Bulk density shows a similar pattern with stratigraphic position to temperature, viscosity and SiO_2 wt% (Fig. 4.15). The trends in bulk density, temperature and viscosity from the onset of North Crater eruptions are opposite to what would be

expected if a closed system, zoned magma chamber was erupting, and instead indicates an open system with complex magmatic processes is controlling the eruptions at North Crater.

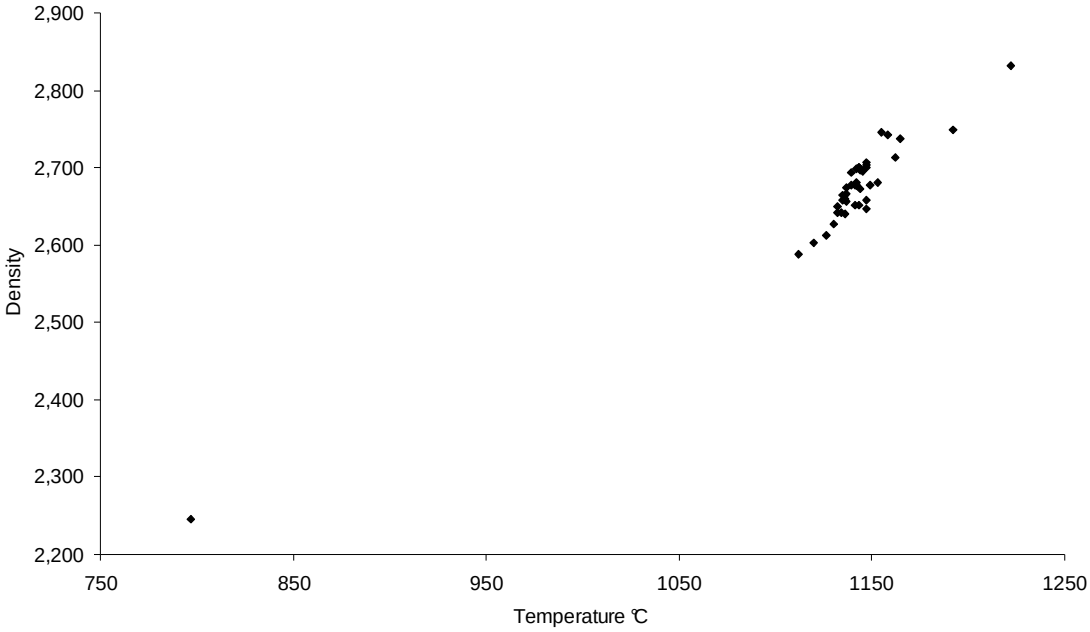

Figure 4.16: *Whole rock bulk density vs temperature for North Crater magmas determined from Kware MAGMA (Wohltez 2005).*

4.9 Summary

Whole rock XRF analysis shows the majority of deposits to be calc-alkaline andesite with limited basaltic-andesite, with the most evolved SiO_2-rich compositions falling in the stratigraphic middle of the North Crater sequence. Harker variation plots of major oxides and trace elements display mainly straight line trends which may indicate magma mingling and processes other than closed system processes to be occurring, i.e. an open magmatic system with multiple magma batches feeding North Crater eruptions. The presence of quartzofeldspathic xenoliths in many of the North Crater samples would indicate that some crustal contamination is also occurring. North Crater deposits show patterns which are similar to other Tongariro vents and the Rotoaira Subgroup.

Plagioclase feldspar is the most abundant mineral phase at North Crater and compositions range from An_{48-77}. Core to rim compositions also vary in many of

the phenocrysts indicating magma disequilibrium, with typically 4-10 mol% An variation within a single phenocryst. Pyroxene is the second most abundant mineral phase, with orthopyroxene compositions ranging from En_{41-70} and clinopyroxenes ranging from $Ca_{39-42}Mg_{41-50}Fe_{9-18}$. Crossed tie lines between clino- and orthopyroxene phenocrysts on a triplot show some pyroxenes in the same rock to be out of equilibrium, indicating mixing and mingling of magmas. Olivine phenocrysts are rarely found in North Crater deposits and range from Fo_{87-76}, and are often rimed by fine grained augite crystals. Fe-Ti oxides occur as abundant spinel and varying rhombohedral (ilmenite) phases. Titanomagmetite ranges from 10.33-18.33 TiO_2 wt% and ilmenite ranges from 46.29-48.55 TiO_2 wt%.

Glass geochemistry show compositions range widely from andesite to rhyolite, with as much as 14 SiO_2 wt% variation within a single clast, indicating large magma heterogeneity. Zones of light and dark coloured glass within single clasts were analysed for chemical differences. Dark glass ranged between 57-71 SiO_2 wt% with a variation of 12 SiO_2 wt% within a single clast. Light glass ranged between 59-73 SiO_2 wt% with a variation of 6 SiO_2 wt% in a single clast. Analyses show that within a single physically mingled clast there are no distinct groupings between the light and dark glass components, indicating that within the subtly contrasting magmas the differences may be more physical (i.e. containing ± microlites) rather than chemical.

Geothermometry calculations with Fe-Ti oxide pairs showed nearly all pairs to be in disequilibrium (according to the Mg/Mn partitioning test of Bacon and Hirschmann (1988)). However the calculations did prove the oxide pairs were formed in different magma bodies and were mingled and erupted together at North Crater. Only one pair fell within the error envelope, indicating equilibrium, and gave a temperature of 898 °C and fO_2 of -11.71.

Magma viscosity, bulk density and liquidus temperature for North Crater samples was calculated using the Kware MAGMA software. Effective viscosity for North Crater magma was determined to range between 2.88×10^0 and 8.58×10^4 log Pa-s, with an average viscosity of 2.69×10^4 Pa-s, which falls within the general range for andesitic magma. Varying magma viscosities in a single magma

chamber or conduit is an effective barrier to efficient mixing between contrasting magmas, resulting in streaky and mingled clasts. Liquidus temperatures have been determined to range generally between 1112-1222 °C, i.e. much higher than that calculated by the Fe-Ti geothermometry. Temperature, viscosity and SiO_2 wt% all show similar patterns with stratigraphic level in the North Crater sequence. Calculated bulk density measurements for North Crater deposits range between 2246-2831 kg m-3, which are similar or slightly higher than those determined in the laboratory. These bulk densities fall within the range for typical andesitic magmas.

Interpretation of these results will provide constraints on eruptive processes from magma chamber to vent dynamics to be determined, and will be discussed in the following chapter.

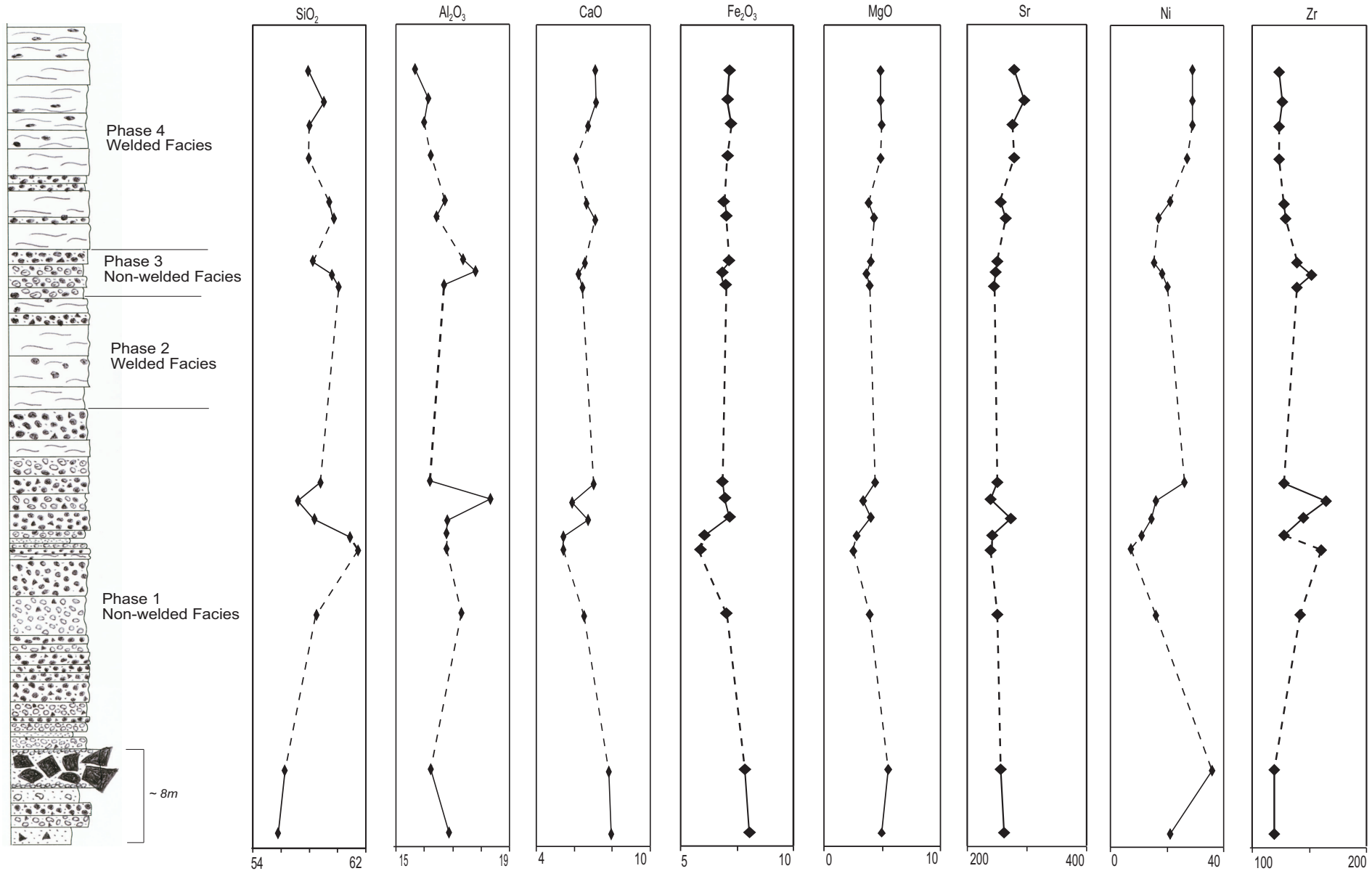

Figure 4.3: *Stratigraphic column of complete North Crater eruptive products,showing vertical variations in SiO_2 wt%, selected major oxides and trace elements through the stratigraphic sequence.*

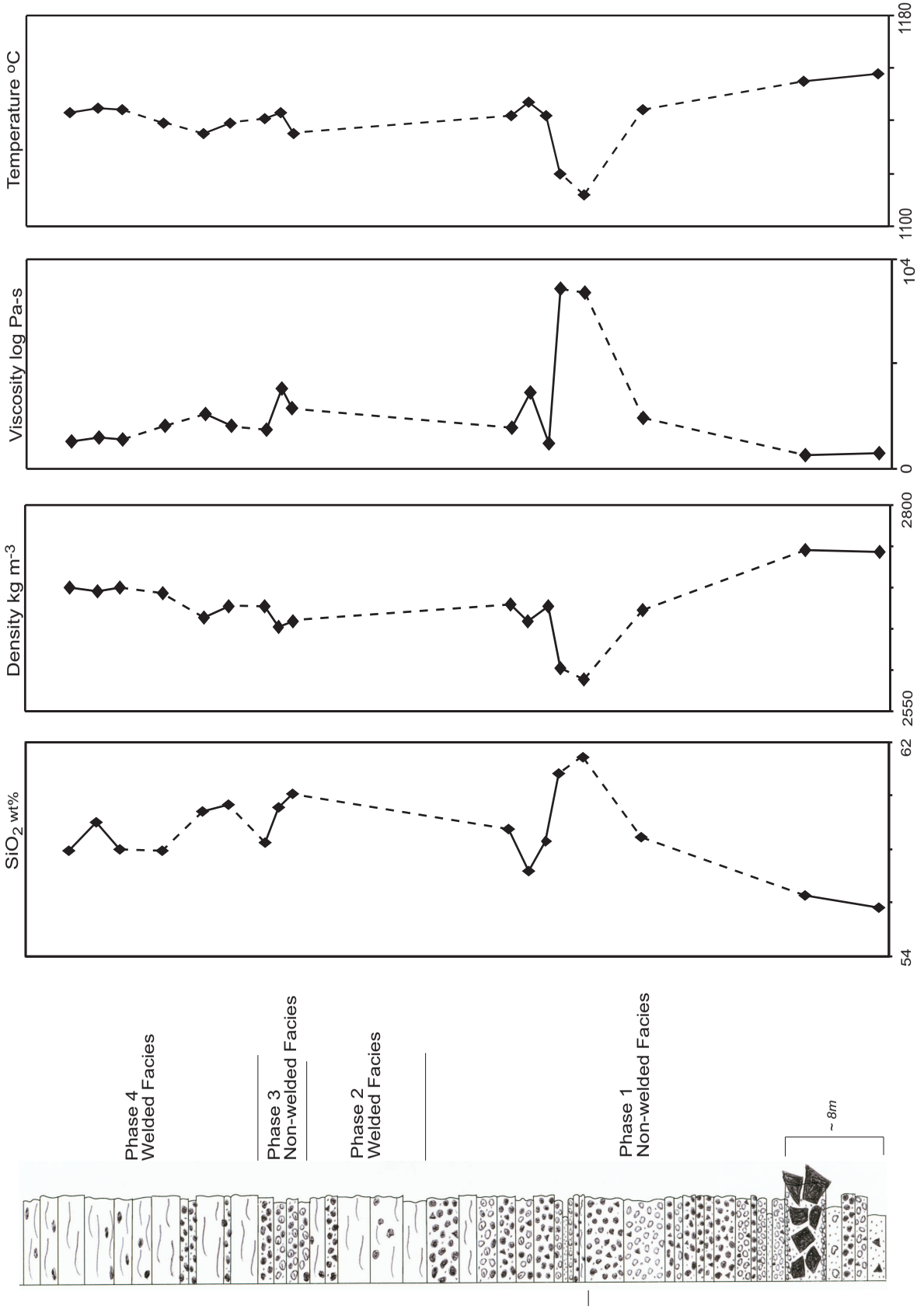

Figure 4.15: *SiO_2 wt%, bulk density, effective viscosity and temperature for North Crater magmas in the complete stratigraphic sequence.*

Chapter 5

Eruptive Processes and History

5.1 Introduction

North Crater is a large composite cone in the north-west quadrant of the TgVC. The major cone forming events, involving sub-plinian and vigorous lava-fountaining activity, took place between 14-12 ka. This chapter discusses the inferred eruptive processes involved in the cone formation of North Crater and describes its eruption history. The hazard impacts associated with a similar North Crater style eruption at TgVC will also be discussed.

5.2 Andesite Cone Volcanism

Most constructional volcano edifices are built from erupted material that extends over the original topography of the vent, and vary in size and shape, where shape is a function of slope angle. At one end of the scale are shield cones characterised by their extremely low slope angles, while composite cones typically have large slope angles around 25-30°, with magma rheology determining the final cone morphology. These large shield and composite cones are produced by multiple eruptions over tens to hundreds of thousands of years and built up of diverse eruptive products. The smallest volcanic structures include lava domes and

scoria/tuff cones, often built from a single eruption episode and are small isolated features (Davidson and de Silva 2000).

5.2.1 Composite Cones

Composite cones are defined as "relatively large, long-lived constructional volcanic edifices, comprising lava and volcaniclastic products erupted from one or more vents, and their recycled equivalents" (Davidson and de Silva 2000). They consist primarily of lava flows that alternate with beds of pyroclastics, often with weak contacts between the layers. They are typically andesitic to dacitic cones found above subduction zones, and are characterised by having the greatest diversity of volcanogenic products over any other volcanic landform (Davidson and de Silva 2000). Composite cones are constructed over long periods of time with frequent large eruptions, with the location of the volcanism remaining relatively constant at a single vent (Marti and Ernst 2005). Geophysical studies at active composite volcanoes have identified the presence of shallow (5-10 km) magma chambers, confirmed by petrographic studies identifying plagioclase rich porphyritic magmas typical of shallow reservoir depths. It is also typical for composite cones to have pyroclasts showing evidence of intense magma mixing, typical of shallow magma systems (Marti and Ernst 2005). Fractionation and magma mixing at shallow levels may produce the range of magma types seen in composite cones (Wohletz and Heiken 1992).

The volcano flanks are built up by multiple lava flows, pyroclastic deposits and reworked volcaniclastic material forming a distinctive conical shape (Marti and Ernst 2005). Changes in magma composition during an eruption may result in Vulcanian or Plinian activity and the formation of higher convective plumes forming pyroclastic fall units and pyroclastic flows. Fall deposits will mantle the landscape while pyroclastic flows will follow gullies and streams down off the volcano. It is also common at composite volcanoes for debris avalanches to occur and produce widely dispersed and large volume deposits on the lower slopes and ring plain (Davidson and de Silva 2000). Phreatic activity may also occur at composite cones when magma comes into contact with a crater lake, groundwater or a hydrothermal system. Explosive steam eruptions result without the eruption of juvenile tephra or fine-grained ash falls (Wohletz and Heiken 1992).

5.2.2 Compound Volcanoes

A compound volcano is defined as a "volcanic massif formed from coalesced products of multiple, closely spaced, vents" (Davidson and de Silva 2000). Formation of compound volcanoes is favoured when eruptions at a vent are small to moderate in size and relatively frequent (Davidson and de Silva 2000). The formation of a compound volcano could occur as activity migrates over time in response to a moving volcanic front or subduction zone, or migration may be random. Ruapehu volcano is a good example of a compound volcano.

5.2.3 Cone Complexes (e.g. Tongariro Volcano)

Cone complexes are large structures made up of a concentration of closely-spaced, but discrete and partially overlapping cones (Davidson and de Silva, 2000). Tongariro is a good example of a composite cone complex as it comprises of about 30 relatively small, closely spaced vents (Hobden 1997). Because of the random structure of overlapping cones and no basement exposures, complex geometries can exist, and it is often difficult to estimate individual cone volumes (Davidson and de Silva 2000).

5.3 Styles of Andesitic Explosive Activity

Eruptive activity at cone volcanoes is characterised by a diversity of styles and mechanisms which produce a wide range of eruptive products.

5.3.1 Lava Fountaining

Typical Hawaiian style activity usually involves basaltic eruptions with very low viscosity magma (10-100 Pa s) where a pillar-like jet of molten pyroclasts and gas is sprayed hundreds of meters above a central vent where the height of the fountain is controlled by the magma volume flux and volatile content (Wolff and Sumner 2000). They are the least violent form of volcanism with subdued intensity, magnitude and dispersal power as a consequence of low viscosity, and during an erupting episode a vent may expel approximately 50-1000 m^3s^{-1} of lava (Vergniolle and Mangan 2000). Intense lava fountaining volcanism may also

occur in magmas of other compositions (i.e. basaltic andesite or peralkaline rhyolite) when erupted magma is still gas rich and has higher eruption velocities, resulting in large, high lava-fountains which may be sustained for several hours or days (Vergniolle and Mangan 2000; Marti and Ernst 2005). Lava fountaining is a relatively uncommon style of explosive activity at andesite cone volcanoes, but was apparently the dominant mechanism during the later stages of North Crater eruptions, so is considered in some detail.

Fountain structure is determined by the velocity profile and the maximum spread angle, i.e. if it is a narrow jet or a broad spray, but is also dependent on magma gas content and effusion rate (Francis 1993; Sumner *et al.* 2005). High mass effusion rates result in collimated fountains and a high fragment accumulation rate on the ground (Sumner *et al.* 2005). Eruption temperatures are highest in the centre of the fountain, where it is optically thick and has a high clast density creating the incandescent yellow-white glow typical of fire fountains (Francis 1993; Sumner *et al.* 2005). Typical temperatures have been found to range between 1150°C and 1216°C (Vergniolle and Mangan 2000). The outer part of the fountain is the fiery red-orange region where the temperature is cooler, clast density is lower and is optically thinner. This region passes into a sparse, black ring of chilled pyroclasts (Fig. 5.1) (Vergniolle and Mangan 2000).

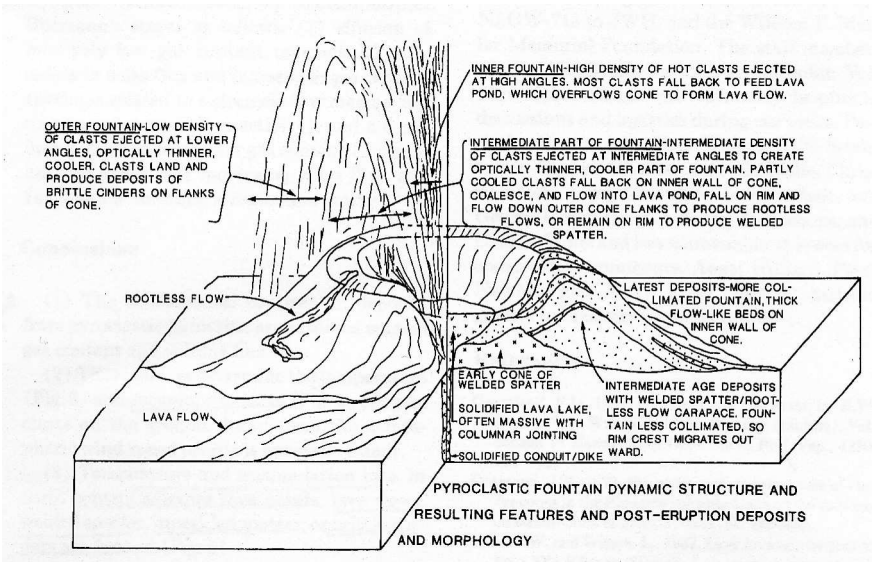

Figure 5.1: *Lava-fountain dynamic structure and associated eruption facies typical of most lava-fountains. From Head and Wilson 1989*

Fragmentation of magma by volatile degassing, and high magma rise rates are the main mechanisms driving lava-fountaining (Wolff and Sumner 2000; Marti and

Ernst 2005). The degree of fragmentation in Hawaiian style volcanism is typically poor resulting in relatively large clots up to several tens of centimetres. Because of the large clast sizes many pyroclasts may remain molten during transport and completely coalesce after fallout to form clastogenic lavas if typical basaltic lava, otherwise welded spatter piles may build up around the vent and form agglutinate or welded deposits (Fig. 5.1) (Francis 1993; Parfitt 2004; Marti and Ernst 2005; Sumner *et al.* 2005). Other smaller clasts or those on the outside of the fountain may cool sufficiently during flight to be deposited as solid tephra or scoria around the vent. Hot fragments may also cool during flight when there is a higher fountain as they have further to travel (Parfitt 2004; Marti and Ernst 2005).

Due to the coarseness of the pyroclasts and the low eruption column associated with Hawaiian style volcanism ejecta usually fall close to the vent, and no further than about 500 m. They can form spatter cones, ramparts and other conical deposits with steep sides, or coalesce to form rootless lava flows, and rates of cone building may exceed 5 mhr^{-1}. A dilute convective plume incorporating volcanic gas, aerosols and ash forms above the erupting fire-fountaining column and contain less than 0.17% of the total mass of lava erupted during typical Hawaiian style volcanism (Vergniolle and Mangan 2000). However, during vigorous andesitic lava-fountaining, concurrent sub-plinian plumes have also been observed (Sumner 1998; Yasui and Koyaguchi 2004).

5.3.2 Strombolian Eruptions

Often associated with lava-fountaining is Strombolian style volcanism. This type of activity involves gas being released as discrete, often rhythmic, bursts which break the cooled surface of the magma column or lava lake and eject a shower of incandescent lava fragments (Parfitt 2004). As the clasts are often already cooler than from lava-fountaining, and cool rapidly during flight they are unable to weld or coalesce on landing and build up loose tephra or scoria cones around the vent (Parfitt 2004). It is not uncommon for rapid changes between fountaining and strombolian style activity as magma rise rates in the conduit fluctuate during an eruption (Vergniolle and Mangan 2000; Parfitt 2004; Schmincke 2004). True strombolian deposits are rare within the North Crater sequences but are important processes at other Tongariro vents (Hobden 1997).

5.3.3 Agglutination and Welding

As defined in chapter 2, agglutination is the instantaneous syn-depositional adhesion and kinetic deformation of clasts, while welding is the post-depositional compaction of a hot pyroclastic deposit under its own weight (Wolff and Sumner 2000). Agglutination occurs syn-depositionally with the adhesion and deformation of hot, fluid clasts on deposition, where clast outlines are partly or wholly retained (Sumner *et al.* 2005). Agglutination typically requires lower viscosities and higher temperatures than simple welding, and clasts with viscosities of less than or equal to 1000 Pa-s agglutinating. These low viscosities and hot temperatures are typical of the inner portion of a basaltic lava-fountain; however as clast viscosities increase with decreasing temperature only the larger fragments will experience deformation on landing. Framework agglutination may occur where piles of predominantly ridged clasts are stuck together by the extruded hot, fluidal cores of bombs (Sumner *et al.* 2005). Welding occurs after deposition to become a coherent rock through load-pressure deformation of the hot, plastic fragments which 'stick' together at point contacts (Wolff and Sumner 2000; Sumner *et al.* 2005). The key factor influencing welding is the clast accumulation rate, with welding favoured when clasts at the surface of the accumulating deposit are unable to cool significantly before being buried and are of a larger clast size. For hot clasts deposited at low accumulation rates, cowpat bombs are common, while high accumulation rates form the compacted and deformed spatter deposits. Also important is if the number density of the falling hot pyroclasts is great enough to minimise radiative heat loss from the falling clasts and accumulation pile (Sumner *et al.* 2005). When welding is accomplished in a matter of seconds it is possible for the deposit to begin to flow and form a clastogenic lava flow (typical in basaltic fountaining eruption), however the development of yield stress from the progressive groundmass crystallisation may be enough to preserve agglutination piles and prevent the formation of clastogenic lava flows (Wolff and Sumner 2000). It is important to note that there is a continuum between agglutination and welding processes which reflects the varying eruption intensity and magmatic properties such as gas content, temperature and crystallinity (Sumner *et al.* 2005).

5.3.4 Andesitic Lava Fountaining Case Study

Izu-Oshima, Japan 1986

Izu-Oshima is a volcanic island of basaltic-andesite composition in central Japan, approximately 100 km SSW of Tokyo where lava-fountain eruptions in 1986 occurred through vents located in the central crater zone (Mannen 2006). Lava-fountaining activity began on 15 November from a fissure in the central crater (fissure A) reaching a climax on 16 November followed by a shift to paroxysmal explosions that continued until 21 November. Late in the day on the 21st a fissure erupted suddenly (fissure B) in the crater floor and produced an eruption column and lava-fountaining reaching several hundred meters and dispersing scoria fallout. This fissure eruption fed a large scoria cone and lava flows as it was accompanied by renewed lava-fountaining activity from fissure A; however the intensity of fissure A was considerably weaker (Sumner 1998; Mannen 2000; Kaneko and Wooster 2005). Lava-fountaining at fissure B initially was mild, but abruptly intensified approximately 50 minutes after the onset of the eruption, the maximum plume height was reported to be 16 km. However accurate information with regard to plume height was difficult to obtain due to limited visual observations. These fissure eruptions ceased in the early hours of the 22nd (Mannen 2006). The fountain behaviour at fissure B progressed from intermittent strombolian through violent strombolian and sustained lava-fountaining at the climax of the eruption. The style of fissure B eruption was not typical Hawaiian style as the fountains were unusually high (1600 m) and developed an associated sub-plinian plume (10-16 km, Sumner 1998). Basaltic andesite lava flows that formed from the fissure B eruption contained remnant clast outlines indicating the flows were spatter fed or clastogenic, and interpreted to have formed by syn-depositional agglutination and coalescence (Sumner 1998). Fountaining also produced an elongate scoria cone from oblique fountain structure which contained beds of incipiently welded, highly vesicular lapilli scoria to highly welded, poorly vesicular, flattened and ragged clots and lumps of agglutinate (Sumner 1998).

Deposits produced around the vent during the eruption at Izu-Oshima were mainly in the form of spatter ramparts and a scoria cone. Sequences through the scoria cone show black and red-brown scoria, bombs and rare lithic fragments. The

scoria and bombs display varying degrees of welding and vesicularity, and the units are often weakly bedded with gradational contacts. Within the scoria cone the beds range from incipiently welded, red-oxidised, highly vesicular, granular scoria to highly welded, dense, poorly vesicular, black, flattened clots and lumps of agglutinate (Sumner 1998). These beds were formed from active lava-fountaining which lasted about 4 hours and built the cone to approximately 40 m. Welded deposits have been formed by the larger clast sizes, with black ribbon-like, elongated clasts and sub-parallel alignment while moderately to incipiently welded units consist of smaller, granular, oxidised, sub-round to sub-angular scoriaceous clasts (Sumner 1998).

North Crater deposits on the upper cone, and the final stages of the eruption, are similar to the deposits in the scoria cone of Izu-Oshima. North Crater welded units are of the larger grain size, while moderately welded units are typically finer grain size. The units also are similar in texture, with the strongly welded deposits having similar ribbon-like, elongated black scoria clasts with nearly no pore space, while the moderately welded units are more granular, sub-angular to elongate and often oxidised.

5.3.5 Sub-Plinian Volcanism

Sub-plinian style volcanism is associated with high eruption plumes which produce widespread tephra sheets blanketing the topography. Plume heights can be sustained for moderate to long periods of time and often reach heights of 20-30 km. Eruptions involving dacite and rhyolite magma are usually involved, but eruptions involving more mafic compositions are also common (Francis 1993).

It is often difficult to separate out sub-plinian from plinian eruptions, but simply put eruptions in the lower ranges of magnitude (~10^{11} kg) and intensity (discharge rate ~10^{6} kg/s) can be classified as sub-plinian, while plinian eruptions will have magnitudes of 10^{11}-10^{13} kg and discharge rates of 10^{6}-10^{8} kg/s. Changes in magma degassing, viscosity, ascent rate and conduit geometry conditions through the eruption can also result in sub-plinian activity (Martin and Nemeth 2006). Sub-plinian activity is often characterised by discharge variations resulting in short phases of sustained eruption separated by varying time breaks or other

eruption styles. The varying discharge rates can result in formation of pyroclastic density currents (PDC) related to unstable conditions in the eruption column. PDC deposits are typically interbedded with fall deposits with no signs of interruption in the fall record (Cioni *et al.* 2000). Because of the lower ranges in magnitude sub-plinian tephra dispersal will be smaller compared to plinian eruptions (Walker 1973). Typical thickness half-distances (b_t) for sub-plinian eruptions are 0.5-4 km, while plinian eruptions have typical b_t values of 2-10 km (refer Fig. 5.7) (Cioni *et al.* 2000).

Complex fragmentation processes are thought to occur during sub-plinian eruptions due to the unsteady and varying nature of the eruption plume (Cioni *et al.* 2000). It is thought syn-eruptive degassing and viscosity increases in a magma column during the filling of the conduit may result in the alternation between sustained columns and relative quiescence. Magma crystallising rapidly in the degassed portion of the conduit causes magma stagnation, and results in build up of pressure eventually reopening the conduit (Sable *et al.* 2006). Each new pulse of the sub-plinian plume may be associated with dome growth and destruction, indicating an important control of volatile content and magma rheology. The varying nature of sub-plinian eruptions could also result from the differences in magma discharge at the surface and rates of magma supply from the magma chamber (Cioni *et al.* 2000).

5.3.6 Pyroclastic Flows and Fallout

Pyroclastic Flows

Two major mechanisms for transport of pyroclastic flows exist and are distinguished by the density of the emerging jet with respect to the atmosphere, i.e. buoyant versus non-buoyant behaviour (Wilson and Houghton 2000). Two end-member types of pyroclastic density currents have been identified, dilute and concentrated, where dilute currents are known as pyroclastic surges and concentrated currents are known as pyroclastic flows (Wilson and Houghton 2000). When an eruption column is formed, the stability is dependent on the density/buoyancy of the column, mass eruption rate and volatile content. If a column (or part of the column) is denser than the atmosphere it will collapse once it leaves the gas thrust region near the vent and loses its momentum collapsing

under gravity. As the erupted mass collapses the potential energy gained in the eruption is transformed to kinetic energy driving the mass at high speed across the ground (Francis 1993).

Dilute currents can travel at tens of meters per second, contain <0.1-1 vol.% of solids and are density stratified with highest particle concentration closest to the ground. The material is primarily transported by turbulent suspension, with a small population salting or sliding along the ground surface (Wilson and Houghton 2000). They typically produce relatively thin, bedded or cross-bedded to massive deposits which can have large run-out distances, about 10 km for sub-plinian eruptions (Valentine and Fisher 2000). Dilute currents generate a secondary buoyant plume or ash cloud which rises off the flowing mass (Wilson and Houghton 2000).

Concentrated density currents travel at similar speeds to surge flows, and velocities greater than 200-300 ms^{-1} have not been observed but can be inferred from the heights of obstacles climbed. These concentrated flows contain tens of volume percent of solids, have a free surface above which the solids concentration diminishes rapidly and transport the material by a combination of particle-particle contact, fluidisation support, matrix support, dispersive pressure and buoyancy (Wilson and Houghton 2000). Turbulence may or may not be present in the flow, but is not dominant as a particle support mechanism like in surge flows (Wilson and Houghton 2000). Ignimbrites and block and ash flow deposits are the product of concentrated density currents and are predominantly massive, poorly sorted, ash-rich deposits laid down by a particulate, gaseous flow. Ignimbrites are pumiceous, ash-rich deposits, while block and ash flows are small-volume deposits containing dense to moderately vesicular juvenile bombs and blocks in an ash matrix (Freundt *et al.* 2000).

Pyroclastic Fall

Pyroclastic fall deposits are produced by the fallout of clasts from an eruption plume during an explosive eruption and are highly variable depending on the kind of eruption, changes in eruption style, composition and distance to source (Francis 1993; Houghton *et al.* 2000). Pyroclastic falls are of two main types: ballistic fall

produced from gas-thrust, and convective fall from a buoyant plume. Ballistic fall and cone accumulation is favoured when clasts are too coarse to be buoyant in the plume, and the distance travelled is a function of initial gas exit velocity and ejection angle. Convective fall is favoured when finer material (ash and lapilli) is buoyant in the plume and falls from the umbrella region; dispersal is a function of plume height, fall velocity and wind. These convective falls mantle the landscape and are typically well sorted, decreasing in grain size with distance from source (Houghton *et al.* 2000).

5.3.7 Andesitic Sub-Plinian Case Study

Asama Volcano, Japan, 1783

Asama volcano is an andesitic cone in central Japan which produced a three month long sub-plinian to plinian eruption during 1783. During the eruption period the eruption styles changed with time from pumice falls through pyroclastic flows to lava flows. The eruption has been divided into six phases, each representing a single eruptive event during the three month eruption. The four initial phases of the eruption from May to early August were characterised by vertical eruption columns producing widespread ash fall and intense pyroclastic falls and intense rumbling and earthquakes (Yasui and Koyaguchi 2004). Phase five is considered to be the climax of the Asama eruption when the duration of eruptive phases and mass of erupted magma increases exponentially. Activity at the onset of phase five was characterised by four sub-phases of plinian activity each lasting 4-5 hours with or without the generation of pyroclastic flows. This was followed by an increase in the eruption intensity and the generation of a pyroclastic flow. The later stages of phase five culminated in a large scale plinian eruption which lasted for ~15 hours and produced a diverse range of deposits with contrasting modes of emplacement, such as pyroclastic flows, lava flows, construction of a cone and pumice falls. A few hours after the close of phase five a large pyroclastic flow and debris avalanche was generated from either an explosion at the summit, a flank eruption or secondary explosion disrupting a lava flow, and is the final phase of the 1783 eruption at Asama (Yasui and Koyaguchi 2004).

The pyroclastic fall deposits produced during the 1783 eruption consist of many thin pumice and ash beds, with dominantly pumice beds in the uppermost, later stage deposits. Those ash beds dispersed in the upper units are thought to be derived from ash clouds of pyroclastic flows. The pyroclastic cone is interpreted to have formed during this eruption from lava fountaining coeval with a plinian eruption and is now scattered with loose lapilli, ash and bombs from eruptions post-1783. The units associated with the 1783 eruption consist of alternations of welded and non-welded deposits, with cooling features such as columnar joints apparent in the densely welded deposits. Partial failure of the cone produced a small lava flow to the north of the cone and is inferred to have occurred during the final stages of phase five (Yasui and Koyaguchi 2004). Pyroclastic flows are widely distributed toward the northeast and reach up to 8 km from the vent. Small, non-welded, scoriaceous pyroclastic flows and associated ash layers interbedded with pumiceous fall material are interpreted to have formed from partial plinian column collapse during the initial stages of phase five. Flow units consisting of dark brown scoria blocks and matrix are characterised by strong welding, with oxidization in the upper 30 cm, while other non-welded scoriaceous flow units are characterised by strong reverse grading. Some thin welded layers are interpreted to have formed by agglutination, rather than post-depositional welding, while the presence of dense blocks indicates generation from collapse at the cone. Andesite lava flows are also recognised on the cone, one is interpreted to be a rootless flow and formed from partial collapse of the cone. The other two identified flows display surface features and internal structures which suggest they were originally formed from rheomorphism of pyroclastic material, i.e. clastogenic lava flows (Yasui and Koyaguchi 2004).

5.4 Nature of North Crater Eruptions

In this section the dynamics and processes involved in the ~14 ka eruption at North Crater will be discussed in detail. Magma chamber processes will first be discussed and interpreted from the geochemical and textural data analysed in the preceding chapters, as well as discussion on the possible eruption triggers. This will be followed by discussion and interpretation on the magma ascent and vent dynamics from the textural analysis and physical properties of the magma. The

final processes involved in the eruption will be discussed by interpreting depositional processes and the cone formation at North Crater, Tongariro.

5.4.1 Magma Chamber Processes

Textural characteristics of North Crater clasts, phenocrysts and glass and whole rock geochemical analysis allows for the interpretation of magma chamber processes occurring beneath North Crater. It has previously been established that andesitic magma is produced beneath TgVC by complex magmatic processes involving fractional crystallisation and assimilation in an open, complex plumbing system associated with the nearby subduction zone (Graham and Hackett 1987; Hobden 1997; Price *et al.* 2005). The porphyritic texture of the plagioclase-dominated pyroxene andesites of North Crater is indicative of derivation from magmas which ascended slowly and stagnated at shallow depths in the crust prior to eruption. The inclusion of crustal xenoliths also indicates some crustal assimilation occurred during magma rise from depth.

Physical evidence for magma mingling and mixing is strong in North Crater magmas with the presence of glass colour banding, phenocryst sieve textures and reverse and oscillatory zoning (see chapter 4). Physical mingling is visible in many clasts associated with North Crater deposits as banding of dark and light glass. Geochemical analysis has identified the compositions of these glasses to be similar in composition, but slight variations indicate the mingling of magma prior to eruption. Composition of the magma alone does not account for the distinct physical differences between the two glass types, indicating other properties play a major role in controlling the differences. The presence of microlites in only the dark glass may influence the cooling rate of the magma and account for these observed differences.

The heterogeneous nature of North Crater SiO_2 content also indicates mixing and mingling of subtly contrasting magmas prior to eruption (see chapter 4). Variation exists within the majority of units found on North Crater, even those deposits and clasts which appear physically homogeneous. Glass SiO_2 compositions for proximal deposits range from 57.66 to 73.72 wt%, and within one clast there is as much as 14 wt% SiO_2 variation. These wide ranging compositional variations

indicate complex shallow level magma chamber processes and mingling of magmas.

SiO_2 trends through the North Crater stratigraphic sequence indicate complex processes are also occurring during the eruption (refer Fig. 4.15). At the start of phase 1 it appears there has been some triggering event to completely overturn a stratified magma chamber, which has lead to the eruption. A large semi-isolated magma chamber residing in the shallow crust beneath North Crater may have differentiated by fractional crystallisation and assimilation (AFC), which has had a magma injected into it, of a similar composition, from a neighbouring chamber. A marked change in SiO_2, viscosity, temperature, and density part way through phase 1 indicates the reinjection, replenishment or incorporation of a more silicic, cooler magma, possibly fed from a neighbouring chamber, either into the erupting chamber, or connected and fed straight to the conduit, mingling with the erupting magma there. The presence of mingled and disequilibrium textures in phenocrysts throughout phase one would indicate mingling of magmas is occurring either in the magma chamber or in the conduit immediate prior to eruption. Due to the lack of data for the final stages of phase 1 it is difficult to interpret magma chamber processes occurring in the later stages. Mingling of magmas appears to be persistent throughout most of the eruption, due to the presence of mingling and disequilibrium textures in many of the deposits.

It is possible some of the phenocryst sieve textures represent resorption due to decompression, although some phenocrysts display sieves in distinct breaks and ringed sieved zones which indicate magma mixing and mingling (Sigurdsson *et al*. 1990, Browne *et al.* 2006; Humphreys *et al*. 2006). Often in the same rock there may be a combination of zoned or unzoned phenocrysts, with or without sieve and resorption textures, suggesting the mingling of two partially crystallised magmas (Nakagawa *et al*. 2002).

Trends on Harker variation plots of both whole rock major oxides and trace elements show fractional crystallisation or magma mingling to be the main magmatic processes occurring at North Crater. However the presence of abundant xenoliths in the majority of deposits indicates crustal assimilation was also an

important process. No systematic changes with time are apparent in any of the variation plots indicating the emptying of a simple zoned magma chamber was not involved in the North Crater eruptions. Instead semi-isolated magma batches may have been mingled and overturned prior to eruption. Magma bodies which have interacted have not been able to sufficiently mix and completely homogenise prior to eruption and instead produced mingled magmas. The lack of trends with height through key stratigraphic sections around North Bluff (refer Fig 4.15) also indicates there is no progression through time and magma mingling must be occurring.

Strong evidence for magma mingling is the variation between Fe-Ti oxides in North Crater deposits. Only one Fe-Ti pair was found to be in equilibrium (using the Mg/Mn method of Bacon and Hirschmann 1988), while all the other pairs all fell outside the equilibrium envelope indicating disequilibrium. Disequilibrium between Fe-Ti oxide pairs suggests crystallisation in different magma bodies which have then mingled and erupted relatively quickly, inhibiting re-equilibration. Disequilibrium between a few analysed orthopyroxene and clinopyroxene phenocrysts from the same clast is also apparent, and also suggests magma mingling from separate magma chambers (Sigurdsson *et al.* 1990).

The evidence for magma mixing and mingling at North Crater is strong, with variations in phenocryst textures, crystal disequilibrium and varying whole-rock geochemistry, indicating multiple, small, semi-isolated magma batches feeding North Crater eruptions. It may be there is feeding into and mixing of magmas inside a single magma chamber prior to eruption, however mixing and mingling inside the conduit may also be occurring for some (or all) of the magmas.

5.4.2 Eruption Trigger

It has been suggested by many authors (e.g. Sparks *et al.* 1977; Eichelberger 1980; Huppert *et al.* 1982; Takeuchi & Nakamura 2001; Nakagawa *et al.* 2002; Carrasco-Nunez *et al.* 2005; Beier *et al.* 2006) that the intrusion of a physically and chemically contrasting magma into the base of a magma body would drastically alter the equilibrium causing the magma at the base of the chamber to

become superheated. The superheated magma would then be less dense than the overlying magma and vigorous convection will be initiated along with vesiculation. The heating and vesiculation cause pressures to increase inside the magma chamber, resulting in fractures to form in the volcano and an eruption to be triggered (Sparks *et al.* 1977).

It has also been suggested that 'second boiling' of a dominant volatile phase may be an effective eruption trigger (Turner and Verhoogen 1960; Tait *et al.* 1989; Woods and Cardodo 1997). This occurs when the intermediate to silicic magma cools and crystallises, causing volatiles (water) to become increasingly concentrated in the residual melt, eventually becoming saturated and exsolved causing a rise in the magma pressure and resulting in eruption. In basaltic melts the dominant volatile phase is carbon dioxide which during second boiling causes decreases in the magma chamber pressure. As the volatile bubbles separate and rise the decompression of the rising bubbles can increase the chamber pressure and trigger the eruption (Turner and Verhoogen 1960; Tait *et al.* 1989; Woods and Cardodo 1997). If pressures in the shallow chamber grow to around 10 MPa it is sufficient to trigger an eruption. As the magma chamber convects bubbles will rise and be concentrated near the roof, allowing the base of the chamber to become progressively undersaturated, while the concentration of bubbles near the roof causes the volatile content of the lower magma to decrease. Magma tapped from this volatile rich upper portion of the magma chamber may lead to explosive lava-fountaining (Woods and Cardodo 1997).

Another model has been suggested for eruption trigger involving bubble rise and overpressure of a closed magma system (Pyle and Pyle 1995). However as the magma system at North Crater, and TgVC, is considered to be an open magmatic system, this model is thought to be unlikely.

The presence of olivine crystals partially or completely reacted to clino- or orthopyroxene may indicate the injection of a melt into a slightly contrasting magma chamber beneath North Crater resulting in olivine disequilibrium. The injection of a contrasting melt may have caused excess pressure in the magma chamber and ultimately lead to eruption. As suggested earlier (see chapter 4) there

may be an event immediately prior to the start of phase one of the North Crater eruptions which has initiated the convection and overturning of the semi-isolated magma chamber, and lead to the subsequent eruption by increasing pressure, vesiculation and caused the fracturing of country rock. This triggering event would have caused the neighbouring magma bodies to become unstable and possibly help feed the eruption via the connecting plumbing system.

Although the evidence is strong for the eruption to have been triggered by the injection of a contrasting magma, it is not possible to discount the likelihood of the eruption, or a later phase, being triggered by second boiling. It may also be possible the later phase of the eruption was also triggered and fed by a magma chamber which had undergone second boiling.

5.4.3 Magma Ascent and Vent Dynamics

As ascending magma nears the Earth's surface it becomes a mixture of gas and liquid. In magmas of low viscosity, eruptions may involve decoupled degassing, where gas bubbles are able to move relatively quickly up through the slowly ascending magma and erupt effusively. However, the presence of dissolved gas in mafic magmas will result in explosive volcanic eruptions, unless significant gas is lost prior to eruption (Parfitt 2004; Sable *et al.* 2006). When magmas are more silicic, coupled degassing occurs where gas bubbles are immobile to the magma and rise at the same speed (Sable *et al.* 2006). Eruptive behaviour is related to the ability of magma to degas through bubble permeability and the degree of bubble coalescence. Bubble permeability is related to the rate of magma ascent as bubbles grow and coalesce as a result of lower pressure (Jaupart 1996; Szramek *et al.* 2006). Typical Hawaiian style lava-fountaining is associated with low degrees of bubble coalescence and high magma ascent rates, which lead to partially coupled behaviour in the shallow conduit.

Two models have been suggested for the formation of lava-fountaining in mafic magmas, which could be applied to the formation of lava-fountaining in andesitic magmas. The first, termed the rise speed dependent model (RSD), depends on the rise rate of magma and bubbles in the conduit (Head and Wilson 1987; Parfitt *et*

al. 1995; Parfitt and Wilson 1999). The magma and gas rise as a homogenous, partially coupled, 2-phase flow and gas bubbles grow from diffusion and decompression. When the bubble fraction becomes large enough the magma will fragment. The rising magma will accelerate as it rises due to the decompression and expansion of gas, and after fragmentation the acceleration will become more pronounced due to the reduction in conduit wall friction. This will result in the continuous eruption of jetted magma clots and gas. This eruption model is very similar to that for plinian eruptions, although the larger grain size produced during lava-fountaining compared with plinian eruptions is the main difference (Parfitt 2004).

The second model, termed the collapsing foam model (CF), suggests magma and gas rise as a separate 2-phase flow, with the rise rates of the two phases significantly different. This may occur when bubbles collecting at the top of a magma chamber form a foam which then collapses, with bubbles coalescing into a large gas pocket. Lava-fountaining eruptions then occur from the complete and instantaneous collapse of the foam which then rises as a single body up the conduit. This is termed annular flow where the rising gas core is surrounded by magma which is dragged up the conduit margins and erupted with the gas core (Jupart and Vergniolle 1988; Jupart 2000; Parfitt 2004). The collapsing foam model has been investigated by many authors, but a review by Parfitt (2004) concludes this separated 2-phase flow for Hawaiian eruptions does not stand up to detailed scrutiny and existing observational evidence suggests lava-fountaining is produced by homogenous two-phase flow (the RSD model) (Parfitt 2004).

At North Crater, eruptions were not typical Hawaiian style fire-fountains involving basaltic magma, however, we can assume the andesitic magma displayed similar high magma ascent rates and homogenous 2-phase flow to allow the formation of lava-fountains. To form lava-fountaining of andesitic magmas there must have been sustained high magma ascent and eruption rate, with low to moderate, partially coupled gas content. The viscosity of andesite magma is usually not as low as that of basalt (typical of Hawaiian style fire-fountaining) so features such as spatter piles are typically preserved around the vent, rather than formation of clastogenic lava flows (Wolff and Sumner 2000).

Changes in exsolved volatile content and vesiculation rates can lead to changes between explosive andesitic lava-fountaining and plinian style eruptions (Sable *et al.* 2006). Assuming magma chamber pressure and conduit radius do not change, variation between explosive plinian and vigorous lava-fountaining can be controlled by the gas content at the vent, specifically the mass fraction of exsolved gas (Jaupart 1996). Sub-plinian and plinian eruptions involve coupled degassing which allows high magma ascent velocities to produce an explosive eruption. Plinian eruptions are favoured over Hawaiian style eruptions when bubble nucleation is initially delayed, volatile supersaturation develops in the magma and final bubbles nucleate without coalescence accompanied by major acceleration. If the amount of exsolved gas increases, then magma fragmentation will also increase resulting in a decrease in the mean clast size (Sable *et al.* 2006). As the mass flux becomes larger and the clasts become more crowded and stay hotter for longer the coupling between clasts and gas permits the change to buoyant or collapsing plumes and generation of pyroclastic falls and flows (Head and Wilson 1989). This coupled degassing occurs when the melt is viscous and bubble coalescence is inhibited, and is common in high-silica magmas (Sable *et al*. 2006; Szramek *et al*. 2006).

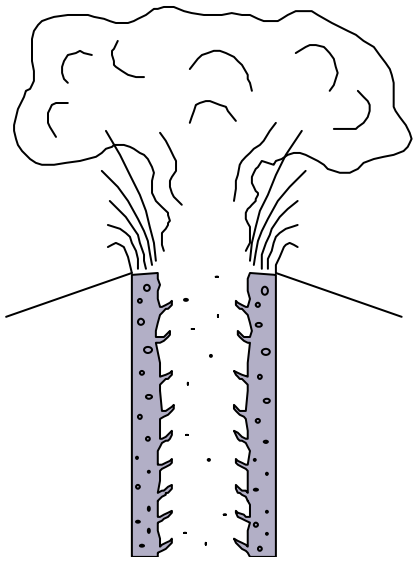

Figure 5.2: *Zones of pumice, scoria and mingled clast formation. Scoria forms in the slower moving more degassed and cooler conduit margins. Pumice forms in the faster moving, hotter central conduit. Mingling between the two zones can occur to form the mingled clasts. Scoria and mingled clasts erupt as lava-fountain and ballistic fallout, pumice erupts in an eruption plume.*

During the explosive eruption plume phase magma may be carried initially by laminar flow at high ascent rates with similar bubble rise speeds. When the magma begins to rapidly vesiculate and reaches a gas content of greater than 75% the magma will fragment and rise as a dispersed flow, where magma fragments are carried by the rapidly expanding gas (Jaupart 2000). The intensity of the andesitic explosive behaviour is determined by the amount of gas decoupling from the melt, which is a function of the relative bubble and melt ascent rates and extent of bubble coalescence. The rapid magma ascent in the eruption plume phases could also have been induced by the rapid decompression of the magma as it rose rapidly from depth.

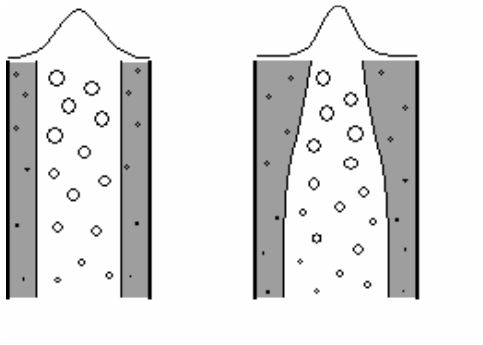

a) early phase b) later phase

Figure 5.3: *Cartoon diagram depicting the conduit at different stages of the North Crater eruptions. Curved lines along top represent laminar velocity profiles near fragmentation surface. a) early phase eruptions dominated by gas-rich, highly vesicular magma, with minor gas-poor magma present, b) later phase eruptions dominated by gas-poor, poorly vesicular magma, with smaller proportions of gas-rich magma (modified from Sable et al. 2006).*

The texturally mixed facies suggests lava-fountaining may have occurred concurrently with an eruption plume at North Crater. This may have occurred by the formation of a velocity profile over the conduit width. Near the margins of the conduit the flow will be slower due to viscous drag, allowing minor crystallisation, bubble coalescence and partial degassing, forming cooler, more crystalline and more vesicular clasts. Magma ascent rates will be higher towards the centre of the conduit and allow the formation of hotter, poor to finely vesicular clasts (Sable *et al.* 2006). Black scoria clasts tend to show higher vesicularities and larger coalesced bubbles, indicating formation along the cooler, slower moving, conduit walls. Pumice tend to show finer, more regular bubble shapes indicating formation in the central, high velocity portion of the conduit. Coupled flow would be able to develop in the central zone and allow explosive fragmentation of the gas region (Sable *et al.* 2006). Formation of mingled clast

textures could occur in the magma conduit prior to eruption where a velocity gradient produces slightly physically contrasting magmas. The magma from the centre of the conduit may mingle with the magma from the conduit walls at the fragmentation surface, resulting in mingled textures formed by contrasting magma cooling rates, bubble coalescence and crystallisation (Figs. 5.2 & 5.3).

Vent and conduit geometry are also important in controlling the eruption dynamics, as they may not remain the same shape during a single eruption. If the magma flow is energetic and powerful it may be enlarged by erosion or partial collapse, and often the presence of wall rock lithics in volcanic deposits will attest to this (Jaupart 2000). In a low intensity eruption the vent may become choked by the cooling of magma along its margins and close up. Conduits vary in width often from 10-100 m depending on the style of eruption, and will flare out at the surface, the vent being much larger in width than the conduit (Jaupart 2000). The stability of an eruption column also depends on the vent radius, along with magma discharge rate, exit velocity and exsolved water content (Cioni *et al.* 2000). If there is a large vent radius then typically a collapsing column will be produced, if the magma discharge rate increases or the exit velocity decreases then a collapsing column will also be produced (Cioni *et al.* 2000). The presence of minor shallow-derived wall rock lithics in the majority of North Crater deposits would indicate the vent underwent some modification by erosion. Crater collapse could have also occurred during the explosive sub-plinian eruptions in order to form the large summit crater/vent and lead to a collapsing column producing pyroclastic flows.

5.4.4 Depositional Processes & Cone Formation

Lava-Fountaining

Lava-fountain heights are a function of several different factors; the amount of exsolved gas in the magma, the eruptive volume flux, amount of re-entrainment of degassed lava, the magma rise speed and subsequent degree of bubble coalescence and hence magma degassing (Parfitt *et al.* 1995). Theoretical and observational analysis predict that exsolved magma gas contents of about 0.4 wt% (Head and Wilson 1989) should result in fountain heights of about 200 m for basaltic eruptions. However as andesitic magma typically contains a larger wt% (sometimes up to 6 wt%, Wolff and Sumner 2000) of exsolved gas, resulting lava-

fountains are expected to be higher, and more vigorous, than those involving basaltic magma (e.g. Izu-Oshima, Japan, ~1600 m lava-fountain, Sumner 1998). Factors such as lava-re-entrainment, shallow vent ponds and bubble coalescence can significantly reduce the height of the fountain or even suppress fountains completely (Parfitt *et al.* 1995). Magma gas content and eruption rate also determine the structure of the lava-fountain by influencing: a) size distribution of pyroclasts; b) velocity and spread angle of pyroclasts leaving the vent; and c) the continuous nature of the eruption (sustained fountaining) (Head and Wilson 1989). The structure of the fountain is closely linked to the structure and morphology of near vent deposits and the build up of material around the vent.

The spread angle of the fountain and the magma eruption velocity determines the path of pyroclasts in a fountain, cooling times and accumulation rates on the ground. Two main factors are important in controlling the structure and morphology of lava-fountain deposits: a) temperature of clasts as they land on the ground, and b) the accumulation rate of clasts on the ground. The relationship between pyroclastic temperature and accumulation rate defines a broad area in which most types of pyroclast deposits occur (Fig. 5.4) (Head and Wilson 1989).

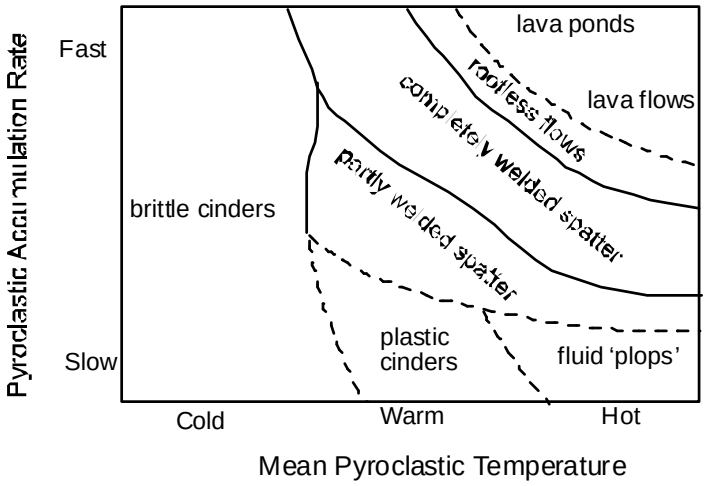

Figure 5.4: *Pyroclastic/deposit diagram illustrating the relationship between mean pyroclastic temperature and pyroclastic accumulation rate. From Head and Wilson (1989).*

For cold clasts falling from the outer portion of the fountain accumulation rate is irrelevant and scoria/cinder cones are formed. Warm clasts with low accumulation rates typically produce plastic scoria and framework-agglutinated spatter ramparts, high accumulation rate yield completely welded spatter, while moderate

accumulation rates produce partly welded spatter and build up spatter cones. Hot clasts with low accumulation rates form individual fluid bombs or cowpat bombs (Sumner *et al.* 2005), while high accumulation rates often produce lava flows and ponds through clast coalescence (Fig. 5.4); these are associated with the inner hottest part of a lava-fountain. Due to the range of temperatures produced in a spreading fountain at any one time a range of deposits can be formed from a single fountain (Head and Wilson 1989). Rapid accumulation of clasts as a scoria or spatter cone allows a cone to be built around the vent with often thick deposits formed from a vigorous, sustained lava-fountain. However, the degree of welding progressively decreases away from the vent as clasts become finer and cool during longer flight times (Head and Wilson 1989; Stevenson and Wilson 1997; Sumner *et al.* 2005).

Cone formation at North Crater occurred in part from vigorous lava-fountaining producing strongly welded deposits and agglutinates, some of which contain sub-parallel stretched ribbon clast outlines which indicate rapid accumulation of hot pyroclasts which have deformed on impact. Some lateral transport may have occurred to produce the strongly attenuated and thin ribbon like clast outlines in these intensely to strongly welded deposits. Thick welded deposits are present near the crater rim predominantly on the northern, western and southern sides. The overall fall origin (with some lateral transport) and unit thinning is consistent with initial deposition from a lava-fountain (Allen 2004; Sable *et al.* 2006).

Flow textures in welded deposits provide some information on the emplacement processes during eruption. Agglutinated and welded deposits can have wavy clast ribbons which interfinger laterally and are evidence of spatter fed lava where semi-fluidal clasts have undergone shear movement after deposition from a sustained lava-fountain. Complete homogenisation of these spatter-fed units may be prevented by cooler clast rims on deposition (i.e. North Crater strongly welded facies), however where no clast outlines are visible and the units appear homogenous clast coalescence may have occurred (i.e. North Crater intensely welded facies) (Stevenson and Wilson 1997). Where spatter accumulation rates exceed agglutination rates (very high eruption intensity) then the porosity of the deposit will be reduced and particle outlines will be eliminated. Clast outlines, and

sometimes poorly welded basal zones will only remain at the basal contact where rapid cooling on contact with the ground preserves clast shapes (Stevenson and Wilson 1997). At Pantelleria, Italy (a peralkaline rhyolite volcano) the association of welded, spatter fed lavas interbedded with pyroclastic fall units supports a fountain-fed eruptive origin. The lava-like units have been interpreted to have formed by clast coalescence after fallout from a sustained lava-fountain due to the presence of smeared spatter and ribbon-like features. These features indicate a clastogenic, fallout origin with clasts undergoing agglutination, and post-depositional shear movement to attenuate and smear clasts (Stevenson and Wilson 1997). These features in the strongly welded units at Pantelleria are similar to the features seen in the intensely and strongly welded facies from North Crater, indicating fallout from a vigorous lava fountain is occurring.

At Summer Coon volcano, Colorado, spatter rich deposits have been interpreted as deposited by pyroclastic flow, as large flattened clasts are deposited against each other at a low angle imbricated pattern (Valentine *et al.* 2000). Other features such as clasts stretched into tatters on their lee side, from shearing of the overriding current, coarse tail grading and abundance of lithic clasts at the base of the units also indicates deposition from pyroclastic flow (Valentine *et al.* 2000). The changes in welding with distance from vent also indicates the initially welded units have been deposited by pyroclastic flow mechanisms. Pyroclastic flow deposition of spatter-rich deposits has also been suggested at Santorini, Greece, by the presence of contorted and folded spatter clasts, as well as slight clast imbrication and changes in welding with distance from vent (Mellors and Sparks 1991).

The lack of imbrication and concentration of dense lithics at the base of some moderately welded facies at North Crater, like those at Summer Coon and Santorini, suggests that deposition occurred via fallout from a vigorous lava-fountain, rather than as a spatter-fed pyroclastic flow. Some units in the moderately welded facies, where clast outlines are retained and there is no clast imbrication or fine matrix, suggests the accumulation rate from the lava-fountain must have been low enough to restrict compaction and retain clast shapes, although still hot enough to cause post-depositional welding. A few units within

the moderately welded facies however do show some faint imbrication and fine matrix, these units also change down slope to poorly welded and indicate a pyroclastic flow origin.

Comparison of North Crater welded deposits with spatter agglomerate in the Siwi pyroclastic sequence, Tanna, Vanuatu, would also indicate the majority of North Crater welded deposits have formed from fallout from a sustained lava-fountain which have then undergone lateral transport. The proximal Siwi spatter agglomerate lacks evidence for lateral deposition due to the variable nature of welding, lack of matrix and layering of clasts parallel to the basal slope profile. The distribution of the Siwi spatter agglomerate, up to 1 km from the vent is also within the range predicted to be plausible for "ballistic" fallout (Fig 5.5) (Allen 2004). The Siwi spatter agglomerate also shows medial variations that indicate pyroclastic fallout has undergone lateral transport by pyroclastic flow as clast imbrication and ash matrix become apparent. These lateral changes, such as reduced welding with distance from vent and incorporation of fine matrix, are apparent in some units of the welded facies at North Crater indicating a change to pyroclastic flow deposition may have occurred further from the vent after the main deposition by lava-fountain fallout (Allen 2004).

These welded North Crater deposits are confined primarily to the main cone area due to magma physical properties and fountain dispersal, but build up and strengthen the cone. Because of the dispersal over most of the upper cone, initial fountain heights must have been high and spreading with high magma ascent rates. Wind direction may have also played an important role in the dominance of these deposits to the north, west and south. The large crater structure formed during the explosive sub-plinian eruption would have trapped some of the hotter lava which fell from the centre of the lava-fountain. The accumulation of lava in this crater would have lead to increased degassing of the magma and re-entrainment of the lava into the fountain, resulting in lower spreading fountain heights and accumulation closer to the vent in the later stages of the fountaining episode.

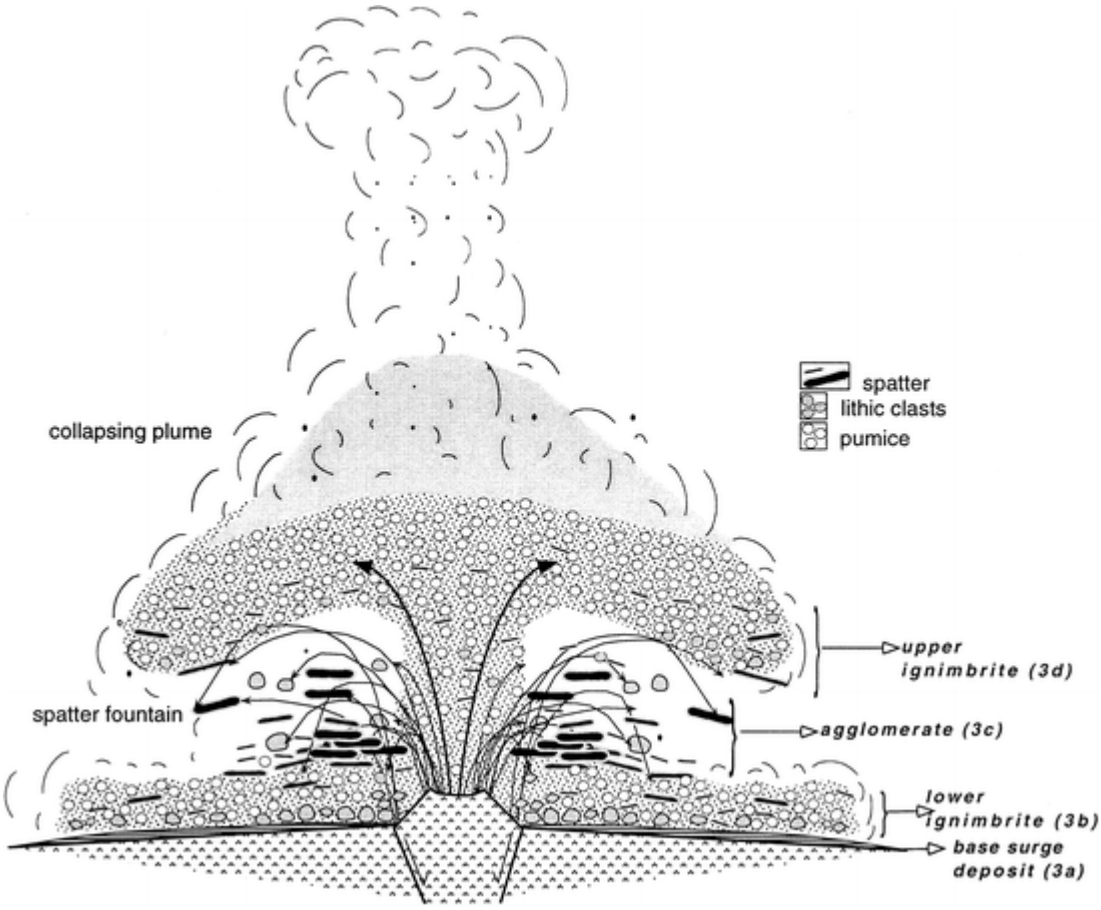

Figure 5.5: *Production of spatter fountain in association with a partially collapsing plume during the Siwi pyroclastic sequence. Produced spatter agglutinate and pumiceous flow deposits. From Allen (2004).*

Sub-Plinian Fallout

A sub-plinian eruption is a scaled down version of a plinian eruption and are often a very common eruption style (Mannen 2006). There is a continuous gradation in the magma discharge rate between plinian and sub-plinian eruptions and often a clear distinction cannot be made between the two deposits based on their fragmentation and dispersal (Mannen 2006; Cioni *et al.* 2000). However Walker (1973) suggest sub-plinian eruptions have a dispersal area of 5-500 km, while plinian eruptions have a dispersal area of more than 500 km. Lower degrees of fragmentation correspond to sub-plinian eruptions and generation of fine particles in a mafic sub-plinian eruption is less than that in a Plinian, but considerably higher than fragmentation in a Hawaiian eruption (Mannen 2006).

Based on the mapping of the Rotoaira Lapilli by Doyle (2006) it is possible to determine the thickness decay of the fallout associated with the eruption plume at North Crater. The thickness decay (b_t) has been calculated from Doyle's (2006) isopach map to be about 1 km, while the clast half distance (b_c) has been

calculated at about 3.5 km. This would indicate the North Crater eruption to involve a sub-plinian to plinian eruption plume (Fig. 5.6). However, Doyle (2006) notes that erosion during and post-eruption of the Rotoaira Subgroup means a loss of the complete tephra record has occurred and her isopach map can only be taken as minimum values. One facies on North Crater has been described as having originated from a buoyant sub-plinian plume with fallout deposition in the proximal environment at North Crater; this facies has been correlated to the distal Rotoaira Lapilli found on the ring plain. These units are interpreted to be deposited as fallout from a buoyant sub-plinian to plinian plume due to their massive bedding, relatively well sorted character and thickness decay rates.

In the distal environment the orangey yellow pumice beds are separated by distinctive dark grey ash beds. Previous authors (e.g. Topping 1974; Doyle 2006) have suggested these ash beds have been reworked (due to their massive to discontinuously cross bedded nature) and are not the original deposits. New work (this study) involving SEM analysis of the ash from these units reveals intense clast rounding (Fig. 3.12, group two) has occurred as no delicate glass textures remain (indicating lateral transport). This confirms the early suggestions of these deposits having undergone reworking and lateral transport. Due to the reworked nature, it is difficult to suggest an original origin/mode of transport for these ash units. They may have originated as ash cloud or co-ignimbrite surge deposits rising off a pyroclastic flow. These pyroclastic flow and associated ash cloud deposits have been observed at various volcanoes (e.g. Unzen, Japan, and Merapi, Java, Freundt *et al.* 2000; Bezymianny, Belousov *et al.* 2002). However, these ashes may also represent products from a phreatomagmatic eruption, due to their poorly vesicular nature, which have undergone lateral transport and abrasion after initial deposition.

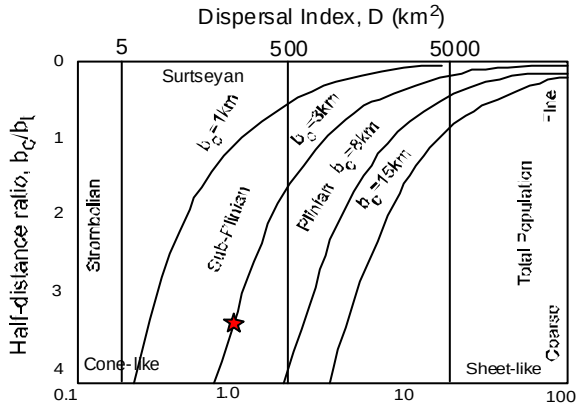

Figure 5.6: *Classification for explosive eruptions based on characteristics of fall deposits,star indicates North Crater eruption dispersal, from Pyle (1989).*

Pyroclastic Flows

Collapsing eruption plumes are common when magma discharge rates increase, amount of exsolved water decreases, eruption velocity decreases or the vent radius increases due to erosion and collapse (Cioni *et al.* 2000). If there was an initially buoyant plume then collapse may be achieved by an increase in magma discharge rate or extraction of a magma progressively depleted in volatiles (Cioni *et al.* 2000). The formation of pyroclastic flows from an initially buoyant eruption plume is a function of the plume's density, if the plume is less dense than the surrounding atmosphere then it can rise buoyantly, otherwise collapse occurs. Pumice and scoria flows are formed from dense eruption columns which collapse under gravity. They form pumice and scoria flows which contain abundant fine matrix material, are poorly sorted, contain moderately vesicular round to sub-round clasts, and are massive to reversely graded and often show a fine basal shear zone (Freundt *et al.* 2000; Wilson and Houghton 2000).

At Fuji volcano, Japan a pyroclastic flow facies has been described which consists of basaltic bombs, scoria lapilli and lithics supported in an ash matrix. The pyroclastic material which fell onto the steep slopes (>33 degrees) was unstable and tumbled down slope and were remobilised as granular flows. However in the main facies the poor sorting and massive appearance are characteristic of deposition from a highly concentrated hot flow and produces poorly to moderately welded deposits (Yamamoto *et al.* 2005). Pyroclastic flow deposits at Latera Volcanic Complex, Italy, also display massive, poorly sorted and fine basal shear zone characteristics. These deposits are interpreted to have formed by

concentrated, high-energy pyroclastic flows (Taddeucci and Palladino 2002). These massive flow deposits at Mt Fuji and Latera are similar in appearance to the massive flow deposits observed on North Crater, and display similar componentry, sorting and welding characteristics, so it is possible to interpret these North Crater deposits as having formed by highly concentrated, high-energy pyroclastic flows.

Experimental work by Taddeucci and Palladino (2002), Cagnoli and Manga (2005) and Choux *et al*. (2004) have found that during lower energy granular flows density and size segregation will occur. Cagnoli and Manga (2005) found that in a mixed density flow lighter particles (vesicular pumice and scoria) moved toward the top, while denser particles (lithics) moved toward the bottom. In polymodal size flows larger clasts always moved to the top, while smaller clasts always moved toward the bottom. These features produce reverse graded deposits and can be interpreted as being produced by lower-concentration, lower-energy granular flow of cooler or cooled clasts to produce non-welded deposits (Cagnoli and Manga 2005). On North Crater reverse graded facies are present and due to the nature of the grading and non welded appearance it is possible to interpret them as having formed by lower-energy granular flow. These North Crater deposits are similar to those deposits seen at Latera Volcanic Complex which display reverse grading, non-welding and are interpreted to have formed by lower-energy, lower-concentration pyroclastic (granular) flow (Taddeucci and Palladino 2002).

Lava-fountaining concurrent with eruption plumes have been observed at a number of volcanoes in recent history (e.g. Izu-Oshima, Japan, Sumner 1998; Asama volcano, Japan, Yasui and Koyaguchi 2004). Small spatter fountains simultaneous with eruption plumes have been described in the Siwi pyroclastic sequence, Tanna, Vanuatu, where scoria spatter clasts are present in varying amounts in the pumiceous flow units. This indicates the small-scale lava-fountain persisted during formation of a partially collapsing eruption plume (Allen 2004). Allen (2004) also suggests the combination of scoria spatter and pumice clasts in a deposit are a feature of explosive eruptions involving relatively low-viscosity magma and a wide vent. Few descriptions have been made on the conditions in

the magma chamber and vent which lead to simultaneous eruption of lava-fountains and eruption plumes, although a scenario for this concurrent activity was suggested in section 5.4.3, and may produce a fountain and plume similar to that described by Allen (2004) (Fig 5.6).

The presence of the texturally mixed massive bomb mingled facies at North Crater may indicate lava-fountaining with a concurrent partially collapsing eruption plume. The presence of end-member pumice and scoria along with mingled and streaky clasts may indicate the mingling of lower velocity, cooling conduit margin magma with central high velocity conduit magma just prior to fragmentation as discussed earlier. Conduit margin and mingled magma would be erupted as a small lava-fountain, while central conduit magma would be erupted as pumiceous partially collapsing plume material. A collapsing plume would then produce pyroclastic flows which would incorporate ballistic material falling from the fountains producing the poorly to non welded mingled facies.

Pyroclastic fall and flow deposits would have rapidly accumulated and built up the cone, becoming stable by welding and compaction forming a cone with slopes of ~30°. The dispersal of these deposits would have been controlled by the topography of the neighbouring vents and the proto-North Crater vent. The presence of Tongariro Trig and Blue Lake vents would have controlled the deposition of the pyroclastic flows toward the north and west, and eruption through the proto-North Crater vent allowed the existing cone to be built over. The lack of Rotoaira Lapilli deposits to the west and south of North Crater would also indicate wind direction played an important role during the sub-plinian eruption, controlling the deposition of plume fallout to the north and east.

5.5 North Crater Explosive Eruption History

Phase 1

Explosive eruptions at North Crater may have been triggered by mixing of compositionally similar andesitic magmas from adjacent shallow magma reservoirs, or from the ‘second boiling’ of volatiles in a magma chamber. It has

been suggested eruptions at Blue Lake (or other unknown northern Tongariro vents, T Kobayashi, pers. comm. 2006) may have started prior to North Crater (Hobden *et al.* 2001) and may have caused other nearby magma chambers to become unstable. The injection of magma or second boiling caused overturning and mingling of a shallow, fractionated magma chamber which lead to pressure increases and likely triggered the onset of eruption at North Crater about 14 ka ago. Magma chambers and vents may have been established during eruptions of the proto-North Crater, with the new eruptions occurring from the same summit vent system. Magma ascent rates were high due to the increased magma chamber pressure forcing magma towards the surface and resulting in delayed vesiculation and explosive fragmentation to form a sub-plinian eruption of gaseous magma. The sub-plinian eruption formed a buoyant plume and produced pyroclastic fall deposits (distal Rotoaira Lapilli) as well as small, localised pyroclastic flows from the collapsing low margins of the plume (Fig. 5.7). The pyroclastic fall material consisted mainly of finely vesicular, pumiceous lapilli, while the pyroclastic flow material consists mainly of moderately to highly vesicular scoriaceous bombs and blocks with limited pumiceous material. These differences could be due to the velocity profile developed over the width of the conduit allowing slower moving, cooler and more vesicular magma to form along the margins, and fast moving, hotter and poorly vesicular magma to form in the centre of the conduit and erupt as a sub-plinian plume. The slower moving, cooler material near the margins may have been erupted as ballistic material and as part of a partially collapsing column. Just prior to fragmentation these contrasting magmas may have undergone mingling in the conduit, to produce the physically contrasting but chemically similar mingled clasts. At some stage during this phase it is thought the vent has undergone erosion and collapse to produce a wide vent radius and allow a change from predominantly buoyant plume activity to predominantly collapsing plume activity (Fig. 5.7).

Midway through phase one there is a sudden geochemical, viscosity and temperature change, indicating the incorporation or injection of a contrasting magma into the conduit. Once the eruption at North Crater had been triggered other chambers in the complex system beneath North Crater would have become unstable and caused other magma chambers to feed into the eruption via the

network of feeder pipes. The new magma incorporated into the system appears to still be gaseous and explosive, with high ascent rates which has continued to result in an explosive eruption forming predominantly pyroclastic flow deposits and minor fall deposits. The conduit mingling of magma is still persisting throughout this phase due to the presence of mingled units and indicates small scale fountaining was occurring with the collapsing eruption plumes. The presence of dense wall rock lithics throughout this explosive phase indicates vent erosion is still occurring.

Phase 2

The onset of vigorous lava-fountaining marks the start of phase 2 and marks a change from explosive fragmentation and eruption at North Crater (Fig. 5.7). The deposited hot, semi-fluidal pyroclasts are initially deposited as fall deposits close to the vent and welded and agglutinate together forming thick intensely to strongly welded deposits which have undergone some lateral transport. Further from vent these deposits have undergone a change to pyroclastic flow transport and deposition which have tapered out with distance and produce some moderately welded deposits. Other moderately welded deposits show no flow features and are thought to be produced solely from fallout from a lava-fountain. The sharp contact between these welded units would indicate breaks between unit depositions were long enough to allow sufficient surface cooling. Fluctuating fountain heights may have been an important controlling factor in this phase. There may have been a weak buoyant plume stoked off the top of the lava-fountain allowing deposition of minor ash fall deposits which may only be visible in the medial to distal environment.

Phase 3

At the start of phase 3 a new physically different but compositionally similar magma batch may have been tapped, which was gas rich, and as this began to rise rapidly, delayed vesiculation would have caused shallow-level fragmentation and resulted in an explosive, collapsing eruption plume (Fig. 5.7). The presence of mingled and disequilibrium textures through out this phase would indicate the explosive eruption may have been triggered by the injection and mingling of contrasting magmas into the plumbing system below. This has resulted in a short

lived collapsing plume with concurrent small-scale lava-fountaining and the deposition of localised pyroclastic flow deposits many of which display mingled textures. Concurrent lava-fountaining has been produced in the same way as described from phase one. Minor erosion of the enlarged vent has occurred with the presence of dense wall rock lithics throughout this phase.

Phase 4

The initiation to vigorous lava-fountaining may mark the climactic phase of the North Crater eruptions at the start of this phase. The magma contrasts between marginal and central conduit zones becomes more pronounced in the early stages of this phase and the fragmentation surface becomes dominated by the gas-poor magma at the conduit margins (Fig. 5.2); alternatively the proportion of degassed magma may have increased during the later stages of the eruption by tapping of a gas poor magma chamber, from the same or a separate vent. During this phase vigorous lava-fountaining dominated involving a high spreading fountain, with deposition occurring initially from fallout from the fountain with subsequent lateral transport and change to pyroclastic flow further from the vent (Fig. 5.7). The dominance of intensely welded facies and associated gas-poor magma in the final stages of the eruption could be due to the fallback and accumulation of hot lava in the central crater and the formation of a degassing lava body.

Phase 5

Late stage eruption through the accumulated lava body would cause waning towards the end of the eruption due to the completely degassed nature of the body as eruption rate slowed significantly (Fig. 5.7). At the Amphitheatre dipping beds of welded pyroclasts are seen to butt up against the solidified ponded lava, indicating these deposits had cooled significantly to retain the lava in the central crater. It could be possible the magma rise rates were still high enough to inject magma into the crater, but the presence of the cooling and degassed ponded lava was enough to inhibit lava-fountaining and eruption. This would have instead caused the lava lake to continue to rise as magma was injected into the bottom and low fountain heights. The eruption would have ceased when magma rise slowed and stopped completely.

Fig 5.7

- Ponded lava

After the main explosive eruptions ceased the ponded lava would continue to degas and cool significantly over the following months. Heat would be lost rapidly from the surface by radiation and convection, and more slowly from the walls and floor by conduction of heat into the surrounding rock. A study at Kilauea volcano, Hawaii, on the Alae lava lake found the 15 x 250 m lava lake cooled and solidified after about 400 days (Schmincke 2004), so it could be possible to assume the North Crater ponded lava took a similar or longer time as it is much wider (~1000 m diameter), but has an undetermined depth (but at least 70 m deep from depth of explosion pit). The presence of platy jointing, and folded structures seen in the middle section of the solidified lava (see Fig. 2.17) would suggest that while the upper and lower portions had sufficiently cooled, lava in the centre was still hot and fluid enough to move and overturn causing the folded and platy structure.

- Explosion Pit

The formation of the explosion pit is interpreted to have occurred prior to the Taupo ~181 AD eruption due to the presence of Taupo pumice on the summit plateau and inside the explosion pit. The explosion pit reveals the platy, massive and jointed internal structure of the solidified lava lake, and must have been formed sometime after the complete cooling and solidification of the ponded lava. Deposits from the explosion pit consist mainly of large (>1 m) blocks, found up to 700 m from the pit, and assorted smaller blocks and debris. The pit forms a slight rise above the crater plateau and consists of prismatic jointed lava which may have formed from the growth of a partially degassed lava dome prior to the initial (possibly steam driven) explosion. The presence of nearby Ketetahi geothermal area may have caused pressure build up beneath the crater and resulted in the explosion at North Crater.

5.6 Hazard Impacts of a North Crater Style Eruption at Tongariro Volcanic Centre

Previous work on Tongariro has identified limited evidence for small-scale pyroclastic flows, however this study has identified multiple, extensive layers of welded and non-welded andesitic pyroclastic material which are the products of extremely hot pyroclastic flows associated with explosive lava-fountaining and eruption plume activity. These flow deposits represent a potentially devastating

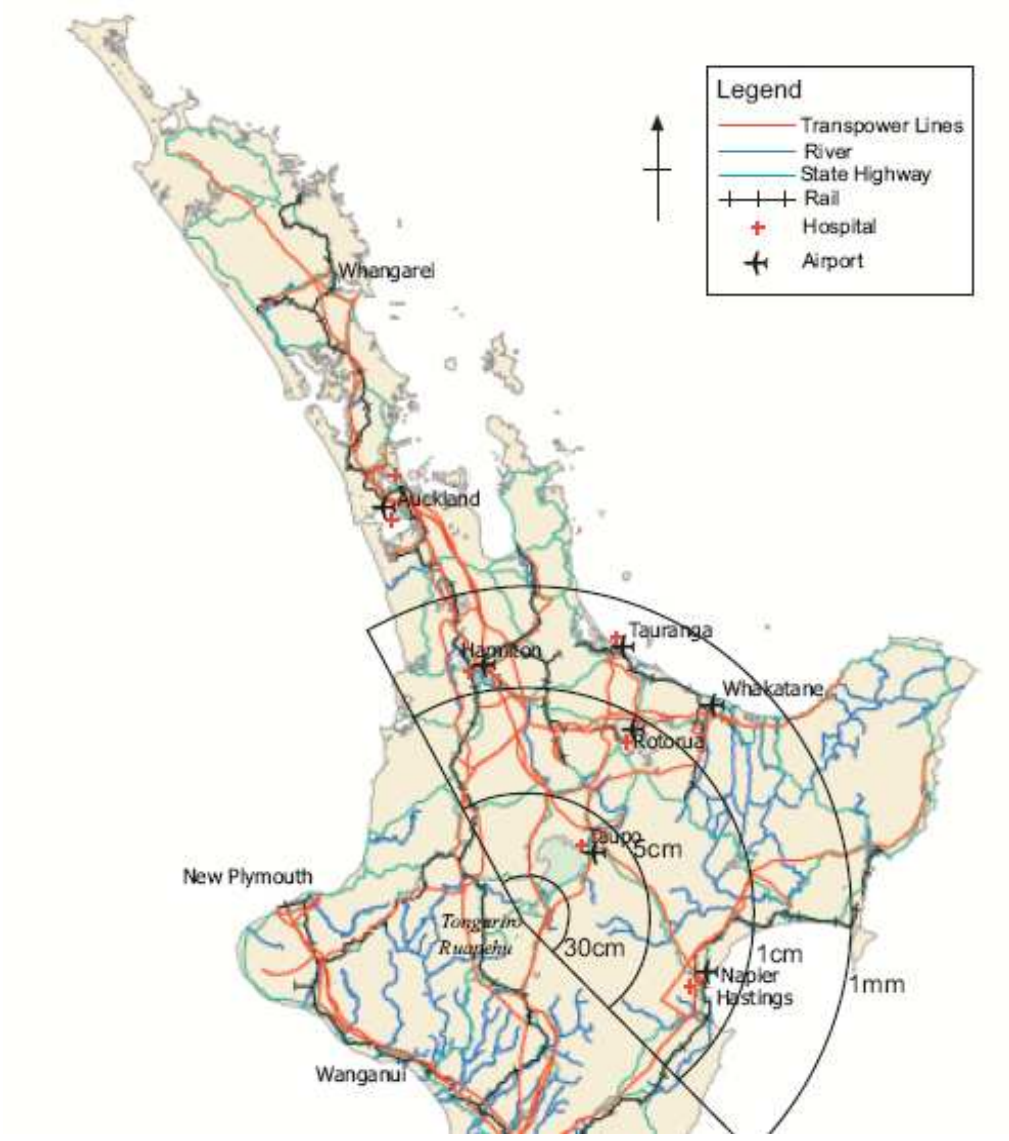

Figure 5.8: *Isopach map showing generalised ash fall thickness from a sub-plinian – Plinian plume associated with an eruption at Tongariro with prevailing SW winds. Main lifeline networks are shown to indicate the extent of the damage in the central North Island. Map based on field observations of fall deposits from past North Crater eruptions.*

hazard which may impact on a wide area of the central North Island. The pyroclastic rocks have been interpreted to be the products of hot, initially turbulent mass flows of frothy andesite spatter, shed from the margins of a vigorous, pulsating incandescent fountain or sub-plinian plume.

Pyroclastic flows occurred simultaneously with widespread fall deposits at North Crater as the eruption intensity varied and produced flows of varying energy, most travelling at least 3-4 km from the vent. Flows to the north and west were the hottest, and as flows moved down slope depositing material and losing heat and mass they became more granular. Associated with these hot pyroclastic flows were hot and turbulent ash clouds. These ground-hugging flows were extremely mobile and ash layers found in road- and trackside sections to the north of North Crater are interpreted as ash cloud deposits associated with North Crater pyroclastic flows. The widespread fall deposits consisting of ash and lapilli layers were deposited up to 20-40 cm thick on the Tongariro ring plain and record the fallout from a high sub-plinian plume (Fig. 5.8). Dispersal from this convecting plume was probably episodic, and concurrent with vigorous explosive lava fountaining of varying intensity.

Ballistic fallout from a high, vigorous fire-fountain would pose less of a hazard than the pyroclastic flows and associated ash clouds, as much of the risk would be contained to within 2-3km of the vent (Fig. 5.9). Cold blocks and hot bombs from a fire-fountain can leave the vent at ballistic trajectories impacting the local area close to the vent. The hot temperatures of the molten bombs potentially can cause fires in the surrounding vegetation and DOC infrastructure, and fallout of these are hazardous to any public in close proximity to the vent, i.e. walking the Tongariro Crossing track.

5.6.1 Hazard Scenarios

Andesite pyroclastic flows may extend for several km beyond their source at speeds of up to 10-100 m/s (Nakada 2000). North Crater flows probably travelled no further than 4 km from the vent (Fig. 5.9 and Fig. 5.10), but the associated hot, mobile ash clouds would be capable of significant physical impacts as they

decouple from the parent flow and could travel to 6-8 km (Fig. 5.9). Impacts from this ash cloud surge may include ignition of fires in the surrounding National Park and exotic forestry, and widespread ash fallout. These ground-hugging ash clouds may be the most dangerous aspect of even low energy pyroclastic flows, and their

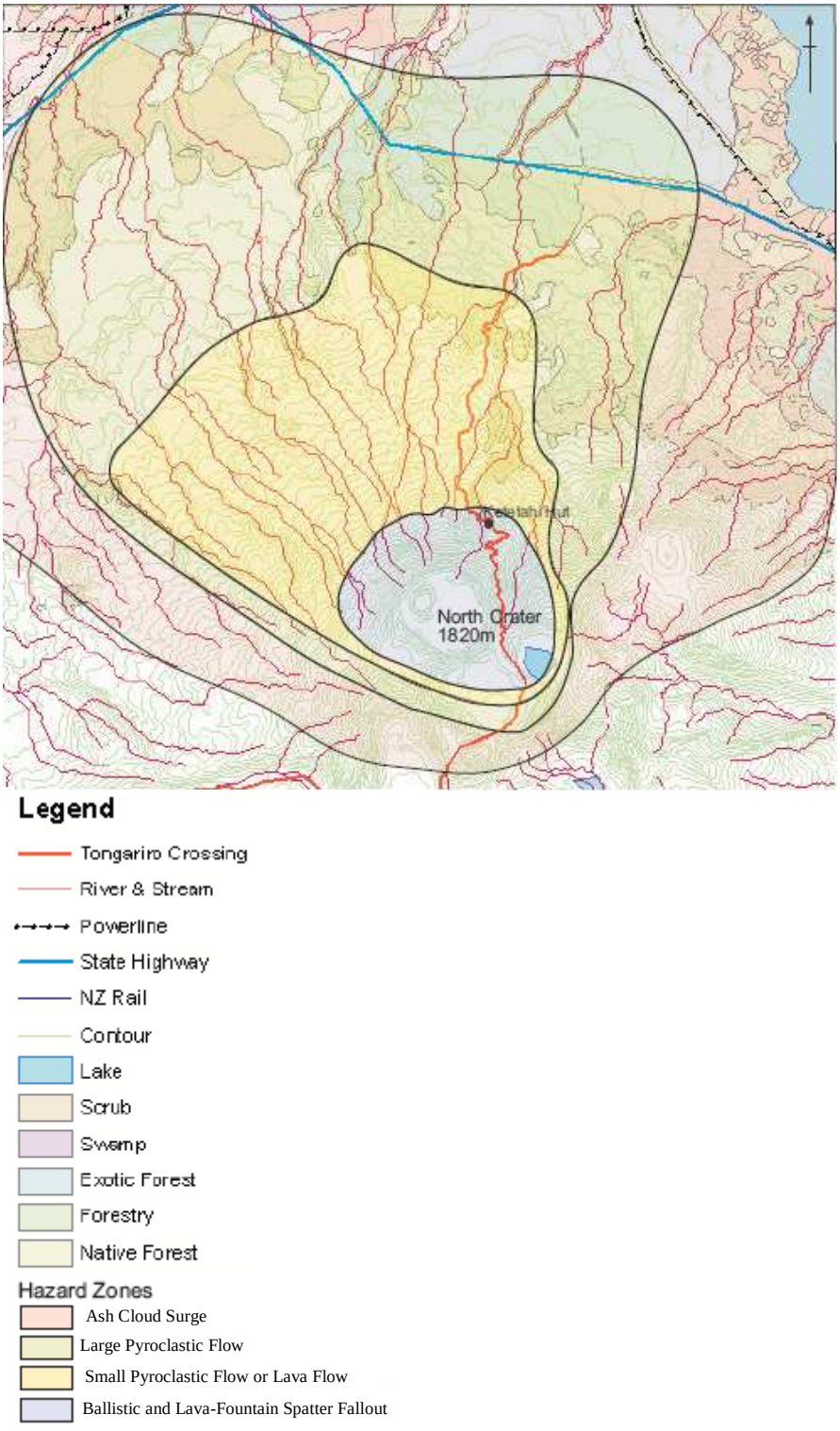

Fig 5.9: *Hazard map of north and western sectors of Tongariro National Park depicting potential hazard zones for pyroclastic flows, lava flows and lava-fountain fallout. Determined from field observations and likely fall zone of pyroclastic fall or flow path if topographically controlled flows. Zones based on scenario involving winds from south and southwest.*

movement is not constricted to valleys like the parent flow. The ash cloud may spread rapidly over any terrain, jumping catchments and out-running the parent flow (Nakada 2000). Features at risk include DOC tracks and associated infrastructure, roads, power lines and networks (including the hydropower Tongariro Power Scheme), forestry plantations and waterways.

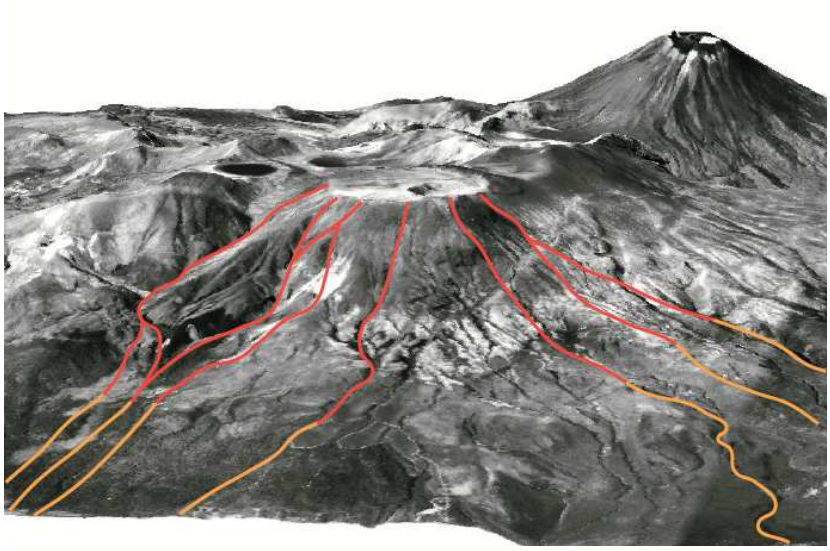

Figure 5.10: *Digital Elevation Model (DEM) looking south over Tongariro National Park, centred on North Crater. Red lines depict potential flow paths of pyroclastic flows down gullies and streams during a large eruption with prevailing winds from the south and west. Orange lines indicate a distal hazard from mixing of pyroclastic flows with water to produce destructive lahars.*

Snowmelt or rainfall accompanying this eruption scenario could sweep away fresh, loose tephra from the steep slopes of the volcano to form destructive lahars flowing down confined valleys (Fig. 5.10). These lahars potentially extend the area of impacts well beyond the National Park boundary, putting at risk major transport networks (roading and rail), power lines (hydropower scheme), pipelines, water resources, forestry, farmland and local settlements in the surrounding area (Rodolfo 2000).

Ash and lapilli fall from a sub-plinian plume also has the potential to impact a large portion of the central North Island, depositing 1 mm of ash as far as North Waikato, Tauranga, Whakatane and Hastings (Fig. 5.8). Ash will disrupt airports, affect livestock, create respiratory problems, contaminate water and cause minor building damage. Machinery and equipment with moving parts can also be damaged through clogging or abrasion. If the eruption plume is sufficiently

buoyant to reach the stratosphere it can cause severe risk to aircraft as their radar is not capable of detecting ash clouds allowing ash to be passed through the engines and cause severe abrasion to leading edges (Miller and Casadevall 2000). GeoNet monitoring should provide sufficient warnings of eruption activity capable of producing widespread ash fall in New Zealand.

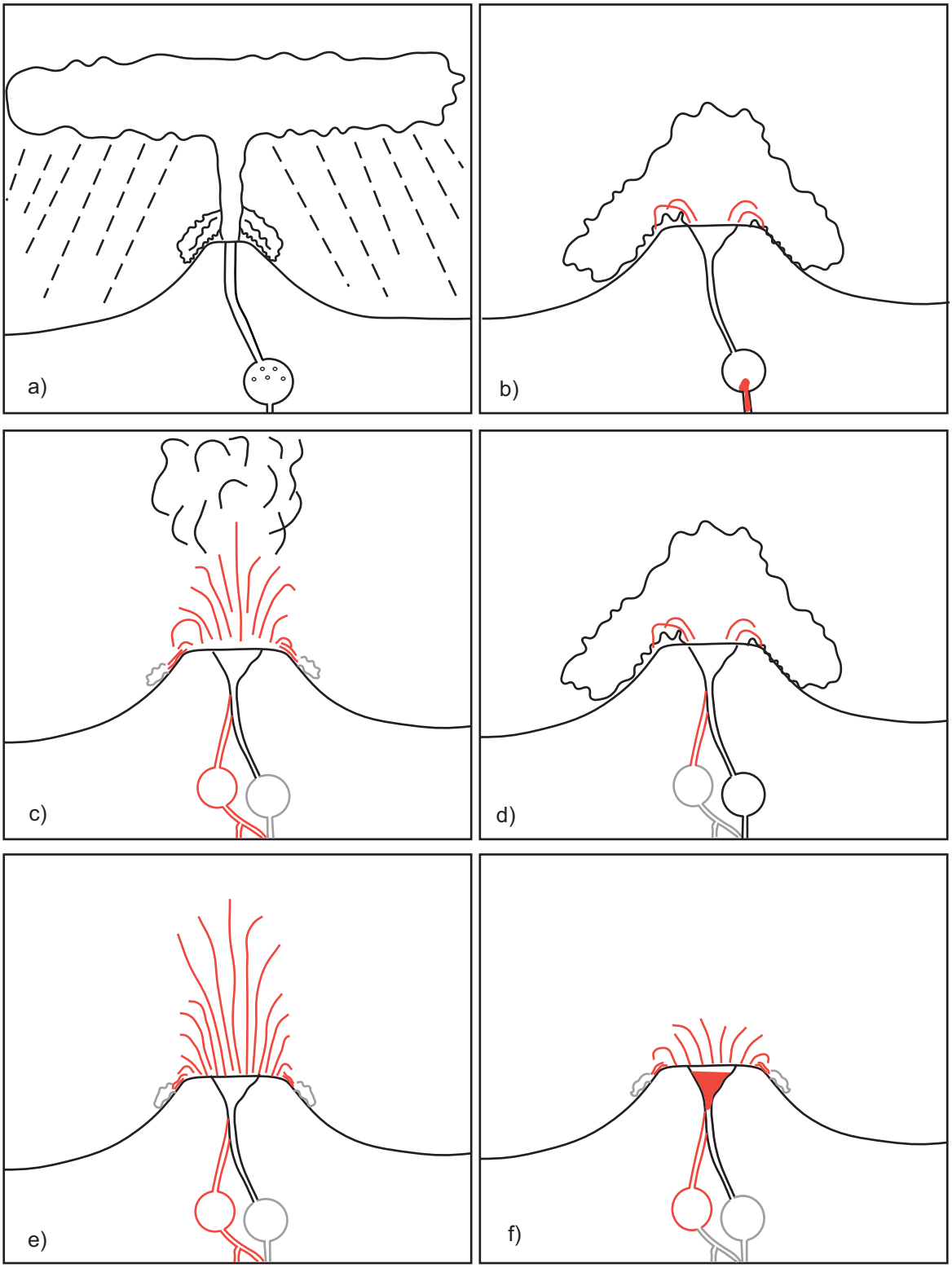

Figure 5.7: *Eruption history at North Crater. a) Phase 1 - initial eruption at North Crater forms buoyant sub-plinian plume with local small-scale pyroclastic flows from partial column collapse. b) incorporation or injection of a varying magma lead to vent erosion and resulted in change to dominant collapsing plume activity, associated with small-scale lava-fountaining producing mingled facies and other pyroclastic flows. c) Phase 2 - lava-fountaining with eruption column to produce welded fall deposits near vent which have undergone lateral transport with distance from vent. d) Phase 3 - change back to predominantly collapsing plume activity with small-scale lava-fountaining to produce pyroclastic flow deposits. e) Phase 4 - Climax of eruption at start of phase, vigorous lava-fountaining producing high, spreading fountain and welded fall deposits which have undergone lateral transport further from vent. f) Phase 5 - waning stages, lava fall back and accumulation in the summit crater allows magma degassing. Result in lower fountain heights and formation of ponded, degassed lava, eventually causes eruption to cease.*

Chapter 6
Summary and Conclusions

North Crater is a young vent on Tongariro volcano which was active around 14-12 ka ago with late stage activity to form the explosion pit. Little previous work has been carried out on North Crater; although recent geochemical work by Doyle (2006) established a geochemical link between proximal North Crater deposits and the distal Rotoaira Lapilli. The wide, flat top summit crater geomorphology of North Crater is distinct compared with other andesite cone volcanoes. The formation of the cone may have also been controlled by the neighbouring Blue Lake and Tongariro Trig vents and underlying proto-North Crater topography.

North Crater stratigraphy, correlations and facies characteristics were compiled from extensive field work on North Crater and involved the logging and mapping of 80 field sites in the proximal, medial and distal environments. In many of the outcrops in the proximal environment sequences of welded and non to poorly welded deposits can be seen. The intensely, strongly and moderately welded facies show varying degrees of clast outlines and are relatively dense, cohesive units. Some poorly to non-welded facies show characteristics of pyroclastic fall deposition, while the majority show characteristics of pyroclastic flow deposition.

Although there are rapid stratigraphic changes both horizontally and vertically, correlation of units in the proximal environment is possible, allowing a complete stratigraphy of North Crater to be compiled. Correlations between proximal units and those units in the medial and distal environment are also possible. This allows correlations between the proximal cone-building deposits to be made with the Rotoaira Lapilli and confirms the North Crater source for this distal tephra, rather than from Te Maari. However, further correlation between more medial sites may be needed to establish the stratigraphic correlation of individual beds.

Laboratory analyses of representative samples collected from proximal, medial and distal stratigraphic sections were carried out in order to characterise the various facies at North Crater. This included grain size, componentry, petrography, SEM studies and clast density and vesicularity to determine spatial and temporal differences in the deposits. The majority of samples collected in the proximal environment show coarse mean grain size and relatively poor sorting, suggesting deposition by pyroclastic flow. Limited fall deposits are indicated by their well sorted character. Deposits in the distal environment display characteristics typical of fall deposits (mantle bedded, well-sorted) and are of finer mean grain size.

The welded deposits in the proximal environment show relatively high bulk density but grain sizes generally cannot be established because particle boundaries are not discernible. Non-welded deposits are typically moderately to highly vesicular, with units made up of both coarsely vesicular scoria and finely vesicular pumice. All deposits are crystal rich and contain plagioclase>clinopyroxene>orthopyroxene>opaques>olivine. Plagioclase phenocrysts show complex disequilibrium textures, such as sieve, oscillatory zoning and dissolution, which indicates complex magma chamber processes in an open magmatic system. Olivine phenocrysts show reaction to fine grained augite and indicates disequilibrium with the enclosing magma. The inclusion of quartzofeldspathic xenoliths in the majority of samples would suggest crustal assimilation is also an important process. Some clasts display varying degrees of mingled groundmass textures between dark and light coloured glass. SEM studies

confirm the presence of microlites in only the dark glass, whereas the light glass contains no microlites.

SEM analysis of ash clast morphology revealed distinct groups contained in matrix and fall deposits. Ash clasts which display delicate structures are moderately to highly vesicular and have suffered little edge modification and abrasion and are interpreted to have been deposited as fall units or as low energy pyroclastic flows. Ash which is poorly vesicular, shows no delicate structures and has suffered extensive edge modification, and is interpreted to have formed from high energy, high concentration pyroclastic flow. SEM analysis of polished thin sections revealed vesicle morphology in pyroclastic clasts. Clasts with higher vesicularities displayed larger and more complex bubble shapes and suggests bubble coalescence. Clasts with lower vesicularities displayed medium to smaller bubbles with smoother shapes and a denser packing arrangement and indicate time for bubble growth was restricted.

Geochemical whole rock analysis showed the majority of deposits to be calc-alkaline andesite with limited basaltic andesite. Harker variation plots display mainly straight line trends between SiO_2 poor and SiO_2 rich magma, which may indicate magma mixing and processes involving an open magmatic system with multiple magma batches feeding North Crater eruptions. Phenocryst mineralogy of plagioclase indicates magma disequilibrium with varying core to rim compositions. Some clino- and orthopyroxenes in the same sample also show disequilibrium, and indicate magma mingling and mixing is occurring.

Groundmass glass geochemistry shows melt compositions range widely from andesite to rhyolite, with as much as 14 wt% SiO_2 variation within a single clast. Dark glass ranged between 57-71 SiO_2 wt% with a variation of 12 wt% SiO_2 within a single clast. Light glass ranged between 59-73 wt% SiO_2 with a variation of 6 wt% SiO_2 in a single clast. This suggests at least two subtly contrasting magmas are mixing, and the physical appearance is due to the presence of microlites, rather than chemical differences. Geothermometry calculations of titanomagnetite-ilmenite pairs indicates they are in disequilibrium, again suggesting that magma mixing and mingling is occurring. Calculated magma

viscosity, density and temperature measurements using the MAGMA software all fall within the typical range of andesite whole rock values.

The evidence for magma mixing and mingling at North Crater is strong, with variations in phenocryst textures, crystal disequilibrium and geochemical trends. Magma may be feeding into and mixing inside magma chambers prior to eruption, although mixing and mingling inside the conduit may also be an important process. The injection and mingling of magma in a magma chamber may also be important for triggering eruptions at North Crater, however 'second boiling' may also have initiated eruptions. At North Crater andesitic magma is thought to have displayed high magma ascent rates, low degrees of bubble coalescence and homogenous 2-phase flow to allow the formation of lava-fountains. The viscosity of andesite magma is usually not as low as that of typical basaltic Hawaiian style fire-fountaining and results in features such as spatter piles and welded agglutinates preserved around the vent. Magma chamber differences may have lead to changes between explosive andesitic lava-fountaining and large eruption plumes at North Crater. Possible changes in vent radius may also have allowed the formation of a collapsing plume after the initial sub-plinian eruption.

Cone formation at North Crater occurred in part from vigorous lava-fountaining producing strongly welded deposits and agglutinates in the proximal environment. Shear movement may have occurred to produce the strongly attenuated and thin ribbon-like clast outlines in some welded deposits. After initial deposition as fallout from a lava-fountain further down slope, fountain fallout has changed to lateral transport and deposition as pyroclastic flows. Many of the non to poorly welded deposits on the slopes of North Crater have been interpreted to have formed from pyroclastic flow, both as high energy, high concentration pyroclastic flows and as lower concentration, lower energy granular pyroclastic flows. Some of these poorly welded units are seen to grade from the welded facies close to the vent. Concurrent buoyant eruption plumes with lava-fountaining can be interpreted from the presence of texturally mixed facies. End member scoria and pumice are present with varying intensity mingled clasts. These mingled textures may have formed in the conduit as physical variations between magma in the conduit margin and centre became apparent, and was mingled just prior to

fragmentation. This would have allowed margin magma to erupt as a small scale lava-fountain and the central magma to erupt as an eruption plume. Sub-plinian eruption plumes have also occurred during the North Crater eruptions. These plumes have deposited pumiceous tephra in the medial and distal environment, and produced the regionally dispersed Rotoaira Lapilli. These deposits display typical fall features, although dark grey ash layers found in the upper Rotoaira Lapilli has been reworked but initial deposition has occurred from either fallout from a plume or as a co-ignimbrite ash cloud surge associated with pyroclastic flows higher on the cone.

Previous work elsewhere on Tongariro has identified limited evidence for small-scale pyroclastic flows, but at North Crater there is evidence of extremely hot pyroclastic flows associated with explosive lava-fountaining and eruption plume activity which represents a potentially devastating hazard. North Crater flows did not travel far from the vent, but the associated hot, mobile ash clouds would be capable of significant physical impacts as they have the potential to travel much further. Impacts from this ash cloud surge may include ignition of fires in the surrounding National Park and exotic forests, as well as widespread ash fallout. Snowmelt or rainfall mixing with loose tephra on the flanks of the volcano could form destructive lahars down confined valleys and streams, especially on the northern slopes of Tongariro. Features at risk include DOC tracks and associated infrastructure, roads, power lines and networks (including the hydropower Tongariro Power Scheme), forestry plantations and waterways. Ash and lapilli fall from an eruption plume also have the potential to impact a large portion of the central North Island, depositing ash perhaps as far as North Waikato, Tauranga, Whakatane and Hastings.

References

Allan, S.R., 2004, Complex spatter- and pumice-rich pyroclastic deposits from an andesitic caldera-forming eruption: the Siwi pyroclastic sequence, Tanna, Vanuatu. *Bulletin of Volcanology*, *67*, 27-41.

Bacon, C.R., Hirschmann, M.M., 1988, Mg/Mn partitioning as a test for equilibrium between coexisting Fe-Ti oxides. *American Mineralogist*, *73*, 57-61.

Basher, R., Physical volcanology and future risk from Te Maari Craters, Tongariro. Unpublished Masters of Science Thesis, University of Waikato, Hamilton, 2005.

Beier, C., Haase, K.M., Hansteen, T.H., 2006, Magma evolution of the Sete Cidades Volcano, Sao Miguel, Azores. *Journal of Petrology*, *47*, 1375-1411.

Belousov, B., Voight, B., Belousova, M., Petukhin, A., 2002, Pyroclastic surges and flows from the 8-10 May 1997 explosive eruption of Bezymianny volcano, Kamchatka, Russia. *Bulletin of Volcanology*, *64*, 455-471.

Bottinga, Y.A., Weill, D.F., 1972, The viscosity of magmatic silicate liquids: a model for calculation. *American Journal Science*, *272*, 438-473.

Browne, B.L., Eichelberger, J.C., Patino, L.C., Vogel, T.A., Uto, K., Hoshizumi, H., 2006, Magma mingling as indicated by texture and Sr/Ba ratios of plagioclase phenocrysts from Unzen volcano, SW, Japan. *Journal of Volcanology and Geothermal Research, 154*, 103-116.

Cagnoli, B., Manga, M., 2005, Vertical segregation granular mass flows: A shear cell studying. *Geophysical Research Letters*, *32*, Art. No. L10402.

Carmichael, I.S.E., 1967, The iron-titanium oxides of silicic volcanic rocks and their associated ferromagnesian silicates. *Contributions to Mineral Petrology, 14*, 36-64.

Carrasco-Nunez, G., Righter, K., Chesley, J., Siebert, L., Aranda-Gomez, J., 2005, Contemporaneous eruption of calc-alkaline and alkaline lavas in a continental arc (Eastern Mexican Volcanic Belt): chemically heterogeneous but isotopically homogeneous source. *Contributions to Mineralogy and Petrology, 150*, 423-440.

Castro, J..M., Mercer, C., 2004, Microlite textures and volatile contents of obsidian from the Inyo volcanic chain, California, *Geophysical Research Letters*, *31*, L18605.

Chappell, B., 1992, Trace element analysis of rocks by x-ray spectrometry. *Advances in X-ray Analysis, 34*, 263–276.

Choux, C., Druitt, T., Thomas, N., 2004, Stratification and particle segregation in flowing polydisperse suspensions, with applications to the transport and sedimentation of pyroclastic density currents. *Journal of Volcanology and Geothermal Research, 138*, 223-241.

Cioni, R., Marianelli, P., Santacroce R., Sbrana, A., Plinian and Sub-plinian Eruptions, In: *Encyclopaedia of Volcanoes*, H. Sigurdsson (Ed). Academic Press, New York, 2000.

Cole, J., 1978, Andesites of the Tongariro Volcanic Centre, North Island, New Zealand. *Journal of Volcanology and Geothermal Research, 3*, 121-153.

Davidson, J., de Silva, S., Composite Volcanoes, In *Encyclopaedia of Volcanoes*, H. Sigurdsson (Ed). Academic Press, New York, 2000.

Davis, B.K., McPhie J., 1996, Spherulites, quench fractures and relict perlite in a Late Devonian rhyolite dyke, Queensland, Australia. *Journal of Volcanology and Geothermal Research, 71*, 1-11.

Donoghue, S., Gamble, J., Palmer, A., Stewart, R., 1995a, Magma mingling in an andesite pyroclastic flow of the Pourahu Member, Ruapehu Volcano, New Zealand. *Journal of Volcanology and Geothermal Research, 68*, 177-191.

Donoghue, S.L., Neall V.E., Palmer A.S.,1995b, Stratigraphy and chronology of late Quaternary Andesitic tephra deposits, Tongariro Volcanic Centre, New Zealand. *Journal of the Royal Society of New Zealand*, *25*, 115-206.

Doyle, L.R., The geochemistry of the 22.6-13.8 Ka Rotoaira eruptive sequence, Tongariro volcano, New Zealand, Masters of Science thesis, University of Auckland, Auckland, 2006.

Eichelberger, J.C., 1980, Vesiculation of mafic magma during replenishment of silicic magma reservoirs. *Nature, 288*, 446-450.

Francis, P., *Volcanoes*: *a planetary perspective*, First Edition. Oxford University Press, New York, 1993.

Freundt, A., Wilson, C.J.N., Carey, S.N., Ignimbrites and block and ash flow deposits. In: *Encyclopaedia of Volcanoes*, H. Sigurdsson (Ed). Academic Press, New York, 2000.

Froggatt, P.C., Lowe D.J., 1990, A review of late Quaternary silicic and some other tephra formations from New Zealand: their stratigraphy,

nonclameture, distribution, volume and age. *New Zealand Journal of Geology and Geophysics*, *33*, 89-109.

Graham, I., Hackett, W., 1987, Petrology of calc-alkaline lavas from Ruapehu volcano and related vents, Taupo Volcanic Zone, New Zealand. *Journal of Petrology, 28*, 531-567.

Graham, I.J., Grapes, R.H., Kifle, K., 1988, Buchitic metagreywacke xenoliths from Mt Ngauruhoe, Taupo Volcanic Zone, New Zealand. *Journal of Volcanology and Geothermal Research, 35*, 205-216.

Graham, I., Cole, J., Briggs, R., Gamble, J., Smith, I., 1995, Petrology and petrogenesis of volcanic rocks from Taupo Volcanic Zone: a review. *Journal of Volcanology and Geothermal Research, 68*, 59-87.

Gregg, D.R., 1960, *The Geology of the Tongariro Subdivision*. New Zealand Geological Survey Bulletin, #40.

Gurioli, L., Houghton, B.F., Cashman, K.V., Cioni, R., 2005, Complex changes in eruption dynamics during the 79 AD eruption of Vesuvius. *Bulletin of Volcanology*, *67*, 144-159.

Hammer, J.E., Rutherford M.J., 2002, An experimental study of the kinetics of decompression-induced crystallization in silicic melt. *Journal of Geophysical Research, 107,* (B1) Act. No. 2021.

Head, J.W., Wilson, L., 1987, Lava fountain heights at Pu' u 'O'o, Kilauea, Hawaii: indicators of amount and variations of exsolved magma volatiles. *Journal of Geophysical Research*, *92*, 13715–13719.

Head, J.W., Wilson, L., 1989, Basaltic pyroclastic eruptions: influence of gas-release patterns and volume fluxes on fountain structure and the formation of cinder cones, spatter cones, rootless flows, lava ponds and lava flows. *Journal of Volcanology and Geothermal Research, 37*, 261-271.

Heiken, G., Wohletz, K., *Volcanic Ash*. University of California Press, Los Angeles, 1985.

Hobden, B.J., Houghton, B.F., Lanphere M.A., Nairn I., 1996, Growth of the Tongariro Volcanic complex: new evidence from K-AR age determinations. *New Zealand Journal of Geology Geophysics, 39*, 151-154.

Hobden, B., Modelling magmatic trends in time and space: eruptive and magmatic history of Tongariro Volcanic Complex, New Zealand, Doctor of Philosophy thesis, University of Canterbury, Christchurch, 1997.

Hobden, B., Houghton, B., Davidson, J., Weaver, S., 1999, Small and short-lived magma batches at composite volcanoes: time windows at Tongariro volcano, New Zealand. *Journal of the Geological Society, London, 156*, 865-868.

Hobden, B., Price, R., Gamble, J., Stewart, R., Growth and magmatic evolution of Tongariro and Ruapehu Volcanoes, New Zealand. In: *Geological Society of New Zealand Annual Conference – Advances in Geoscience Fieldtrip Guides*, R. Smith (Ed), University of Waikato, Geological Society of New Zealand misc. publication 110A, 2001.

Hobden, B., Houghton, B., Nairn, I., 2002, Growth of a young, frequently active composite cone: Ngauruhoe volcano, New Zealand. *Bulletin of Volcanology, 64*, 392-409.

Houghton, B.F., Wilson, C.J.N., Hassan, M., 1988, Density measurements for pyroclasts and pyroclastic rocks. *New Zealand Geological Survey Record, 35*, 73-76.

Houghton, B.F., Smith, R., 1993, Recycling of juvenile clasts during explosive eruptions: estimating the true juvenile content of phreatomagmatic volcanic deposits. *Bulletin of Volcanology, 55*, 414-420.

Houghton, B.F., Wilson, C.J.N., Pyle, D.M., Pyroclastic fall deposits. In: *Encyclopaedia of Volcanoes*, H. Sigurdsson (Ed). Academic Press, New York, 2000.

Humphreys, M.C.S., Blundy, J.D., Sparks, R.S.J., 2006, Magma evolution and open-system processes at Shiveluch Volcano: Insights from phenocryst zoning. *Journal of Petrology, 47*, 2303-2334.

Huppert, H.E., Sparks, R.S.J., Turner, J.S., 1982, Effects of volatiles on mixing in calc-alkaline magma systems. *Nature, 297*, 554-557.

Jaupart, C., 1996, Physical models of volcanic eruptions. *Chemical Geology, 128*, 217-227.

Jaupart, C., Magma ascent at shallow levels. In: *Encyclopaedia of Volcanoes*, H. Sigurdsson (Ed). Academic Press, New York, 2000.

Jaupart, C., Vergniolle, S., 1988, Laboratory models of Hawaiian and Strombolian eruptions. *Nature, 331*, 58-60.

Kaneko, T., Wooster, M.J., 2005, Satellite thermal analysis of the 1986 Izu-Oshima lava flows. *Journal of Volcanology and Geothermal Research, 148*, 355-371.

Klug, C., Cashman, K.V., 1996, Permeability development in vesiculating magmas: implications for fragmentation. *Bulletin of Volcanology, 58*, 87-100.

Mannen, K., 2006, Total size distribution of a mafic sub-plinian tephra, TB-2, from the 1986 Izu-Oshima eruption, Japan: An estimation based on a theoretical model. *Journal of Volcanology and Geothermal Research, 155*, 1-17.

Marti, J., Ernst, G., *Volcanoes and the Environment*. Cambridge University Press, Cambridge, 2005.

Martin, U., Nemeth K., 2006, How strombolian is a "strombolian" scoria cone? Some irregularities in scoria cone architecture from the Transmexican Volcanic Belt, near Volcan Ceboruco, (Mexico) and Al Haruj (Libya). *Journal of Volcanology and Geothermal Research, 155,* 104-118.

Mathews, W.H., 1967, A contribution to the geology of the Mount Tongariro massif, North Island, New Zealand. *New Zealand Journal of Geology and Geophysics, 10,* 1027-1038.

Mellors, R.A., Sparks, R.S.J., 1991, Spatter-rich pyroclastic flow deposits on Santorini, Greece. *Bulletin of Volcanology, 53,* 327-342.

Miller, T.P., Casadevall, T.J., Volcanic ash hazards to aviation. In: *Encyclopaedia of Volcanoes*, H. Sigurdsson (Ed). Academic Press, New York, 2000.

Nairn, I., Kobayashi T., Nakagawa M., 1998, The ~10ka multiple vent pyroclastic eruption sequence at Tongariro Volcanic Centre, Taupo Volcanic Zone, New Zealand: Part 1. Eruptive processes during regional extension. *Journal of Volcanology and Geothermal Research, 86,* 19-44.

Nakada, S., Hazards from pyroclastic flows and surges. In: *Encyclopaedia of Volcanoes*, H. Sigurdsson (Ed). Academic Press, New York, 2000.

Nakagawa, M., Nairn, I., Kobayashi, T., 1998, The ~10ka multiple vent pyroclastic eruption sequence at Tongariro Volcanic Centre, Taupo Volcanic Zone, New Zealand Part 2. Petrological insights into magma storage and transport during regional extension. *Journal of Volcanology and Geothermal Research, 86,* 45-65.

Nakagawa, M., Wada, K., Wood, C.P., 2002, Mixed magmas, mush chambers and eruption triggers: Evidence from zoned clinopyroxene phenocrysts in andesitic scoria from the 1995 eruptions of Ruapehu volcano, New Zealand. *Journal of Petrology, 43,* 2279-2303.

Newnham, R., Lowe, D., Williams, P., 1999, Quaternary environmental change in New Zealand: a review. *Progress in Physical Geography, 23,* 567-610.

Norrish, K., Hutton, J. T., 1977, An accurate x-ray spectrographic method for the analysis of a wide range of geological samples. *Geochimica et Cosmochimica Acta, 33,* 431–441.

Parfitt, E.A., 2004, A discussion of the mechanisms of explosive basaltic eruptions. *Journal of Volcanology and Geothermal Research, 134,* 77-107.

Parfitt, E.A., Wilson, L., 1999, A Plinian treatment of fallout from Hawaiian lava fountains. *Journal of Volcanology and Geothermal Research, 88,* 67–75.

Parfitt, E.A., Wilson, L., Neal, C.A., 1995, Factors influencing the height of Hawaiian lava fountains: implications for the use of fountain height as an indicator of magma gas content. *Bulletin of Volcanology, 57*, 440–450.

Price, R., Gamble, J., Smith, I., Stewart, R., Eggins, S. Wright, I., 2005, An integrated model for the temporal evolution of andesites and rhyolites and crustal development in New Zealand's North Island. *Journal of Volcanology and Geothermal Research, 140*, 1-24.

Pyle, D.M., 1989, The thickness, volume and grainsize of tephra fall deposits. *Bulletin of Volcanology, 51*, 1-15.

Pyle, D.M., Pyle, D.L., 1995, Bubble migration and the initiation of volcanic eruptions. *Journal of Geothermal Research, 67*, 227-232.

Rodolfo, K.S., The hazards from lahars and jokulhlaups. In: *Encyclopaedia of Volcanoes*, H. Sigurdsson (Ed). Academic Press, New York, 2000.

Sable, J.E, Houghton, B.F., Del Carlo, P., Coltelli, M., 2006, Changing conditions of magma ascent and fragmentation during the Etna 122 BC basaltic Plinian eruption: Evidence from clast microtextures. *Journal of Volcanology and Geothermal Research, 158*, 33-354.

Schmincke, H., *Volcanism*. Springer-Verlag, New York, 2004.

Shaw, H. R., 1972, Viscosities of magmatic silicate liquids: an empirical method of prediction. *American Journal Science, 272*, 870-893.

Sigurdsson, H., Carey, S., Palais, J.M., Devine, J., 1990, Pre-eruption compositional gradients and mixing of andesite and dacite magma erupted from Nevado del Ruiz Volcano, Colombia in 1985. *Journal of Volcanology and Geothermal Research, 41*, 127-151.

Sisson, T.W., Grove T.L., 1993, Experimental investigations of the role of H_2O in calc-alkaline differentiation and subduction zone magmatism. *Contributions to Mineralogy and Petrology, 113*, 143-166.

Spera, F. J., Physical Properties of Magma. *In: Encyclopaedia of Volcanoes,* H. Sigurdsson (Ed), Academic Press, New York, 2000.

Sparks, R.S., Sigurdsson, H., Wilson, L., 1977, Magma mixing: a mechanism for triggering acid explosive eruptions. *Nature, 267*, 315-318.

Stevenson, R.J., Wilson, L., 1997, Physical volcanology and eruption dynamics of peralkaline agglutinates from Pantelleria. *Journal of Volcanology and Geothermal Research, 79*, 97-122.

Sumner, J.M., 1998, Formation of clastogenic lava flows during fissure eruption and scoria cone collapse: the 1986 eruption of Izu-Oshima Volcano, eastern Japan. *Bulletin of Volcanology, 60*, 195-212.

Sumner, J.M., Blake, S., Matela, R.J., Wolff J.A., 2005, Spatter. *Journal of Volcanology and Geothermal Research, 142*, 49-65.

Szramek, L., Gardner J.E., Larsen, J., 2006, Degassing and microlite crystallisation of basaltic andesite magma erupting at Arenal Volcano, Costa Rica. *Journal of Volcanology and Geothermal Research, 157*, 182-201.

Taddeucci, J., Palladino, D.M., 2002, Particle size-density relationships in pyroclastic deposits: inferences for emplacement processes. *Bulletin of Volcanology, 64*, 273-284.

Tait, S.R., Jaupart, C., Vergniolle, S., 1989, Pressure, gas content and eruption of a shallow, crystallising magma chamber. *Earth and Planetary Science Letters, 92*, 107-123.

Takeuchi, S., Nakamura, M., 2001, Role of precursory less-viscous mixed magma in the eruption of phenocryst rich magma: evidence from the Hokkaido-Komagatake 1929 eruption. *Bulletin of Volcanology, 63*, 365-376.

Topping, W.W., 1973, Tephrostratigraphy and chronology of late Quaternary eruptives from the Tongariro Volcanic Centre, New Zealand. *New Zealand Journal of Geology and Geophysics 16*, 397-423.

Topping, W.W., Some Aspects of Quaternary history of the Tongariro Volcanic Centre. Doctor of Philosophy thesis, Victoria University, Wellington, 1974.

Turner, F.J., Verhoogen, J., *Igneous and metamorphic petrology*, p 694, McGraw-Hill, New York, 1960.

Valentine, G.A., Fisher, R.V., Pyroclastic surges and blasts. In: *Encyclopaedia of Volcanoes*, H. Sigurdsson (Ed). Academic Press, New York, 2000.

Valentine, G.A., Perry, F.V., WoldeGabriel, G., 2000, Field characteristics of deposits from spatter-rich pyroclastic density currents at Summer Coon volcano, Colorado. *Journal of Volcanology and Geothermal Research, 104*, 187-199.

Vergniolle, S., Mangan M., Hawaiian and Strombolian eruptions. In: *Encyclopaedia of Volcanoes*, H. Sigurdsson (Ed). Academic Press, New York, 2000.

Waight, T.E., Price, R.C., 1999, Stratigraphy and geochemistry of the Turoa area, with implications for andesite petrogenesis at Mt Ruapehu, Taupo Volcanic Zone, New Zealand. *New Zealand Journal of Geology and Geophysics, 42*, 513-532.

Walker G.P.L., 1973, Explosive Volcanic Eruptions – a new classification scheme. *International Journal of Earth Sciences, 62*, 431-446.

Wilson, C.J.N., Houghton, B.F., Pyroclastic transport and deposition. In: *Encyclopaedia of Volcanoes*, H. Sigurdsson (Ed). Academic Press, New York, 2000.

Wilson, C.J.N., Houghton, B., McWilliams, M., Lanphere, M., Weaver, S., Briggs, R., 1995, Volcanic and structural evolution of Taupo Volcanic Zone, New Zealand – A review. *Journal of Volcanology and Geothermal Research, 68*, 1-28.

Wohletz, K., 2005, Kware MAGMA- geological software. Los Alamos National Laboratory, version 2.48.0116 (20 October 2005).

Wohletz K., Heiken G., *Volcanology and Geothermal Energy*. University of California Press, Los Angeles, 1992.

Wolff, J.A., Sumner, J.M., Lava fountaining and their products. In: *Encyclopaedia of Volcanoes*, H. Sigurdsson (Ed). Academic Press, New York, 2000.

Woods A.W., Cardoso S.S.S., 1997, Triggering basaltic volcanic eruptions by bubble-melt separation. *Nature, 385*, 6616, 518-520.

Yamamoto, T., Takada, A., Ishizuka, Y., Miyaji, N., Tajima, Y., 2005, Basaltic pyroclastic flows of Fuji volcano, Japan: characteristics of the deposits and their origin. *Bulletin of Volcanology, 67*, 622-633.

Yasui, M., Koyaguchi, T., 2004, Sequence and eruptive style of the 1783 eruption of Asama Volcano, central Japan: a case study of an andesitic explosive eruption generating fountain-fed lava flow, pumice fall, scoria flow and forming a cone. *Bulletin of Volcanology, 66*, 243-262.

Appendix A

Sample Catalogue

					Analyses Undertaken					Hand Specimen Description				
Sample ID	**Waikato #**	**Field Site**	**Easting**	**Northing**	**Sieve**	**TS**	**Density**	**MP**	**XRF**	**Colour**	**Grain Size**	**Vesicularity**	**Texture**	**Other Comments**
AG01	20060116	45	2739054	6228947	N	Y	N	N	Y	Cream	Very fine			Metamorphosed crustal xenolith
AG02	20060045	47	2739215	6228562	N	Y	Y	N	N	Greyish red	fine	10-15%	Vitrophyric /porphyritic	Dense welded unit. Bands of redder less vesicular, 3.8mm wide, with wider greyish red mod-vesic, 1-1.3cm wide bands
AG03	20060046	9	2738965	6228810	N	Y	Y	N	Y	Pinkish med grey	fine	10-15%	Porphyritic	Dense welded unit. Large cryst in v fine groundmass. Possible recrystalised xenoliths seen as sugar like inclusion 3mm by 12mm
AG04	20060047	10	2739022	6228818	N	Y	Y	N	Y	Brownish red	fine to coarse	15-20%	Vitrophyric /Porphyritic	Dense welded unit. Minor concentration of dark minerals in informal bands or clusters, ~20%dense sub-ang inclusions 5-15mm of v dark grey, scoria clast
AG05	20060048	57	2738605	6228686	N	Y	Y	N	N	Very dark grey	fine-med	10-15%	Porphyritic	Dense welded unit. Red sub-rnd clast 3-6mm seen, some crystals seem sub-parallel
AG06	20060049	57	2738605	6228686	N	Y	Y	N	N	Pinkish Dark grey	fine-med	20-25%	Porphyritic	Dense welded unit. Inside vesicles reddish colour, rounded inclusion can be seen, some large crysts or clusters of crysts seen
AG07	20060050	58	2738552	6228587	N	Y	Y	N	N	Light grey	fine	5-10%	Porphyritic	Vesicles small, in dense/strongly welded unit
AG08	20060051	59	2738630	6228380	N	Y	Y	N	Y	Med grey	fine	<5%	Porphyritic/ vitrophyric	Appears to be strongly/densely welded unit as minor vesicles
AG09	20060052	60	2738537	6228329	N	Y	Y	N	N	Med grey	fine to med	5%	Porphyritic/ vitrophyric	Dense welded unit. Phenocrysts mostly large 3-4mm, possibly some squashed lithics, and stretched clasts.
AG10	20060053	2	2739327	6228093	N	Y	Y	N	N	Greyish red	fine	30-40%	Vitrophyric /trachytic	Dense welded unit. Conc of dark minerals/colours along bands, with low vesic, crystals aligned sub-parallel
AG11	20060054	2	2739327	6228093	N	N	Y	N	N	Slight pinkish grey	fine	5-10%	Porphyritic/ vitrophyric	Dense welded unit. Inclusions of dense angular lithics

Sample ID	Waikato #	Field Site	Easting	Northing	Analyses Undertaken					Hand Specimen Description				
					Sieve	TS	Density	MP	XRF	Colour	Grain Size	Sieve	Texture	Other Comments
AG12	20060055	2	2739327	6228093	N	Y	Y	N	N	Greyish pink	fine	15-20%	Vitrophyric /trachytic	Dense welded unit. Conc of dark minerals in informal bands or clusters, dense round inclusions 15mm seen
AG14	20060056	61	2739173	6227889	N	Y	Y	N	N	Dark grey/black	med	5-10%	Porphyritic	Dense black scoria clast, vesicles small and compacted.dense angluar inclusions seen inside 10x8mm
AG15	20060057	62	2739157	6227849	N	Y	Y	N	N	Pinkish grey	fine	5-10%	Vitrophyric /porphyritic	Dense welded unit. Bands of darker grey minerals & glass with lighter pinker bands between.
AG16	20060058	63	2738228	6228439	N	Y	Y	N	Y	Dark grey	fine to med	25-35%	Porphyritic	Densly welded black scoria. Small vesicles, large crystals
AG17	20060059	66	2738652	6228818	N	N	N	N	N	Greyish pink	fine to med	10-15%	Vitrophyric /porphyritic	Dense welded unit. Conc of dark minerals into informal bands or clusters.
AG18	20060060	66	2738652	6228818	N	Y	Y	N	N	Very dark grey	fine	10-15%	Porphyritic	Vesicles tiny, from dense/intensly welded flow in stream below hut. Lower older lava unit?
AG19	20060061	69	2739447	6231023	Y	N	N	N	N	Black	med		Vitrophyric /porphyritic	Loose black scoria lapilli unit, uniform size and colour, unsure if NC source
AG20	20060062	69	2739447	6231023	N	Y	Y	N	Y	Black	fine	30-40%	Vitrophyric /porphyritic	Black scoria bomb taken from Block & Ash flow, see dense angular inclusions 30x8mm
AG21	20060063	69	2739447	6231023	Y	N	Y	N	N	Orangey brown	med		Vitrophyric /porphyritic	Loose pumice & scoria lapilli deposit, predom poor vesicular clasts
AG22	20060064	19	2739290	6228426	N	Y	Y	N	Y	Light grey	fine-med	<5%	Porphyritic	Dense welded unit. Sub-rnd slightly elongated inclusion of lighter grey/white colour, ~50% cryst, sub-ang dense inclusion also seen 15mm.

AG23	20060065	20	2739290	6228424	N	Y	Y	N	Y	Rusty red	fine	30-40%	Vitrophyric /porphyritic	Dense welded unit. Conc of dark minerals/glass in bands in some areas, dense sub-rnd inclusions 8mm

					Analyses Undertaken					Hand Specimen Description				
Sample ID	**Waikato #**	**Field Site**	**Easting**	**Northing**	**Sieve**	**TS**	**Density**	**MP**	**XRF**	**Colour**	**Grain Size**	**Vesicularity**	**Texture**	**Other Comments**
AG24	20060066	52	2739324	6229134	N	Y	Y	N	N	Pinkish grey	med	20-25%	Porphyritic/ vitrophyric	Dense welded unit. Mainly med grey but faint areas of pinkish grey clast shapes in sub-parallel alignment, slightly elongated shapes.
AG25	20060067	23	2739595	6228443	Y	Y	Y	Y	YY	Mixed black, brown and yellow.	fine	10-15%	Porphyritic/ vitrophyric	Loose scoria lapilli deposit, some clasts are intensely mingled, other just black or yellow end member clasts, some pinkish red lapilli and dense lithics
AG26	20060068	25	2739548	6228399	Y	Y	Y	N	Y	Black, irridescent blue	fine	5-10%	Porphyritic/ vitrophyric	Loose scoria lapilli unit, dense lithics crystal rich clasts
AG27	20060069	25	2739548	6228399	Y	N	Y	N	YY	Brownish orange	fine	5-10%	Porphyritic/ vitrophyric	Loose scoria/pumice lapilli unit, coarse matrix, dense lithics, cryst rich
AG28	20060070	24	2739578	6228431	Y	N	N	N	N	Bluish grey	fine-med	-	-	Slightly consolidated ash
AG29	20060071	45	2739054	6228947	N	Y	N	Y	Y	Black and creamy brown	fine	40-45%	Vitrophyric /porphyritic	Intensely mingled/banded pumice & scoria, cryst rich
AG30	20060072	70	2753313	6238262	Y	N	N	N	N	Orangey brown	fine-med	20-30%		Loose fall deposit, minor lapilli mostly coarse ash, clasts sub-round, ring plain
AG31	20060073	70	2753313	6238262	Y	N	N	N	N	Orangey brown	fine	20-30%		Loose fall deposit all ash apart from very minor small lap, ring plain
AG32	20060074	72	2751703	6231907	Y	N	N	N	N	Orangey grey	fine	20-30%	Porphyritic/ vitrophyric	Loose lapilli fall deposit, ring plain
AG33	20060075	72	2751703	6231907	Y	N	N	N	N	Orangey grey	fine	20-30%	Porphyritic/ vitrophyric	Loose lapilli fall deposit, ring plain
AG34	20060076	72	2751703	6231907	Y	N	N	N	N	Dark grey	fine			Loose ash fall deposit, ring plain

AG35	20060077	72	2751703	6231907	Y	Y	Y	N	Y	Orangey brown	fine	20-30%	Porphyritic/ vitrophyric	Loose lapilli fall deposit, ring plain
AG36	20060078	74	2749739	6232073	Y	Y	Y	Y	Y	Orangey yellow	fine	20-30%	Porphyritic/ vitrophyric	Loose lapilli fall deposit, ring plain
					Analyses Undertaken					**Hand Specimen Description**				
Sample ID	**Waikato #**	**Field Site**	**Easting**	**Northing**	**Sieve**	**TS**	**Density**	**MP**	**XRF**	**Colour**	**Grain Size**	**Vesicularity**	**Texture**	**Other Comments**
AG37	20060079	74	2749739	6232073	Y	N	N	N	N	Dark grey	fine			Loose ash fall deposit, ring plain
AG38	20060080	74	2749739	6232073	Y	N	N	N	N	Orangey yellow	fine	20-30%	Porphyritic/ vitophyric	Loose lapilli fall deposit, ring plain
AG39	20060081	75	2748196	6232419	Y	N	N	N	Y	Yellow brown	fine	20-30%	Porphyritic/ vitrophyric	Loose lapilli fall deposit, ring plain
AG40	20060082	75	2748196	6232419	Y	N	N	N	N	Dark grey	fine			Loose ash fall deposit, ring plain
AG41	20060083	75	2748196	6232419	Y	N	Y	N	Y	Yellow brown	fine	20-30%	Porphyritic/ vitrophyric	Loose lapilli fall deposit, ring plain
AG42	20060084	76	2739875	6232923	Y	Y	N	YY	Y	Dark redish brown	med	10-20%	Porphyritic/ vitrophyric	Loose fall deposit, dense sub-rnd to rnd juveniles and dense lithics with coarse ash
AG43	20060085	76	2739875	6232923	Y	N	N	N	N	Orange brown	coarse			Loose ash fall deposit, distal
AG44	20060086	76	2739875	6232923	Y	N	N	N	N	Blackish grey	med	10-20%	Porphyritic/ vitrophyric	Loose lapilli fall deposit, distal
AG45	20060087	16	2739569	6228598	Y	Y	Y	N	YY	Orange brown	med-coarse	10-20%	Vitrophyric /porphyritic	Loose pumice & scoria deposit, denser red scoria and creamy pumice with coarse ash. Chips off large clasts unable to bring back to lab to do vesic work
AG46	20060088	16	2739569	6228598	Y	Y	Y	N	N	Black	med-coarse	10-20%	Vitrophyric /porphyritic	Loose scoria lap deposit, chips off larger clasts unable to bring back
AG47	20060089	38	2739686	6228639	Y	N	Y	N	YYY	Yellow brown	med-coarse	10-20%	Vitrophyric /porphyritic	Loose pumice lapilli deposit, some clasts with mingled textures

AG48	20060090	1	2739446	6228547	Y	Y	Y	N	Y	Orange brown	med-coarse	10-20%	Vitrophyric /porphyritic	Loose pumice & scoria deposit, lapilli and coarse ash, some dense red scoria, round and dense lithics (cream). Chips off larger clasts not able to bring back
AG49	20060091	1	2739446	6228547	Y	N	Y	N	Y	Brown black	med-coarse	5-15%	Vitrophyric /porphyritic	Loose scoria & pumice lapilli with coarse ash, poor vesic, hard to tell if any mingled clasts at this stage, need to clean up clasts. Chips off larger clasts unable to bring back to do vesic work
					Analyses Undertaken					**Hand Specimen Description**				
Sample ID	**Waikato #**	**Field Site**	**Easting**	**Northing**	**Sieve**	**TS**	**Density**	**MP**	**XRF**	**Colour**	**Grain Size**	**Vesicularity**	**Texture**	**Other Comments**
AG50	20060092	1	2739446	6228547	Y	N	Y	N	Y	Orange brown	med - coarse	5%	Vitrophyric /porphyritic	Loose pumice & scoria lapilli and coarse ash
AG51	20060093	1	2739446	6228547	N	Y	Y	N	Y	Rusty red	fine	30-35%	Vitrophyric /porphyritic	Scoria from welded unit, very fine vesicular
AG52	20060094	36	2739624	6228444	Y	N	Y	N	Y	Creamy brown and dark brown	med-coarse	15-20%	Vitrophyric /porphyritic	Loose pumice & mingled scoria unit, large lapilli & some dense ang lithics. Chips off larger clasts unable to bring back to do vesicularity on.
AG53	20060095	27	2739499	6228381	Y	Y	Y	N	N	Brownish black	med-coarse	5-10%	Vitrophyric /porphyritic	Loose scoria lapilli and coarse ash
AG54	20060096	27	2739499	6228381	Y	N	Y	N	N	Yellowish brown	med-coarse	5-15%	Vitrophyric /porphyritic	Mix of yellowish brown pumice lap & denser black/dark grey scoria (minor) lapilli with coarse ash. Chips of larger clasts not able to bring back for vesic work
AG55	20060097	78	2739177	6227901	Y	N	Y	N	YY	Reddish black	med-coarse	5%	Vitrophyric /porphyritic	Loose scoria lapilli deposit with coarse ash
AG56	20060098	78	2739177	6227901	N	N	N	N	N	Rusty red	fine	40-45%	Porphyritic	Scoria clast from mod welded unit below cave. Can see some clast shapes(small) where app scoria have stuck together
AG57	20060099	62	2739157	6227849	N	Y	Y	N	Y	Brownish black	fine	25-30%	Porphyritic	Welded black scoria unit, partially weathered

AG58	20060100	79	2738983	6227803	N	Y	Y	N	Y	med-dark grey	med	<5%	Porphyritic	Dense/strongly welded unit, from lava lake which has spilled over the west lip, lithics inclusions seen, some pinkish grey tinges in patches
AG60	20060101	80	2738833	6227731	N	Y	Y	N	Y	Dark pinkish grey	fine	10-15%	Porphyritic	Part of welded scoria unit
AG61	20060102	80	2738833	6227731	N	Y	Y	N	Y	Greyish red	fine	15-20%	Porphyritic	Dense scoria unit. Minor flow bands with concentration of dark minerals in some areas
					Analyses Undertaken					**Hand Specimen Description**				
Sample ID	**Waikato #**	**Field Site**	**Easting**	**Northing**	**Sieve**	**TS**	**Density**	**MP**	**XRF**	**Colour**	**Grain Size**	**Vesicularity**	**Texture**	**Other Comments**
AG62	20060103	55	2738329	6228446	N	Y	Y	Y	Y	Medium grey	fine	<5%	Porphyritic	Dense strongly welded unit, some flow banding/stretched clasts
AG63	20060104	55	2738329	6228446	N	Y	Y	N	Y	Light-med grey	fine-coarse	5%	Porphyritic	Dense strongly welded unit, some stretched banding/clasts
AG64	20060105	9	2738965	6228810	N	Y	Y	N	N	Greyish black	fine	5%	Porphyritic	Dense strongly welded unit
AG65	20060106	9	2738965	6228810	Y	Y	Y	N	Y	Brownish black	med-coarse	5-15%	Vitrophyric /porphyritic	Loose scoria lapilli deposit with coarse ash
AG66	20060107	9	2738965	6228810	N	Y	Y	N	N	Rusty brown red	fine	35-40%	Vitrophyric /porphyritic	Part of scoria clast, appears red exterior and blackish brown interior.
AG67	20060108	44	2739045	6228906	Y	N	Y	N	Y	Black	med-coarse	10-20%	Vitrophyric /porphyritic	Loose black scoria lapilli deposit with coarse ash. Chips off larger clasts couldn't bring home to do vesic work
AG68	20060109	45	2739054	6228947	Y	Y	Y	Y	YY	Yellow brown	med-coarse	10-15%	Vitrophyric /porphyritic	Loose pumice lapilli deposit, some clasts show faint mingling, crystal rich, minor denser scoria/pumice of darker brown colour. Chips off larger clasts couldn't bring home to do vesic work

AG69	20060110	45	2739054	6228947	Y	N	Y	N	Y	Blackish brown	med-coarse	10-20%	Vitrophyric /porphyritic	Loose scoria lapilli deposit with coarse ash and lithics. Chips off larger clasts unable to bring home to do vesic work
AG70	20060111	15	2739121	6228992	Y	Y	Y	Y	Y	Blackish brown	med-coarse	10-20%	Vitrophyric /porphyritic	Loose scoria deposit with coarse ash. Chips of larger clasts couldn't bring home to do vesic work
AG71	20060112	15	2739121	6228992	Y	N	Y	N	N	Dark orange brown	med-coarse	10-15%	Vitrophyric /porphyritic	Loose scoria lapilli and ash deposit, some mingled pumice & scoria. Chips of larger clasts unable to bring home to do vesic work.
AG72	20060113	15	2739121	6228992	N	Y	Y	N	N	Brownish red	fine	10-15%	Vitrophyric /porphyritic	Weathered red scoria from welded unit
					Analyses Undertaken					**Hand Specimen Description**				
Sample ID	**Waikato #**	**Field Site**	**Easting**	**Northing**	**Sieve**	**TS**	**Density**	**MP**	**XRF**	**Colour**	**Grain Size**	**Vesicularity**	**Texture**	**Other Comments**
AG73	20060114	50	2739134	6228835	N	N	N	N	N	Brownish orange outside with black inside	fine	10-15%	Vitrophyric /porphyritic	Weathered scoria clasts from moderate welded scoria unit. Partial welding at some point contacts but not all, mainly clast supported unit. Clast has large vesicles in the centre and smaller ones on the outside.
AG74	20060115	53	2738480	6228017	N	Y	Y	N	Y	Dark grey with minor pink	med	2%	Porphyritic	Dense strongly welded unit, some minor stretched out ribbons of clasts.
BL01					N	Y	Y	Y	Y	Black	fine	10%	Vitrophyric /porphyritic	From welded units on the side of Blue Lake, partway downslope, possible North Crater source.

Appendix B
Stratigraphic Columns

Stratigraphic Column

Field Trip: Eastern Gully 1 - North Crater

Date: 16 (day) 1 (month) 2006 (year)

Field Site: 1

Region: North Crater Tongariro National Park - Tongariro

Location: 2739446 6228547

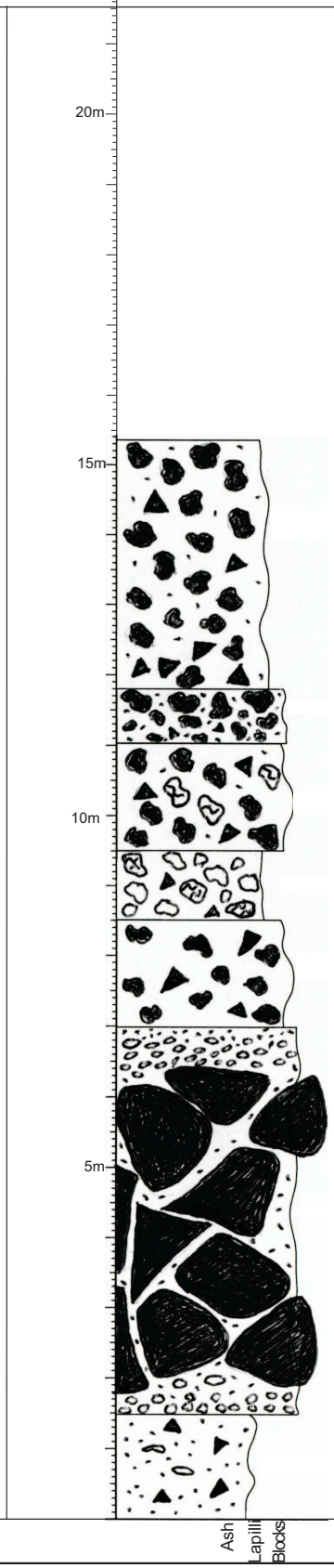

Black scoria unit, non-poorly welded lapilli and bomb, massive unit. Juvenile clasts 8-10cm max 35cm, moderately vesicular. Dense angular blocks 10-15% size 8-10cm, rare >1m and appear to be wall rock lithics, angular to sub-angular. Juvenile clasts sub-angular to sub-round. Predominantly clast supported, very minor matrix. Appears to be a concentration of dense clasts near base of unit, which has a sharp contact with lower unit.

Red-black scoria non-welded unit, clasts appeared weathered on outside to red/brown colour. Clasts coarse lapilli and bomb size 4-6cm up to 12-15cm, moderately vesicular. Some black and cream mingled scoria and pumice, moderate-high vesicular. Predominantly clast supported, but minor matrix bearing of coarse ash. Some dense angular lithics 10-15%. Has a sharp contact with the lower unit.

Black scoria non-welded unit. Clasts bomb and blocks of size 8-10cm and poor-moderately vesicular. Clasts have ragged appearance and are sub-angular to sub-round. Some dense angular lithics <10%, max size 12cm. Unit has a sharp contact with lower unit.

Creamy yellow pumice unit. Massive, poorly sorted, non-welded lapilli to small bombs 5-8cm. Dense juveniles of black and red scoria, mingled pumice/scoria. Dense angular lithics 10-15% size 4-6cm, max 12cm. Unit clast supported with weak matrix support. Unit appears to lens in and out further up and down slope.

Black scoria non-welded unit. Clasts bomb and blocks of size 7-10cm poor-moderately vesicular. Clasts have ragged appearance and are sub-angular to sub-round. Some dense angular lithics <10%, max size 12cm. Unit has a sharp contact with lower unit.

Black coarse ash bed not seen here, possible lenses out at this site, or been removed during deposition of upper unit.

Red-orange breccia unit. Very coarse ash and lapilli with dense clasts grades quickly down into very large clasts 50cm-1m, poorly sorted weathered red-orange colour, with agglomerate zones (possible margins of large clasts). Rugged spatter like clasts >1m with irregular boundaries, interspersed with non-welded fine scoria zones. Presence of dense angular lithics indicate pyroclastic origin. Juveniles dense to poor vesicular. Very dense blocks at base of breccia.

Greenish-cream tuff. Exposed in lower stream cutting below breccia. Highly consolidated. Very fine ash with some pumice lapilli, mud like deposit, contains dense lithics and rounded mud like balls 1-2cm diameter - possible accretionary lapilli. Disintegrate when try to extract from face. Unit possibly highly weathered as so mudlike.

Stratigraphic Column

Field Trip: Eastern Bluff - North Crater

Date: 16 (day) 1 (month) 2006 (year)

Field Site 2

Region: North Crater Tongariro National Park - Tongariro

Location: 2739327 6228093

Thick. (m)	Graphic Log	Sample No	Description
20m			
			Pinky red scoria unit strongly welded, some weathering to brown-red. Top surface is very knobbly spatter, clasts appear sub-rnd to slight cowpat-like, 3-6 cm, mod/poor vesic, cryst rich. Quickly grades down into clasts being less visible, entire unit strongly welded. Grades down to clast outlines not visible, intensly welded. Minor dense angular WRL, dark grey, 8-12cm max 45cm. Slight gradational contact with lower unit.
10m		AG10	Pink/grey scoria unit. Some pink stretched clast ribbons in pinky grey groundmass. Strongly welded. Minor dense angular WRL 8-10 cm.
			Grey scoria unit, strong/intense welded, poor-mod vesic, cryst rich. Columnar joints seen giving some areas smooth face, other areas have knobble face like below. Some clast shapes seen, cowpat-like, -6-8cm. Some dense angular WRL 10-15cm, dark grey/black, cryst rich.
		AG12	Red scoria unit, strongly welded, cryst rich, minor dense lithics (dark grey). Can see some clast shapes which appear elongate and slightly flattened. Columnar jointing at regular intervals (~2m), smooth face where jointing has occurred, knobbly in some areas where no jointing. Unit appears to lens in at base on the bluff at this site and tapers out quickly.

Ash Lapilli Blocks

Stratigraphic Column

Field Trip: North Bluff - North Crater

Date: 23 (day) 1 (month) 2006 (year)

Field Site: 7

Region: North Crater Tongariro National Park - Tongariro

Location: 2739101 6229057

Thick. (m)	Graphic Log	Sample No	Description
40m			
30m			
20m			
10m			Black scoria unit, poorly welded/compacted at base 30cm, moderatly welded above. Clasts appear sub-rnd to rnd and moderatly vesicular and 6-7cm in upper mod welded section. Dense angular WRL 5-7cm dark grey/black. Matrix and some clast support. Black scoria unit poorly welded/compacted at base 40cm, moderatly welded above. Clasts appear sub-rnd to rnd and moderatly vesicular and 6-7cm in upper mod welded section. Dense angular lithics 5-7cm dark grey/black with large white crystals and sub-angular. Matrix support and some clast support. Greyish brown pumice lapilli unit. Similar to seen earlier. Pumice poor vesicular outside but high vesicular inside, and crystal rich with large black crystals <4mm. Clasts 6-8cm max 15cm, min 1cm. Clasts weathered to greyish brown outside but have brown interior. Clast supported, massive, non-welded. Dense ang WRL dark grey to black, 4-7cm, max 12cm. Scree ledge Pinkish red scoria unit. Highly weathered outside to dark grey, some thin bedding (cm scale) can be seen which tapper out with distance. Strongly welded unit. Dense sub-ang WRL seen.

Ash Lapilli Blocks

Stratigraphic Column

Field Trip: North Bluff - North Crater

Date: 23 (day) 1 (month) 2006 (year)

Field Site: 8

Region: North Crater Tongariro National Park - Tongariro

Location: 2739001 6228885

Thick. (m)	Graphic Log	Sample No	Description
40m			
30m			
20m			
10m	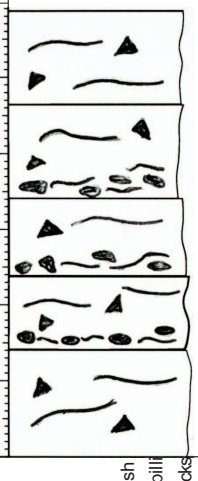		Greyish black scoria unit, intensely welded, medium grey to black colour, crystal rich. Some dense angular WRL, but cannot see scoria clasts. Unit tappers out quickly over 40m to the north. Irregular fractures or columnar joints extend partway into the unit below. Greyish black scoria unit, strongly welded with smooth rock face where jointing has caused blocks to fall off. Dense angular lWRL seen, dark grey, 4-6cm. Some stretched out/elongated dark grey clasts. Basal 10cm moderalty welded can see knobble clast appearance to face where some erosion has occured and forms narrow ledge into unit below. Greyish black scoria unit, strongly welded, some dense angular WRL(~20%) 3-6cm dark grey. Cannot see indivitual clast shapes and sizes but face has a knobbly appearance. Base 10cm mod welded as narrow ledge formed into unit below. Greyish black scoria unit, strongly welded. Dense angular WRL 3-6cm dark grey. Hard to make out indivitual clast shapes and sizes but face has a knobbly appearance. Base 10cm moderately welded as narrow ledge formed to unit below. Greyish black scoria unit, strongly welded, some dense dark grey WRL 3-5cm . Clast appear 6-8cm, with knobbly appearance to face, dip of unit ~29-30'.

Ash Lapilli Blocks

Stratigraphic Column

Field Trip: North Bluff - North Crater

Date: 28 (day) 1 (month) 2006 (year)

Field Site 9

Region: North Crater Tongariro National Park - Tongariro

Location: 2738965 6228810

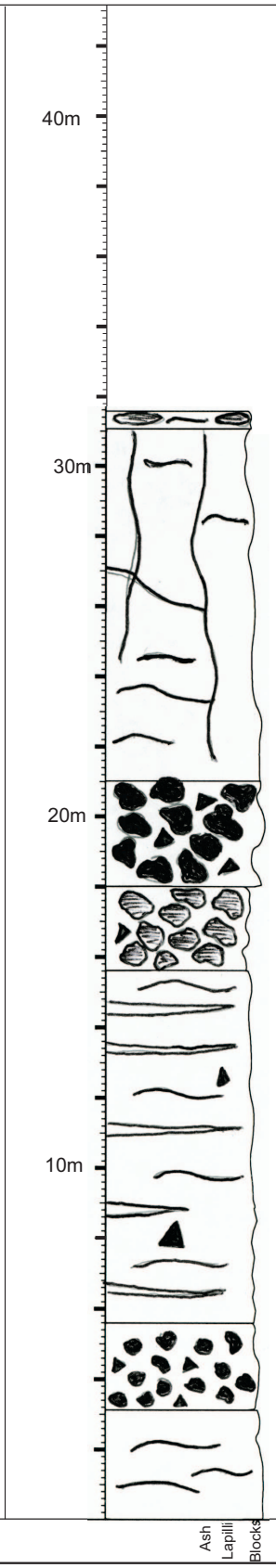

Pinky red scoria. Srongly welded cowpat like clasts.

Medium grey intensly welded scoria unit. Irregular jointing seen with informal columnar jointing. Clasts can no longer be seen. Appears non-graded, massive and jointing has caused smooth face surfaces in some areas. Blocks are 1.5-2m wide and 2.5-3m high. Some lithic seen 2-4cm

Non to poorly welded black scoria unit, still porous and vesicular in some areas (not compacted). Clast supported with minor matrix support. Scoria poor-mod vesicular and sub-rnd, sixe 8-15cm max 20cm, but also smaller 2-4cm mixed in. Poorly sorted seems, massive. Some dense angular WRL 3-4cm light grey fine-med grained.

Red scoria unit non-welded. Clast supported with minor matrix support. Clasts sub-angular to sub-rounded, some slightly elongated. Some clasts have others stuck to them. Scoria mod-poor vesicular, size 12-18cm max 22cm. Crystal rich 1-2mm, some clasts show weathered. Forms narrow scree ledge.

Strongly welded pinkish red scoria unit. Where jointing has occured and blocks fallen off areas of bedding can be seen on dm scale. Some irregular fractures have caused blocky appearance to upper face. Unit crystal rich 1-2mm, dense sub-angular WRL present (~20%) 8-18cm max 85cm.

Black scoria unit, clast and minor matrix supported. Some lWRL (~5%) of 4-8cm. Unit is non welded but some consolidation,massive and poorly sorted. Scoria clasts sub-rnd and poor-mod vesicular, crystal rich. Forms a narrow scree ledge.

Pinkish red scoria unit, strongly welded can see occasional stretched clast outline off lighter grey colour. Red scoria appears moderatly vesicular when breaking sections off. Some minor bedding features can be seen in the upper half on dm scale. Has a wavy bottom contact with the unit below.

Stratigraphic Column

Field Trip: North Bluff - North Crater

Date: 28 (day) 1 (month) 2006 (year)

Field Site 10

Region: North Crater Tongariro National Park - Tongariro

Location: 2739022 6228818

Thick. (m)	Graphic Log	Sample No	Description
			Pinky red scoria agglutinate. Strongly welded cowpat like clasts.
			Medium grey dense/intensly welded scoria agglutinate unit. Irregular jointing seen with informal columnar jointing. Welding is so intense clasts can no longer be seen. Appears non-graded, massive and jointing has caused smooth face surfaces in some areas. Blocks are 1.5-2m wide and 2.5-3m high. Some lithic seen 2-4cm.
			Non to poorly welded black scoria unit, still porous and vesicular in some areas (not compacted). Clast supported with minor matrix support, scoria poor-mod vesicular and rounded, size 8-15cm max 20cm, but also smaller 2-4cm mixed in. Poorly sorted seems to be no grading. Some dense angular lithics 3-4cm light grey fine-med grained. Scoria weathered on the outside to grey colour. scoria is very crystal rich (plagioclase)
			Red scoria unit non-welded, clast supported with minor matrix support. Clasts sub-angular to sub-rounded with irregular shapes and some slightly elongated. Some clasts have others stuck to them. Scoria mod-poor vesicular, size 12-18cm max 22cm, minor 4-6cm(broken fragments). Some mingled clasts present. Crystal rich 1-2mm. Forms narrow scree ledge to unit above.
		AG04	Strong/densly welded pinkish red agglutinate unit. Where jointing has occured and blocks fallen off areas of bedding can be seen indicating flow movement on the scale of 20-50cm. Some irregular fractures have caused blocky appearance to upper face. Possibly some areas of squashed and smeared black scoria clasts, but hard to distinguish as up too high. Unit crystal rich 1-2mm, dense sub-angular lithics present (~20%) (poss juvenile) 8-18cm max 85cm.
			Weathered scoria to light pinky brown colour, not seen at site 9. Non-poorly welded, clast supported with minor matrix. Clasts sub-round to round and mod vesicular, forms an undercut notch to unit above.
			Black scoria unit, clast and minor matrix supported. Some lithics seen (~5%) of 4-8cm. Non welded but some consolidation, non graded and poorly sorted. Scoria clasts sub-round and poor-mod vesicular. Cannot distinguish actual base of unit but forms a narrow scree ledge. Scoria is crystal rich 1-2mm.

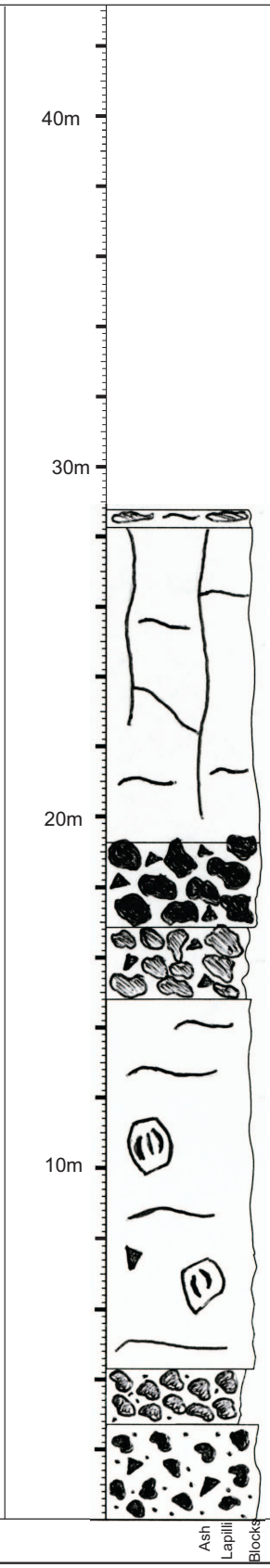

Stratigraphic Column

Field Trip: Eastern Gully 1 - North Crater

Date: 27 (day) 1 (month) 2006 (year)

Field Site 12

Region: North Crater Tongariro National Park - Tongariro

Location: 2739448 6228565

Thick. (m)	Graphic Log	Sample No	Description
			Black scoria unit, moderately welded some dense angular WRL about 12-20cm.
			Scree ledge
			Black scoria unit, partial welded, but pockets of poor welding. Clasts mod vesic, 10-15cm max 20cm. Some red scoria <5cm, poor vesic present. Dense angular WRL, light grey 3-8cm max 30cm, one large block 1.8x0.7m 'floating' in unit.
			Light orange/red scoria unit. Scoria 1-4cm, with some small WRL 3-5cm, non-welded, forms small scree ledge. Grades down into lower unit.
			Orange/red breccia. Lenses out suddenly 1m downslope from here. Large blocks 20-40cm max 1m. At top of unit grades quickly from red scoria 8-10cm into the breccia, near base grades back into red scoria 1-4cm (about 10cm), sharp base contact.
			Greenish cream ash and pumice tuff. Highly consolidated. V. fine ash w. dense lithics and rounded weathered? mud like balls <2cm, and some pumice lapilli. Poss higly weathered? very mud like.
			Black scoria unit, non-welded, clasts 2-3cm &6-8cm, max 18cm, mod-vesic, sub-rnd. Dense angular WRL 4-6cm. Some matrix support but mainly clast supported.
			Rubbley creamy grey pumice unit. Some mingled clasts present. Some matrix and clast support. Clasts crystal rich, rounded, 2-5cm. Dense angular light grey WRL 5-7cm, minor dark weathered scoria 6-7cm, mod vesic.

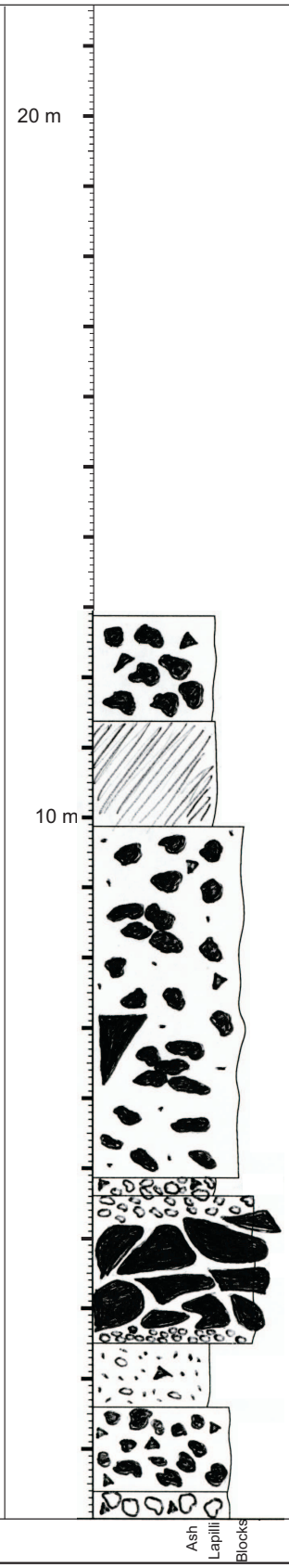

Stratigraphic Column

Field Trip: Eastern Gully 1 - North Crater

Date: 27 (day) 1 (month) 2006 (year)

Field Site 13

Region: North Crater Tongariro National Park - Tongariro

Location: 2739395 6228513

Thick. (m)	Graphic Log	Sample No	Description
10 m			
5 m			Brownish black scoria unit, poorly welded. Clasts mod-vesic, 8-15cm max 20cm. Dense angular WRL blocks 'floating' in, 20-30cm max 80cm, dark grey. Black scoria, looks like smaller clast size w. more matrix. Above is the brownish black unit again.
			Blackish brown (weathered) scoria unit. Poorly welded or compacted with clasts 8-12cm. Dense angular WRL blocks (~25%), 18-25cm, dark grey. Some red dense scoria <5cm. Top forms a ledge to the unit above
			Yellow/brown pumice unit, non-welded, clast supported. Clasts 8-10cm max 13cm, mod-poor vesic, sub-rnd. Minor dense red scoria, sub-rnd to sub-ang, 5-8cm max 15cm. Dense angular WRL, 3-5cm.dark grey. Mingled clasts (~15%), 8-10cm. Gradational contact with upper unit, scree below.

Ash Lapilli Blocks

Stratigraphic Column

Field Trip: North Bluff - North Crater

Date: 18 (day) 1 (month) 2006 (year)

Field Site: 15

Region: North Crater Tongariro National Park - Tongariro

Location: 2739121 6228992

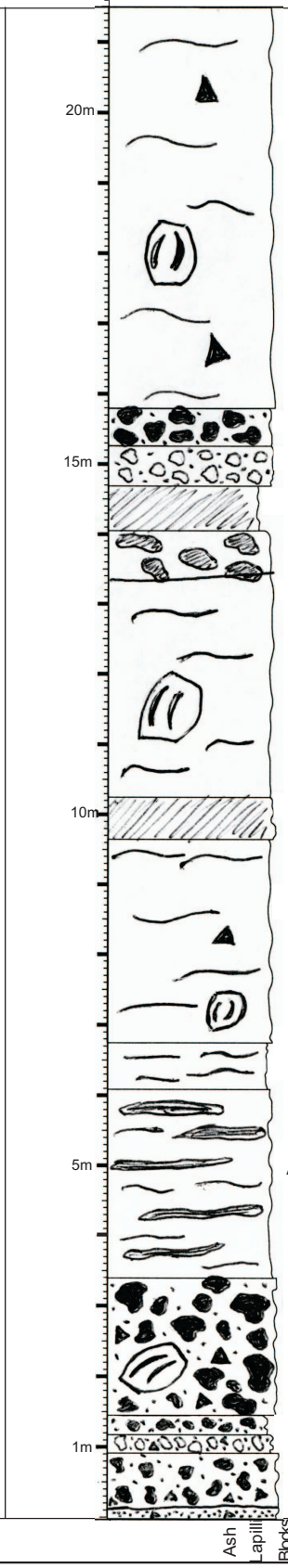

Thick. (m)	Graphic Log	Sample No	Description
			Pinkish red scoria unit - highly weathered outside to dark grey and covered in moss some thin beds can be distinguished, appear to tapper out with distance? highly welded unit, containing welded pinkish red spatter and dense lithics (wall rock or juveniles??). bedding structures are visible about 20-30cm
			whitish grey pumice unit, non welded
			Scree slope, forms a narrow but steep ledge
			Pinkinsh red scoria spatter deposit, strongly welded. Similar characteristics to the upper pinkish red unit. Contains large dense angular lithic blocks max 25cm.
			Whitish grey pumice unit, non welded, possibly similar to upper pumice unit.
			Pinkish red scoria spatter unit., similar to units above
			Pinkish red scoria spatter unit. Has sharp contacts with upper and lower units of the same characteristics. Knobbly base can be seen on overhangs. Strongly welded, unit can be traced around the outcrop and above cave.
			Pinkish red scoria agglutanate unit, moderatly welded, can see scoria clasts sub-rounded and slightly elongated, semi cool when landed but not as hot a previous units as not as strongly welded. Clast supported with some matrix
		AG72	Black scoria unit, contains large dense blocks (35%) (wall rock and juvenile) some w. surface cracking, are dark grey and cryst rich, size 15-30cm, max 40cm. Scoria is rounded and has some matrix support, size 8-15cm to lapilli size. Some scoria contains sugur like lumps of quartz crystals. Small rounded pinkish red scoria clasts also seen, size 4-6cm (~5%). Some scoria near base in weathered to lighter brown/grey w. dark grey/brown middle. Sugar lump of quartz cryst.
			Black scoria unit. rare to no lithics and non welded. scoria clasts range 6-8cm, max 10cm. minor matrix to clast supported. scoria clasts in bottom of unit show alteration/weathering to light brown colour, inside of clast still black. clasts mod to well vesicular and sub-angular to sub-rounded. in this photo cannot see upper contact with black scoria+lithic unit seen in above photo. estimated unit thickness of max 25cm. sharp contact with unit below
			Creamy grey pumicious unit. moderate to highly vesicular. inside clast larger vesicles seen in centre with high concentration of small vesicles within 1-2cm of clast surface.. clast supported with minor amounts of matrix - possibly from pumice rubbing together though? non-welded and forms small scree surface. sharp contact with unit below.
		AG70 AG71	Black scoria and lithic unit. dense lithics range 8-15cm, min 2cm, max 40cm. clasts show red/brown iron weatheing near top of unit. concentration of lithics near base of unit. clast supported and non-welded, rather compaction instead. desnse lithics predominantly dark to medium grey, with some pinkish red. lithics angular and blocky. scoria clasts sub-rounded and moderatly vesicular. near base of unit minor pumice (~5%) weathered/alteration of scoria and pumice near base contact to brownish orange colour with 'fresh' interiors. Sharp basal contact with unit below.
			Basal fine grey ash unit with dense angular WRL (5-10cm)

Stratigraphic Column

Field Trip: Eastern Gully 1 - North Crater

Date: 1 (day) 2 (month) 2006 (year)

Field Site 17

Region: North Crater Tongariro National Park - Tongariro

Location: 2739396 6228616

Thick. (m)	Graphic Log	Sample No	Description
	10 m		
	5 m		Redish/brown agglutinate unit. Moderately welded but not compacted as can see clast shapes and gaps between clasts. Clasts sub-rnd (some elightly elongate)parallel, 5-6cm and smaller 2-3cm. Dense angular WRL 5-6cm (~25%). Unit appears massive i.e. no bedding visible, possible failed joints have given face smooth appearance.
			Redish/brown scoria agglutinate unit. Clasts 2-6cm, mod-high vesic, few poor-vesic (dense juvenile ~10%) 2-3cm. Rare dense WRL (~5%) 2-3cm. Grades from lower unit.
			Redish/brown scoria unit. Non welded, minor matrix support, mostly clast support. Clasts appear slightly broken/ground up/irregular, 0.5-1cm, others 5-8cm. Few dense angular WRL (~5%), 4-6cm. Grades into upper unit.

Ash Lapilli Blocks

Stratigraphic Column

Field Trip: Amphitheatre - North Crater

Date: 1 (day) 2 (month) 2006 (year)

Field Site 19

Region: North CraterTongariro National Park - Tongariro

Location: 2739290 6228426

Thick. (m)	Graphic Log	Sample No	Description
	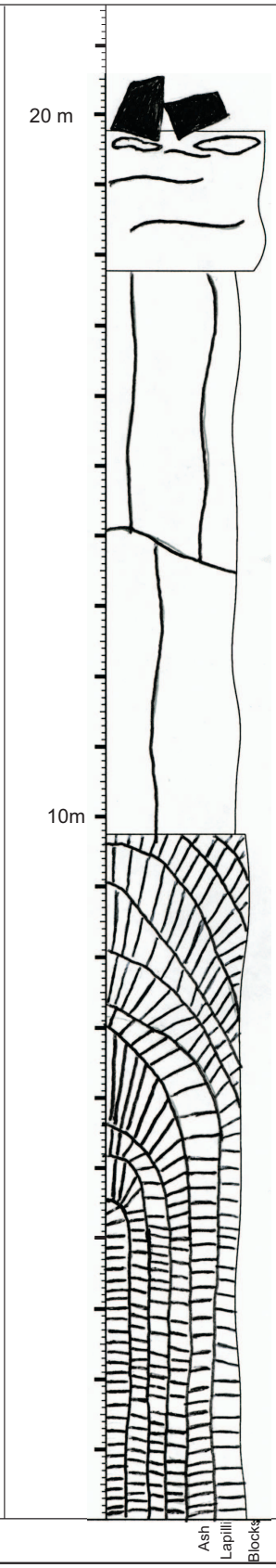		Minor pinkish agglutinate lower part and large blocky boulders covering the top. Boulders possibly from the explosion pit as similar light grey colour and crystal rich.
		AG22	Massive light/med grey andesite lava, crystal rich. Some irregular to columnar jointing (large blocks), some blocks have curving fractures. Very similar to unit below and to those in explosion pit.
			Light grey andesite lava unit - possible part of lava lake in crater as at the crater lip and has eroded out to form an ampitheatre. Unit appears massive but is higly broken up by parallel and irregular platy fractures. Some vertical/horizontal while others start of vertical but then curve over, some just irregular patterns. Is crystal rich. Lava is very dense/intensely welded, can distinguish some xenoliths 2-5cm, creamy white colour, quartz like lumps also seen.

Stratigraphic Column

Field Trip: Amphitheatre - North Crater

Date: 1 (day) 2 (month) 2006 (year)

Field Site 20

Region: North Crater Tongariro National Park - Tongariro

Location: 2739289 6228424

Thick. (m)	Graphic Log	Sample No	Description
20 m			
		AG23	Pinkish red agglutinate, strongly welded, some bedding seen, knobbly clast appearance to face. Clasts seen 8-12cm, sub-rnd slightly cowpat, poor vesic. Possibly less welded at base as small notch/ledge formed.
10m			Pinkish red scoria agglutinte unit. Strongly/densely welded, but messy looking face but hard to distinguish individual clasts. Moderalty welded at very base as forms a small notch/ledge in face.
			Strongly welded pinkish red agglomerate unit. Ghost clasts clearly seen as stretched 1-2cm thick, grey ribbons parallel to slope dip. Some faint red/grey bedding seen on 20cm scale. Informal columnar jointing present. Welding decreases to moderatly/poorly welded quickly downslope. unit tappers out quickly down slope.

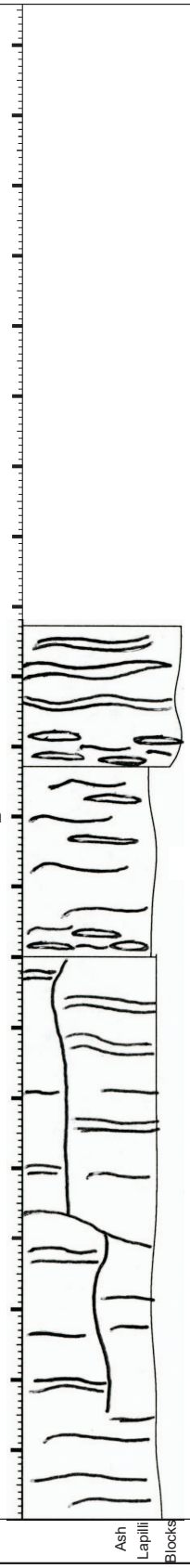

Stratigraphic Column

Field Trip: Eastern Gully 2 - North Crater

Date: 2 (day) 2 (month) 2006 (year)

Field Site 24

Region: North Crater Tongariro National Park - Tongariro

Location: 2739578 6228431

Thick. (m)	Graphic Log	Sample No	Description
			Pinkish red scoria unit, grades into lower unit. From base grades up from non welded to partially welded pockets. Non welded areas clast supported with minor matrix support. From base clast size reversly graded, bottom clasts 3-4cm, middle 8-10cm to 20-30cm, some larger seen dispersed in unit with very irregular shapes. This unit thickens considerable upslope, has nearly tappered out at this site.
			Black (and minor brown) scoria unit. Large brownish black(weathered) scoria clasts, 12-18cm, mixed with smaller irridescent blue scoria, 3-6cm (max 8cm), all clasts sub round. Poor/mod sorted, mod/high vesic. Few WR lithics (1-4cm) dense, angluar very dark grey. Non welded, predominantly larger scoria near top (minor reverse grading). Grades into upper and lower units.
			Orangy brown scoria/pumice lapilli unit, lighter (more weathered) brown in upper portion and more orangy in bottom portion. Clasts (sub)round, with some clast and matrix support, matrix is coarse ash and small lap. Clast poor/mod vesic, clasts slightly larger at top, 3-4cm and grade down to 1-<1cm. Clasts crystal rich, small amounts of mingled pumice seen. Seen to lens in and out down slope. Some dense angular lithics dark grey/black and cryst rich. Grades into upper unit.
			Sharp, but wavy contact with lower unit. Bluish grey fine/very fine ash unit. Very narrow grey ash bed halfway through unit of slightly coarser ash. Rest of unit is massive.
			Grades (slightly) from below into purplish grey med/fine ash, can see interbedding of slightly browner ash of finer grain size. Few minor lapilli size pumice clast cen be seen.
			Black scoria unit, some irridescent blue scoria seen. Near top smaller 1-3cm size with matrix.Cannot see past 5cm depth because of too much scree. Has a gradational contact with the upper unit. Contains some dense sub-ang lithics very dark grey/black (3-4cm, ~10%). Non welded matrix to minor clast supported. Clast mod to high vesic and poor to mod sorted.
			Scree

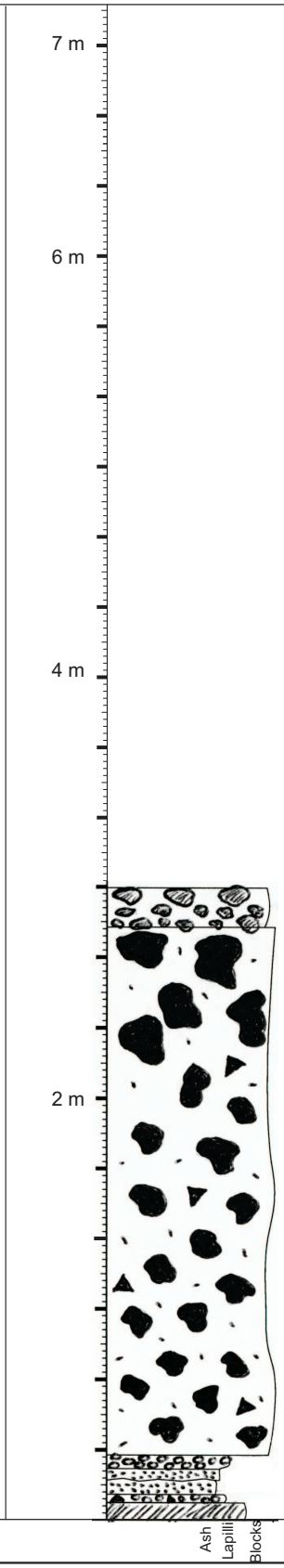

Stratigraphic Column

Field Trip: Eastern Gully 2 - North Crater

Date: 2 (day) 2 (month) 2006 (year)

Field Site 25

Region: North Crater Tongariro National Park - Tongariro

Location: 2739548 6228439

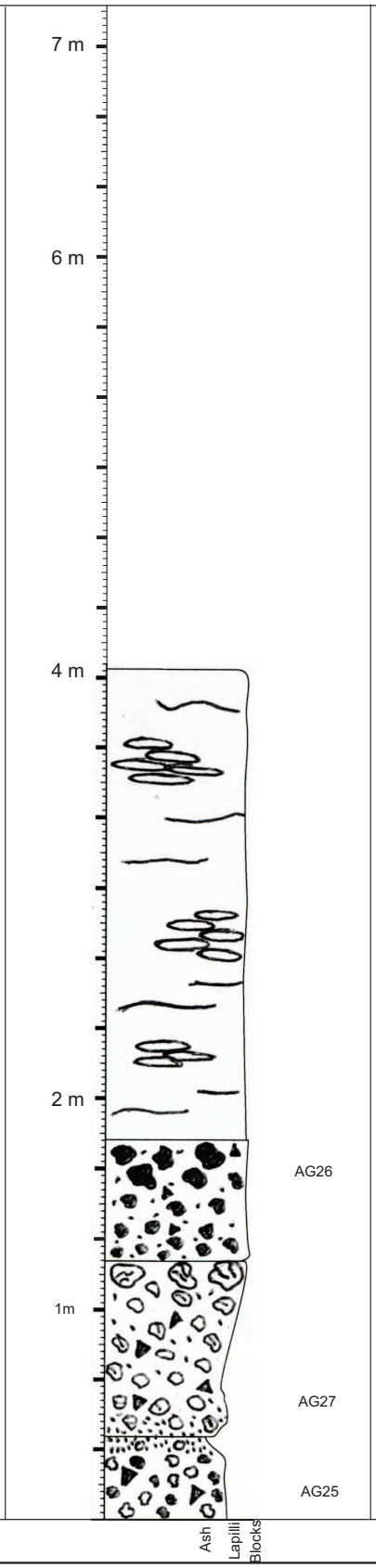

Pinkish red scoria unit. Moderately welded pockets rest poorly welding agglutinate unit. Knobbly appearance to face, scoria clasts appear 3-4cm and mainly clast support. Clasts sub-rnd to minor elongate. Hard to well define unit as no easy access, but appears to fit with the red scoria unit at site 27.

Black (and minor brown) scoria unit clast supported. Large brownish black(weathered) scoria clasts, 12-15cm (max 20cm) irregular clasts in top portion,middle of unit clasts 4-8cm (max 10cm) mixed with smaller irridescent blue scoria, all clasts sub round. Poor/mod sorted, mod-high vesic. Few WR lithics (4-7cm) dense, angluar very dark grey and cryst rich. Some red scoria lap poor vesic. Non welded but consolidated, predominantly larger scoria near top (minor reverse grading). Some clasts show mingling.

Orangy brown pumice lapilli unit, clasts poor-mod vesice, crystal rich, 4-7cm (max 9cm)and round to sub-rnd. At top clasts large 6-8cm and browner. Clast with some matrix support, matrix is very coarse ash and small lap. Some dense angular lithics dark grey/black and cryst rich. Minor mingled pumice (faint brown colour) and minor black mod-vesic scoria lapilli. Sharp upper and lower contacts but near base of unit grades down into smaller 2-4cm lapilli and orangy red colour with very coarse ash matrix at base.

Mixed scoria lapilli unit, some irridescent blue scoria seen with mingled scoria clasts and minor creamy brown pumice and some pinkish red scoria, clasts 2-4cm, but most 1-2cm. Contains some dense sub-ang WR lithics very dark grey/black (1-3cm, ~5%) and cryst rich. Non welded matrix supported with very coarse ash. Clast poor vesic and poor to mod sorted. Upper 5cm contains predominantly very coarse ash and small lapilli.

Stratigraphic Column

Field Trip: Eastern Gully 2 - North Crater

Date: 2 (day) 2 (month) 2006 (year)

Field Site 27

Region: North Crater Tongariro National Park - Tongariro

Location: 2739499 6228381

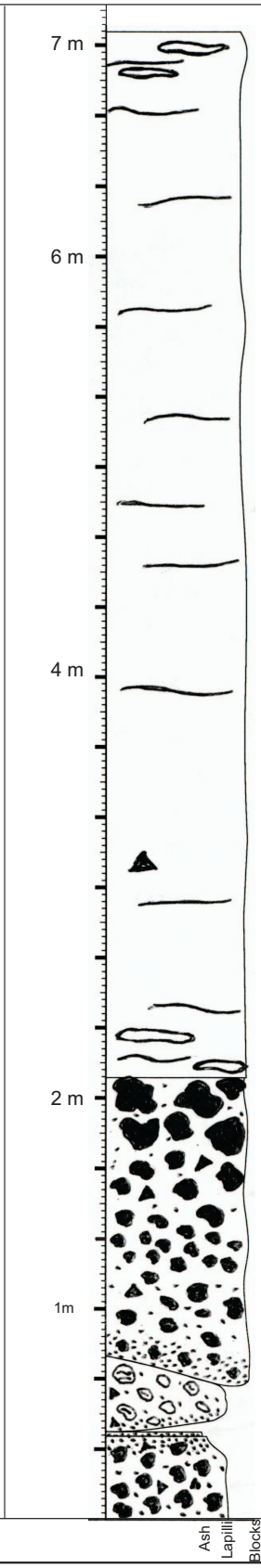

Description

Pinkish red scoria unit. Strongly welded agglutinate unit. Knobbly appearance to face with irregular jointing. Hard to well define unit as no easy access, but appears to fit with the red scoria (non welded) unit at site 25.

Black (and minor brown) scoria unit. Large brownish black(weathered) scoria clasts, 18-25cm (max 85cm) irregular clasts in top portion,middle of unit clasts 4-8cm (max 10cm) mixed with smaller irridescent blue scoria, all clasts sub round. Bottom 10cm very coarse dark grey/black ash with some scoria clasts (3-5cm). Poor/mod sorted, mod/high vesic. Few lithics (4-7cm) dense, angluar very dark grey and cryst rich. Some red scoria lapilli poor vesic. Non welded but consolidated, predominantly larger scoria near top (minor reverse grading). Some clasts show red mingling. In the middle of this unit there is a ~20cm section where ther black scoria grades into orangy brown and red scoria lapilli, the clasts are non welded, poorly sorted and mod-vesic.

Orangy brown pumice lapilli unit, clasts poor vesice, crystal rich, 4-7cm (max 9cm)and round to sub-rnd. Unit waves in and out up/down slope. Clast with some matrix support. Matrix is very coarse ash and small lap. Some dense angular lithics dark grey/black and cryst rich. Minor mingled pumice (faint brown colour) and minor black mod-vesic scoria lap. Sharp upper and lower contacts.

Narrow wedge of consolidated blue/grey fine ash. Minor orangy pumice lapilli. Is only a narrow wedge here but thickens both up and down slope by some cm's.

Black scoria unit, some irridescent blue scoria seen, clasts 3-5cm. Contains some dense sub-ang lithics very dark grey/black (1-3cm, ~5%) and cryst rich. Non welded, matrix supported. Clast mod to high vesic and poor to mod sorted. Upper 5cm contains predominantly very coarse ash and small lapilli. Minor pinkish red scoria lap <1-1.5cm

Stratigraphic Column

Field Trip: Eastern Gully 2 - North Crater

Date: 2 (day) 2 (month) 2006 (year)

Field Site 28

Region: North Crater Tongariro National Park - Tongariro

Location: 2739481 6228384

Thick. (m)	Graphic Log	Sample No	Description
7 m			
6 m			Poorly welded agglutinate unit. Large scoria bombs can be distinguished with other scoria clasts stuck to outside in flight or rolling. Clasts 40-50cm with some smaller 6-10cm and poor-mod vesicular. Most rounded to slightly elongated. Dense angular lithics 6-12cm are dark grey to black with large white crystals (rich). Clast supported, minor matrix. Near base grades into partially welded and the changes to strongly welded scoria agglutinate
4 m			Pinkish red scoria unit. Strongly welded agglutinate unit. Smooth appearance to face where jointed blocks have fallen off with iregular jointing. Upper contact is gradational from the non welded unit, but has a sharp contact with unit below. Unit is massive and crystal rich with minor WR lithics seen.
2 m			Black (and minor brown) scoria unit. Large brownish black(weathered) scoria clasts, 6-8cm (max 15cm) irregular clasts in top portion. Poor/mod sorted, mod/high vesic. Few WR lithics (8-12cm) dense, angluar very dark grey and cryst rich. Some red scoria lapilli poor vesicular. Non welded but consolidated, predominantly larger scoria near top (minor reverse grading).
			Orangey brown pumice lapilli unit, clasts poor vesice, crystal rich, 6-12cm (max 20cm)and round to sub-rnd. Clast with some matrix support. Matrix is very coarse ash and small lapilli. Some dense angular WR lithics dark grey/black and cryst rich. Mingled pumice and minor black mod-vesic scoria lap. Grades into units above and below
1m			Black scoria unit, some irridescent blue scoria seen, clasts 3-5cm. Contains some dense sub-ang lithics very dark grey/black (1-3cm, ~5%) and cryst rich. Non welded matrix supported. Clast mod to high vesicular and poor to mod sorted.Grades into units above and below
			Orangey brown pumice lapilli unit, clasts poor vesicular, crystal rich, 2-4cm (max 5cm)and round to sub-rnd. Clast with some matrix support. Matrix is very coarse ash and small lapilli. Some dense angular lithics dark grey/black and cryst rich. Minor mingled pumice and minor black mod-vesic scoria lapilli. Grades into unit above.

Ash Lapilli Blocks

Stratigraphic Column

Field Trip: Eastern Gully 2 - North Crater

Date: 2 (day) 2 (month) 2006 (year)

Field Site 29

Region: North Crater Tongariro National Park - Tongariro

Location: 2739441 6228381

Thick. (m)	Graphic Log	Sample No	Description
			Pinkish red scoria unit, poorly welded (strongly weathered). Clasts 6-15cm min 3cm, poor vesic, sub-rnd. Minor matrix very coarse ash but clast supported. Some clasts with red weathered outside w. grey/black poor vesic inside. Minor dense angular WRL ~10%, dark grey, 3-5cm. Some clasts have others stuck to them to give irregular shape, some have breadcrust outside.
			Black scoria unit, blue irredescent colour, mod sorted, poorly welded, compact clast supported w. minor matrix. Clasts 8-12cm, min 2cm, max 18cm, sub-ang to sub-rnd. ~10% red scoria, poor vesic/dense, rnd, cryst rich, 5-6cm. Dense angular WRL 8-15cm, min 3cm max 22cm. Quartz xenoliths (sugar lumps) <2cm found
			Creamy brown pumice unit, poor welded. Clasts 5-9cm max 12cm, min 2cm, poor-mod vesic, sub-rnd some slightly elongate. Most clast support with minor matrix of small lapilli & coarse ash. Some small black scoria 1-3cm ~10%, dense angular WRL, dark grey, cryst rich, 8-12cm, dense juvenile clasts sub-rnd 5-7cm. Minor mingled pumice visible.
			Reddish/brown scoria unit (joins top unit from site 28), pooly welded with pockets of moderate welded. Clast supported with minor matrix, clasts 4-7cm min 1cm, max 10cm, poor vesic, cryst rich. Dense angular WRL, dark grey, 1-4cm, cryst rich. Larger clasts have weathered red outside with mod-vesic black inside

10 m

5m

Ash Lapilli Blocks

Stratigraphic Column

Field Trip: East Slope - North Crater

Date: 7 (day) 2 (month) 2006 (year)

Field Site 36

Region: North Crater Tongariro National Park - Tongariro

Location: 2739624 6228444

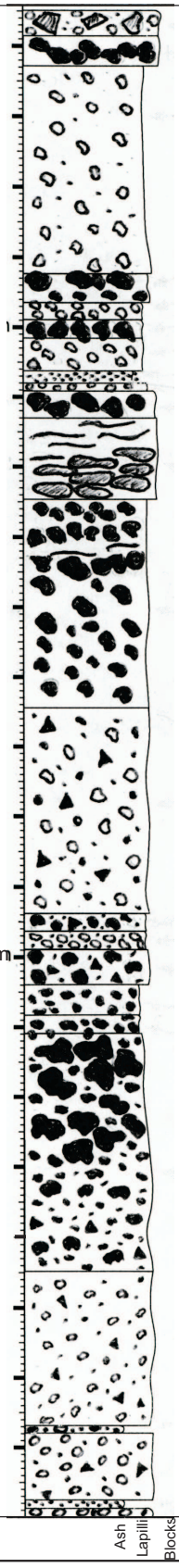

Thick. (m)	Sample No	Description
		Small debris type avalance or block'n'ash flow
		Black scoria, mod welded, clasts appear 5-10cm, mod vesic. Some weathered to brown on top.
		Yellow/brown pumice lapilli unit, minor mingled clasts. Clast supported, 1-3cm, cryst rich, poor vesic, minor coarse ash matrix. Dense WRL 2-3cm.
		Black scoria, grades from non-welded scoria lapilli 1-3cm to welded bombs 5-10cm, some with breadcrust features, minor mingled clasts. Grades into upper unit.
		Yellow/brown pumice lapilli, poor-mod vesic cryst rich. Mix of yellow pum with small red & black scoria, minor mingled clasts, .8-3cm max 7cm. Minor matrix but clast supported. Dense WRL.
		Grades from lower unit. Black scoria, irridescent blue in some, clasts 5-10cm max 18cm, sub-rnd, some weathered, moderatly welded, minor WRL.
		Yellow/brown pumice lapilli, 0.5-1.5cm max 3cm,cryst rich, poor vesic. ~10% WRL. Minor black & red scoria <1cm. Grades up into black scoria 4-6cm. Minor coarse ash matrix.
		Purplish grey med ash, w. poor vesic scoria <1.5cm and WRL, no bedding visible.
		Orangy/brown pumice lapilli, crystal rich, mod/poor vesic. Minor mingled clasts. Matrix of coarse ash
		Grades from below into weathered black scoria, moderatly welded, mod vesic, cryst rich, minor WRL.
		Red scoria unit, stongly welded at top grades down to moderatly welded. knobbly appearance, mod vesic, 4-8cm and poorly welded at very base (grades into lower unit). Minor WRL 2-4cm.
	AG52	Black scoria unit, poorly welded bottom ~1m, clast supported. Irridescent blue black, mod-well vesic, minor small lapilli to 3-5cm max 8cm, cryst rich. Mingled clasts (~15-20%) & some light grey clasts 1-2cm present. Some poor vesic/dense juvenile clasts. Grades up into moderately welded black scoria for ~80cm, some irregular jointing & clasts indistingushable. Grades into poorly welded black scoria lapilli 2-4cm, sub-rnd, some large poor vesic scoria ~15-20cm max 30cm slightly elongate.
		Yellow/brown pumice lapilli unit. Similar to earlier units, round clasts, 3-4cm and 1-4cm. Dense angular WRL 3-6cm dark grey, cryst rich. Minor black & red scoria <1cm, poor vesic. Minor matrix v. coarse ash. Mainly clast supported.
		Black scoria unit. Non welded, clasts sub-rnd to sub-ang, 20-30cm, some smaller 8-10cm and 4-6cm. Dense angular WRL 6-8cm. Clast supported.
		Orangy/brown pumice lapilli, clasts sub-rnd, 3-4cm, cryst rich, poor vesic. Minor coarse ash matrix, clast supported, similar to orangy/brown units below. Minor WRL
		Black scoria lapilli, grades quickly from lower unit. Clasts 4-6cm, poor vesic, cryst rich, some weathering. Grades up into moderate welding in middle and back to poor welded at top. Few mingled clasts seen near top/bottom. Dense angular WRL <1cm, & dense juvenile w. breadcrust texture.
		Blackish/brown (weathered) scoria lapilli, 0.5-1.5cm sub-rnd. Matrix of very coarse ash. Some black & red scoria poor vesic, <1cm. Minor mingled clasts (~10%). Minor dense angular WRL <1cm.
		Grades from lower unit into non-welded purplish/black scoria lapilli 1-2cm. Weathered.
		Lower 1.2m black scoria lapilli, sub-rnd, poor vesic, 0.8-1.5cm, larger 5-7cm mod-vesic scoria and 12-20cm scoria. Clast supported, dense angular WRL 8-15cm. Grades up into ~1m poorly welded black scoria, clasts 1-4cm, poor vesic, WRL. Grades up into top section of moderately welded black scoria, sub-rnd, 4-6cm.
		Grades from lower unit into orange/brown pumice lapilli , clasts 2-4cm max 8cm, mod vesic, cryst rich, sub-rnd. ~5% mingled clasts. Red & black scoria <1cm, round, poor vesic. Dense angular WRL 1-4cm dark grey (~20%). Minor coarse ash matrix. 1.8m up from base small lens of black poor vesic scoria/lapilli 5-8cm, sub-rnd w. minor dark grey/black ash matrix.
		Grades from below into band of weathered scoria (brown/black), sub-rnd, 6-10cm max 15cm. Mixed with grey/brown lapilli.
		Orange/brown pumice lapilli. Pumice 3-5cm &<1cm, sub-rnd. ~25% mingled clasts. Mod vesic & cryst rich. Some clasts pinky-orange. Matrix of coarse-med ash. Some black & red scoria ~0.5cm. Dense angular WRL dark grey, cryst rich, angular 2-4cm max 6cm.
		Fine light grey ash. No bedding seen, consolidated, sharp upper & lower contacts.
		Orange/brown pumice lapilli. Non-welded, poor sorted, clasts mod/poor vesic, sub-rnd, 0.5-2cm max 4cm. Matrix v. coarse-med ash, with black & red poor vesic scoria, sub-rnd. Pumice cryst rich. Some mingled clasts, sub-rnd. Dense angular WRL 6-8cm dark grey. Cannot see base of unit.

Stratigraphic Column

Field Trip: Eastern Slope - North Crater

Date: 7 (day) 2 (month) 2006 (year)

Field Site 38

Region: North Crater Tongariro National Park - Tongariro

Location: 2739686 6228639

Thick. (m)	Graphic Log	Sample No	Description
			Large grey, massive andesitic bounders sitting on top (from lava flow or deposited here). Very similar to the massive lava unit seen at site 37, possible tumbled down from the bluffs up slope.
			Block & ash flow draping topography. Large block 0.5-1.5m, some also 10-20cm and 2-5cm. Floating in ash matrix, no apparent grading. Very similar in appearance to that at site 36 but w. larger blocks.
			Red scoria agglutinate unit. Poor to mod welded, clasts appear 2-4cm & football/elongate. Dense angular WRL 5-8cm, max 30cm
			Black scoria lapilli unit, clast supported, clasts 3-6cm, poor vesic, cryst rich, rounded. Dense angular WRL 7-12cm, dark grey (~30%)
			Yellow brown pumice lapilli unit clast supported, clasts 2-3cm, round, cryst rich, poor/mod vesic. Minor dense angular WRL 4-6cm.
			Black scoria lapilli unit clast supported, clasts 2-4cm, mod vesic, cryst rich, sub-rnd to sub-ang. Minor dense angular WRL, dark grey 5-7cm.
			Yellow brown pumice lapilli unit clast supported, clasts 2-3cm, round, cryst rich, poor/mod vesic. Minor dense angular WRL 4-6cm
			Purplish black fine ash, fine wavy bedding seen
		AG47	Yellow brown pumice lapilli unit clast supported, clasts 1-5cm max 8cm, mod vesic, minor black scoria 5-9cm, mod vesic. Dense angular WRL 2-4cm, dark grey, can see cryst easily.
			Purplish black med-coarse ash, wavey, grades into lower unit.
			Brown/black (weathered) scoria lapilli unit poor vesic <1cm, & minor yellow/brown pumicle lapilli 2-3cm. Dense angular WRL, dark grey. Some very coarse dark grey ash. Interbedded with few thin black units, appear very coarse ash or small lapilli.
			Yellow brown pumice lapilli, clasts <2cm max 3cm, round, cryst rich, poor-mod vesic. Larger dense angular WRL 4-8cm

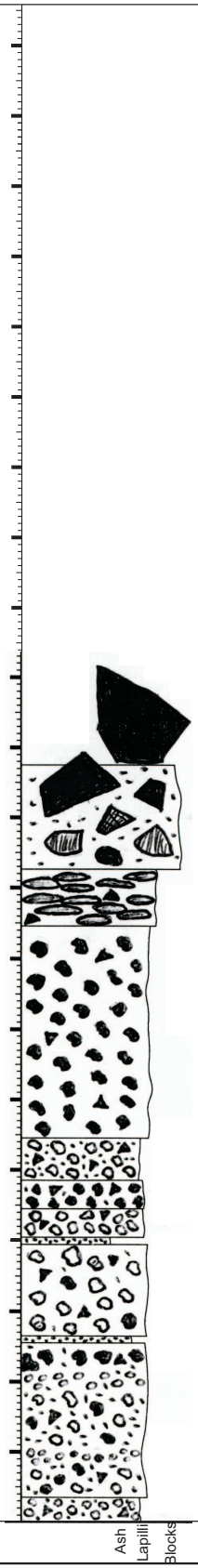

Stratigraphic Column

Field Trip: Eastern Gully 1 - North Crater

Date: 8 (day) 2 (month) 2006 (year)

Field Site 39

Region: North Crater Tongariro National Park - Tongariro

Location: 2739710 6228700

Thick. (m)	Graphic Log	Sample No	Description
	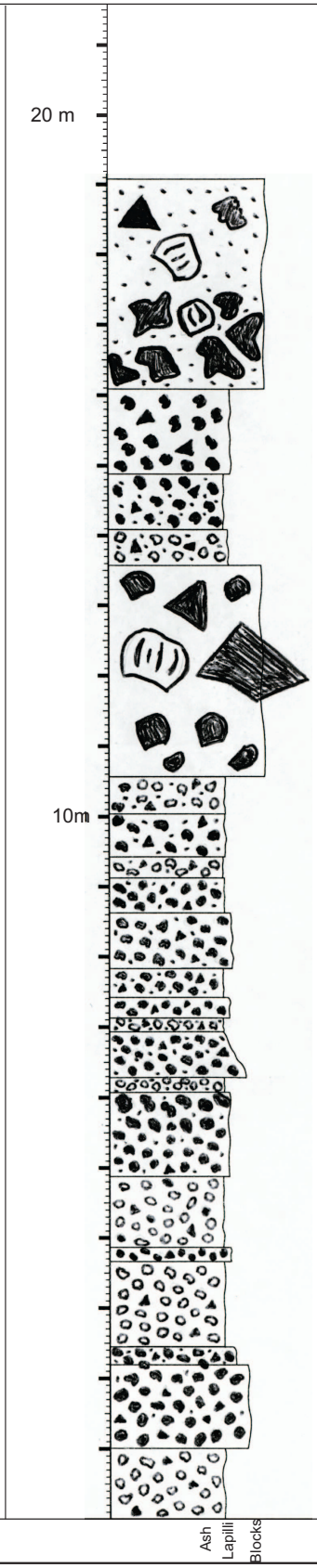		
			Block & ash flow, some coarse ash bedding seen in very top w. blocks 8-10cm, grades down from low concentration of block at top to high concn near bottom blocks 0.5-1m max 1.5m. Matrix supported
			Red scoria unit, mod-poorly welded, clasts 2-4cm & 8-10cm. Some dense angular WRL 5-8cm & dense juveniles 15-30cm, sub-rnd to sub-ang (some stuck together).
			Black scoria lapilli unit, clasts 1-3cm max 5cm, mod vesic, sub-rnd. Some minor matrix coarse ash, minor dense angular WRL 1-2cm.
			Yellow brown pumice lapilli unit, clasts 1-3cm max 6cm, poor vesic, cryst rich, round. Some red & black scoria round <1cm, minor dense angular WRL 1-3cm.
			Block & ash flow, weathered blocks 15-40cm max 2m, mix of dense red and dense grey blocks sub-rnd. Minor dense angular WRL 20-30cm. Fine-med ash matrix blocks 'floating' in w. some lapilli 1-2cm.
			Yellow brown pumice lapilli unit, clasts 1-3cm max 5cm. Some minor red & black scoria <1cm. Minor dense angular WRL 1-3cm, dark grey.
			Black scoria lapilli unit, clasts 1-3cm max 5cm, minor red scoria <1cm, dense angular WRL 1-2cm max 4cm, dark grey.
			Yellow brown pumice lapilli unit, clasts 1-3cm max 5cm. Some minor red & black scoria <1cm. Minor dense angular WRL 1-3cm, dark grey.
			Blackish brown scoria lapilli unit. Clasts 1-3cm max 4cm, some red scoria (<1cm). Dense angular WRL 1-3cm dark grey. Clast supported.
			Black scoria lapilli unit, clasts 1-3cm, mod vesic, sub-round. Minor dense angular WRL 1-3cm max 8cm.
			Redish brown scoria lapilli unti, <2cm max 4cm, poor vesic, w. minor black scoria 1-2cm.
			Blackish brown (weathered) scoria lapilli unit. Clasts 1-3cm max 4cm, some red scoria (<1cm). Dense angular WRL 1-3cm dark grey. Clast supported.
			Yellow orange pumice lapilli unit, clasts round <2cm, poor/mod vesic, cryst rich w. coarse ash. Minor black scoria (<1cm) poor vesic.
			Black scoria unit. At top lapilli <2cm grades down into 5-8cm w. mixed lap in middle and grades into lower section dense scoria 12-18cm. All clasts poor vesic, sub-rnd. Some pockets of mod welding, very base is non welded. Clast supported rest.
			Yellow brown pumice lapilli, <2cm round, poor vesic. Dense angular WRL 1-2cm, minor coarse ash.
			Black scoria lapilli unit, clasts 2-4cm (some <1cm), poor vesic grades into clasts 4-6cm and grades into clasts 20-35cm. All sub-rnd poor/mod vesic. Clast supported.
			Yellow brown pumice lapilli unit 0.5-1.5cm, minor black scoria (round) <1cm. Minor dense angular WRL, dark grey 2-4cm.
			Small lense in the pumice unit. Black scoria 1-3cm, poor vesic, minor dense angular WRL 2-3cm
			Yellow brown pumice lapilli unit 0.5-1.5cm, minor black scoria (round) <1cm. Minor dense angular WRL, dark grey 2-4cm.
			Reddish/brown scoria lapilli unit. Some large sub-rnd scoria w. black centres, few mingled clasts 6-9cm. Most lapilli 2-4cm & some black <1cm. Minor matrix coarse ash, slight gradational contact into lower unit.
			Black scoria unit, clast supported, some 9-15cm sub-rnd others 6-8cm, most 0.5-2cm. Mod vesic. Minor dense angular WRL 1-3cm.
			Yellow brown pumice lapilli unit, clasts <2cm, poor vesic w. very coarse ash. Minor black round scoria <2cm. Minor dense angular WRL 1-2cm. Few lenses of black scoria <1.5cm in middle.

Stratigraphic Column

Field Trip: Eastern Slope - North Crater

Date: 13 (day) 2 (month) 2006 (year)

Field Site 42

Region: North Crater Tongariro National Park - Tongariro

Location: 2739529 6228784

Thick. (m)	Graphic Log	Sample No	Description
2m	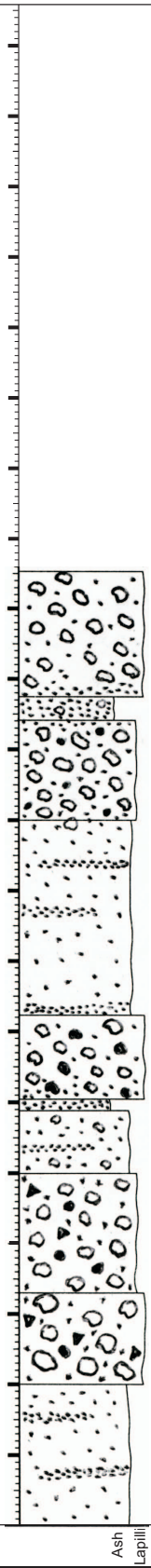		Yellow/brown pumice lapilli unit. Clasts 2-4cm max 7cm, poor/mod vesic, rnd, clast supported, cryst rich. Some red scoria mod vesic, rnd. No lithics, unit weathered near top.
			Dark grey fine ash, with minor pumice lapilli, grades into lower unit.
			Yellow/brown pumice lapilli with minor red/black scoria, matrix supported. Clasts 1-4cm, few <1cm, matrix med/coarse ash dark grey + yellow/red, no lithics, grades into lower unit.
			Coarse ash, dark grey + yellow/red small lenses. Minor pumice+scoria <1cm in ash. Bed of darker grey coarse/med ash at very bottom
1m			Yellow/brown pumice and reddish brown scoria lapilli, clast supported, clasts mod/high vesic, sub-rnd, 2-3cm min 0.8cm max 8cm. Some dense angular WRL 2-4cm dark grey. Some pumice poor/mod vesic, minor matrix of coarse ash and very small lapilli. Grades into lower unit.
			Dark grey fine/med ash, grades into lower unit.
			Very coarse ash. Band of fine/med dark grey+red+yellow ash in middle. Back into very coarse ash then band of fine/med ash at bottom again. In the finer ash bands some lapilli can be seen.
			Yellow brown pumice lapilli, 2-2.5cm, sub-rnd. Some black scoria & some weathered with black interior, lots of very coarse ash. Clast supported, clasts rnd, 0.5-1.5cm max 2.5cm, poor vesic, cryst rich, minor coarse ash matrix. Minor dense WLR.
			Grades into large yellow brown pumice lapilli, poor/mod vesi 2.5-5cm.
			Coarse ash, some med/dark grey with minor very coarse red/orange ash. Small lens of red/orange very coarse ash ~5cm down from top mod/well sorted, no bedding seen.

Ash Lapilli Blocks

Stratigraphic Column

Field Trip: North Bluff - North Crater

Date: 18 (day) 2 (month) 2006 (year)

Field Site 44

Region: North Crater Tongariro National Park - Tongariro

Location: 2739045 6228906

Thick. (m)	Graphic Log	Sample No	Description
			Pinky red scoria agglutinate. Strongly welded cowpat like clasts
			Medium grey dense/intensly welded scoria agglutinate unit. Irregular jointing seen with informal columnar jointing. Welding is so intense clasts can no longer be seen. Appears non-graded, massive and jointing has caused smooth face surfaces in some areas. Blocks are 1.5-2m wide and 2.5-3m high. Some lithic seen 2-4cm
			Non to poorly welded black scoria unit, still porous and vesicular in some areas (not compacted). Clast supported with minor matrix support. Scoria poor-mod vesicular and rounded, size 8-15cm max 20cm, but also smaller 2-4cm mixed in. Poorly sorted seems to be no grading. Some dense angular lithics 3-4cm light grey fine-med grained. Scoria weathered on the outside to grey colour. Scoria is very crystal rich
			Red scoria unit non-welded. Clast supported with minor matrix support. Clasts sub-angular to sub-rounded with irregular shapes and some slightly elongated. Some clasts have others stuck to them. Scoria mod-poor vesicular, size 12-18cm max 22cm, minor 4-6cm. Some mingled clasts. Crystal rich 1-2mm. Some clasts show yellow/red colour (poss weathered). Forms narrow scree ledge.
			Strong/densly welded pinkish red agglutinate unit. Where jointing has occured and blocks fallen off areas of bedding can be seen indicating flow movement on the scale of 20-50cm. Some irregular fractures have caused blocky appearance to upper face. Possibly some areas of stretched and smeared black scoria clasts, but hard to distinguish as up too high. Unit crystal rich 1-2mm, dense sub-angular lithics present (~20%) (poss juvenile) 8-18cm max 85cm
			Black scoria unit, clast and minor matrix supported. Some lithics seen (~5%) of 4-8cm. Non welded but some consolidation. Non graded and poorly sorted. Scoria clasts sub-round and poor-mod vesicular. Cannot distinguish actual base of unit but forms a narrow scree ledge. Scoria is crystal rich 1-2mm.
			Pinkish red agglutinate, strongly/densly welded, can see occasional stretched out ghost clasts off lighter grey colour. Some small lithics but hard to distinguish because of the weathered face. Red scoria appears moderatly vesicular when breaking sections off, but hard to see any clast shape or size as welded. Some minor bedding features can be seen in the upper half. Has a wavy bottom contact with the unit below.
			Weathered black scoria to med brown/yellow colour. Has a irregular upper surface (thickness of 80-15cm). Is clast supported with minor lithics (<5%). Clasts sub-round to round and mod vesicular. They still have black colour on inside of clast.
			Black scoria unit (fresh) consolidated but poorly welded. At base a very coarse ash and lapilli size material with lithics size 2-3cm of dark grey colour (is ~8cm thick), then band of larger black scoria poor vesicular and crystal rich clasts 8-12cm and dense angular lithics 8-10cm. Grades up again into being clasts of 2-6cm max 12cm poor vesicular clast supported with minor matrix, has large dense sub-angular lithics 10-18 cm (~15%)
			Yellow/brown pumice unit. Larger more vesicular pumice at the top 4-8cm, grades into lapilli 1-2cm max 4cm, poor vesicular, crystal rich. Minor black scoria seen of .4-.8cm poor vesic, dense angular lithics 3-4cm. Very coarse ash also seen, so poorly sorted. Sharp contact with above.
			Black/brown scoria unit, clast support with minor matrix support clasts sub-rnd to rnd and 5-8cm at base and others 1-2cm. Crystal sugar lumps seen 1-2cm. Scoria mod vesic, minor lithiscs angular (black w. white crystals) <2cm. One large bomb (juvenile) seen 45cm with jigsaw cracks.
			Yellow/brown pumice clasts 3-5cm in some coarse ash matrix, some lithics (~20%) dense angular, dark grey similar to those in unit above.
		AG67	Red/black weathered unit, strongly welded with knobbly appearance on face. Can see squashed, cowpat-like black scoria. Clasts appear sub-rnd, mod vesicular, minor sub-ang/rnd lithics 4-7cm, with smaller 1-3cm clasts near base contact.
			Strongly welded black scoria unit, grades from clasts 1-2cm to 8-12cm over 70cm Dense angular dark grey WRL 4-8cm, poor-mod vesicular scoria. Appears to be pinkish red welded scoria underneath but hard to tell.

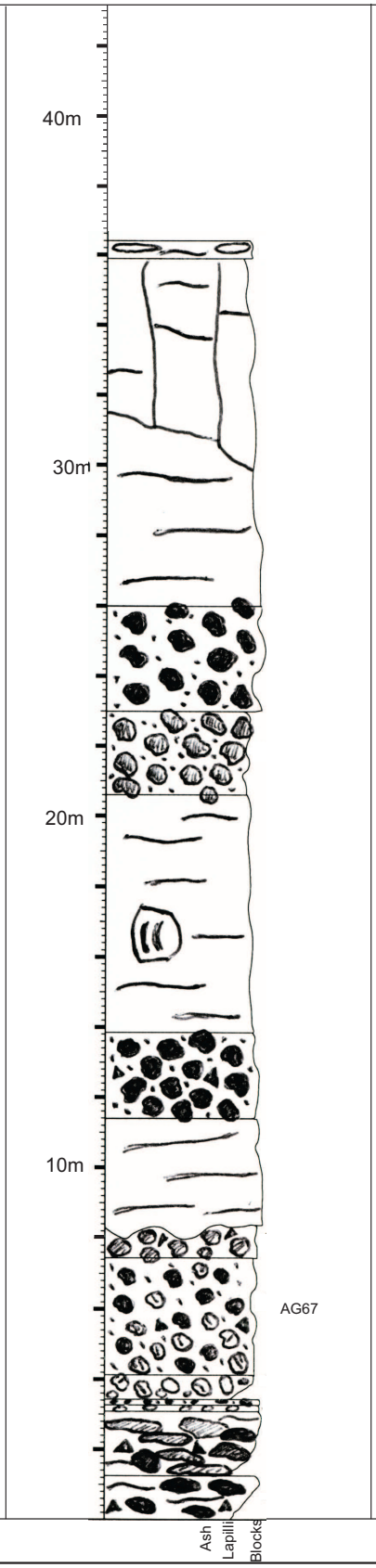

Stratigraphic Column

Field Trip: North Bluff - North Crater

Date: 13 (day) 2 (month) 2006 (year)

Field Site: 45

Region: North Crater Tongariro National Park - Tongariro

Location: 2739054 6228947

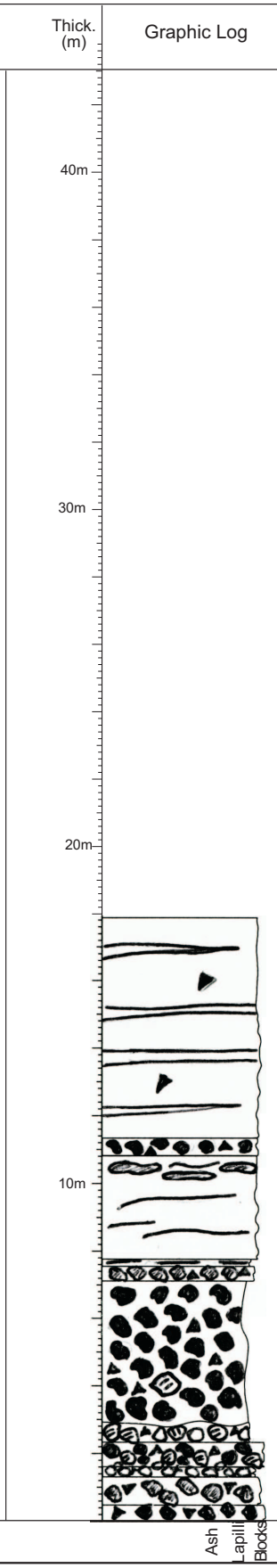

Red/grey scoria unit, strong/intensly welded. Bedding structures can be seen in more welded areas on 30-40cm scale. In less compacted beds can still see some clast shapes. Some irregular fractures. Dense angular lithics can be seen in fresh face appear 5-10cm.

Black scoria unit, non welded, clast supported with minor coarse matrix. Clasts appear 5-10cm but hard to tell. Dense angular lithics seen(10%), 5-10cm.

Red scoria unit. Bottom ~2.5m is strong/densley welded with stretched clast ribbons, can see some clast outlines in fresh section to face. Minor dense angluar lithics. Grades into upper 0.5m of unit is mod welded red scoria, clasts appear 5-15cm

Strongly welded red scoria unit, some minor bedding, dm scale

Scoria unit weathered to yellow/brown. Red interior to clasts, non welded, clast supported, sharp upper and lower contact.

Black scoria unit, poorly welded/compacted. Clasts sub-rnd to rnd and moderatly vesicular. Dense angular WRL 2-5cm dark grey. Some juvenile 30-40cm very dense but show breadcrust or jigsaw cracking on outside. Clast supported with minor matrix. Bedding can be seen in more welded areas cm-dm scale.

Yellow/brown pumice lapilli unit. Clasts 1-3cm some <1cm, max 6cm, cryst rich. Minor mingled yellow and brown pumice, some very coarse ash to fine lapilli matrix but predom clast supported. Minor weath brown scoria 3-5cm. Dense angular WRL 1-2cm max 4cm. Found creamy green crustal xenolith.

Black/brown scoria unit. Contains mingled pumice clasts 3-4cm moderate vesicular, minor 1-2cm pumice. Minor dense red scoria (<5%), minor dense angular WRL dark grey to black, 4-8cm concentrated in centre of unit. In centre of unit lens/bed of red/yellow weathered scoria, clasts 5-12cm poor vesic to dense and crystal rich.

Yellow/brown pumice lapilli unit. Minor black scoria, moderate vesicular, max 6cm, pumice moderate vesicular and crystal rich, 3-6cm max 8cm. Mainly clast supported some matric coarse ash. Dense angular WRL dark grey to black, 3-4cm, min1cm. Grades into above unit over 5cm

Red scoria unit. Some clasts have black interior with red weath outside. Clasts 2-4cm, max 10cm, min <1cm. Moderatly/poorly welded unit. Scoria poor vesicular, but black interior is moderatly versicular, cryst rich. Minor dense angular WRL(10%), dark grey to black, crystal rich (white cryst) and 2-3cm max 6cm. Grades into unit above over 5cm.

Black/brown scoria lapilli unit. Dense angular WRL, 2-4cm. Clast supported (minor ash matrix) and non-welded, compaction instead. Dense lithics(10%) predominantly dark grey to black. Scoria clasts sub-rnd, moderatly vesicular, 2-4cm max 8cm, few <1cm, cryst rich. Grades into unit above over 5cm.

Stratigraphic Column

Field Trip: North Bluff - North Crater

Date: 14 (day) 2 (month) 2006 (year)

Field Site: 48 - Horseshoe

Region: North Crater Tongariro National Park - Tongariro

Location: 2739191 6228768

Thick. (m)	Graphic Log	Sample No	Description
20m	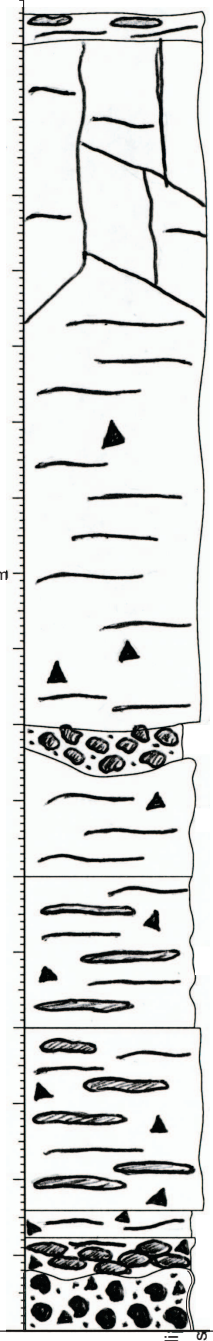		Top capping unit of red agglutinate, similar to what seen at other sites
			Red/grey unit strongly/intensly welded with informal columnar joints and some irregular fractures. At base appears moderately welded and can see knobbly clast face which grades up into stongly/intensly welded. Where joints have failed can see smooth face. Few dense angular WRL visible in base area, but cannot distinguish clasts in unit.
10m			Red/brown weathered scoria unit. Poor-mod welded, clasts appear sub-rnd, ~4-6cm, but hard to see.
			Pink/grey unit, strongly/intensly welded, can see stretched clast ribbons, are irregular and 'wavey' not just horizontal. Thinkness of unit varies along outcrop.
			Red/brown scoria unit. Moderatly welded, forms a bit of a ledge as less welding than lower unit. Clast shaps visible as cowpat/compact. Looks similar to lower unit but just not so strongly welded. Hard to distinguish many features as bit covered by grass.
			Red/brown scoria unit. Strongly welded, but clasts not squashed or too compacted. Very knobbly appearance to face, clasts appear 5-10cm & poor vesic, cryst rich. Dense angular WRL (~5%) 2-5cm, dark grey.
			Medium grey agglutinate unit. Strongly welded with stretched clast ribbons. Cannot see clast shapes in face. Dense angular WRL 3-5cm max 15cm visible.
			Red/brown scoria agglutinate unit. Moderaly welded, but poorly welded at base, clasts 2-3cm, poor-mod vesic. Dense angular WRL (~10%) 3-4cm max 6cm, clast supported, no matrix.
			Black scoria unit, non welded, 2-4cm max 8cm, moderate vesicular, sub-ang to sub-rnd. ~30% red scoria poor vesic, cryst rich, sub-rnd 2-4cm. Dense angular WRL and juvenile clasts dark grey/black, cryst rich. Top 15cm mod welded. Possibly base contact with a red scoria agglutinate unit.

Ash Lapilli Blocks

Stratigraphic Column

Field Trip: South Bluff - North Crater

Date: 15 (day) 2 (month) 2006 (year)

Field Site 53

Region: North Crater Tongariro National Park - Tongariro

Location: 2738480 6228017

Thick. (m)	Graphic Log	Sample No	Description
	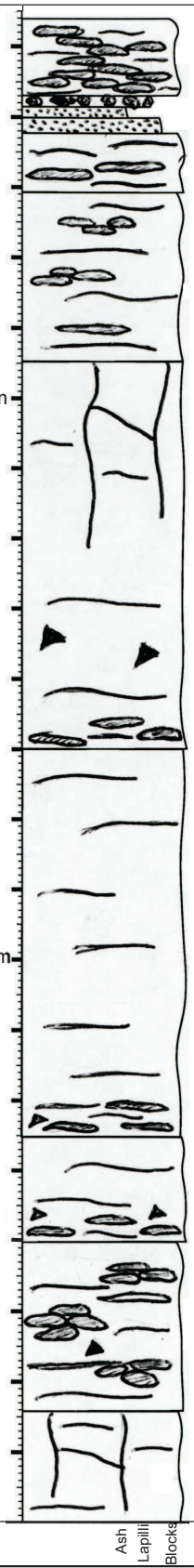	AG74	Weathered red scoria unit. Moderatly welded, mod-poor vesicular, cryst rich. Some dense black/grey scoria included in (most 6-10cm) some cowpat like.
			Orangy brown scoria unit. Weathered. Some black scoria 1-1.5cm poor vesicular, some dense WRL <1cm
			Med-fine grey ash. Weathered, from younger Tongariro vents?
			Very weathered fine ash unit to grey/yellow. Found several red scoria <1cm.
			Reddish scoria poorly welded grades into moderately welded at base. Clasts flat/cowpat like.
			Possible upper section to unit below. Strongly welded but has knobbly clast appearance to face. Clasts sub-rnd to elongate shape. Some minor ribbon features seen pinching out. Crystal rich, poor-mod vesicular scoria.
			Pink/grey unit, very similar to base unit. Some clasts visible near base (moderately welded), but quickly grades up to strongly/intensely welded. Can see pink ribbons of clasts stretched out 1-3mm thick. Dense sub-ang WRL 3-5cm. Scoria clasts seen stretched out to 25-30cm long/4-5cm thick. columnar jointing 3-4m apart with irregular fractures near top.
			Red scoria unit mod welded at base quick gradational change to strongly/intensely welded. Some clasts still visible in areas - knobbly face. But some stretched clast ribbons. Clasts appear 6-8cm max 15cm, sub-round/elongate to flat, cryst rich. Dense sub-ang WRL 6-10cm max 15cm, some columnar jointing.
			Red/black scoria unit. Moderate welded gradational at base where forms small notch. Grades up into strongly welded. See black clasts mod-poor vesicular, sub-rnd to elongate shape, 4-6cm, others stretched clast ribbons. Red scoria 4-6cm poor vesicular, cryst rich. Dense sub-ang WRL 3-5cm max 15cm. Minor columnar joints.
			Red scoria unit with grey/black scoria, areas strongly welded some stretched clast ribbons and flatened clasts visible. Other areas less compacted but just as welded can easily see sub-rounded clast shape welded at contacts, few clasts flattened or football shape, 1-3cm wide/3-5cm flat. Dense sub-ang WRL 3-5cm max 8cm.
			Grey/pink scoria unit, with very long thin (1-3mm)pink and grey stretched out clast ribbons. Strongly/intensly welded, cryst rich & coarse vesicular like texture. Some irregular fractures and columnar joints seen through heigh of exposed blocks.

Stratigraphic Column

Field Trip: South Bluff - North Crater

Date: 15 (day) 2 (month) 2006 (year)

Field Site 54

Region: North Crater Tongariro National Park - Tongariro

Location: 2738726 6227840

Thick. (m)	Graphic Log	Sample No	Description
	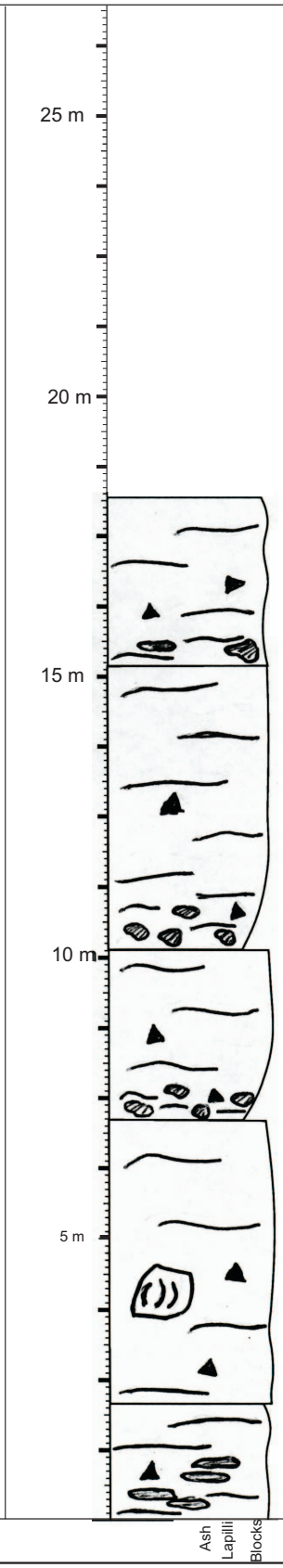		
			Grey/pink scoria unit, stongly welded upper with stretched clast ribbons, can see clasts easier at base (moderate welding) appear large 20-30cm. Some dense angular WRL 4-8cm, but hard to tell because of weathered face.
		AG61	Red scoria unit, strongly welded with stretched grey ribbons. Dense angular WRL 8-15cm light grey (~5%). Grades to moderately welded at base where slight notch is formed. Clasts appear 10-15cm, poor/moderate vesicular, sub-rnd to sub-ang.
		AG60	Redish/grey unit strongly welded with lots ofstretched grey ribbons. Dense angular WRL 6-8cm max 10cm (~5%). Strongly welded grades to moderatly welded at base where notch formed. Clasts appear 10-13cm, poor/moderate vesicular and sub-rnd to sub-ang.
			Red scoria unit, with knobbly face, clasts appear cowpat like and 4-8cm, some joined/smeared together. Some black scoria seen, moderately vesicular (<10%). Dense angular WRL (~30%) med grey, some have breadcrust outside so possible mixture of juvenile lithics 6-8cm max 40cm. Grades down to intensely/strongly welded with some areas of stretched clast rivbbons, other areas no clasts visible.
			Red/grey unit. Strongly welded with stretched clast ribbons. Clasts stretched out to ribbons <1cm thick. Dense angular WRL 6-10cm and dark grey. Grades down into knobbly face mod welded and point contacts. Clasts seen are cowpat and flat 4-6cm elongate, with some areas more compacted. Dense angular WRL 8-15cm, max 80cm.

Stratigraphic Column

Field Trip: South Bluff - North Crater

Date: 15 (day) 2 (month) 2006 (year)

Field Site 55

Region: North Crater Tongariro National Park - Tongariro

Location: 2738329 6228095

Thick. (m)	Graphic Log	Sample No	Description
	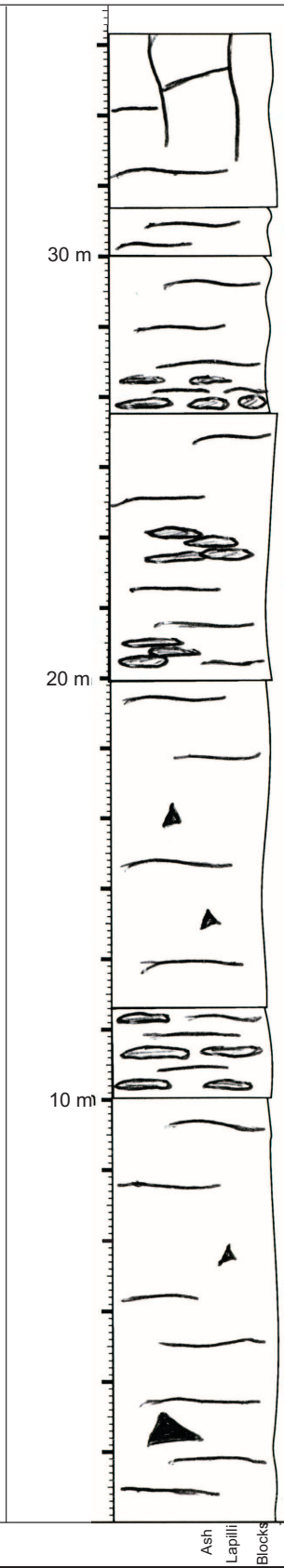		Pink/grey unit. Can see clasts stretch out, but not into thin ribbons as below. moderately/strongly welded with irregular/informal columnar jointing up through unit.
			Pink/grey unit. Strongly welded, shows stretched clast ribbons.
			Pink/grey strongly welded (stretched clast ribbons) but moderatly welded near base where clast shapes seen. Clasts appear black poor vesic scoria, sub-rnd 4-7cm grades up quickly into stretched out grey ribbons. Some irregular jointing (informal columnar jointing) seen through unit.
			Grey/black scoria unit. Moderate to strong welded with varying flow (stretched ribbons) and non flow areas (cowpat clasts). Flow banding can be seen with stretched out ribbions of black scoria, other areas of cowpat-like clasts with no flow, but still strongly welded.
		AG63	Pink/grey agglutinate flow. Intensely welded with banding patterns of stretched pink and grey ribbons. Hard to distinguish WRL in face as weathered.
			Possible upper section to unit below. Moderatly welded, and forms slight notch. Clasts seen are flat/cowpat like. Mainly dark grey poor vesicular scoria 5-8cm. Some dense angular WRL seen 5-8cm max 10cm.
		AG62	Red/grey unit. Strongly welded with massive with informal columnar jointing. Clasts stretched out to ribbons <1cm thick. Dense angular WRL 6-10cm and dark grey. Shows coarse crystal rich interior.

30 m

20 m

10 m

Ash Lapilli Blocks

Stratigraphic Column

Field Trip: Explosion Pit, stand alone pinnacle - North Crater

Date: 17 (day) 2 (month) 2006 (year)

Field Site: 59

Region: North Crater Tongariro National Park - Tongariro

Location: 2738630 6228380

Thick. (m)	Graphic Log	Sample No	Description
40m			
30m			
20m			Massive single unit. Hard to distinguish too many features as most of visible exposure has some weathering or moss growth. Upper half to the unit is intensly welded massive lava. Informal columnar to irregular jointing but many of the joints dont join up some only partial blocks formed and result in concentric 'blocks' still sitting locked together. Bottom half of unit contains highly fractured or platy fractures- 'stacked pancake' look. The main vertical joints swing from vertical to near horizontal and broken between by much smaller platy joints, the joints are 5-10cm apart and 3-5cm high. The very base of the unit is more of a messy and irregular fracture zone with no defined pattern. Unit is a uniform med grey and very crystal rich large white crystals 1-3mm and some black crystals, and non to very poor vesicular. No clast shapes are seen.
10m		AG08	
			Scree

Ash Lapilli Blocks

Stratigraphic Column

Field Trip: Explosion Pit, stand alone pinnacle - North Crater

Date: 17 (day) 2 (month) 2006 (year)

Field Site: 60

Region: North Crater Tongariro National Park - Tongariro

Location: 2738537 6228329

Thick. (m)	Graphic Log	Sample No	Description
		AG09	Massive single unit. Hard to distinguish too many features as most of visible exposure has some weathering or moss growth. Upper 5-6m to the unit is intensly welded massive lava. Informal columnar to irregular jointing but many of the joints dont join up some only partial blocks formed and result in concentric 'blocks' still sitting locked together. Middle 3-3.5meters of unit contains highly fractured or platy fractures- 'stacked pancake' look in intensly welded lava. The main vertical joints swing from vertical to near horizontal and broken between by much smaller platy joints, the joints are 5-10cm apart and 3-5cm high. Lower 2-2.5m of unit gardes back into intensly welded lava which is broken by some informal columns - some concentric shapes seen. Unit is a uniform med grey and very crystal rich, large white crystals 1-3mm and some black crystals, and non to very poor vesicular. Cannot see any clast outlines.
			Scree

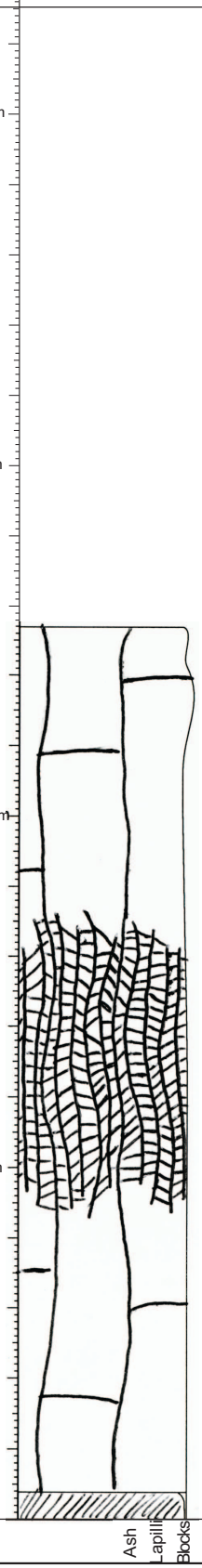

Stratigraphic Column

Field Trip: Pimple Rock - North Crater

Date: 21 (day) 2 (month) 2006 (year)

Field Site 62

Region: North Crater Tongariro National Park - Tongariro

Location: 2739157 6227849

Thick. (m)	Graphic Log	Sample No	Description
	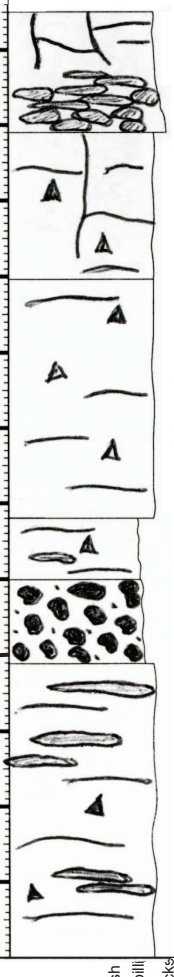	AG57	Pinish grey aggultinate strongly welded some irregular jointing, on very top large block broken by jigsaw cracks but still sitting together, blocks 0.5-1.5m. Grades into messy poorly black scoria, with minor pink scoria, clasts sub-rnd to cowpat-like, 8-12cm.
		AG15	Pinish grey unit. Intensely/strongly welded, stretched clasts (thin pinkish ribbons) seen, poor vesicular, cryst rich. Dense angular WRL 3-4cm. Some irregular jointing into large blocks
			Pinish grey unit. Strongly welded, some minor flow or stretched clasts (pinkish thick ribbions) seen, mod-poor vesicular. Dense angular WRL 5-10cm.
			Red scoria unit, mod-strongly welded, poor/mod vesicular. Hard to see clast shapes but appear 3-6cm. Dense angular WRL 3-6cm.
			Black scoria unit, clasts sub-rnd, mod/well vesicular, 4-7cm, poor sorting & some <2cm and minor matrix. Some irridescent blue scoria seen. Only found unit by digging into the scree slope.
			Red scoria agglutinate unit, clasts poor vesic, cryst rich, clasts appear 3-5 cm, poorly welded but pockets of mod welded. Minor dense angular WRL 3-5 cm. Scree slope below limits amount of unit seen.

20m

10m

Ash Lapilli Blocks

Stratigraphic Column

Field Trip: Northern Slope - North Crater

Date: 23 (day) 2 (month) 2006 (year)

Field Site 69

Region: North Crater Tongariro National Park - Tongariro

Location: 2739447 6231023

Thick. (m)	Graphic Log	Sample No	Description
			Brown fine ash, highly weathered to clay (possibly Ngaruhoe ash?), no distinctive features.
			Creamy white pumice deposit (Taupo pumice?), well sorted, highly vesicular, no crystals, 2-4cm.
			Grey ash weathered to clay in some areas, can still see some parallel bedding features. More weathereing at top of unit.
			Weathered fine brown ash, highly weathered to clay, no distinguishable features.
			Orangy brown lapilli unit. Most .4-.8cm some 1-1.5cm, poor vesic pumice, some minor black scoria mixed in. Minor dense WRL, 3-4cm, one large block 2m x1.2m.
		AG21	Medium ash, dark grey/black
			Black scoria lapilli unit, poor vesic, 2-5cm, minor yellow/brown pumice mixed in cryst rich, poor vesic <1.5cm. Dense WRL <1.5cm.
			Orangey/brown scoria lapilli unit. Black rnd scoria & reddish orange scoria <1cm, poor vesic. Dense angular WRL <1cm and 3-4cm.
			Medium ash, dark grey/black
		AG19	Black scoria lapilli unit, poor vesic, 2-5cm, minor yellow/brown pumice mixed in cryst rich, poor vesic <1.5cm. Dense WRL <1.5cm.
			Very coarse ash, black/brown, similar to below.
			Coarse ash, black/brown w. minor red & orange ash seen.
			Med/coarse ash, dark grey, well sorted
		AG20	Block & Ash flow, black scoria bombs sub-rnd to rnd, moderate vesicular, 30-80 cm max 1.2m, most have breadcrust texture, minor clast supported in areas with high conc blocks, rest is matrix supported in fine/med ash some areas weath to clay. No WRL. In stream just below can see intensly welded lava unit, assume b'n'a flow sits on this but cannot see the contact.

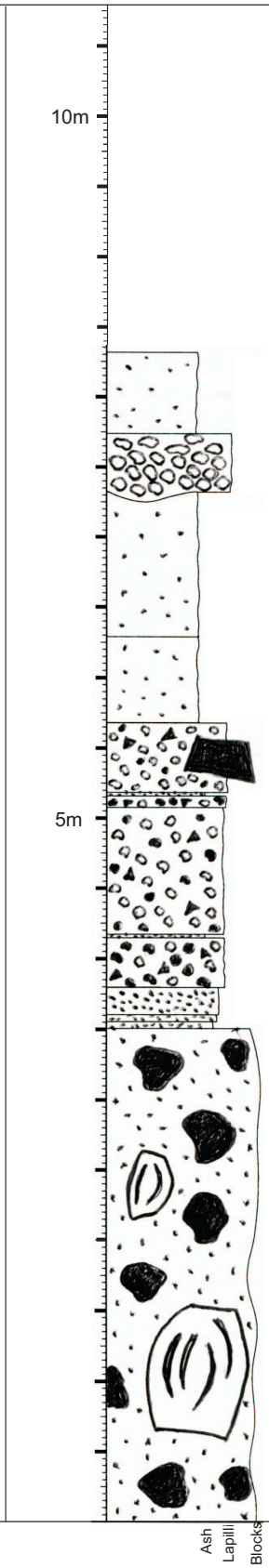

Stratigraphic Column

Field Area: Ring Plain- North Crater

Date: 23 (day) 3 (month) 2006 (year)

Field Site: 70

Region: North Crater Tongariro National Park - Tongariro

Location: 2753313 6238262

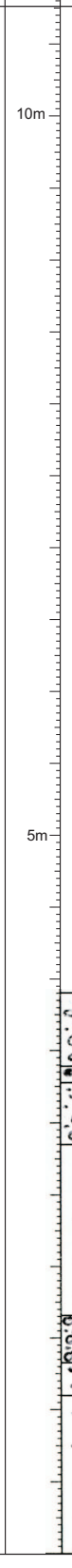

Thick. (m)	Sample No	Description
		Medium to fine lapilli, orange/brown, massive unit. Clasts <2 cm, sub-round, clast supported with very minor ash matrix. Slightly weathered. Possibly the Potou Lapilli.
		Dark greyish brown lapilli unit. Clasts <2 cm, clast supported but minor dark ash. Slightly weathered.
		Orangey brown lapilli unit. Lapilli <2 cm in the base cm grades up into coarse ash.
		Orangey brown medium to coarse ash, slightly weathered face.
	AG30 AG31	Rotoaira Lapilli. Orange yellow lapilli bedded with fine black ash. Upper most lapilli bed lapilli 2-3 cm, clast supported. Middle lapilli very similar. Lower lapilli bed fine <1.5cm and lighter orange yellow colour.
		Coarse brown ash unit
		Pale pinkish brown, coarse ash and pumice unit, minor lithics with occasional large pumice. Kawakawa Tephra/Oruanui Ignimbrite.

Stratigraphic Column

Field Area: Ring Plain- North Crater

Date: 23 (day) 3 (month) 2006 (year)

Field Site: 72

Region: North Crater Tongariro National Park - Tongariro

Location: 2751703 6231907

Thick. (m)	Graphic Log	Sample No	Description
10m			
5m			
			Medium to fine lapilli, orange/brown, massive unit. Clasts <2 cm, sub-round, clast supported with very minor ash matrix. Slightly weathered. Possibly the Potou Lapilli.
			Vegetation and scree
			Brownish yellow lapilli unit. Clasts <2 cm, clast supported but minor dark ash. Slightly weathered. Grades from lower unit.
			Orangey brown lapilli unit. Fine lapilli with coarse dark ash. Slightly weathered. Grades from lower unit.
			Brownish yellow fine to medium ash, well sorted, massive
		AG32	Rotoaira Lapilli. Orange grey fine lapilli, massive, well sorted, <3cm clasts
			Rotoaira Lapilli. Steel grey medium to coarse ash
		AG33	Rotoaira Lapilli. Orange grey fine lapilli, massive, well sorted
		AG34	Rotoaira Lapilli. Dark grey medium ash, minor bedding, but not continuous
		AG35	Rotoaira Lapilli. Medium orange yellow pumice lapilli, fine lapilli and coarse ash lithics and pumice in upper 3cm, grades from above.

Ash Lapilli Blocks

Stratigraphic Column

Field Area: Ring Plain- North Crater

Field Site: 74

Date: 23 (day) 3 (month) 2006 (year)

Region: North Crater Tongariro National Park - Tongariro

Location: 2750582 6232080

Thick. (m)	Graphic Log	Sample No	Description
10m			
			Taupo Pumice, medium to coarse, cream pumice lapilli unit.
			Ngauruhoe Tephra, fine brownish grey ash unit. Very well sorted, some beds defined by slight colour and grainsize changes.
5m			Brownish green medium lapilli. Very well sorted, massive unit. Poutu Lapilli
			Fine dark grey ash, well sorted, massive interbedded with fine pumice lapilli <2cm
			Medium to fine lapilli <2cm, orange/brown, between medium to coarse ash beds.
			Brownish yellow medium to fine ash unit.
			Brown very coarse ash and fine lapilli
			Brownish yellow medium to fine ash unit.
		AG37	Rotoaira Lapilli. Orangey brown lapilli unit. Fine lapilli with coarse dark ash. Slightly weathered. Grades from lower unit.
		AG36	Rotoaira Lapilli. Brownish yellow fine to medium ash, well sorted, massive
			Rotoaira Lapilli. Orange grey fine lapilli, massive, well sorted, <3cm clasts
		AG38	Rotoaira Lapilli. Steel grey medium to coarse ash
			Rotoaira Lapilli. Orange grey fine lapilli, massive, well sorted
			Rotoaira Lapilli. Dark grey medium ash, minor bedding, but not continuous
			Rotoaira Lapilli. Medium orange yellow pumice lapilli, fine lapilli and coarse ash lithics and pumice in upper 3cm, grades from above.
			Oruanui Fm, pinkish cream tephra

Ash Lapilli Blocks

Stratigraphic Column

Field Area: Ring Plain- North Crater

Field Site: 75

Date: 23 (day) 3 (month) 2006 (year)

Region: North Crater Tongariro National Park - Tongariro

Location: 2748196 6232419

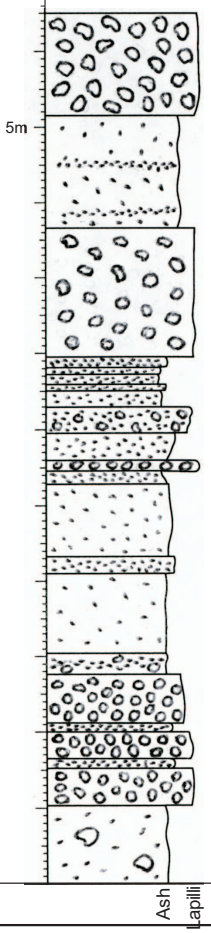

Thick. (m)	Sample No	Description
		Taupo Pumice, medium to coarse, cream pumice lapilli unit.
		Ngauruhoe Tephra, fine brownish grey ash unit. Very well sorted, some beds defined by slight colour and grainsize changes.
		Brownish green medium lapilli. Very well sorted, massive unit. Poutu Lapilli
		Brownish green fine ash. Wharepu Tephra
		Yellowish cream, fine rhyolitic ash
		Brown medium ash, Ohinepango Tephra.
		Reddish brown coarse ash and fine lapilli , Waihohonu Fm.
		Fine brown ash
		Very dark grey coarse ash and fine yellow lapilli
		Taurewa Fm, coarse ash grades down into fine ash
		Brownish red fine lapilli and lithics, Bullot Fm.
		Brownish yellow fine ash coarsening down
		Brownish yellow medium to fine ash unit.
		Brown very coarse ash and fine lapilli
		Brownish yellow medium to fine ash unit.
		Rotoaira Lapilli. Reworked dark grey ash with minor pumice lapilli, some bedding but is discontinuous.
	AG37	Rotoaira Lapilli. Orange grey fine lapilli, massive, well sorted, <3cm clasts, with lens of dark grey coarse ash
	AG36	Rotoaira Lapilli. Steel grey medium to coarse ash
		Rotoaira Lapilli. Orange grey medium lapilli, massive, well sorted
		Rotoaira Lapilli. Dark grey very coarse ash, minor bedding, but not continuous
	AG38	Rotoaira Lapilli. Fine orange yellow pumice lapilli, fine lapilli unit.
		Scree and pinkish cream fine ash, Oruanui Ignimbrite

Stratigraphic Column

Field Trip: Lower Ketetahi Track - Waterfall - North Crater

Date: 23 (day) 3 (month) 2006 (year)

Field Site 76

Region: North Crater Tongariro National Park - Tongariro

Location: 2739875 6232923

Thick. (m)	Graphic Log	Sample No	Description
			Brown med ash, weathered, (Ngaruhoe Ash?), no distinguishing features and partly covered by plants etc.
			Pumice lapilli unit (Taupo Pumice), clasts 3-5cm, mod-high vesic, no cryst.
			Dark brown fine-med ash highly weathered to clay, cannot distinguish any features in unit.
			Yellow brown pumice very coarse ash and lapilli unit. Some weathering of ash to clay. Some dense round juveniles 3-6cm.
			Reddish brown scoria, very coarse ash to fine lapilli, mix of red and black scoria, minor dense angular WRL <2cm.
		AG42	Brownish orange very coarse ash
		AG43	Black fine lapilli and very coarse ash, grades into lower unit.
		AG44	Black/grey scoria lapilli unit. Clasts <2cm, poor vesic, minor dense angular WRL 1-2cm.
			Orangey/brown medium ash interbedded with 3 very coarse ash beds, each about 2-3cm thick.
			Block'n'ash flow, hard to distinguish as mostly covered in stream debris, moss and ferns. Can see a few large dense angular/sub-round blocks 20-60cm juvenile. Matrix appears to be orangey ash but is probably highly weathered from being in the stream.

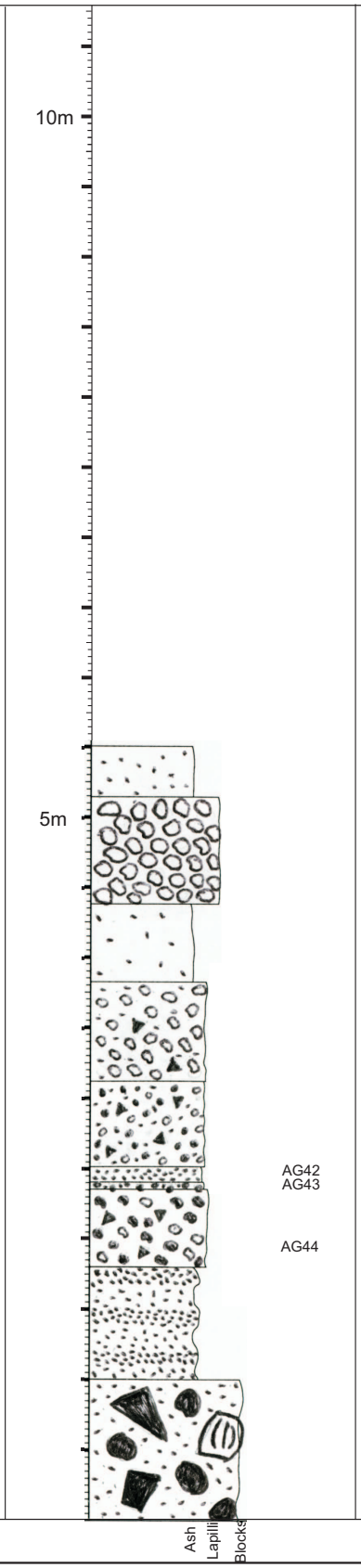

Stratigraphic Column

Field Trip: Eastern Crater Rim - near Pimple Rock

Date: 19 (day) 4 (month) 2006 (year)

Field Site 78

Region: North Crater Tongariro National Park - Tongariro

Location: 2739177 6227901

Thick. (m)	Graphic Log	Sample No	Description
		AG56	Red scoria agglutinate unit. Strongly welded in upper 2m where can see some stretch ribbions of clasts, grades into moderately welded at base. Base clasts poor/moderately vesicular, 1-3cm max 5cm, some black mod vesic scoria in base. Minor dense angular WRL 2-3cm.
		AG55	Consolidated yellow/black lapilli unit. Some mingled pumice, with black scoria. Large clasts show more mingling texture. Clasts 1-3cm rare 4-6cm, cryst rich, mod/poor vesicular. Minor dense angular WRL 1-5cm max 20cm.
			Red scoria unit. Large scoria bombs, poor/mod vesic, sub-rnd moderately welded with small areas poorly welded. Messy broken up structure so hard to distinguish features about clasts.
			Consolidated yellow/black lapilli unit. Some mingled pumice, with black scoria. Large clasts show more mingling texture. Clasts 1-3cm rare 4-6cm, cryst rich, mod/poor vesicular. Minor dense angular WRL 1-5cm max 15cm. Scree slope hides bottom contact so don't know true thickness.

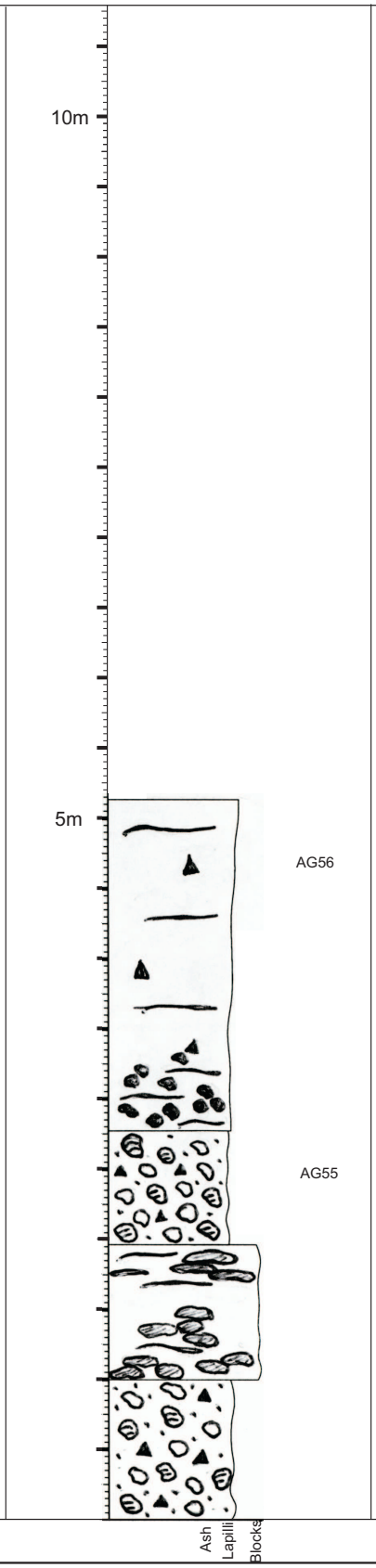

Appendix C

Density, Vesicularity & Componentry Data

Sample	**AG21**							
Componentry	**Dry**	**Wet**	**Ballast**	**Wax**	**Density**	**Vesicularity**	**Clast no.**	
dense lithic	9.25	5.68	0.00	0.00	2.59	0.3	1	-4phi
Pumice	14.11	101.12	92.91	1.00	2.40	7.7	2	
Pumice	8.29	4.09	0.00	0.00	1.97	24.1	3	
Pumice	8.27	4.27	0.00	0.00	2.07	20.5	4	
Pumice	4.94	1.93	0.00	0.00	1.64	36.9	5	
Pumice	6.43	3.87	0.00	0.00	2.51	3.4	6	
Pumice	2.49	0.79	0.00	0.00	1.46	43.7	7	-3.5phi
Pumice	3.28	1.92	0.00	0.00	2.41	7.2	8	
Pumice	2.17	0.95	0.00	0.00	1.78	31.6	9	
Pumice	1.75	0.56	0.00	0.00	1.47	43.4	10	
Pumice	1.84	0.63	0.00	0.00	1.52	41.5	11	
Pumice	2.38	1.05	0.00	0.00	1.79	31.2	12	
Pumice	3.08	1.74	0.00	0.00	2.30	11.6	13	
Pumice	2.06	1.14	0.00	0.00	2.24	13.9	14	
dense lithic	2.84	1.74	0.00	0.00	2.58	0.7	15	
Pumice	1.70	0.62	0.00	0.00	1.57	39.5	16	
Pumice	1.45	0.43	0.00	0.00	1.42	45.3	17	
Dense lithic	3.41	2.09	0.00	0.00	2.58	0.6	18	
	3.49	mean mass			1.97	16.12	mean	
	3.48	standard dev			0.44	16.95	standard deviation	
	14.11	max mass			1.42	45.32	minimum density value	
	1.45	min mass			2.59	0.34	maximum density value	
					2.31	1.85	average 3 minimum density	
					1.79	23.63	average 3 maximum density	

Sample	**AG25**							
Componentry	**Dry**	**Wet**	**Ballast**	**Wax**	**Density**	**Vesicularity**	**Clast no.**	
Minor mingling	156.19	148.32	160.79	6	0.93	64.4	27	-6phi
Pumice	103.76	127.73	160.79	5.5	0.76	70.8	23	-5.5phi
Scoria	108.63	28.92	92.91	4	0.63	75.8	24	
Pumice	46.31	79.94	92.91	4	0.78	69.9	25	
Minor mingling	60.83	73.24	92.91	4	0.76	70.9	26	
Scoria	34.83	8.90	0.00	3.00	1.35	48.2	1	-5phi
Scoria	16.44	92.60	92.91	3.00	0.99	62.1	2	
Minor mingling	19.20	87.20	92.91	4.00	0.77	70.3	3	
Pumice	33.13	82.74	92.91	6.00	0.77	70.5	4	
Minor mingling	17.07	90.43	92.91	3.00	0.88	66.3	5	
Scoria	38.95	93.67	92.91	4.00	1.02	60.7	6	
Minor mingling	31.44	92.57	92.91	4.00	0.99	61.9	7	
Pumice	42.74	81.76	92.91	5.00	0.79	69.4	8	
Scoria	23.87	92.35	92.91	4.00	0.98	62.3	9	
Minor mingling	21.52	2.94	0.00	3.00	1.16	55.3	10	
Scoria	41.29	93.34	92.91	5.00	1.01	61.0	11	
Intense mingling	33.65	86.91	92.91	5.00	0.85	67.3	12	
Scoria	7.27	91.29	92.91	2.00	0.82	68.4	13	-4.5phi
Scoria	7.57	89.94	92.91	2.00	0.72	72.3	14	
Scoria	12.73	89.54	92.91	3.00	0.79	69.5	15	
Scoria	9.07	92.20	92.91	2.00	0.93	64.2	16	
Scoria	6.73	92.94	92.91	1.00	1.01	61.3	17	
Scoria	11.37	91.84	92.91	3.00	0.92	64.7	18	
Scoria	5.71	93.08	92.91	1.00	1.03	60.2	19	
Minor mingling	16.71	92.63	92.91	2.00	0.99	62.1	20	
Minor mingling	5.60	91.78	92.91	2.00	0.84	67.8	21	
Minor mingling	11.43	91.95	92.91	2.00	0.93	64.4	22	
Minor mingling	6.66	90.58	92.91	2.00	0.74	71.4	23	
Minor mingling	5.78	90.92	92.91	1.00	0.75	71.3	24	
Minor mingling	6.12	91.72	92.91	2.00	0.84	67.6	25	
Intense mingling	9.66	88.68	92.91	2.00	0.70	73.2	26	
Intense mingling	12.29	90.79	92.91	2.00	0.86	67.1	27	
Intense mingling	9.16	91.19	92.91	2.00	0.85	67.5	28	
Intense mingling	13.03	88.98	92.91	3.00	0.77	70.3	29	
Intense mingling	12.24	87.68	92.91	2.00	0.70	73.0	30	
Intense mingling	21.59	3.45	0.00	2.00	1.19	54.1	31	
Intense mingling	12.59	95.90	92.91	1.00	1.31	49.5	32	
Intense mingling	4.98	90.20	92.91	2.00	0.65	75.0	33	
Pumice	10.53	89.49	92.91	2.00	0.76	70.9	34	

AG25 continued

Scoria	4.47	92.39	92.91	2.00	0.90	65.3	35	-4 phi
Scoria	3.65	92.99	92.91	1.00	1.03	60.5	36	
Scoria	2.39	92.01	92.91	1.00	0.73	71.9	37	
Scoria	1.70	91.87	92.91	1.00	0.63	76.0	38	
Scoria	2.96	92.87	92.91	1.00	0.99	61.8	39	
Scoria	3.15	91.98	92.91	1.00	0.78	70.2	40	
Scoria	6.27	93.78	92.91	1.00	1.17	55.2	41	
Scoria	2.75	92.09	92.91	1.00	0.77	70.2	42	
Minor mingling	3.21	92.06	92.91	1.00	0.79	69.4	43	
Minor mingling	5.16	93.10	92.91	1.00	1.04	59.9	44	
Minor mingling	3.59	91.46	92.91	1.00	0.72	72.5	45	
Minor mingling	4.52	90.65	92.91	1.00	0.67	74.3	46	
Minor mingling	3.78	93.12	92.91	1.00	1.06	59.0	47	
Minor mingling	2.95	91.81	92.91	1.00	0.73	71.8	48	
Minor mingling	3.99	92.43	92.91	1.00	0.90	65.5	49	
Pumice	1.68	91.90	92.91	1.00	0.63	75.8	50	
Pumice	3.71	91.21	92.91	1.00	0.69	73.5	51	
Pumice	4.07	92.80	92.91	1.00	0.98	62.4	52	
Pumice	3.41	92.71	92.91	1.00	0.95	63.5	53	
Pumice	2.88	91.98	92.91	1.00	0.76	70.8	54	
Pumice	6.93	91.15	92.91	1.00	0.80	69.3	55	
Pumice	3.22	92.01	92.91	1.00	0.79	69.8	56	
Scoria	1.55	11.34	11.38	1.00	0.99	62.0	57	-3.5phi
Scoria	2.03	11.71	11.38	1.00	1.21	53.5	58	
Scoria	2.45	11.44	11.38	1.00	1.03	60.2	59	
Scoria	1.79	11.44	11.38	1.00	1.05	59.7	60	
Scoria	1.17	11.25	11.38	1.00	0.91	64.8	61	
Scoria	3.35	11.64	11.38	1.00	1.09	58.0	62	
Scoria	1.18	11.26	11.38	1.00	0.92	64.5	63	
Scoria	1.14	11.04	11.38	1.00	0.78	70.0	64	
Minor mingling	1.20	11.45	11.38	1.00	1.08	58.4	65	
Minor mingling	1.59	11.67	11.38	1.00	1.24	52.2	66	
Minor mingling	2.67	11.15	11.38	1.00	0.93	64.3	67	
Minor mingling	2.05	11.26	11.38	1.00	0.95	63.3	68	
Minor mingling	1.44	11.09	11.38	1.00	0.84	67.6	69	
Minor mingling	1.45	10.96	11.38	1.00	0.78	69.9	70	
Minor mingling	1.38	11.46	11.38	1.00	1.08	58.5	71	
Pumice	1.80	10.89	11.38	1.00	0.79	69.5	72	
Pumice	1.80	10.78	11.38	1.00	0.76	70.9	73	
Pumice	2.19	10.88	11.38	1.00	0.82	68.5	74	
Pumice	1.33	11.14	11.38	1.00	0.86	67.0	75	
Pumice	1.34	11.01	11.38	1.00	0.79	69.5	76	
Pumice	0.98	10.89	11.38	1.00	0.68	74.0	77	
Pumice	1.18	11.16	11.38	1.00	0.86	67.1	78	

6.01	mean mass	0.87	62.96	mean
24.89	standard dev	0.16	6.24	standard deviation
156.19	max mass	0.63	75.96	minimum density value
0.98	min mass	1.35	48.22	maximum density value
		0.72	69.35	average 3 minimum density
		0.77	67.19	average 3 maximum density

Sample	**AG26**							
Componentry	**Dry**	**Wet**	**Ballast**	**Wax**	**Density**	**Vesicularity**	**Clast no.**	
Scoria	243.12	185.22	92.91	6.00	1.61	37.9	29	-6phi
Scoria	57.59	83.60	92.91	6.00	0.86	66.8	1	-5phi
Scoria	49.73	100.70	92.91	6.00	1.19	54.3	2	
Scoria	29.21	95.90	92.91	4.00	1.12	57.0	3	
Dense lithic	41.40	22.28	0.00	2.00	2.17	16.5	4	-4.5phi
Scoria	21.85	95.60	92.91	2.00	1.14	56.0	5	
Scoria	8.99	91.87	92.91	2.00	0.90	65.4	6	
Scoria	12.05	93.91	92.91	2.00	1.09	57.9	7	
Scoria	21.39	97.07	92.91	2.00	1.24	52.1	8	
Scoria	9.85	92.64	92.91	2.00	0.98	62.4	9	
Minor mingling	18.09	91.95	92.91	2.00	0.95	63.4	10	
Minor mingling	10.68	93.41	92.91	2.00	1.05	59.5	11	
Minor mingling	10.66	94.48	92.91	2.00	1.18	54.7	12	
Minor mingling	9.57	92.37	92.91	2.00	0.95	63.4	13	
Minor mingling	11.45	95.19	92.91	2.00	1.25	51.8	14	
Minor mingling	11.55	93.66	92.91	2.00	1.07	58.7	15	
Minor mingling	10.09	92.70	92.91	2.00	0.98	62.2	16	
Minor mingling	9.73	92.53	92.91	2.00	0.97	62.8	17	
Minor mingling	21.29	93.95	92.91	3.00	1.05	59.4	18	
Minor mingling	12.19	95.12	92.91	2.00	1.23	52.8	19	
Minor mingling	14.28	93.93	92.91	2.00	1.08	58.5	20	
Minor mingling	10.55	92.84	92.91	2.00	1.00	61.6	21	
Minor mingling	9.08	93.48	92.91	2.00	1.07	58.8	22	

AG26 continued

Minor mingling	12.10	94.18	92.91	2.00	1.12	56.9	23	
Minor mingling	9.67	95.12	92.91	2.00	1.30	49.9	24	
Minor mingling	8.80	91.31	92.91	2.00	0.85	67.3	25	
Minor mingling	8.97	94.80	92.91	2.00	1.27	51.0	26	
Minor mingling	22.18	92.57	92.91	3.00	0.99	62.0	27	
Minor mingling	7.45	93.23	92.91	2.00	1.05	59.6	28	
Dense lithic	9.99	73.10	67.94	1.00	2.08	20.1	29	-4phi
Scoria	3.25	67.86	67.94	1.00	0.98	62.2	30	
Scoria	2.56	68.13	67.94	1.00	1.09	58.1	31	
Scoria	4.72	68.84	67.94	1.00	1.24	52.2	32	
Scoria	3.38	67.39	67.94	1.00	0.86	66.8	33	
Scoria	3.02	68.03	67.94	1.00	1.04	60.1	34	
Scoria	5.52	67.51	67.94	1.00	0.93	64.2	35	
Scoria	4.11	68.81	67.94	1.00	1.28	50.9	36	
Scoria	5.12	68.71	67.94	1.00	1.18	54.5	37	
Scoria	3.41	67.38	67.94	1.00	0.86	66.8	38	
Scoria	3.48	67.58	67.94	1.00	0.91	65.0	39	
Scoria	3.83	67.82	67.94	1.00	0.97	62.5	40	
Scoria	4.35	67.85	67.94	1.00	0.98	62.1	41	
Minor mingling	4.12	67.70	67.94	1.00	0.95	63.5	42	
Minor mingling	6.42	68.96	67.94	1.00	1.19	54.1	43	
Minor mingling	8.45	68.02	67.94	2.00	1.01	61.0	44	
Minor mingling	5.47	68.77	67.94	1.00	1.18	54.5	45	
Minor mingling	3.77	92.08	92.91	1.00	0.82	68.3	46	
Minor mingling	4.92	67.17	67.94	1.00	0.87	66.6	47	
Minor mingling	3.30	67.59	67.94	1.00	0.91	65.0	48	
Minor mingling	5.17	67.51	67.94	1.00	0.93	64.4	49	
Minor mingling	6.89	67.48	67.94	1.00	0.94	63.8	50	
Minor mingling	10.69	67.79	67.94	1.00	0.99	62.0	51	
Dense lithic	6.56	3.85	0.00	1.00	2.44	6.2	52	-3.5phi
Minor mingling	2.04	67.80	67.94	1.00	0.94	63.7	53	
Minor mingling	2.38	67.83	67.94	1.00	0.96	62.9	54	
Minor mingling	2.86	68.69	67.94	1.00	1.37	47.4	55	
Minor mingling	1.14	67.20	67.94	1.00	0.61	76.4	56	
Minor mingling	1.16	67.33	67.94	1.00	0.66	74.5	57	
Minor mingling	1.64	67.25	67.94	1.00	0.71	72.7	58	
Minor mingling	2.26	68.46	67.94	1.00	1.31	49.5	59	
Minor mingling	2.14	67.89	67.94	1.00	0.99	62.1	60	
Minor mingling	2.20	68.13	67.94	1.00	1.11	57.5	61	
Minor mingling	1.75	67.99	67.94	1.00	1.04	59.9	62	
Minor mingling	2.43	67.89	67.94	1.00	0.99	62.0	63	
Minor mingling	1.87	67.76	67.94	1.00	0.92	64.6	64	
Scoria	2.23	67.83	67.94	1.00	0.96	63.0	65	
Scoria	1.64	68.09	67.94	1.00	1.12	57.1	66	
Scoria	1.43	67.85	67.94	1.00	0.95	63.3	67	
Scoria	1.89	68.02	67.94	1.00	1.06	59.4	68	
Scoria	1.07	67.65	67.94	1.00	0.80	69.3	69	
Scoria	1.90	68.03	67.94	1.00	1.06	59.2	70	
Scoria	1.89	67.59	67.94	1.00	0.85	67.3	71	
Scoria	1.69	68.00	67.94	1.00	1.05	59.6	72	
Scoria	1.79	67.99	67.94	1.00	1.04	60.0	73	
Scoria	2.77	68.13	67.94	1.00	1.08	58.4	74	

5.74	mean mass	1.05	55.53	mean
28.96	standard dev	0.28	10.87	standard deviation
243.12	max mass	0.61	76.43	minimum density value
1.07	min mass	2.44	6.21	maximum density value
		1.05	55.47	average 3 minimum density
		1.06	54.84	average 3 maximum density

Sample **AG27**

Componentry	**Dry**	**Wet**	**Ballast**	**Wax**	**Density**	**Vesicularity**	**Clast no.**	
Minor mingling	29.37	94.84	92.91	3.00	1.07	58.7	1	-5phi
Pumice	14.90	89.14	92.91	3.00	0.80	69.2	2	
Minor mingling	8.31	91.75	92.91	2.00	0.88	66.1	3	-4.5phi
Minor mingling	12.34	92.96	92.91	2.00	1.01	61.3	4	
Minor mingling	8.94	93.51	92.91	2.00	1.08	58.6	5	
Minor mingling	12.58	92.94	92.91	2.00	1.01	61.3	6	
Minor mingling	12.68	94.63	92.91	2.00	1.16	55.3	7	
Minor mingling	8.41	92.12	92.91	2.00	0.92	64.7	8	
Minor mingling	8.14	90.16	92.91	2.00	0.75	71.1	9	
Minor mingling	8.08	93.28	92.91	2.00	1.05	59.5	10	

AG27 continued

Minor mingling	10.56	92.37	92.91	2.00	0.95	63.3	11	
Minor mingling	7.87	93.17	92.91	1.00	1.04	60.1	12	
Minor mingling	9.17	93.45	92.91	1.00	1.07	59.0	13	
Minor mingling	6.61	92.70	92.91	1.00	0.97	62.6	14	
Minor mingling	5.60	91.81	92.91	1.00	0.84	67.8	15	
Pumice	7.18	89.22	92.91	2.00	0.66	74.5	16	
Pumice	5.80	90.77	92.91	2.00	0.73	71.8	17	
Pumice	10.57	88.65	92.91	2.00	0.71	72.5	18	
Pumice	9.65	89.64	92.91	2.00	0.75	71.2	19	
Pumice	16.99	92.67	92.91	1.00	0.99	62.0	20	
Pumice	8.92	90.90	92.91	2.00	0.82	68.5	21	
Pumice	9.12	91.12	92.91	2.00	0.84	67.7	22	
Minor mingling	3.28	68.11	67.94	1.00	1.06	59.2	23	-4phi
Minor mingling	2.94	68.01	67.94	1.00	1.03	60.3	24	
Minor mingling	3.58	67.95	67.94	1.00	1.01	61.2	25	
Minor mingling	3.14	68.17	67.94	1.00	1.09	58.2	26	
Minor mingling	3.40	68.34	67.94	1.00	1.14	56.1	27	
Minor mingling	5.85	67.38	67.94	2.00	0.92	64.7	28	
Minor mingling	6.95	68.43	67.94	2.00	1.08	58.4	29	
Minor mingling	3.68	68.19	67.94	1.00	1.08	58.5	30	
Intense mingling	2.17	67.32	67.94	1.00	0.78	69.9	31	
Intense mingling	1.82	67.60	67.94	1.00	0.85	67.3	32	
Intense mingling	5.44	68.63	67.94	1.00	1.15	55.8	33	
Intense mingling	3.94	67.41	67.94	1.00	0.89	65.9	34	
Intense mingling	1.96	67.24	67.94	1.00	0.74	71.4	35	
Intense mingling	2.08	67.24	67.94	1.00	0.75	71.0	36	
Intense mingling	1.70	67.73	67.94	1.00	0.90	65.4	37	
Pumice	2.85	66.72	67.94	1.00	0.70	72.9	38	
Pumice	3.58	66.31	67.94	2.00	0.69	73.4	39	
Pumice	5.04	67.28	67.94	1.00	0.89	65.9	40	
Pumice	2.50	66.95	67.94	1.00	0.72	72.3	41	
Pumice	2.20	66.82	67.94	1.00	0.67	74.4	42	
Pumice	3.20	67.47	67.94	1.00	0.88	66.3	43	
Pumice	2.59	67.03	67.94	2.00	0.75	71.2	44	
Dense lithic	5.45	3.13	0.00	1.00	2.37	8.9	45	-3.5phi
Dense lithic	7.27	4.32	0.00	1.00	2.48	4.6	46	
Minor mingling	1.06	11.33	11.42	1.00	0.94	63.9	47	
Minor mingling	1.20	11.33	11.42	1.00	0.94	63.7	48	
Minor mingling	1.66	11.45	11.42	1.00	1.03	60.3	49	
Minor mingling	1.80	11.59	11.42	1.00	1.12	57.0	50	
Minor mingling	1.81	11.48	11.42	1.00	1.05	59.8	51	
Minor mingling	2.31	11.51	11.42	1.00	1.05	59.6	52	
Minor mingling	1.68	11.70	11.42	1.00	1.22	53.2	53	
Minor mingling	2.09	11.33	11.42	1.00	0.97	62.8	54	
Minor mingling	1.00	10.79	11.42	1.00	0.62	76.1	55	
Minor mingling	1.57	11.08	11.42	1.00	0.83	68.1	56	
Minor mingling	2.42	11.39	11.42	1.00	1.00	61.7	57	
Minor mingling	2.26	11.19	11.42	1.00	0.91	64.8	58	
Minor mingling	1.75	11.06	11.42	1.00	0.84	67.8	59	
Some mingling	1.85	11.37	11.42	1.00	0.98	62.2	60	
Intense mingling	1.47	11.25	11.42	1.00	0.91	65.1	61	
Intense mingling	0.89	11.23	11.42	1.00	0.84	67.7	62	
Intense mingling	1.56	11.02	11.42	1.00	0.80	69.1	63	
Intense mingling	2.94	11.40	11.42	1.00	1.00	61.5	64	
Intense mingling	1.67	10.84	11.42	1.00	0.75	71.2	65	
Intense mingling	1.37	11.03	11.42	1.00	0.79	69.7	66	
Intense mingling	1.42	11.00	11.42	1.00	0.78	70.0	67	
Pumice	1.67	11.19	11.42	1.00	0.89	65.8	68	
Pumice	1.75	67.32	67.45	1.00	0.94	63.8	69	
Pumice	1.70	67.36	67.45	1.00	0.96	63.1	70	
Pumice	0.85	66.75	67.45	1.00	0.56	78.6	71	
Pumice	1.62	67.24	67.45	1.00	0.90	65.6	72	

3.54	mean mass	0.92	60.86	mean
4.77	standard dev	0.29	11.14	standard deviation
29.37	max mass	0.56	78.63	minimum density value
0.85	min mass	2.48	4.57	maximum density value
		0.91	61.22	average 3 minimum density
		0.78	66.74	average 3 maximum density

Sample AG35

Componentry	Dry	Wet	Ballast	Wax	Density	Vesicularity	Clast no.	
Pumice	5.05	65.08	67.94	1.00	0.64	75.4	1	-4.5phi
Pumice	1.94	66.26	67.94	1.00	0.54	79.3	2	-4phi
Pumice	1.97	66.39	67.94	1.00	0.56	78.4	3	
Pumice	1.70	66.73	67.94	1.00	0.59	77.4	4	
Pumice	3.59	63.96	67.94	1.00	0.48	81.7	5	
Pumice	1.92	67.08	67.94	1.00	0.70	73.2	6	
Pumice	3.01	67.01	67.94	1.00	0.77	70.5	7	
Pumice	1.53	66.58	67.94	1.00	0.53	79.5	8	
Pumice	1.17	66.68	67.94	1.00	0.49	81.3	9	
Pumice	1.90	67.02	67.94	1.00	0.68	73.9	10	
Pumice	1.37	66.83	67.94	1.00	0.56	78.6	11	-3.5phi
Pumice	1.37	66.85	67.94	1.00	0.56	78.4	12	
Pumice	1.43	66.99	67.94	1.00	0.61	76.7	13	
Pumice	1.41	67.06	67.94	1.00	0.62	76.1	14	
Pumice	1.45	67.10	67.94	1.00	0.64	75.4	15	
Pumice	0.94	67.24	67.94	1.00	0.58	77.7	16	
Pumice	1.14	66.62	67.94	1.00	0.47	82.0	17	
Pumice	1.11	67.34	67.94	1.00	0.66	74.7	18	
Pumice	0.83	67.13	67.94	1.00	0.51	80.3	19	
Pumice	1.68	67.84	67.94	1.00	0.95	63.3	20	

1.65	mean mass	0.60	74.59	mean
1.00	standard dev	0.11	4.35	standard deviation
5.05	max mass	0.47	82.03	minimum density value
0.83	min mass	0.95	63.29	maximum density value
		0.58	75.36	average 3 minimum density
		0.68	70.86	average 3 maximum density

Sample AG36

Componentry	Dry	Wet	Ballast	Wax	Density	Vesicularity	Clast no.	
Pumice	1.85	66.89	67.94	1.00	0.64	75.3	1	-4phi
Pumice	1.83	66.24	67.94	1.00	0.52	79.9	2	
Pumice	2.32	66.41	67.94	1.00	0.61	76.7	3	
Intense mingling	2.25	67.22	67.94	1.00	0.76	70.7	4	
Pumice	1.34	65.78	67.94	1.00	0.39	85.2	5	
Intense mingling	4.25	66.39	67.94	1.00	0.74	71.7	6	
Pumice	2.01	65.28	67.94	1.00	0.43	83.4	7	
Pumice	2.71	67.03	67.94	1.00	0.75	71.0	8	
Pumice	1.83	65.73	67.94	1.00	0.46	82.5	9	
Pumice	1.29	66.47	67.94	1.00	0.47	81.9	10	
Pumice	1.45	66.51	67.94	1.00	0.51	80.5	11	
Pumice	2.25	67.16	67.94	1.00	0.75	71.2	12	
Pumice	1.87	66.23	67.94	1.00	0.53	79.8	13	
Pumice	1.04	66.66	67.94	1.00	0.45	82.6	14	
Pumice	0.85	66.53	67.94	1.00	0.38	85.4	15	-3.5phi
Pumice	1.75	66.56	67.94	1.00	0.56	78.4	16	
Pumice	1.05	66.90	67.94	1.00	0.51	80.5	17	
Pumice	1.10	67.05	67.94	1.00	0.56	78.5	18	
Pumice	0.96	66.91	67.94	1.00	0.49	81.3	19	
Pumice	1.28	67.19	67.94	1.00	0.64	75.5	20	
Pumice	1.15	66.87	67.94	1.00	0.52	79.9	21	
Pumice	0.79	66.97	67.94	1.00	0.45	82.5	22	
Pumice	1.08	66.75	67.94	1.00	0.48	81.5	23	

1.53	mean mass	0.54	77.19	mean
0.77	standard dev	0.12	4.47	standard deviation
4.25	max mass	0.38	85.41	minimum density value
0.79	min mass	0.76	70.66	maximum density value
		0.59	75.00	average 3 minimum density
		0.48	79.37	average 3 maximum density

Sample	**AG41**							
Componentry	**Dry**	**Wet**	**Ballast**	**Wax**	**Density**	**Vesicularity**	**Clast no.**	
Pumice	7.18	62.28	67.94	2.00	0.56	78.4	1	-4.5phi
Pumice	2.56	67.02	67.94	1.00	0.74	71.5	2	-4phi
Intense mingling	2.76	66.44	67.94	1.00	0.65	75.0	3	
Intense mingling	2.91	66.83	67.94	1.00	0.73	72.0	4	
Pumice	3.64	66.65	67.94	1.00	0.74	71.5	5	
Pumice	2.58	67.48	67.94	1.00	0.85	67.1	6	
Pumice	1.72	66.63	67.94	1.00	0.57	78.0	7	
Pumice	2.44	67.16	67.94	1.00	0.76	70.7	8	
Pumice	1.86	67.32	67.94	1.00	0.76	70.9	9	
Pumice	1.78	66.93	67.94	1.00	0.64	75.3	10	-3.5phi
Pumice	2.34	67.17	67.94	1.00	0.76	70.9	11	
Pumice	1.55	67.33	67.94	1.00	0.72	72.1	12	
Intense mingling	1.27	67.30	67.94	1.00	0.67	74.2	13	
Pumice	1.78	67.34	67.94	1.00	0.75	71.0	14	
Pumice	1.68	66.75	67.94	1.00	0.59	77.3	15	
Pumice	1.50	66.62	67.94	1.00	0.54	79.4	16	
Pumice	1.31	67.20	67.94	1.00	0.65	75.2	17	
Pumice	1.63	67.28	67.94	1.00	0.72	72.4	18	
Pumice	1.81	67.59	67.94	1.00	0.85	67.5	19	
Pumice	1.77	67.49	67.94	1.00	0.80	69.1	20	
Pumice	1.93	67.49	67.94	1.00	0.82	68.5	21	
Pumice	0.91	67.35	67.94	1.00	0.61	76.4	22	
Pumice	1.84	67.21	67.94	1.00	0.72	72.2	23	
	2.00	mean mass			0.70	70.26	mean	
	1.25	standard dev			0.09	3.48	standard deviation	
	7.18	max mass			0.54	79.40	minimum density value	
	0.91	min mass			0.85	67.14	maximum density value	
					0.65	72.49	average 3 minimum density	
					0.71	69.65	average 3 maximum density	

Sample	**AG45**							
Componentry	**Dry**	**Wet**	**Ballast**	**Wax**	**Density**	**Vesicularity**	**Clast no.**	
Intense mingling	75.38	81.51	92.91	4.00	0.87	66.6	29	-5.5phi
Intense mingling	68.78	78.69	92.91	4.00	0.83	68.1	30	
Intense mingling	38.60	61.55	67.94	3.00	0.86	67.0	1	-5phi
Pumice	12.10	64.40	67.94	2.00	0.78	70.2	2	-4.5phi
Intense mingling	16.59	63.09	67.94	2.00	0.78	70.2	3	
Scoria	14.10	6.01	0.00	1.00	1.75	32.8	4	
Scoria	10.08	71.31	67.94	1.00	1.51	42.0	5	-4phi
Pumice	5.03	66.78	67.94	1.00	0.82	68.6	6	
Intense mingling	4.72	66.20	67.94	1.00	0.73	71.8	7	
Minor mingling	10.70	67.71	67.94	1.50	0.98	62.2	8	
Minor mingling	6.55	68.93	67.94	1.00	1.18	54.5	9	
Minor mingling	3.29	67.42	67.94	1.00	0.87	66.6	10	
Intense mingling	4.40	69.23	67.94	1.00	1.42	45.2	11	
Scoria	10.66	6.25	0.00	1.00	2.43	6.6	12	
Minor mingling	2.81	67.98	67.94	0.50	1.02	60.8	13	
Scoria	4.08	69.14	67.94	0.50	1.42	45.3	14	
Intense mingling	2.90	67.78	67.94	0.50	0.95	63.4	15	
Minor mingling	2.78	68.04	67.94	0.50	1.04	60.0	16	
Minor mingling	3.55	68.24	67.94	0.50	1.10	57.9	17	
Scoria	4.56	69.03	67.94	0.50	1.32	49.3	18	
Scoria	3.38	68.54	67.94	0.50	1.22	53.1	19	-3.5phi
Intense mingling	1.48	67.71	67.94	0.50	0.87	66.5	20	
Minor mingling	4.13	69.28	67.94	0.50	1.49	42.9	21	
Minor mingling	2.82	68.23	67.94	0.50	1.12	57.0	22	
Minor mingling	3.20	68.79	67.94	0.50	1.37	47.4	23	
Minor mingling	1.78	68.06	67.94	0.50	1.08	58.5	24	
Scoria	2.07	68.02	67.94	0.50	1.05	59.8	25	
Intense mingling	1.02	67.95	67.94	0.50	1.02	60.8	26	
Minor mingling	1.17	67.80	67.94	0.25	0.90	65.5	27	
Minor mingling	1.33	67.96	67.94	0.25	1.02	60.8	28	
	5.16	mean mass			1.10	53.14	mean	
	18.20	standard dev			0.36	13.82	standard deviation	
	75.38	max mass			0.73	71.81	minimum density value	
	1.02	min mass			2.43	6.61	maximum density value	
					0.80	65.86	average 3 minimum density	
					0.96	59.32	average 3 maximum density	

Sample **AG46**

Componentry	Dry	Wet	Ballast	Wax	Density	Vesicularity	Clast no.	
Scoria	34.46	103.43	92.91	2.00	1.44	44.5	1	-5phi
Pumice	34.28	97.66	92.91	2.00	1.16	55.3	2	
Minor mingling	19.82	86.12	92.91	2.00	0.75	71.3	3	
Scoria	31.78	91.85	92.91	2.00	0.97	62.7	4	
Scoria	26.15	94.16	92.91	2.00	1.05	59.5	5	
Scoria	13.63	94.03	92.91	1.00	1.09	58.0	6	-4.5phi
Scoria	10.25	93.09	92.91	1.00	1.02	60.8	7	
Scoria	19.91	97.49	92.91	1.00	1.30	50.0	8	
Scoria	11.66	95.05	92.91	1.00	1.23	52.8	9	
Scoria	27.29	97.92	92.91	1.00	1.23	52.8	10	
Scoria	17.45	94.59	92.91	2.00	1.11	57.3	11	
Scoria	27.33	99.50	92.91	2.00	1.32	49.2	12	
Scoria	12.00	94.40	92.91	1.00	1.14	56.0	13	
Scoria	12.14	92.08	92.91	1.00	0.94	63.9	14	
Scoria	12.76	95.28	92.91	1.00	1.23	52.7	15	
Scoria	11.47	92.57	92.91	2.00	0.97	62.5	16	
Scoria	16.64	9.06	0.00	1.00	2.20	15.3	17	
Scoria	7.12	93.30	92.91	1.00	1.06	59.2	18	-4phi
Scoria	6.48	94.28	92.91	1.00	1.27	51.0	19	
Scoria	5.80	94.08	92.91	1.00	1.26	51.6	20	
Scoria	7.89	92.68	92.91	1.00	0.97	62.5	21	
Scoria	5.98	93.70	92.91	1.00	1.16	55.5	22	
Scoria	4.82	93.29	92.91	1.00	1.09	58.1	23	
Scoria	5.42	93.31	92.91	1.00	1.08	58.3	24	
Scoria	8.77	94.98	92.91	1.00	1.31	49.5	25	
Scoria	7.99	93.60	92.91	1.00	1.10	57.8	26	
Scoria	7.42	93.74	92.91	1.00	1.13	56.6	27	
Scoria	4.96	92.65	92.91	1.00	0.95	63.3	28	
Scoria	64.40	100.22	92.91	4.00	1.13	56.6	29	-5phi
Scoria	1.00	1.00	1.00	1.00	1.02	60.8	30	
	56.68	30.18	0.00	4.00	2.15	17.5	31	larger clast chips
	104.53	59.88	0.00	4.00	2.35	9.8	32	
	68.03	30.61	0.00	4.00	1.82	29.9	33	
	67.80	28.84	0.00	4.00	1.74	32.9	34	
	78.71	19.74	0.00	4.00	1.34	48.6	35	
	57.98	32.31	0.00	4.00	2.27	12.9	36	
	15.95	mean mass			1.25	46.62	mean	
	25.33	standard dev			0.40	15.31	standard deviation	
	104.53	max mass			0.75	71.31	minimum density value	
	1.00	min mass			2.35	9.80	maximum density value	
					1.08	54.16	average 3 minimum density	
					1.74	25.90	average 3 maximum density	

Sample **AG47**

Componentry	Dry	Wet	Ballast	Wax	Density	Vesicularity	Clast no.	
Pumice	66.57	123.70	160.02	4.00	0.65	75.1	29	-5.5phi
Intense mingling	33.00	88.24	92.91	2.00	0.88	66.3	1	-5phi
Pumice	26.58	82.87	92.91	3.00	0.73	72.0	2	
Pumice	34.40	53.59	67.93	3.00	0.71	72.8	3	
Minor Mingling	45.07	69.98	67.93	3.00	1.05	59.6	4	
Pumice	18.18	62.83	67.93	2.00	0.78	69.9	5	-4.5phi
Intense mingling	14.29	67.57	67.93	2.00	0.98	62.4	6	
Pumice	5.95	65.65	67.93	1.00	0.72	72.1	7	
Pumice	5.53	65.97	67.93	1.00	0.74	71.5	8	
Intense mingling	12.50	65.23	67.93	2.00	0.82	68.3	9	
Scoria	26.01	90.01	92.91	2.00	0.90	65.3	10	
Minor Mingling	21.42	71.90	67.93	2.00	1.23	52.7	11	
Scoria	33.04	96.92	92.91	2.00	1.14	56.2	12	
Pumice	2.67	67.09	67.93	0.50	0.76	70.7	13	-4phi
Pumice	1.77	67.21	67.93	0.50	0.71	72.5	14	
Pumice	2.28	67.14	67.93	0.50	0.75	71.3	15	
Pumice	1.89	67.49	67.93	0.50	0.81	68.7	16	
Pumice	1.60	67.28	67.93	0.50	0.71	72.5	17	
Intense mingling	3.11	67.65	67.93	0.50	0.92	64.6	18	
Pumice	2.19	67.40	67.93	0.50	0.81	68.9	19	
Pumice	5.03	68.42	67.93	0.50	1.11	57.3	20	
Pumice	5.58	67.16	67.93	1.00	0.88	66.1	21	
Pumice	2.35	67.40	67.93	0.50	0.82	68.5	22	
Pumice	2.27	67.12	67.93	0.50	0.74	71.6	23	

AG47 continued

Minor Mingling	6.23	92.13	92.91	0.50	0.89	65.8	24	
Dense lithic	8.28	4.93	0.00	0.50	2.48	4.7	25	
Pumice	2.84	67.39	67.93	0.50	0.84	67.6	26	-3.5phi
Minor Mingling	2.61	68.32	67.93	0.50	1.18	54.6	27	
Pumice	1.48	67.37	67.93	0.50	0.73	72.0	28	

7.01	mean mass	0.89	62.30	mean
16.13	standard dev	0.34	13.10	standard deviation
66.57	max mass	0.71	72.82	minimum density value
1.48	min mass	2.48	4.65	maximum density value
		0.77	67.38	average 3 minimum density
		0.93	60.51	average 3 maximum density

Sample AG48

Componentry	Dry	Wet	Ballast	Wax	Density	Vesicularity	Clast no.	
Pumice	103.51	101.30	160.79	4.00	0.64	75.6	29	-6phi
Intense mingling	111.32	113.32	160.79	4.50	0.70	73.0	30	
Pumice	15.81	59.73	67.94	2.00	0.66	74.6	1	-5phi
Dense lithic	39.37	22.90	0.00	2.00	2.40	7.8	2	-4.5phi
Pumice	5.77	63.63	67.94	1.00	0.57	77.9	3	
Pumice	10.00	62.61	67.94	1.00	0.65	74.9	4	
Pumice	6.28	64.25	67.94	1.00	0.63	75.7	5	
Intense mingling	8.09	65.67	67.94	1.00	0.78	69.9	6	
Scoria	5.93	2.09	0.00	1.00	1.55	40.3	7	-4phi
Dense lithic	7.68	4.47	0.00	1.00	2.41	7.4	8	
Pumice	2.10	66.57	67.94	1.00	0.61	76.6	9	
Intense mingling	4.58	67.98	67.94	1.00	1.01	61.0	10	
Intense mingling	6.25	68.81	67.94	1.00	1.17	55.2	11	
Minor mingling	5.71	68.28	67.94	1.00	1.07	59.0	12	
Intense mingling	5.59	68.94	67.94	0.50	1.22	53.1	13	
Intense mingling	3.05	67.16	67.94	0.50	0.80	69.3	14	
Pumice	3.64	66.12	67.94	0.50	0.67	74.3	15	
Pumice	1.75	67.04	67.94	0.50	0.66	74.5	16	
Pumice	3.97	68.78	67.94	0.50	1.27	51.1	17	
Intense mingling	2.05	67.08	67.94	0.50	0.71	72.8	18	
Pumice	2.14	66.76	67.94	0.50	0.65	75.1	19	
Intense mingling	3.46	67.26	67.94	0.50	0.84	67.8	20	
Scoria	3.34	68.26	67.94	0.50	1.11	57.3	21	
Pumice	2.05	67.31	67.94	0.50	0.77	70.5	22	
Dense lithic	11.62	6.96	0.00	0.50	2.50	3.9	23	
Pumice	1.09	67.54	67.94	0.25	0.73	71.8	24	-3.5phi
Pumice	1.23	67.25	67.94	0.25	0.64	75.3	25	
Intense mingling	2.67	68.15	67.94	0.50	1.09	58.1	26	
Minor mingling	0.94	67.56	67.94	0.25	0.71	72.5	27	
Pumice	1.05	67.49	67.94	0.25	0.70	73.0	28	

4.93	mean mass	0.92	60.85	mean
26.73	standard dev	0.56	21.36	standard deviation
111.32	max mass	0.57	77.94	minimum density value
0.94	min mass	2.50	3.89	maximum density value
		0.97	58.82	average 3 minimum density
		0.70	70.11	average 3 maximum density

Sample AG49

Componentry	Dry	Wet	Ballast	Wax	Density	Vesicularity	Clast no.	
Scoria	72.45	101.39	92.91	4.00	1.13	56.4	29	-5.5phi
Scoria	19.46	87.06	92.91	2.00	0.77	70.4	1	-5phi
Minor Mingling	31.77	92.69	92.91	2.00	0.99	61.8	2	
Intense mingling	17.83	90.64	92.91	2.00	0.89	65.8	3	-4.5phi
Minor Mingling	8.14	90.99	92.91	1.00	0.81	68.8	4	
Minor Mingling	9.52	92.17	92.91	1.00	0.93	64.2	5	
Minor Mingling	16.08	93.53	92.91	2.00	1.04	59.9	6	
Pumice	7.12	92.48	92.91	1.00	0.95	63.6	7	
Scoria	5.68	92.96	92.91	1.00	1.01	61.1	8	
Minor Mingling	8.28	93.21	92.91	1.00	1.04	60.0	9	
Scoria	8.28	89.26	92.91	1.00	0.70	73.3	10	
Dense lithic	40.50	24.00	0.00	2.00	2.46	5.4	11	
Dense lithic	32.24	19.14	0.00	2.00	2.47	5.1	12	
Pumice	5.69	91.54	92.91	1.00	0.81	68.9	13	-4phi
Intense mingling	4.53	90.97	92.91	1.00	0.70	73.0	14	

AG49 continued

Minor Mingling	8.95	94.33	92.91	1.00	1.19	54.2	15	
Minor Mingling	6.35	93.01	92.91	1.00	1.02	60.8	16	
Pumice	6.54	93.58	92.91	1.00	1.12	57.0	17	
Minor Mingling	10.95	95.11	92.91	1.00	1.25	51.8	18	
Pumice	2.82	92.28	92.91	1.00	0.82	68.4	19	
Scoria	2.15	92.16	92.91	1.00	0.75	71.3	20	
Minor Mingling	5.38	93.81	92.91	1.00	1.21	53.6	21	
Minor Mingling	5.93	91.59	92.91	1.00	0.82	68.5	22	
Scoria	4.81	92.90	92.91	1.00	1.00	61.5	23	
Minor Mingling	1.48	92.65	92.91	1.00	0.86	66.9	24	-3.5phi
Minor Mingling	3.39	94.11	92.91	1.00	1.56	39.9	25	
Intense mingling	0.98	92.74	92.91	1.00	0.87	66.6	26	
Pumice	1.74	92.72	92.91	1.00	0.91	65.0	27	
Pumice	1.02	92.71	92.91	1.00	0.85	67.3	28	

6.99	mean mass	1.01	57.18	mean
15.24	standard dev	0.44	16.84	standard deviation
72.45	max mass	0.70	73.26	minimum density value
0.98	min mass	2.47	5.05	maximum density value
		0.88	62.57	average 3 minimum density
		0.88	62.55	average 3 maximum density

sample AG50

Componentry	Dry	Wet	Ballast	Wax	Density	Vesicularity	Clast no.	
Pumice	108.48	115.02	92.91	4.00	1.26	51.6	1	-5.5phi
Pumice	4.05	94.38	92.91	0.50	1.58	39.4	2	-4phi
Pumice	5.80	95.78	92.91	0.50	1.99	23.6	3	
Pumice	4.97	95.37	92.91	0.50	1.99	23.5	4	
Pumice	8.93	97.53	92.91	0.50	2.08	20.1	5	
Pumice	5.89	96.11	92.91	0.50	2.20	15.5	6	
Pumice	1.88	93.39	92.91	0.25	1.35	48.2	7	-3.5phi
Pumice	2.28	93.66	92.91	0.25	1.50	42.5	8	

6.41	mean mass	1.71	27.38	mean
36.71	standard dev	0.36	13.94	standard deviation
108.48	max mass	1.26	51.65	minimum density value
1.88	min mass	2.20	15.47	maximum density value
		1.58	32.82	average 3 minimum density
		1.64	30.12	average 3 maximum density

Sample AG52

Componentry	Dry	Wet	Ballast	Wax	Density	Vesicularity	Clast no.	
Intense mingling	29.45	90.11	92.91	2.00	0.91	64.8	1	-5phi
Intense mingling	38.78	93.04	92.91	2.00	1.00	61.4	2	
Intense mingling	23.59	88.84	92.91	2.00	0.85	67.2	3	
Intense mingling	35.66	81.73	92.91	2.00	0.76	70.7	4	
Intense mingling	21.64	91.83	92.91	2.00	0.95	63.3	5	
Pumice	13.14	93.10	92.91	2.00	1.02	60.9	6	-4.5phi
Dense lithic	26.14	14.62	0.00	2.00	2.28	12.4	7	
Intense mingling	13.32	90.69	92.91	2.00	0.86	66.9	8	
Intense mingling	20.24	92.77	92.91	2.00	1.00	61.7	9	
Pumice	15.96	88.18	92.91	2.00	0.77	70.3	10	
Intense mingling	18.11	88.55	92.91	2.00	0.81	68.9	11	
Intense mingling	14.98	88.94	92.91	2.00	0.79	69.5	12	
Intense mingling	8.99	90.64	92.91	2.00	0.80	69.2	13	
Pumice	9.26	88.63	92.91	2.00	0.69	73.6	14	
Intense mingling	9.20	90.84	92.91	2.00	0.82	68.5	15	
Intense mingling	20.33	91.75	92.91	2.00	0.95	63.5	16	
Minor mingling	14.36	92.92	92.91	2.00	1.00	61.4	17	
Pumice	8.56	90.02	92.91	2.00	0.75	71.1	18	
Pumice	7.10	91.67	92.91	1.00	0.85	67.2	19	
Pumice	6.57	92.25	92.91	1.00	0.91	65.0	20	-4phi
Pumice	6.20	90.80	92.91	1.00	0.75	71.2	21	
Dense lithic	15.96	9.13	0.00	1.00	2.34	9.9	22	
Pumice	6.56	94.42	92.91	1.00	1.30	49.8	23	
Pumice	5.83	92.94	92.91	1.00	1.01	61.2	24	
Pumice	3.83	91.06	92.91	1.00	0.68	74.0	25	
Pumice	5.14	93.20	92.91	1.00	1.06	59.1	26	
Pumice	4.40	91.95	92.91	1.00	0.82	68.3	27	
Pumice	3.41	92.29	92.91	1.00	0.85	67.3	28	

AG52 continued

11.71	mean mass	0.94	60.12	mean
9.60	standard dev	0.40	15.27	standard deviation
38.78	max mass	0.68	73.97	minimum density value
3.41	min mass	2.34	9.86	maximum density value
		0.92	60.76	average 3 minimum density
		0.91	61.41	average 3 maximum density

Sample AG53

Componentry	Dry	Wet	Ballast	Wax	Density	Vesicularity	Clast no.	
Scoria	18.79	65.00	67.93	2.00	0.87	66.7	1	-5phi
Scoria	37.18	76.94	67.93	2.00	1.32	49.2	2	
Scoria	42.69	72.46	67.93	2.00	1.12	56.9	3	
Scoria	33.90	72.51	67.93	2.00	1.16	55.5	4	
Scoria	10.75	68.18	67.93	1.00	1.03	60.5	5	-4.5phi
Scoria	13.49	68.26	67.93	1.00	1.03	60.5	6	
Scoria	10.88	67.81	67.93	1.00	0.99	61.9	7	
Scoria	10.01	67.46	67.93	1.00	0.96	63.2	8	
Scoria	7.99	65.73	67.93	1.50	0.79	69.8	9	
Scoria	11.55	68.93	67.93	1.50	1.10	57.8	10	
Scoria	12.33	68.17	67.93	1.50	1.02	60.7	11	
Scoria	10.17	65.40	67.93	1.00	0.80	69.2	12	
Scoria	6.63	66.15	67.93	1.00	0.79	69.6	13	
Scoria	10.06	67.95	67.93	1.00	1.00	61.4	14	-4phi
Scoria	8.21	68.19	67.93	1.00	1.04	60.2	15	
Scoria	10.26	71.30	67.93	1.00	1.49	42.6	16	
Scoria	3.52	68.19	67.93	0.50	1.08	58.3	17	
Scoria	5.13	66.91	67.93	1.00	0.84	67.8	18	
Scoria	5.60	68.37	67.93	1.00	1.09	58.1	19	
Scoria	7.10	69.04	67.93	1.00	1.19	54.3	20	
Scoria	5.12	67.31	67.93	1.00	0.90	65.6	21	
Scoria	9.42	68.14	67.93	1.00	1.03	60.6	22	
Scoria	3.11	67.33	67.93	0.50	0.84	67.7	23	
Scoria	1.79	67.92	67.93	0.50	1.00	61.5	24	-3.5phi
Scoria	2.58	68.71	67.93	0.50	1.44	44.6	25	
Scoria	2.40	68.27	67.93	0.50	1.17	55.0	26	
Scoria	1.83	67.90	67.93	0.50	0.99	62.0	27	
Scoria	2.03	67.81	67.93	0.50	0.95	63.5	28	

7.60	mean mass	1.02	56.50	mean
10.45	standard dev	0.18	6.83	standard deviation
42.69	max mass	0.79	69.75	minimum density value
1.79	min mass	1.49	42.56	maximum density value
		1.09	53.76	average 3 minimum density
		1.03	56.09	average 3 maximum density

Sample AG54

Componentry	Dry	Wet	Ballast	Wax	Density	Vesicularity	Clast no.	
Minor mingling	73.76	89.85	92.91	3.00	0.96	63.0	29	-5.5phi
Pumice	38.47	78.10	92.91	4.00	0.72	72.2	1	-5phi
Minor mingling	38.62	93.35	92.91	4.00	1.01	61.0	2	
Dense lithic	59.06	32.92	0.00	4.00	2.27	12.8	3	
Intense mingling	22.22	89.10	92.91	4.00	0.86	67.1	4	
Minor mingling	11.49	68.14	67.94	2.00	1.02	60.7	5	-4.5phi
Pumice	11.16	64.55	67.94	2.00	0.77	70.4	6	
Intense mingling	16.47	67.27	67.94	2.00	0.96	63.0	7	
Dense lithic	24.70	14.44	0.00	2.00	2.42	7.0	8	
Intense mingling	13.11	63.33	67.94	2.00	0.74	71.5	9	
Intense mingling	10.37	65.89	67.94	2.00	0.84	67.8	10	
Intense mingling	14.91	65.34	67.94	2.00	0.85	67.2	11	
Pumice	9.29	67.28	67.94	2.00	0.94	63.9	12	
Pumice	7.44	65.06	67.94	2.00	0.72	72.2	13	
Pumice	5.31	65.56	67.94	1.00	0.69	73.4	14	
Pumice	8.47	68.55	67.94	1.00	1.08	58.4	15	
Intense mingling	8.02	67.33	67.94	1.00	0.93	64.2	16	
Intense mingling	9.88	67.75	67.94	1.00	0.98	62.2	17	
Pumice	7.46	65.88	67.94	1.00	0.79	69.8	18	
Scoria	3.79	68.60	67.94	1.00	1.22	53.1	19	-4phi
Intense mingling	2.43	67.29	67.94	1.00	0.79	69.5	20	

AG54 continued

Pumice	6.64	66.89	67.94	1.00	0.87	66.7	21	
Intense mingling	5.02	67.08	67.94	1.00	0.86	67.1	22	
Pumice	6.47	68.06	67.94	1.00	1.02	60.7	23	
Dense lithic	10.36	74.07	67.94	1.00	2.46	5.4	24	
Dense lithic	13.96	76.31	67.94	1.00	2.51	3.6	25	
Intense mingling	5.93	66.96	67.94	1.00	0.86	66.9	26	
Pumice	5.05	65.55	67.94	1.00	0.68	73.8	27	
Intense mingling	4.87	66.66	67.94	1.00	0.79	69.4	28	

10.89	mean mass	1.00	57.36	mean
16.78	standard dev	0.56	21.65	standard deviation
73.76	max mass	0.68	73.82	minimum density value
2.43	min mass	2.51	3.60	maximum density value
				average 3 minimum
		1.18	49.60	density
				average 3 maximum
		0.74	68.71	density

Sample **AG55**

Componetry	Dry	Wet	Ballast	Wax	Density	Vesicularity	Clast no.	
Scoria	69.36	92.29	92.91	4.00	0.99	61.8	29	-5.5phi
Minor mingling	36.37	97.23	92.91	2.00	1.14	56.3	1	-5phi
Scoria	22.64	96.46	92.91	2.00	1.19	54.3	2	
Intense mingling	25.31	90.28	92.91	2.00	0.91	65.1	3	
Pumice	18.28	93.91	92.91	2.00	1.06	59.2	4	-4.5phi
Minor mingling	11.42	94.95	92.91	1.00	1.22	53.1	5	
Minor mingling	11.88	95.16	92.91	1.00	1.24	52.5	6	
Pumice	11.31	93.72	92.91	1.00	1.08	58.5	7	
Scoria	12.45	94.84	92.91	1.00	1.19	54.4	8	
Scoria	12.46	93.14	92.91	2.00	1.02	60.7	9	
Minor mingling	10.53	94.75	92.91	1.00	1.21	53.3	10	
Intense mingling	9.97	94.87	92.91	1.00	1.25	52.0	11	
Pumice	6.60	93.16	92.91	1.00	1.04	59.9	12	
Minor mingling	8.45	94.86	92.91	1.00	1.30	49.8	13	-4phi
Minor mingling	6.78	94.49	92.91	0.50	1.31	49.8	14	
Intense mingling	5.32	94.19	92.91	0.50	1.32	49.2	15	
Pumice	5.11	93.15	92.91	0.50	1.05	59.6	16	
Scoria	6.74	93.83	92.91	0.50	1.16	55.4	17	
Scoria	5.36	92.47	92.91	0.50	0.93	64.4	18	
Pumice	5.89	94.10	92.91	0.50	1.26	51.7	19	
Minor mingling	4.03	93.67	92.91	0.50	1.24	52.5	20	
Scoria	4.63	94.27	92.91	0.50	1.42	45.4	21	
Minor mingling	4.16	93.23	92.91	0.50	1.09	58.2	22	
Intense mingling	2.90	93.26	92.91	0.50	1.14	56.1	23	
Pumice	2.08	93.06	92.91	0.50	1.08	58.3	24	-3.5phi
Minor mingling	2.60	93.30	92.91	0.25	1.18	54.6	25	
Minor mingling	2.37	93.50	92.91	0.25	1.34	48.6	26	
Scoria	2.90	93.63	92.91	0.25	1.33	48.7	27	
Intense mingling	1.87	92.62	92.91	0.25	0.87	66.6	28	

7.49	mean mass	1.15	50.88	mean
13.64	standard dev	0.14	5.29	standard deviation
69.36	max mass	0.87	66.63	minimum density value
1.87	min mass	1.42	45.38	maximum density value
		1.07	54.47	average 3 minimum density
		1.08	54.23	average 3 maximum density

Sample **AG65**

Componentry	Dry	Wet	Ballast	Wax	Density	Vesicularity	Clast no.	
Minor mingling	41.07	96.67	92.91	2.00	1.10	57.6	1	-5phi
Scoria	26.81	95.97	92.91	2.00	1.13	56.5	2	
Scoria	44.18	94.79	92.91	3.00	1.05	59.8	3	
Dense lithic	67.80	40.29	0.00	3.00	2.47	5.0	4	
Scoria	11.08	94.03	92.91	1.00	1.11	57.1	5	-4.5phi
Scoria	12.40	93.96	92.91	1.00	1.09	57.9	6	
Scoria	9.95	93.65	92.91	1.00	1.08	58.4	7	
Minor mingling	11.12	96.13	92.91	1.00	1.41	45.7	8	
Scoria	11.96	94.15	92.91	1.00	1.12	57.0	9	
Scoria	6.89	93.56	92.91	1.00	1.11	57.4	10	-4phi

AG65 continued

Scoria	5.72	93.30	92.91	1.00	1.08	58.6	11	
Scoria	7.59	96.38	92.91	1.00	1.85	28.8	12	
Scoria	3.89	93.01	92.91	0.50	1.03	60.4	13	
Scoria	4.57	93.20	92.91	0.50	1.07	58.8	14	
Scoria	4.90	93.37	92.91	0.50	1.11	57.5	15	
Scoria	4.03	92.71	92.91	0.50	0.95	63.3	16	
Scoria	4.52	92.96	92.91	0.50	1.01	61.0	17	
Scoria	3.85	92.97	92.91	0.50	1.02	60.8	18	
Dense lithic	12.17	7.22	0.00	1.50	2.47	4.9	19	
Scoria	6.74	93.47	92.91	0.75	1.09	58.0	20	
Scoria	2.76	0.48	0.00	0.00	1.21	53.4	21	
Scoria	1.80	33.43	33.26	0.00	1.10	57.5	22	-3.5phi
Scoria	2.14	0.45	0.00	0.00	1.27	51.3	23	
Scoria	1.43	0.15	0.00	0.00	1.12	57.0	24	
Scoria	2.12	33.67	33.26	0.00	1.24	52.3	25	
Scoria	1.82	0.32	0.00	0.00	1.21	53.3	26	
Scoria	2.03	0.69	33.26	0.00	0.06	97.7	27	
Scoria	2.09	0.28	33.26	0.00	0.06	97.7	28	

6.28	mean mass	0.97	58.55	mean
15.49	standard dev	0.49	19.00	standard deviation
67.80	max mass	0.06	97.74	minimum density value
1.43	min mass	2.47	4.86	maximum density value
		1.09	53.52	average 3 minimum density
		0.16	93.11	average 3 maximum density

Sample AG67

Componentry	Dry	Wet	Ballast	Wax	Density	Vesicularity	Clast no.	
Scoria	35.24	59.44	67.94	2.00	0.81	69.0	1	-5phi
Scoria	19.82	61.85	67.94	3.00	0.77	70.5	2	
Scoria	31.20	71.94	67.94	2.00	1.15	55.8	3	
Scoria	61.87	70.90	67.94	4.00	1.05	59.6	4	
Scoria	25.88	63.26	67.94	2.25	0.85	67.4	5	
Scoria	28.83	61.44	67.94	2.00	0.82	68.6	6	
Scoria	19.02	65.94	67.94	2.00	0.91	65.1	7	-4.5phi
Scoria	7.31	65.14	67.94	1.00	0.72	72.1	8	
Scoria	8.49	66.98	67.94	1.25	0.90	65.4	9	
Dense lithic	16.08	8.50	0.00	0.00	2.12	18.4	10	
Scoria	9.99	65.91	67.94	1.00	0.83	68.0	11	
Dense lithic	38.71	90.89	67.94	1.00	2.46	5.4	12	
Minor mingling	4.50	67.27	67.94	1.00	0.87	66.4	13	-4phi
Minor mingling	2.90	68.20	67.94	0.50	1.10	57.6	14	
Scoria	2.83	67.25	67.94	0.50	0.81	69.0	15	
Scoria	2.47	66.89	67.94	0.50	0.70	72.9	16	
Scoria	3.89	68.03	67.94	0.50	1.03	60.5	17	
Scoria	2.49	67.20	67.94	0.50	0.77	70.3	18	
Scoria	2.08	67.30	67.94	0.50	0.77	70.5	19	
Scoria	2.33	66.86	67.94	0.50	0.69	73.6	20	
Scoria	2.01	66.82	67.94	0.50	0.64	75.2	21	
Scoria	3.44	68.44	67.94	0.50	1.17	54.8	22	-3.5phi
Scoria	2.31	68.13	67.94	0.50	1.09	57.9	23	
Scoria	1.71	67.44	67.94	0.25	0.78	70.2	24	
Scoria	2.18	67.41	67.94	0.25	0.81	69.0	25	
Scoria	2.40	68.11	67.94	0.25	1.08	58.5	26	
Scoria	2.42	68.28	67.94	0.50	1.17	55.0	27	
Scoria	1.48	67.43	67.94	0.50	0.75	71.3	28	

6.21	mean mass	0.93	60.25	mean
15.12	standard dev	0.40	15.50	standard deviation
61.87	max mass	0.64	75.22	minimum density value
1.48	min mass	2.46	5.41	maximum density value
		0.89	62.03	average 3 minimum density
		0.98	58.28	average 3 maximum density

Sample AG68

Componentry	Dry	Wet	Ballast	Wax	Density	Vesicularity	Clast no.	
Minor mingling	90.58	85.11	92.91	4.00	0.92	64.6	29	-5.5phi
Minor mingling	52.66	88.69	92.91	2.00	0.93	64.4	30	
Dense lithic	87.98	50.51	0.00	5.00	2.35	9.5	1	-5phi

AG68 continued

Intense mingling	25.53	89.77	92.91	4.00	0.89	65.7	2	
Scoria	40.82	19.36	0.00	2.00	1.91	26.7	3	
Intense mingling	54.72	83.97	92.91	4.00	0.86	66.9	4	
Minor mingling	27.47	90.09	92.91	4.00	0.91	65.0	5	
Intense mingling	16.65	85.85	92.91	3.00	0.70	72.9	6	
Intense mingling	17.14	91.80	92.91	2.00	0.94	63.8	7	-4.5phi
Intense mingling	18.88	90.42	92.91	2.00	0.89	66.0	8	
Intense mingling	13.10	91.93	92.91	2.00	0.93	64.1	9	
Pumice	10.49	89.57	92.91	2.00	0.76	70.7	10	
Pumice	8.39	90.63	92.91	2.00	0.79	69.6	11	
Intense mingling	14.17	91.19	92.91	2.00	0.89	65.6	12	
Pumice	10.97	90.11	92.91	2.00	0.80	69.3	13	
Intense mingling	6.56	91.87	92.91	1.00	0.87	66.7	14	
Intense mingling	7.24	92.34	92.91	1.00	0.93	64.3	15	
Intense mingling	17.97	89.44	92.91	2.00	0.84	67.7	16	
Pumice	8.54	92.39	92.91	1.00	0.94	63.7	17	
Intense mingling	7.74	92.49	92.91	1.00	0.95	63.4	18	
Dense lithic	19.65	104.48	92.91	1.00	2.44	6.2	19	-4phi
Minor mingling	5.15	92.47	92.91	1.00	0.92	64.4	20	
Intense mingling	4.51	91.50	92.91	1.00	0.76	70.6	21	
Pumice	3.57	92.02	92.91	1.00	0.80	69.1	22	
Intense mingling	5.02	92.90	92.91	1.00	1.00	61.5	23	
Pumice	5.01	91.95	92.91	1.00	0.84	67.6	24	
Intense mingling	3.73	91.68	92.91	1.00	0.76	71.0	25	
Minor mingling	7.28	92.16	92.91	1.00	0.91	65.0	26	
Intense mingling	3.11	91.97	92.91	1.00	0.77	70.3	27	
Intense mingling	4.28	92.70	92.91	1.00	0.96	63.2	28	

12.33	mean mass	0.95	59.42	mean
23.17	standard dev	0.44	17.07	standard deviation
90.58	max mass	0.70	72.92	minimum density value
3.11	min mass	2.44	6.23	maximum density value
		1.59	32.42	average 3 minimum density
		0.96	59.26	average 3 maximum density

Sample **AG69**

Componentry	**Dry**	**Wet**	**Ballast**	**Wax**	**Density**	**Vesicularity**	**Clast no.**	
Scoria	18.18	84.70	92.91	2.00	0.69	73.5	1	-5phi
Scoria	28.94	94.46	92.91	2.00	1.06	59.3	2	
Scoria	25.99	88.53	92.91	2.00	0.86	67.0	3	
Minor mingling	37.66	88.82	92.91	3.00	0.90	65.3	4	
Minor mingling	12.03	94.24	92.91	1.00	1.13	56.7	5	-4.5phi
Scoria	12.95	91.13	92.91	2.00	0.88	66.1	6	
Dense lithic	39.27	23.33	0.00	1.00	2.47	5.1	7	
Minor mingling	6.53	89.46	92.91	1.00	0.66	74.8	8	
Scoria	13.10	90.33	92.91	1.00	0.84	67.8	9	
Scoria	7.00	89.56	92.91	1.00	0.68	73.9	10	
Scoria	20.41	93.72	92.91	2.00	1.04	59.9	11	
Dense lithic	22.15	13.37	0.00	0.00	2.52	3.0	12	
Minor mingling	6.60	91.37	92.91	1.00	0.81	68.7	13	-4phi
Pumice	5.53	91.60	92.91	1.00	0.81	68.8	14	
Minor mingling	5.09	91.46	92.91	1.00	0.78	70.0	15	
Pumice	3.00	91.99	92.91	1.00	0.77	70.4	16	
Minor mingling	2.60	92.07	92.91	0.50	0.76	70.8	17	
Minor mingling	2.36	92.30	92.91	0.75	0.80	69.3	18	
Scoria	6.59	92.63	92.91	1.00	0.96	63.0	19	
Intense mingling	3.88	92.46	92.91	1.00	0.90	65.4	20	
Minor mingling	5.95	90.94	92.91	1.00	0.75	71.0	21	
Minor mingling	5.40	92.68	92.91	1.00	0.96	63.0	22	
Minor mingling	4.09	91.90	92.91	1.00	0.81	69.0	23	
Intense mingling	1.74	92.88	92.91	0.00	0.98	62.2	24	-3.5phi
Scoria	1.07	92.95	92.91	0.00	1.04	60.0	25	
Scoria	1.84	93.08	92.91	0.00	1.10	57.6	26	
Pumice	1.72	92.99	92.91	0.00	1.05	59.7	27	
Intense mingling	1.87	92.97	92.91	0.00	1.03	60.3	28	

6.65	mean mass	0.94	59.82	mean
11.01	standard dev	0.44	17.01	standard deviation
39.27	max mass	0.66	74.78	minimum density value
1.07	min mass	2.52	2.97	maximum density value
		0.86	63.61	average 3 minimum density
		1.06	54.86	average 3 maximum density

Sample **AG70**

Componentry	Dry	Wet	Ballast	Wax	Density	Vesicularity	Clast no.	
Scoria	95.05	22.05	0.00	4.00	1.30	49.9	1	-5.5phi
Scoria	82.85	94.10	92.91	4.00	1.02	60.9	2	
Minor mingling	124.94	18.26	0.00	4.00	1.17	54.9	3	
Minor mingling	78.94	95.22	92.91	4.00	1.03	60.3	4	
Minor mingling	32.16	87.49	92.91	2.00	0.86	67.1	5	-5phi
Scoria	80.18	10.83	92.91	4.00	0.49	81.0	6	
Intense mingling	18.42	83.74	92.91	2.00	0.67	74.3	7	
Minor mingling	17.46	86.78	92.91	2.00	0.74	71.5	8	
Intense mingling	55.56	100.08	92.91	2.00	1.15	55.8	9	
Scoria	16.10	92.81	92.91	2.00	1.00	61.7	10	-4.5phi
Pumice	9.23	90.93	92.91	1.00	0.82	68.3	11	
Minor mingling	17.76	93.32	92.91	2.00	1.03	60.5	12	
Minor mingling	13.33	90.28	92.91	1.00	0.84	67.8	13	
Minor mingling	14.68	92.58	92.91	1.00	0.98	62.3	14	
Dense lithic	28.04	16.79	0.00	1.00	2.50	4.0	15	
Intense mingling	6.32	92.27	92.91	1.00	0.91	65.0	16	
Minor mingling	10.36	91.01	92.91	1.00	0.85	67.4	17	
Minor mingling	8.02	91.18	92.91	1.00	0.82	68.3	18	
Scoria	6.07	94.03	92.91	1.00	1.23	52.6	19	-4phi
Scoria	4.06	90.58	92.91	1.00	0.64	75.5	20	
Scoria	7.14	93.96	92.91	1.00	1.18	54.8	21	
Scoria	3.65	92.16	92.91	0.50	0.83	68.0	22	
Intense mingling	2.60	91.69	92.91	0.50	0.68	73.8	23	
Intense mingling	7.81	94.36	92.91	1.00	1.23	52.6	24	
Pumice	3.98	92.84	92.91	1.00	0.99	62.0	25	
Minor mingling	4.00	93.10	92.91	0.50	1.05	59.5	26	
Minor mingling	4.39	93.83	92.91	0.50	1.27	51.2	27	
Intense mingling	1.21	92.94	92.91	0.00	1.03	60.6	28	-3.5phi
Intense mingling	1.49	92.81	92.91	0.00	0.94	64.0	29	
Scoria	2.20	93.18	92.91	0.00	1.14	56.2	30	
Intense mingling	1.71	92.92	92.91	0.00	1.01	61.3	31	
Intense mingling	1.52	92.95	92.91	0.00	1.03	60.5	32	

10.30	mean mass	0.97	58.63	mean
32.69	standard dev	0.33	12.84	standard deviation
124.94	max mass	0.49	80.99	minimum density value
1.21	min mass	2.50	3.97	maximum density value
		1.16	50.74	average 3 minimum density
		1.06	55.06	average 3 maximum density

Sample **AG71**

Componentry	Dry	Wet	Ballast	Wax	Density	Vesicularity	Clast no.	
Intense mingling	54.97	92.84	92.91	4.00	1.00	61.5	1	-5.5phi
Minor mingling	101.50	106.18	92.91	4.00	1.15	55.7	2	
Intense mingling	31.59	96.18	92.91	2.00	1.12	57.0	3	-5phi
Intense mingling	38.23	102.76	92.91	2.00	1.35	48.1	4	
Scoria	19.51	90.83	92.91	2.00	0.91	65.2	5	
Minor mingling	25.59	92.18	92.91	2.00	0.97	62.5	6	
Minor mingling	28.46	92.72	92.91	2.00	0.99	61.7	7	
Pumice	20.19	92.89	92.91	1.00	1.00	61.5	8	
Minor mingling	27.33	94.31	92.91	1.00	1.05	59.4	9	
Scoria	9.31	93.51	92.91	1.00	1.07	58.8	10	-4.5phi
Minor mingling	13.38	89.59	92.91	1.00	0.80	69.1	11	
Minor mingling	12.74	92.81	92.91	1.00	0.99	61.8	12	
Minor mingling	12.73	90.78	92.91	1.00	0.86	67.0	13	
Intense mingling	10.46	90.18	92.91	1.00	0.79	69.5	14	
Intense mingling	7.59	92.31	92.91	1.00	0.93	64.3	15	
Intense mingling	6.49	92.35	92.91	1.00	0.92	64.5	16	
Intense mingling	8.47	91.95	92.91	1.00	0.90	65.4	17	
Intense mingling	3.83	91.99	92.91	0.50	0.81	68.9	18	-4phi
Pumice	4.09	92.45	92.91	0.50	0.90	65.4	19	
Pumice	2.89	92.91	92.91	0.50	1.00	61.4	20	
Scoria	3.44	91.91	92.91	0.50	0.78	70.1	21	
Intense mingling	6.52	91.29	92.91	0.50	0.80	69.2	22	
Intense mingling	4.36	91.39	92.91	0.50	0.74	71.4	23	
Intense mingling	2.45	92.61	92.91	0.50	0.89	65.6	24	
Minor mingling	2.13	92.90	92.91	0.50	1.00	61.5	25	-3.5phi
Intense mingling	1.98	92.68	92.91	0.50	0.90	65.4	26	
Intense mingling	2.17	93.29	92.91	0.50	1.22	53.1	27	
Pumice	0.99	92.51	92.91	0.50	0.72	72.4	28	
Pumice	1.52	92.87	92.91	0.50	0.98	62.3	29	

AG71 continued

8.43	mean mass	0.94	59.98	mean
20.99	standard dev	0.14	5.53	standard deviation
101.50	max mass	0.72	72.41	minimum density value
0.99	min mass	1.35	48.12	maximum density value
		1.09	53.72	average 3 minimum density
		0.95	59.57	average 3 maximum density

Sample **Welded Rocks**

Dry	Wet	Ballast	Wax	Density	Vesicularity	Clast no.	Sample	Degree of Welding
35.03	12.16	0.00	2.00	1.53	41.0	1	BL01	Moderate
49.63	18.21	0.00	0.00	1.58	39.2	2	BL01	Moderate
9.84	3.91	0.00	1.00	1.66	36.0	3	AG02	Strong
8.03	4.08	0.00	0.00	2.03	21.8	4	AG02	Strong
83.13	50.07	0.00	0.00	2.51	3.3	5	AG03	Intense
53.55	32.01	0.00	0.00	2.49	4.4	6	AG03	Intense
39.69	19.97	0.00	0.00	2.01	22.6	7	AG04	Moderate
26.17	12.48	0.00	1.00	1.91	26.4	8	AG04	Moderate
42.10	23.35	0.00	0.00	2.25	13.6	9	AG05	Intense
32.25	17.70	0.00	0.00	2.22	14.8	10	AG05	Intense
50.04	30.48	0.00	0.00	2.56	1.6	11	AG06	Intense
61.49	36.44	0.00	0.00	2.45	5.6	12	AG06	Intense
56.85	35.02	0.00	0.00	2.60	-0.2	13	AG08	Intense
17.73	10.25	0.00	1.00	2.38	8.6	14	AG08	Intense
90.84	52.95	0.00	0.00	2.40	7.8	15	AG07	Intense
56.59	34.11	0.00	2.00	2.52	3.0	16	AG09	Intense
34.02	20.85	0.00	0.00	2.58	0.6	17	AG09	Intense
94.84	56.30	0.00	0.00	2.46	5.4	18	AG10	Strong
30.96	17.44	0.00	0.00	2.29	11.9	19	AG12	Strong
28.98	16.16	0.00	0.00	2.26	13.1	20	AG12	Strong
42.17	25.94	0.00	0.00	2.60	0.1	21	AG14	Intense
26.09	14.58	0.00	0.00	2.27	12.8	22	AG15	Strong
34.28	18.91	0.00	0.00	2.23	14.2	23	AG15	Strong
34.91	21.04	0.00	0.00	2.52	3.2	24	AG16	Intense
8.72	5.17	0.00	0.00	2.46	5.5	25	AG16	Strong
42.64	25.36	0.00	0.00	2.47	5.1	26	AG18	Intense
28.10	15.76	0.00	0.00	2.28	12.4	27	AG18	Intense
32.68	8.83	0.00	2.00	1.37	47.2	28	AG20	Non
35.07	13.71	0.00	0.00	1.64	36.9	29	AG20	Non
34.63	20.72	0.00	1.00	2.49	4.1	30	AG22	Intense
58.80	29.09	0.00	2.00	1.98	23.8	31	AG23	Strong
49.23	28.90	0.00	0.00	2.42	6.9	32	AG24	Strong
7.85	0.73	0.00	1.00	1.11	57.5	33	AG51	Moderate
12.77	4.07	0.00	0.00	1.47	43.5	34	AG51	Moderate
101.78	55.15	0.00	0.00	2.18	16.0	35	AG57	Strong
44.80	27.52	0.00	0.00	2.59	0.3	36	AG58	Intense
33.54	20.61	0.00	0.00	2.59	0.2	37	AG58	Intense
41.85	21.01	0.00	0.00	2.01	22.8	38	AG60	Strong
61.64	32.29	0.00	0.00	2.10	19.2	39	AG61	Strong
45.02	26.83	0.00	0.00	2.47	4.8	40	AG62	Intense
71.01	43.14	0.00	0.00	2.55	2.0	41	AG63	Intense
43.25	18.50	0.00	2.00	1.75	32.7	42	AG64	Strong
34.29	4.71	0.00	2.00	1.16	55.4	43	AG66	Moderate
18.25	4.20	0.00	1.00	1.30	50.0	44	AG72	Strong
116.52	68.33	0.00	0.00	2.42	7.0	45	AG74	Strong

36.68	mean mass	2.11	10.28	mean
24.60	standard dev	0.43	16.54	standard deviation
116.52	max mass	1.11	57.48	minimum density value
7.85	min mass	2.60	-0.16	maximum density value
		1.59	32.25	average 3 minimum density
		1.54	34.48	average 3 maximum density

Appendix D
Grain Size Data

Sample: AG19

	mm	phi	Cum wt (g)	wt (g)	wt%	cum % finer	Modes
1	64.00	-6	0.00	0.00	0.000	100.00	
2	45.25	-5.5	0.00	0.00	0.000	100.00	
3	32.00	-5	0.00	0.00	0.000	100.00	
4	22.62	-4.5	0.00	0.00	0.000	100.00	
5	16.00	-4	1.61	1.61	0.003	99.74	
6	11.31	-3.5	10.50	8.89	0.015	98.27	
7	8.00	-3	19.55	9.05	0.015	96.79	
8	5.65	-2.5	50.11	30.56	0.050	91.76	
9	4.00	-2	102.91	52.80	0.087	83.08	
10	2.82	-1.5	185.18	82.27	0.135	69.55	
11	2.00	-1	290.01	104.83	0.172	52.32	
12	1.41	-0.5	407.46	117.45	0.193	33.00	mode at -0.8
13	1.00	0	506.32	98.86	0.163	16.75	
14	0.70	0.5	573.60	67.28	0.111	5.69	
15	0.50	1	601.45	27.85	0.046	1.11	
16	0.35	1.5	607.11	5.66	0.009	0.18	
17	0.25	2	608.18	1.07	0.002	0.00	
18	0.17	2.5	608.18	0.00	0.000	0.00	
19	0.12	3	608.18	0.00	0.000	0.00	
20	0.08	3.5	608.18	0.00	0.000	0.00	
21	0.06	4	608.18	0.00	0.000	0.00	
22	0.04	4.5	608.18	0.00	0.000	0.00	
23	0.03	5	608.18	0.00	0.000	0.00	
24	0.02	5.5	608.18	0.00	0.000	0.00	
25	0.01	6	608.18	0.00	0.000	0.00	
26	0.01	6.5	608.18	0.00	0.000	0.00	
27	0.00	7	608.18		0.000	0.00	
28	0.00	7.5	608.18		0.000	0.00	
29	0.00	8	608.18		0.000	0.00	
30	0.00	8.5	608.18		0.000	0.00	
		Sums:	608.18	608.18	1.000		

iles

	phi	*mm*
95%	-2.82	7.073
84%	-2.05	4.150
75%	-1.70	3.252
50%	-0.94	1.919
25%	-0.25	1.192
16%	0.03	0.977
5%	0.57	0.671

Folks' Graphic Stats

	phi	*mm*
Mean (Mz)	-0.99	1.981
Sorting (SI)	1.04	
Skewness (SkI)	-0.09	
Kurtosis (KG)	0.96	

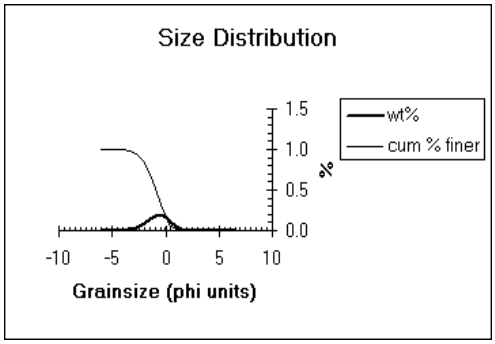

Sample: AG21

	mm	phi	Cum wt (g)	wt (g)	wt%	cum % finer	Modes
1	64.00	-6	0.00	0.00	0.000	100.00	
2	45.25	-5.5	0.00	0.00	0.000	100.00	
3	32.00	-5	0.00	0.00	0.000	100.00	
4	22.62	-4.5	0.00	0.00	0.000	100.00	
5	16.00	-4	50.74	50.74	0.068	93.23	mode at -4.3
6	11.31	-3.5	88.68	37.94	0.051	88.16	
7	8.00	-3	233.38	144.70	0.193	68.84	
8	5.65	-2.5	394.23	160.85	0.215	47.37	mode at -2.8
9	4.00	-2	540.00	145.77	0.195	27.91	
10	2.82	-1.5	649.65	109.65	0.146	13.27	
11	2.00	-1	720.82	71.17	0.095	3.77	
12	1.41	-0.5	742.90	22.08	0.029	0.82	
13	1.00	0	746.93	4.03	0.005	0.28	
14	0.70	0.5	748.11	1.18	0.002	0.12	
15	0.50	1	749.04	0.93	0.001	0.00	
16	0.35	1.5	749.04	0.00	0.000	0.00	
17	0.25	2	749.04	0.00	0.000	0.00	
18	0.17	2.5	749.04	0.00	0.000	0.00	
19	0.12	3	749.04	0.00	0.000	0.00	
20	0.08	3.5	749.04	0.00	0.000	0.00	
21	0.06	4	749.04	0.00	0.000	0.00	
22	0.04	4.5	749.04	0.00	0.000	0.00	
23	0.03	5	749.04	0.00	0.000	0.00	
24	0.02	5.5	749.04	0.00	0.000	0.00	
25	0.01	6	749.04	0.00	0.000	0.00	
26	0.01	6.5	749.04	0.00	0.000	0.00	
27	0.00	7	749.04		0.000	0.00	
28	0.00	7.5	749.04		0.000	0.00	
29	0.00	8	749.04		0.000	0.00	
30	0.00	8.5	749.04		0.000	0.00	
		Sums:	749.04	749.04	1.000		

Percentiles

	phi	*mm*
95%	-4.13	17.520
84%	-3.39	10.500
75%	-3.16	8.934
50%	-2.56	5.902
25%	-1.90	3.734
16%	-1.59	3.017
5%	-1.06	2.092

Folks' Graphic Stats

	phi	*mm*
Mean (Mz)	-2.52	5.718
Sorting (SI)	0.91	
Skewness (SkI)	0.03	
Kurtosis (KG)	1.00	

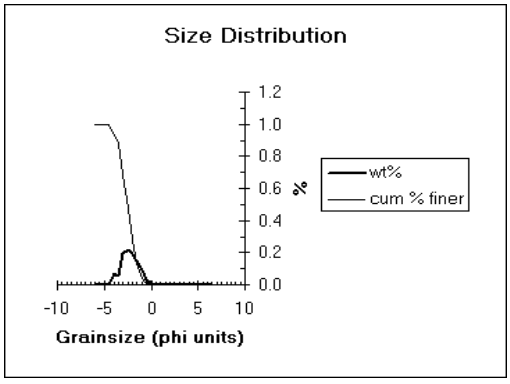

Sample: AG25

	mm	phi	Cum wt (g)	wt (g)	wt%	cum % finer	Modes
1	90.51	-6.5	100.56	100.56	0.032	96.80	
2	64.00	-6	259.84	159.28	0.051	91.72	
3	45.25	-5.5	583.21	323.37	0.103	81.42	
4	32.00	-5	940.14	356.93	0.114	70.04	
5	22.63	-4.5	1390.44	450.30	0.143	55.69	mode at -4.8
6	16.00	-4	1726.44	336.00	0.107	44.99	
7	11.31	-3.5	1956.94	230.50	0.073	37.64	
8	8.00	-3	2165.74	208.80	0.067	30.99	
9	5.66	-2.5	2311.81	146.07	0.047	26.33	
10	4.00	-2	2466.44	154.63	0.049	21.41	mode at -2.3
11	2.83	-1.5	2593.51	127.07	0.040	17.36	
12	2.00	-1	2706.91	113.40	0.036	13.74	
13	1.41	-0.5	2816.27	109.36	0.035	10.26	
14	1.00	0	2910.45	94.18	0.030	7.26	
15	0.71	0.5	3001.48	91.03	0.029	4.36	
16	0.50	1	3096.65	95.17	0.030	1.33	mode at 0.75
17	0.35	1.5	3175.71	79.06	0.025	-1.19	
18	0.25	2	3238.82	63.11	0.020	-3.20	
19	0.18	2.5	3238.82	0.00	0.000	-3.20	
20	0.13	3	3238.82	0.00	0.000	-3.20	
21	0.09	3.5	3238.82	0.00	0.000	-3.20	
22	0.06	4	3238.82	0.00	0.000	-3.20	
23	0.04	4.5	3238.82	0.00	0.000	-3.20	
24	0.03	5	3238.82	0.00	0.000	-3.20	
25	0.02	5.5	3238.82	0.00	0.000	-3.20	
26	0.02	6	3238.82	0.00	0.000	-3.20	
27	0.01	6.5	3238.82		0.000	-3.20	
28	0.01	7	3238.82		0.000	-3.20	
29	0.01	7.5	3238.82		0.000	-3.20	
30	0.00	8	3238.82		0.000	-3.20	
		Sums:	3238.82	3138.26	1.032		

Percentiles

	phi	*mm*
95%	-6.32	80.065
84%	-5.63	49.364
75%	-5.22	37.218
50%	-4.23	18.819
25%	-2.36	5.150
16%	-1.31	2.483
5%	0.39	0.763

Folks' Graphic Stats

	phi	*mm*
Mean (Mz)	-3.72	13.213
Sorting (SI)	2.10	
Skewness (SkI)	0.37	
Kurtosis (KG)	0.96	

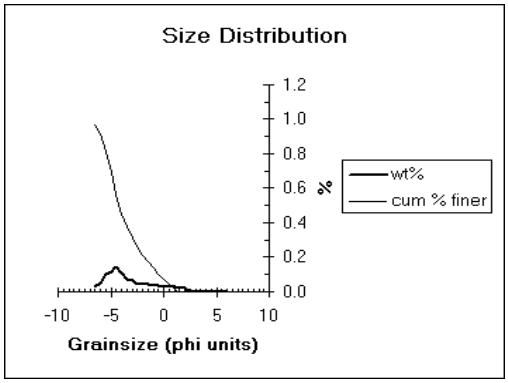

Sample: AG26

	mm	phi	Cum wt (g)	wt (g)	wt%	cum% finer	Modes
1	90.51	-6.5	0.00	0.00	0.000	100.00	
2	64.00	-6	243.56	243.56	0.113	88.68	mode at -6.3
3	45.25	-5.5	254.21	10.65	0.005	88.18	
4	32.00	-5	391.33	137.12	0.064	81.80	
5	22.63	-4.5	801.33	410.00	0.191	62.74	mode at -4.8
6	16.00	-4	1062.73	261.40	0.122	50.59	
7	11.31	-3.5	1256.93	194.20	0.090	41.56	
8	8.00	-3	1394.53	137.60	0.064	35.16	
9	5.66	-2.5	1527.63	133.10	0.062	28.97	
10	4.00	-2	1647.53	119.90	0.056	23.40	
11	2.83	-1.5	1738.23	90.70	0.042	19.18	
12	2.00	-1	1813.70	75.47	0.035	15.67	
13	1.41	-0.5	1881.66	67.96	0.032	12.51	
14	1.00	0	1940.99	59.33	0.028	9.75	
15	0.71	0.5	1998.33	57.34	0.027	7.09	
16	0.50	1	2058.84	60.51	0.028	4.27	mode at 0.75
17	0.35	1.5	2110.06	51.22	0.024	1.89	
18	0.25	2	2150.71	40.65	0.019	0.00	
19	0.18	2.5	2150.71	0.00	0.000	0.00	
20	0.13	3	2150.71	0.00	0.000	0.00	
21	0.09	3.5	2150.71	0.00	0.000	0.00	
22	0.06	4	2150.71	0.00	0.000	0.00	
23	0.04	4.5	2150.71	0.00	0.000	0.00	
24	0.03	5	2150.71	0.00	0.000	0.00	
25	0.02	5.5	2150.71	0.00	0.000	0.00	
26	0.02	6	2150.71	0.00	0.000	0.00	
27	0.01	6.5	2150.71		0.000	0.00	
28	0.01	7	2150.71		0.000	0.00	
29	0.01	7.5	2150.71		0.000	0.00	
30	0.00	8	2150.71		0.000	0.00	
		Sums:	2150.71	2150.71	1.000		

Percentiles

	phi	*mm*
95%	-6.28	77.668
84%	-5.17	36.056
75%	-4.82	28.276
50%	-3.97	15.644
25%	-2.14	4.419
16%	-1.05	2.066
5%	0.87	0.547

Folks' Graphic Stats

	phi	*mm*
Mean (Mz)	-3.40	10.524
Sorting (SI)	2.11	
Skewness (SkI)	0.38	
Kurtosis (KG)	1.09	

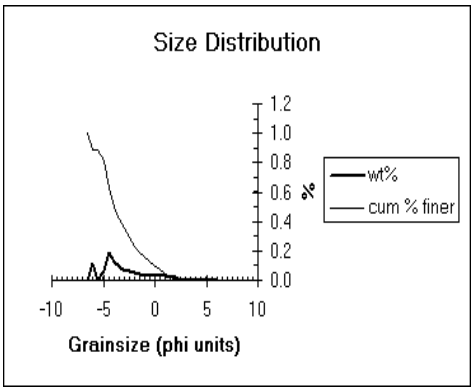

Sample: AG27

	mm	phi	Cum wt (g)	wt (g)	wt%	cum% finer	Modes	
1	64.00	-6	0.00	0.00	0.000	100.00		
2	45.25	-5.5	0.00	0.00	0.000	100.00		
3	32.00	-5	45.83	45.83	0.035	96.54		
4	22.62	-4.5	270.53	224.70	0.170	79.58	mode at	-4.8
5	16.00	-4	478.43	207.90	0.157	63.88		
6	11.31	-3.5	664.43	186.00	0.140	49.84		
7	8.00	-3	798.33	133.90	0.101	39.74		
8	5.65	-2.5	883.33	85.00	0.064	33.32		
9	4.00	-2	940.73	57.40	0.043	28.99		
10	2.82	-1.5	992.53	51.80	0.039	25.08		
11	2.00	-1	1040.63	48.10	0.036	21.45		
12	1.41	-0.5	1082.53	41.90	0.032	18.28		
13	1.00	0	1124.03	41.50	0.031	15.15		
14	0.70	0.5	1173.33	49.30	0.037	11.43		
15	0.50	1	1227.43	54.10	0.041	7.34		
16	0.35	1.5	1284.43	57.00	0.043	3.04	mode at	1.25
17	0.25	2	1324.73	40.30	0.030	0.00		
18	0.17	2.5	1324.73	0.00	0.000	0.00		
19	0.12	3	1324.73	0.00	0.000	0.00		
20	0.08	3.5	1324.73	0.00	0.000	0.00		
21	0.06	4	1324.73	0.00	0.000	0.00		
22	0.04	4.5	1324.73	0.00	0.000	0.00		
23	0.03	5	1324.73	0.00	0.000	0.00		
24	0.02	5.5	1324.73	0.00	0.000	0.00		
25	0.01	6	1324.73	0.00	0.000	0.00		
26	0.01	6.5	1324.73	0.00	0.000	0.00		
27	0.00	7	1324.73		0.000	0.00		
28	0.00	7.5	1324.73		0.000	0.00		
29	0.00	8	1324.73		0.000	0.00		
30	0.00	8.5	1324.73		0.000	0.00		
		Sums:	1324.73	1324.73	1.000			

Percentiles

	phi	*mm*
95%	-4.95	31.008
84%	-4.63	24.767
75%	-4.35	20.451
50%	-3.51	11.357
25%	-1.49	2.808
16%	-0.14	1.099
5%	1.27	0.414

Folks' Graphic Stats

	phi	*mm*
Mean (Mz)	-2.76	6.761
Sorting (SI)	2.07	
Skewness (SkI)	0.52	
Kurtosis (KG)	0.89	

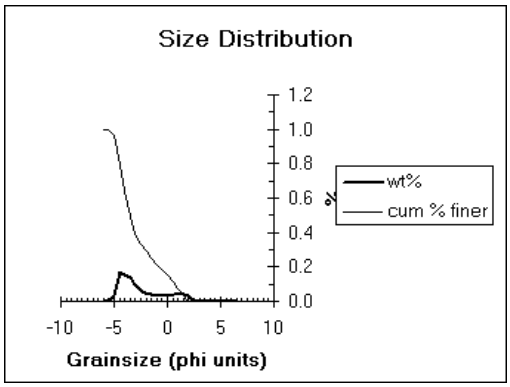

Sample: AG28

	mm	phi	Cum wt (g)	wt (g)	wt%	cum% finer	Modes	
1	64.00	-6	0.00	0.00	0.000	100.00		
2	45.25	-5.5	0.00	0.00	0.000	100.00		
3	32.00	-5	0.00	0.00	0.000	100.00		
4	22.63	-4.5	77.48	77.48	0.193	80.68	mode at	-4.8
5	16.00	-4	152.50	75.02	0.187	61.97		
6	11.31	-3.5	180.90	28.40	0.071	54.88		
7	8.00	-3	188.64	7.74	0.019	52.95		
8	5.66	-2.5	195.74	7.10	0.018	51.18		
9	4.00	-2	202.05	6.31	0.016	49.61		
10	2.83	-1.5	208.76	6.71	0.017	47.93		
11	2.00	-1	216.64	7.88	0.020	45.97		
12	1.41	-0.5	224.78	8.14	0.020	43.94		
13	1.00	0	234.89	10.11	0.025	41.42		
14	0.71	0.5	249.17	14.28	0.036	37.86		
15	0.50	1	269.85	20.68	0.052	32.70		
16	0.35	1.5	296.70	26.85	0.067	26.00	mode at	1.25
17	0.25	2	322.95	26.25	0.065	19.45		
18	0.18	2.5	341.54	18.59	0.046	14.82		
19	0.13	3	367.25	25.71	0.064	8.41	mode at	2.75
20	0.09	3.5	385.13	17.88	0.045	3.95		
21	0.06	4	400.95	15.82	0.039	0.00		
22	0.04	4.5	400.95	0.00	0.000	0.00		
23	0.03	5	400.95	0.00	0.000	0.00		
24	0.02	5.5	400.95	0.00	0.000	0.00		
25	0.02	6	400.95	0.00	0.000	0.00		
26	0.01	6.5	400.95	0.00	0.000	0.00		
27	0.01	7	400.95		0.000	0.00		
28	0.01	7.5	400.95		0.000	0.00		
29	0.00	8	400.95		0.000	0.00		
30	0.00	8.5	400.95		0.000	0.00		
		Sums:	400.95	400.95	1.000			

Percentiles

	phi	*mm*
95%	-4.87	29.255
84%	-4.59	24.017
75%	-4.35	20.369
50%	-2.12	4.361
25%	1.58	0.335
16%	2.37	0.193
5%	3.38	0.096

Folks' Graphic Stats

	phi	*mm*
Mean (Mz)	-1.45	2.725
Sorting (SI)	2.99	
Skewness (SkI)	0.31	
Kurtosis (KG)	0.57	

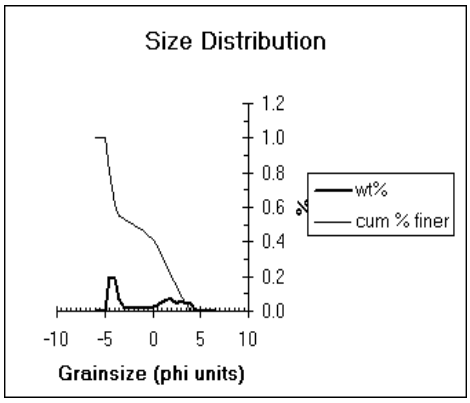

Sample: AG30

	mm	phi	Cum wt (g)	wt (g)	wt%	cum% finer	Modes	
1	64.00	-6	0.00	0.00	0.000	100.00		
2	45.25	-5.5	0.00	0.00	0.000	100.00		
3	32.00	-5	0.00	0.00	0.000	100.00		
4	22.63	-4.5	0.00	0.00	0.000	100.00		
5	16.00	-4	0.00	0.00	0.000	100.00		
6	11.31	-3.5	1.65	1.65	0.004	99.60		
7	8.00	-3	4.73	3.08	0.007	98.87		
8	5.66	-2.5	16.85	12.12	0.029	95.96		
9	4.00	-2	41.91	25.06	0.060	89.95		
10	2.83	-1.5	77.59	35.68	0.086	81.40		
11	2.00	-1	129.47	51.88	0.124	68.96		
12	1.41	-0.5	191.34	61.87	0.148	54.13		
13	1.00	0	254.68	63.34	0.152	38.94	mode at	-0.3
14	0.71	0.5	312.80	58.12	0.139	25.01		
15	0.50	1	349.67	36.87	0.088	16.17		
16	0.35	1.5	369.98	20.31	0.049	11.30		
17	0.25	2	385.99	16.01	0.038	7.46		
18	0.18	2.5	401.31	15.32	0.037	3.79		
19	0.13	3	417.11	15.80	0.038	0.00	mode at	2.75
20	0.09	3.5	417.11	0.00	0.000	0.00		
21	0.06	4	417.11	0.00	0.000	0.00		
22	0.04	4.5	417.11	0.00	0.000	0.00		
23	0.03	5	417.11	0.00	0.000	0.00		
24	0.02	5.5	417.11	0.00	0.000	0.00		
25	0.02	6	417.11	0.00	0.000	0.00		
26	0.01	6.5	417.11	0.00	0.000	0.00		
27	0.01	7	417.11		0.000	0.00		
28	0.01	7.5	417.11		0.000	0.00		
29	0.00	8	417.11		0.000	0.00		
30	0.00	8.5	417.11		0.000	0.00		
		Sums:	417.11	417.11	1.000			

Percentiles

	phi	*mm*
95%	-2.42	5.352
84%	-1.65	3.143
75%	-1.24	2.367
50%	-0.36	1.287
25%	0.50	0.707
16%	1.02	0.494
5%	2.34	0.198

Folks' Graphic Stats

	phi	*mm*
Mean (Mz)	-0.33	1.260
Sorting (SI)	1.39	
Skewness (SkI)	0.09	
Kurtosis (KG)	1.12	

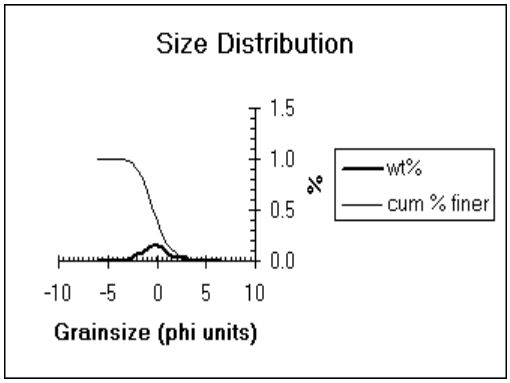

Sample: AG31

	mm	phi	Cum wt (g)	wt (g)	wt%	cum% finer	Modes	
1	64.00	-6	0.00	0.00	0.000	100.00		
2	45.25	-5.5	0.00	0.00	0.000	100.00		
3	32.00	-5	0.00	0.00	0.000	100.00		
4	22.62	-4.5	0.00	0.00	0.000	100.00		
5	16.00	-4	0.00	0.00	0.000	100.00		
6	11.31	-3.5	0.00	0.00	0.000	100.00		
7	8.00	-3	0.00	0.00	0.000	100.00		
8	5.65	-2.5	0.00	0.00	0.000	100.00		
9	4.00	-2	0.48	0.48	0.001	99.90		
10	2.82	-1.5	3.03	2.55	0.005	99.35		
11	2.00	-1	16.55	13.52	0.029	96.48		
12	1.41	-0.5	40.68	24.13	0.051	91.34		
13	1.00	0	87.48	46.80	0.100	81.37		
14	0.70	0.5	170.21	82.73	0.176	63.76		
15	0.50	1	309.42	139.21	0.296	34.11	mode at	0.75
16	0.35	1.5	415.06	105.64	0.225	11.62		
17	0.25	2	448.02	32.96	0.070	4.60		
18	0.17	2.5	459.06	11.04	0.024	2.25		
19	0.12	3	469.63	10.57	0.023	0.00		
20	0.08	3.5	469.63	0.00	0.000	0.00		
21	0.06	4	469.63	0.00	0.000	0.00		
22	0.04	4.5	469.63	0.00	0.000	0.00		
23	0.03	5	469.63	0.00	0.000	0.00		
24	0.02	5.5	469.63	0.00	0.000	0.00		
25	0.01	6	469.63	0.00	0.000	0.00		
26	0.01	6.5	469.63	0.00	0.000	0.00		
27	0.00	7	469.63		0.000	0.00		
28	0.00	7.5	469.63		0.000	0.00		
29	0.00	8	469.63		0.000	0.00		
30	0.00	8.5	469.63		0.000	0.00		
		Sums:	469.63	469.63	1.000			

Percentiles

	phi	*mm*
95%	-0.86	1.810
84%	-0.13	1.096
75%	0.18	0.882
50%	0.73	0.602
25%	1.20	0.434
16%	1.40	0.378
5%	1.97	0.255

Folks' Graphic Stats

	phi	*mm*
Mean (Mz)	0.67	0.630
Sorting (SI)	0.81	
Skewness (SkI)	-0.12	
Kurtosis (KG)	1.13	

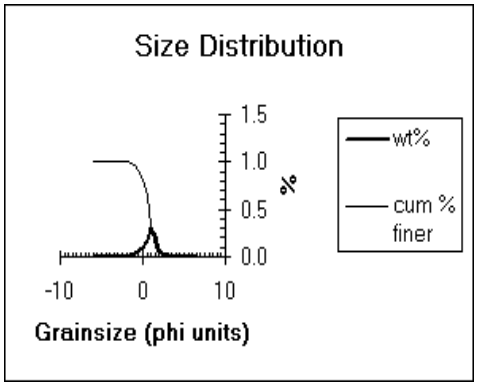

Sample: AG32

	mm	phi	Cum wt (g)	wt (g)	wt%	cum % finer	Modes	
1	64.00	-6	0.00	0.00	0.000	100.00		
2	45.25	-5.5	0.00	0.00	0.000	100.00		
3	32.00	-5	0.00	0.00	0.000	100.00		
4	22.63	-4.5	0.00	0.00	0.000	100.00		
5	16.00	-4	0.00	0.00	0.000	100.00		
6	11.31	-3.5	0.00	0.00	0.000	100.00		
7	8.00	-3	1.01	1.01	0.001	99.87		
8	5.66	-2.5	5.61	4.60	0.006	99.29		
9	4.00	-2	18.43	12.82	0.016	97.66		
10	2.83	-1.5	46.65	28.22	0.036	94.09		
11	2.00	-1	98.33	51.68	0.066	87.54		
12	1.41	-0.5	189.68	91.35	0.116	75.96		
13	1.00	0	316.72	127.04	0.161	59.86		
14	0.71	0.5	489.44	172.72	0.219	37.97		
15	0.50	1	680.41	190.97	0.242	13.76	mode at	0.8
16	0.35	1.5	768.79	88.38	0.112	2.56		
17	0.25	2	788.99	20.20	0.026	0.00		
18	0.18	2.5	788.99	0.00	0.000	0.00		
19	0.13	3	788.99	0.00	0.000	0.00		
20	0.09	3.5	788.99	0.00	0.000	0.00		
21	0.06	4	788.99	0.00	0.000	0.00		
22	0.04	4.5	788.99	0.00	0.000	0.00		
23	0.03	5	788.99	0.00	0.000	0.00		
24	0.02	5.5	788.99	0.00	0.000	0.00		
25	0.02	6	788.99	0.00	0.000	0.00		
26	0.01	6.5	788.99	0.00	0.000	0.00		
27	0.01	7	788.99		0.000	0.00		
28	0.01	7.5	788.99		0.000	0.00		
29	0.00	8	788.99		0.000	0.00		
30	0.00	8.5	788.99		0.000	0.00		
		Sums:	788.99	788.99	1.000			

Percentiles

	phi	*mm*
95%	-1.63	3.090
84%	-0.85	1.799
75%	-0.47	1.385
50%	0.23	0.856
25%	0.77	0.587
16%	0.95	0.516
5%	1.39	0.381

Folks' Graphic Stats

	phi	*mm*
Mean (Mz)	0.11	0.926
Sorting (SI)	0.91	
Skewness (SkI)	-0.21	
Kurtosis (KG)	1.00	

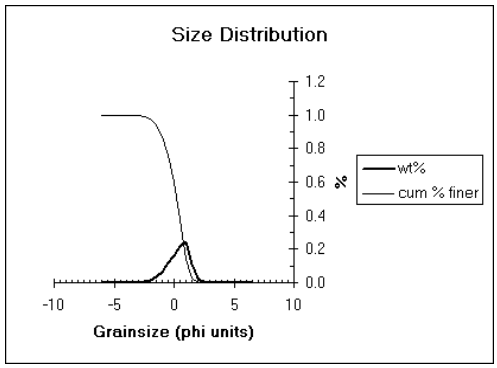

Sample: AG33

	mm	phi	Cum wt (g)	wt (g)	wt%	cum% finer	Modes	
1	64.00	-6	0.00	0.00	0.000	100.00		
2	45.25	-5.5	0.00	0.00	0.000	100.00		
3	32.00	-5	0.00	0.00	0.000	100.00		
4	22.62	-4.5	0.00	0.00	0.000	100.00		
5	16.00	-4	0.00	0.00	0.000	100.00		
6	11.31	-3.5	0.00	0.00	0.000	100.00		
7	8.00	-3	0.78	0.78	0.001	99.90		
8	5.65	-2.5	9.00	8.22	0.011	98.81		
9	4.00	-2	32.58	23.58	0.031	95.70		
10	2.82	-1.5	70.26	37.68	0.050	90.72		
11	2.00	-1	142.57	72.31	0.095	81.18		
12	1.41	-0.5	238.71	96.14	0.127	68.49		
13	1.00	0	351.78	113.07	0.149	53.56		
14	0.70	0.5	502.33	150.55	0.199	33.68		
15	0.50	1	673.56	171.23	0.226	11.08	mode at	0.75
16	0.35	1.5	748.72	75.16	0.099	1.16		
17	0.25	2	757.48	8.76	0.012	0.00		
18	0.17	2.5	757.48	0.00	0.000	0.00		
19	0.12	3	757.48	0.00	0.000	0.00		
20	0.08	3.5	757.48	0.00	0.000	0.00		
21	0.06	4	757.48	0.00	0.000	0.00		
22	0.04	4.5	757.48	0.00	0.000	0.00		
23	0.03	5	757.48	0.00	0.000	0.00		
24	0.02	5.5	757.48	0.00	0.000	0.00		
25	0.01	6	757.48	0.00	0.000	0.00		
26	0.01	6.5	757.48	0.00	0.000	0.00		
27	0.00	7	757.48		0.000	0.00		
28	0.00	7.5	757.48		0.000	0.00		
29	0.00	8	757.48		0.000	0.00		
30	0.00	8.5	757.48		0.000	0.00		
		Sums:	757.48	757.48	1.000			

Percentiles

	phi	*mm*
95%	-1.93	3.810
84%	-1.15	2.216
75%	-0.76	1.690
50%	0.09	0.940
25%	0.69	0.619
16%	0.89	0.539
5%	1.31	0.404

Folks' Graphic Stats

	phi	*mm*
Mean (Mz)	-0.06	1.039
Sorting (SI)	1.00	
Skewness (SkI)	-0.23	
Kurtosis (KG)	0.92	

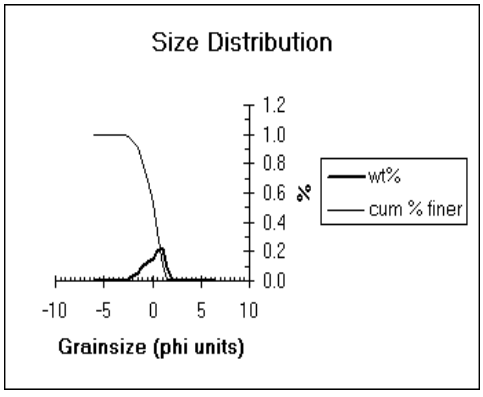

Sample: AG34

	mm	phi	Cum wt (g)	wt (g)	wt%	cum% finer	Modes	
1	64.00	-6	0.00	0.00	0.000	100.00		
2	45.25	-5.5	0.00	0.00	0.000	100.00		
3	32.00	-5	0.00	0.00	0.000	100.00		
4	22.62	-4.5	0.00	0.00	0.000	100.00		
5	16.00	-4	6.88	6.88	0.022	97.79		
6	11.31	-3.5	19.26	12.38	0.040	93.82		
7	8.00	-3	39.91	20.65	0.066	87.20	mode at	-3.3
8	5.65	-2.5	55.41	15.50	0.050	82.23		
9	4.00	-2	63.87	8.46	0.027	79.52		
10	2.82	-1.5	70.23	6.36	0.020	77.48		
11	2.00	-1	74.56	4.33	0.014	76.09		
12	1.41	-0.5	79.07	4.51	0.014	74.64	mode at	-0.8
13	1.00	0	83.03	3.96	0.013	73.37		
14	0.70	0.5	88.02	4.99	0.016	71.77		
15	0.50	1	94.05	6.03	0.019	69.84		
16	0.35	1.5	101.35	7.30	0.023	67.50		
17	0.25	2	121.56	20.21	0.065	61.01		
18	0.17	2.5	172.10	50.54	0.162	44.80		
19	0.12	3	248.13	76.03	0.244	20.42	mode at	2.75
20	0.08	3.5	290.14	42.01	0.135	6.95		
21	0.06	4	311.80	21.66	0.069	0.00		
22	0.04	4.5	311.80	0.00	0.000	0.00		
23	0.03	5	311.80	0.00	0.000	0.00		
24	0.02	5.5	311.80	0.00	0.000	0.00		
25	0.01	6	311.80	0.00	0.000	0.00		
26	0.01	6.5	311.80	0.00	0.000	0.00		
27	0.00	7	311.80		0.000	0.00		
28	0.00	7.5	311.80		0.000	0.00		
29	0.00	8	311.80		0.000	0.00		
30	0.00	8.5	311.80		0.000	0.00		
		Sums:	311.8	311.8	1.000			

Percentiles

	phi	*mm*
95%	-3.65	12.538
84%	-2.68	6.400
75%	-0.62	1.541
50%	2.34	0.198
25%	2.91	0.133
16%	3.16	0.112
5%	3.64	0.080

Folks' Graphic Stats

	phi	*mm*
Mean (Mz)	0.94	0.521
Sorting (SI)	2.56	
Skewness (SkI)	-0.68	
Kurtosis (KG)	0.85	

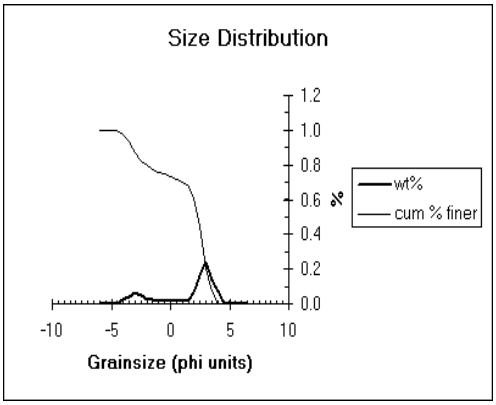

Sample: AG35 :

	mm	phi	Cum wt (g)	wt (g)	wt%	cum% finer	Modes	
1	64.00	-6	0.00	0.00	0.000	100.00		
2	45.25	-5.5	0.00	0.00	0.000	100.00		
3	32.00	-5	0.00	0.00	0.000	100.00		
4	22.63	-4.5	5.07	5.07	0.006	99.40		
5	16.00	-4	28.78	23.71	0.028	96.59		
6	11.31	-3.5	66.66	37.88	0.045	92.09		
7	8.00	-3	130.63	63.97	0.076	84.50		
8	5.66	-2.5	205.19	74.56	0.088	75.66		
9	4.00	-2	296.14	90.95	0.108	64.87		
10	2.83	-1.5	391.39	95.25	0.113	53.57		
11	2.00	-1	491.49	100.10	0.119	41.69	mode at	-1.3
12	1.41	-0.5	572.15	80.66	0.096	32.13		
13	1.00	0	673.05	100.90	0.120	20.16	mode at	-0.3
14	0.71	0.5	762.31	89.26	0.106	9.57		
15	0.50	1	817.32	55.01	0.065	3.04		
16	0.35	1.5	834.71	17.39	0.021	0.98		
17	0.25	2	842.95	8.24	0.010	0.00		
18	0.18	2.5	842.95	0.00	0.000	0.00		
19	0.13	3	842.95	0.00	0.000	0.00		
20	0.09	3.5	842.95	0.00	0.000	0.00		
21	0.06	4	842.95	0.00	0.000	0.00		
22	0.04	4.5	842.95	0.00	0.000	0.00		
23	0.03	5	842.95	0.00	0.000	0.00		
24	0.02	5.5	842.95	0.00	0.000	0.00		
25	0.02	6	842.95	0.00	0.000	0.00		
26	0.01	6.5	842.95	0.00	0.000	0.00		
27	0.01	7	842.95		0.000	0.00		
28	0.01	7.5	842.95		0.000	0.00		
29	0.00	8	842.95		0.000	0.00		
30	0.00	8.5	842.95		0.000	0.00		
		Sums:	842.95	842.95	1.000			

Percentiles

	phi	*mm*
95%	-3.82	14.158
84%	-2.97	7.844
75%	-2.47	5.539
50%	-1.35	2.549
25%	-0.20	1.151
16%	0.20	0.873
5%	0.85	0.555

Folks' Graphic Stats

	phi	*mm*
Mean (Mz)	-1.38	2.594
Sorting (SI)	1.50	
Skewness (SkI)	-0.04	
Kurtosis (KG)	0.84	

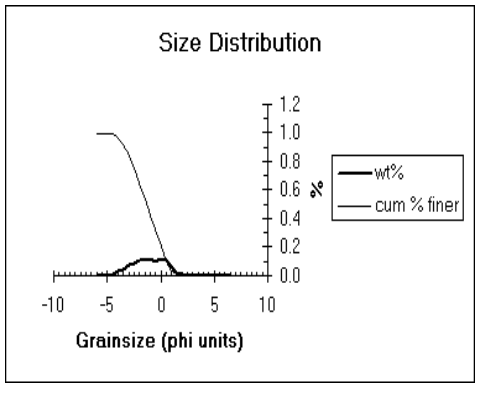

Sample: AG36

	mm	phi	Cum wt (g)	wt (g)	wt%	cum% finer	Modes	
1	64.00	-6	0.00	0.00	0.000	100.00		
2	45.25	-5.5	0.00	0.00	0.000	100.00		
3	32.00	-5	0.00	0.00	0.000	100.00		
4	22.63	-4.5	7.05	7.05	0.009	99.14		
5	16.00	-4	46.29	39.24	0.048	94.35		
6	11.31	-3.5	114.49	68.20	0.083	86.03		
7	8.00	-3	240.07	125.58	0.153	70.71	mode at	-3.3
8	5.66	-2.5	351.99	111.92	0.137	57.06		
9	4.00	-2	442.49	90.50	0.110	46.02		
10	2.83	-1.5	521.57	79.08	0.096	36.37		
11	2.00	-1	591.37	69.80	0.085	27.85		
12	1.41	-0.5	649.92	58.55	0.071	20.71		
13	1.00	0	702.42	52.50	0.064	14.31		
14	0.71	0.5	749.09	46.67	0.057	8.61		
15	0.50	1	789.14	40.05	0.049	3.73		
16	0.35	1.5	809.06	19.92	0.024	1.30		
17	0.25	2	819.68	10.62	0.013	0.00		
18	0.18	2.5	819.68	0.00	0.000	0.00		
19	0.13	3	819.68	0.00	0.000	0.00		
20	0.09	3.5	819.68	0.00	0.000	0.00		
21	0.06	4	819.68	0.00	0.000	0.00		
22	0.04	4.5	819.68	0.00	0.000	0.00		
23	0.03	5	819.68	0.00	0.000	0.00		
24	0.02	5.5	819.68	0.00	0.000	0.00		
25	0.02	6	819.68	0.00	0.000	0.00		
26	0.01	6.5	819.68	0.00	0.000	0.00		
27	0.01	7	819.68		0.000	0.00		
28	0.01	7.5	819.68		0.000	0.00		
29	0.00	8	819.68		0.000	0.00		
30	0.00	8.5	819.68		0.000	0.00		
		Sums:	819.68	819.68	1.000			

Percentiles

	phi	*mm*
95%	-4.07	16.768
84%	-3.43	10.805
75%	-3.14	8.815
50%	-2.18	4.533
25%	-0.80	1.741
16%	-0.13	1.096
5%	0.87	0.547

Folks' Graphic Stats

	phi	*mm*
Mean (Mz)	-1.92	3.772
Sorting (SI)	1.57	
Skewness (SkI)	0.24	
Kurtosis (KG)	0.86	

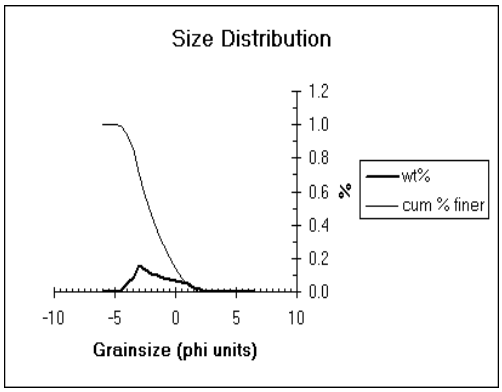

Sample: AG37

	mm	phi	Cum wt (g)	wt (g)	wt%	cum% finer	Modes	
1	64.00	-6	0.00	0.00	0.000	100.00		
2	45.25	-5.5	0.00	0.00	0.000	100.00		
3	32.00	-5	0.00	0.00	0.000	100.00		
4	22.63	-4.5	0.00	0.00	0.000	100.00		
5	16.00	-4	0.00	0.00	0.000	100.00		
6	11.31	-3.5	0.00	0.00	0.000	100.00		
7	8.00	-3	1.57	1.57	0.006	99.44		
8	5.66	-2.5	4.95	3.38	0.012	98.23		
9	4.00	-2	10.80	5.85	0.021	96.14	mode at	-2.3
10	2.83	-1.5	14.88	4.08	0.015	94.68		
11	2.00	-1	25.92	11.04	0.039	90.73		
12	1.41	-0.5	51.93	26.01	0.093	81.43		
13	1.00	0	85.38	33.45	0.120	69.46		
14	0.71	0.5	126.38	41.00	0.147	54.80	mode at	0.25
15	0.50	1	165.20	38.82	0.139	40.91		
16	0.35	1.5	189.33	24.13	0.086	32.28		
17	0.25	2	208.73	19.40	0.069	25.34		
18	0.18	2.5	222.91	14.18	0.051	20.27		
19	0.13	3	245.02	22.11	0.079	12.36	mode at	2.75
20	0.09	3.5	263.85	18.83	0.067	5.63		
21	0.06	4	279.59	15.74	0.056	0.00		
22	0.04	4.5	279.59	0.00	0.000	0.00		
23	0.03	5	279.59	0.00	0.000	0.00		
24	0.02	5.5	279.59	0.00	0.000	0.00		
25	0.02	6	279.59	0.00	0.000	0.00		
26	0.01	6.5	279.59	0.00	0.000	0.00		
27	0.01	7	279.59		0.000	0.00		
28	0.01	7.5	279.59		0.000	0.00		
29	0.00	8	279.59		0.000	0.00		
30	0.00	8.5	279.59		0.000	0.00		
		Sums:	279.59	279.59	1.000			

Percentiles

	phi	*mm*
95%	-1.61	3.053
84%	-0.64	1.557
75%	-0.23	1.174
50%	0.67	0.627
25%	2.03	0.244
16%	2.77	0.147
5%	3.56	0.085

Folks' Graphic Stats

	phi	*mm*
Mean (Mz)	0.93	0.523
Sorting (SI)	1.63	
Skewness (SkI)	0.17	
Kurtosis (KG)	0.93	

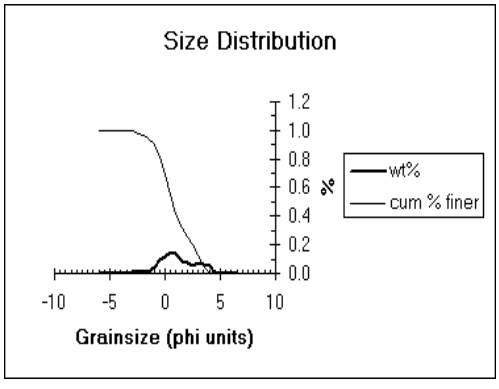

Sample: AG38

	mm	phi	Cum wt (g)	wt (g)	wt%	cum % finer	Modes	
1	64.00	-6	0.00	0.00	0.000	100.00		
2	45.25	-5.5	0.00	0.00	0.000	100.00		
3	32.00	-5	0.00	0.00	0.000	100.00		
4	22.63	-4.5	0.00	0.00	0.000	100.00		
5	16.00	-4	1.89	1.89	0.004	99.61		
6	11.31	-3.5	16.60	14.71	0.031	96.54		
7	8.00	-3	36.40	19.80	0.041	92.41		
8	5.66	-2.5	65.03	28.63	0.060	86.44	mode at	-2.8
9	4.00	-2	91.04	26.01	0.054	81.02		
10	2.83	-1.5	108.19	17.15	0.036	77.45		
11	2.00	-1	133.33	25.14	0.052	72.21		
12	1.41	-0.5	175.80	42.47	0.089	63.36		
13	1.00	0	241.99	66.19	0.138	49.56		
14	0.71	0.5	318.47	76.48	0.159	33.62	mode at	0.3
15	0.50	1	383.14	64.67	0.135	20.14		
16	0.35	1.5	422.13	38.99	0.081	12.01		
17	0.25	2	445.70	23.57	0.049	7.10		
18	0.18	2.5	460.13	14.43	0.030	4.09		
19	0.13	3	479.74	19.61	0.041	0.00	mode at	2.8
20	0.09	3.5	479.74	0.00	0.000	0.00		
21	0.06	4	479.74	0.00	0.000	0.00		
22	0.04	4.5	479.74	0.00	0.000	0.00		
23	0.03	5	479.74	0.00	0.000	0.00		
24	0.02	5.5	479.74	0.00	0.000	0.00		
25	0.02	6	479.74	0.00	0.000	0.00		
26	0.01	6.5	479.74	0.00	0.000	0.00		
27	0.01	7	479.74		0.000	0.00		
28	0.01	7.5	479.74		0.000	0.00		
29	0.00	8	479.74		0.000	0.00		
30	0.00	8.5	479.74		0.000	0.00		
		Sums:	479.74	479.74	1.000			

Percentiles

	phi	*mm*
95%	-3.31	9.941
84%	-2.27	4.838
75%	-1.27	2.406
50%	-0.02	1.011
25%	0.82	0.567
16%	1.25	0.419
5%	2.35	0.196

Folks' Graphic Stats

	phi	*mm*
Mean (Mz)	-0.35	1.270
Sorting (SI)	1.74	
Skewness (SkI)	-0.22	
Kurtosis (KG)	1.11	

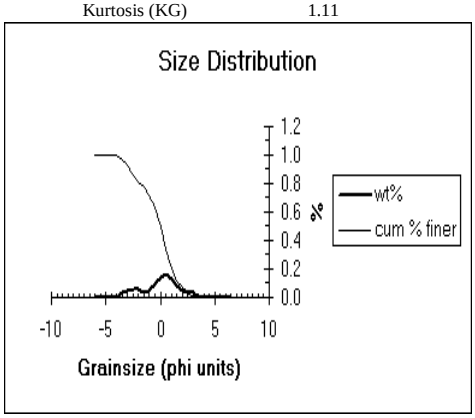

Sample: AG39 :

	mm	phi	Cum wt (g)	wt (g)	wt%	cum% finer	Modes	
1	64.00	-6	0.00	0.00	0.000	100.00		
2	45.25	-5.5	0.00	0.00	0.000	100.00		
3	32.00	-5	0.00	0.00	0.000	100.00		
4	22.63	-4.5	0.00	0.00	0.000	100.00		
5	16.00	-4	0.00	0.00	0.000	100.00		
6	11.31	-3.5	5.12	5.12	0.004	99.64		
7	8.00	-3	36.52	31.40	0.022	97.45		
8	5.66	-2.5	109.53	73.01	0.051	92.36		
9	4.00	-2	215.88	106.35	0.074	84.95		
10	2.83	-1.5	344.23	128.35	0.089	76.00		
11	2.00	-1	495.50	151.27	0.105	65.46		
12	1.41	-0.5	668.24	172.74	0.120	53.41		
13	1.00	0	867.13	198.89	0.139	39.55		
14	0.71	0.5	1106.23	239.10	0.167	22.88	mode at	0.25
15	0.50	1	1330.03	223.80	0.156	7.28		
16	0.35	1.5	1416.23	86.20	0.060	1.27		
17	0.25	2	1434.43	18.20	0.013	0.00		
18	0.18	2.5	1434.43	0.00	0.000	0.00		
19	0.13	3	1434.43	0.00	0.000	0.00		
20	0.09	3.5	1434.43	0.00	0.000	0.00		
21	0.06	4	1434.43	0.00	0.000	0.00		
22	0.04	4.5	1434.43	0.00	0.000	0.00		
23	0.03	5	1434.43	0.00	0.000	0.00		
24	0.02	5.5	1434.43	0.00	0.000	0.00		
25	0.02	6	1434.43	0.00	0.000	0.00		
26	0.01	6.5	1434.43	0.00	0.000	0.00		
27	0.01	7	1434.43		0.000	0.00		
28	0.01	7.5	1434.43		0.000	0.00		
29	0.00	8	1434.43		0.000	0.00		
30	0.00	8.5	1434.43		0.000	0.00		
		Sums:	1434.43	1434.43	1.000			

Percentiles

	phi	*mm*
95%	-2.76	6.769
84%	-1.95	3.855
75%	-1.45	2.737
50%	-0.38	1.299
25%	0.44	0.739
16%	0.72	0.607
5%	1.19	0.438

Folks' Graphic Stats

	phi	*mm*
Mean (Mz)	-0.53	1.448
Sorting (SI)	1.27	
Skewness (SkI)	-0.19	
Kurtosis (KG)	0.86	

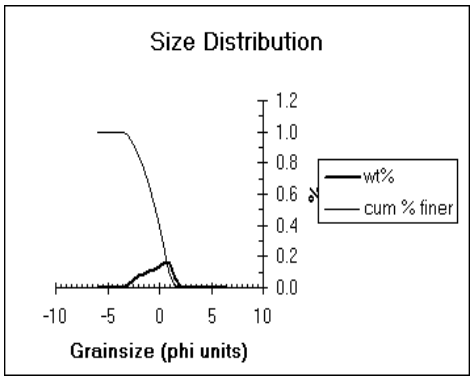

Sample: AG40

	mm	phi	Cum wt (g)	wt (g)	wt%	cum% finer	Modes	
1	64.00	-6	0.00	0.00	0.000	100.00		
2	45.25	-5.5	0.00	0.00	0.000	100.00		
3	32.00	-5	0.00	0.00	0.000	100.00		
4	22.63	-4.5	0.00	0.00	0.000	100.00		
5	16.00	-4	0.00	0.00	0.000	100.00		
6	11.31	-3.5	0.00	0.00	0.000	100.00		
7	8.00	-3	0.00	0.00	0.000	100.00		
8	5.66	-2.5	0.00	0.00	0.000	100.00		
9	4.00	-2	0.00	0.00	0.000	100.00		
10	2.83	-1.5	0.00	0.00	0.000	100.00		
11	2.00	-1	0.00	0.00	0.000	100.00		
12	1.41	-0.5	0.10	0.10	0.000	99.97		
13	1.00	0	0.30	0.20	0.001	99.92		
14	0.71	0.5	0.80	0.50	0.001	99.78		
15	0.50	1	4.10	3.30	0.009	98.85		
16	0.35	1.5	22.60	18.50	0.052	93.68		
17	0.25	2	125.80	103.20	0.288	64.84		
18	0.18	2.5	244.68	118.88	0.332	31.62	mode at	2.25
19	0.13	3	333.80	89.12	0.249	6.71		
20	0.09	3.5	351.71	17.91	0.050	1.70		
21	0.06	4	357.81	6.10	0.017	0.00		
22	0.04	4.5	357.81	0.00	0.000	0.00		
23	0.03	5	357.81	0.00	0.000	0.00		
24	0.02	5.5	357.81	0.00	0.000	0.00		
25	0.02	6	357.81	0.00	0.000	0.00		
26	0.01	6.5	357.81	0.00	0.000	0.00		
27	0.01	7	357.81		0.000	0.00		
28	0.01	7.5	357.81		0.000	0.00		
29	0.00	8	357.81		0.000	0.00		
30	0.00	8.5	357.81		0.000	0.00		
		Sums:	357.81	357.81	1.000			

Percentiles

	phi	*mm*
95%	1.37	0.386
84%	1.67	0.315
75%	1.82	0.282
50%	2.22	0.214
25%	2.63	0.161
16%	2.81	0.142
5%	3.17	0.111

Folks' Graphic Stats

	phi	*mm*
Mean (Mz)	2.23	0.212
Sorting (SI)	0.56	
Skewness (SkI)	0.04	
Kurtosis (KG)	0.91	

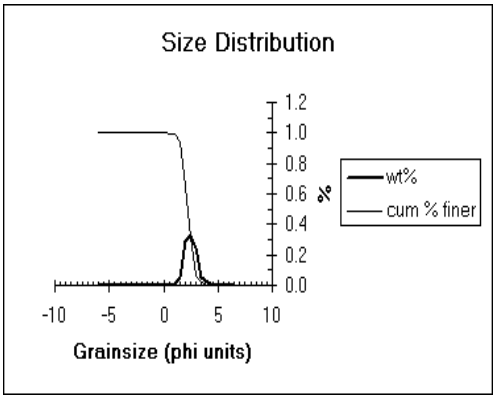

Sample: AG41 :

	mm	phi	Cum wt (g)	wt (g)	wt%	cum% finer	Modes	
1	64.00	-6	0.00	0.00	0.000	100.00		
2	45.25	-5.5	0.00	0.00	0.000	100.00		
3	32.00	-5	0.00	0.00	0.000	100.00		
4	22.63	-4.5	6.65	6.65	0.010	99.02		
5	16.00	-4	26.73	20.08	0.030	96.05		
6	11.31	-3.5	105.80	79.07	0.117	84.37		
7	8.00	-3	195.53	89.73	0.133	71.11	mode at	-3.3
8	5.66	-2.5	271.05	75.52	0.112	59.96		
9	4.00	-2	319.81	48.76	0.072	52.75		
10	2.83	-1.5	373.58	53.77	0.079	44.81		
11	2.00	-1	436.81	63.23	0.093	35.47		
12	1.41	-0.5	507.98	71.17	0.105	24.96		
13	1.00	0	580.55	72.57	0.107	14.24	mode at	-0.3
14	0.71	0.5	634.45	53.90	0.080	6.27		
15	0.50	1	662.46	28.01	0.041	2.13		
16	0.35	1.5	671.50	9.04	0.013	0.80		
17	0.25	2	676.91	5.41	0.008	0.00		
18	0.18	2.5	676.91	0.00	0.000	0.00		
19	0.13	3	676.91	0.00	0.000	0.00		
20	0.09	3.5	676.91	0.00	0.000	0.00		
21	0.06	4	676.91	0.00	0.000	0.00		
22	0.04	4.5	676.91	0.00	0.000	0.00		
23	0.03	5	676.91	0.00	0.000	0.00		
24	0.02	5.5	676.91	0.00	0.000	0.00		
25	0.02	6	676.91	0.00	0.000	0.00		
26	0.01	6.5	676.91	0.00	0.000	0.00		
27	0.01	7	676.91		0.000	0.00		
28	0.01	7.5	676.91		0.000	0.00		
29	0.00	8	676.91		0.000	0.00		
30	0.00	8.5	676.91		0.000	0.00		
		Sums:	676.91	676.91	1.000			

Percentiles

	phi	*mm*
95%	-3.96	15.509
84%	-3.49	11.205
75%	-3.15	8.855
50%	-1.83	3.547
25%	-0.50	1.416
16%	-0.08	1.059
5%	0.65	0.636

Folks' Graphic Stats

	phi	*mm*
Mean (Mz)	-1.80	3.478
Sorting (SI)	1.55	
Skewness (SkI)	0.05	
Kurtosis (KG)	0.71	

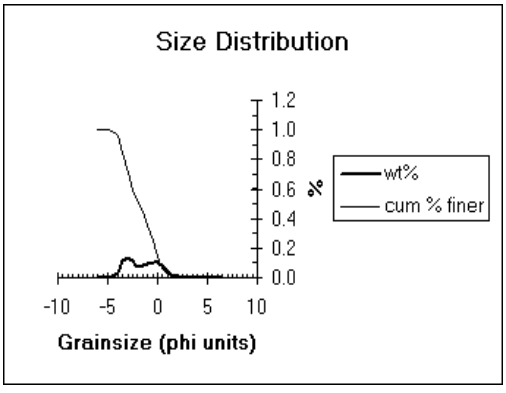

Sample: AG42

	mm	phi	Cum wt (g)	wt (g)	wt%	cum% finer	Modes	
1	64.00	-6	0.00	0.00	0.000	100.00		
2	45.25	-5.5	0.00	0.00	0.000	100.00		
3	32.00	-5	0.00	0.00	0.000	100.00		
4	22.63	-4.5	0.00	0.00	0.000	100.00		
5	16.00	-4	0.00	0.00	0.000	100.00		
6	11.31	-3.5	11.64	11.64	0.010	98.96		
7	8.00	-3	87.06	75.42	0.068	92.19		
8	5.66	-2.5	220.41	133.35	0.120	80.22		
9	4.00	-2	368.63	148.22	0.133	66.91	mode at	-2.3
10	2.83	-1.5	512.08	143.45	0.129	54.04		
11	2.00	-1	662.64	150.56	0.135	40.53		
12	1.41	-0.5	843.05	180.41	0.162	24.33	mode at	-0.8
13	1.00	0	990.68	147.63	0.133	11.08		
14	0.71	0.5	1071.88	81.20	0.073	3.79		
15	0.50	1	1093.40	21.52	0.019	1.86		
16	0.35	1.5	1105.03	11.63	0.010	0.82		
17	0.25	2	1114.16	9.13	0.008	0.00		
18	0.18	2.5	1114.16	0.00	0.000	0.00		
19	0.13	3	1114.16	0.00	0.000	0.00		
20	0.09	3.5	1114.16	0.00	0.000	0.00		
21	0.06	4	1114.16	0.00	0.000	0.00		
22	0.04	4.5	1114.16	0.00	0.000	0.00		
23	0.03	5	1114.16	0.00	0.000	0.00		
24	0.02	5.5	1114.16	0.00	0.000	0.00		
25	0.02	6	1114.16	0.00	0.000	0.00		
26	0.01	6.5	1114.16	0.00	0.000	0.00		
27	0.01	7	1114.16		0.000	0.00		
28	0.01	7.5	1114.16		0.000	0.00		
29	0.00	8	1114.16		0.000	0.00		
30	0.00	8.5	1114.16		0.000	0.00		
		Sums:	1114.16	1114.16	1.000			

Percentiles

	phi	*mm*
95%	-3.21	9.240
84%	-2.66	6.312
75%	-2.30	4.938
50%	-1.35	2.550
25%	-0.52	1.435
16%	-0.19	1.137
5%	0.42	0.749

Folks' Graphic Stats

	phi	*mm*
Mean (Mz)	-1.40	2.635
Sorting (SI)	1.17	
Skewness (SkI)	-0.04	
Kurtosis (KG)	0.83	

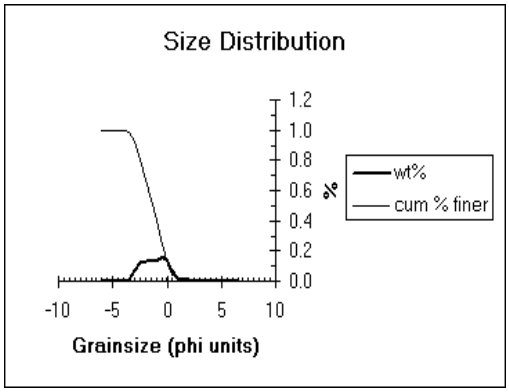

Sample: AG43

	mm	phi	Cum wt (g)	wt (g)	wt%	cum% finer	Modes	
1	64.00	-6	0.00	0.00	0.000	100.00		
2	45.25	-5.5	0.00	0.00	0.000	100.00		
3	32.00	-5	0.00	0.00	0.000	100.00		
4	22.63	-4.5	0.00	0.00	0.000	100.00		
5	16.00	-4	0.00	0.00	0.000	100.00		
6	11.31	-3.5	0.00	0.00	0.000	100.00		
7	8.00	-3	0.00	0.00	0.000	100.00		
8	5.66	-2.5	3.18	3.18	0.005	99.51		
9	4.00	-2	13.73	10.55	0.016	97.87		
10	2.83	-1.5	31.27	17.54	0.027	95.16		
11	2.00	-1	68.55	37.28	0.058	89.38		
12	1.41	-0.5	137.32	68.77	0.107	78.73		
13	1.00	0	238.55	101.23	0.157	63.05		
14	0.71	0.5	341.21	102.66	0.159	47.15	mode at	0.25
15	0.50	1	424.36	83.15	0.129	34.27		
16	0.35	1.5	490.76	66.40	0.103	23.98		
17	0.25	2	534.62	43.86	0.068	17.19		
18	0.18	2.5	565.57	30.95	0.048	12.39		
19	0.13	3	595.31	29.74	0.046	7.79		
20	0.09	3.5	616.54	21.23	0.033	4.50		
21	0.06	4	645.57	29.03	0.045	0.00	mode at	3.75
22	0.04	4.5	645.57	0.00	0.000	0.00		
23	0.03	5	645.57	0.00	0.000	0.00		
24	0.02	5.5	645.57	0.00	0.000	0.00		
25	0.02	6	645.57	0.00	0.000	0.00		
26	0.01	6.5	645.57	0.00	0.000	0.00		
27	0.01	7	645.57		0.000	0.00		
28	0.01	7.5	645.57		0.000	0.00		
29	0.00	8	645.57		0.000	0.00		
30	0.00	8.5	645.57		0.000	0.00		
		Sums:	645.57	645.57	1.000			

Percentiles

	phi	*mm*
95%	-1.49	2.802
84%	-0.75	1.679
75%	-0.38	1.302
50%	0.41	0.752
25%	1.45	0.366
16%	2.12	0.229
5%	3.42	0.093

Folks' Graphic Stats

	phi	*mm*
Mean (Mz)	0.60	0.662
Sorting (SI)	1.46	
Skewness (SkI)	0.21	
Kurtosis (KG)	1.10	

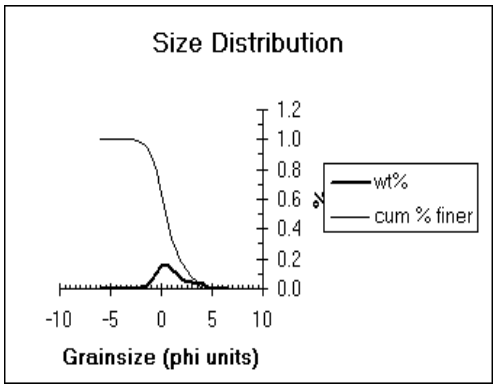

Sample: AG44

	mm	phi	Cum wt (g)	wt (g)	wt%	cum% finer	Modes	
1	64.00	-6	0.00	0.00	0.000	100.00		
2	45.25	-5.5	0.00	0.00	0.000	100.00		
3	32.00	-5	0.00	0.00	0.000	100.00		
4	22.63	-4.5	0.00	0.00	0.000	100.00		
5	16.00	-4	4.58	4.58	0.004	99.65		
6	11.31	-3.5	18.17	13.59	0.010	98.61		
7	8.00	-3	78.90	60.73	0.046	93.97		
8	5.66	-2.5	183.38	104.48	0.080	85.98		
9	4.00	-2	303.70	120.32	0.092	76.78		
10	2.83	-1.5	456.17	152.47	0.117	65.13		
11	2.00	-1	654.83	198.66	0.152	49.94		
12	1.41	-0.5	884.03	229.20	0.175	32.41	mode at	-0.8
13	1.00	0	1110.43	226.40	0.173	15.11		
14	0.71	0.5	1252.44	142.01	0.109	4.25		
15	0.50	1	1299.98	47.54	0.036	0.61		
16	0.35	1.5	1306.96	6.98	0.005	0.08		
17	0.25	2	1308.02	1.06	0.001	0.00		
18	0.18	2.5	1308.02	0.00	0.000	0.00		
19	0.13	3	1308.02	0.00	0.000	0.00		
20	0.09	3.5	1308.02	0.00	0.000	0.00		
21	0.06	4	1308.02	0.00	0.000	0.00		
22	0.04	4.5	1308.02	0.00	0.000	0.00		
23	0.03	5	1308.02	0.00	0.000	0.00		
24	0.02	5.5	1308.02	0.00	0.000	0.00		
25	0.02	6	1308.02	0.00	0.000	0.00		
26	0.01	6.5	1308.02	0.00	0.000	0.00		
27	0.01	7	1308.02		0.000	0.00		
28	0.01	7.5	1308.02		0.000	0.00		
29	0.00	8	1308.02		0.000	0.00		
30	0.00	8.5	1308.02		0.000	0.00		
		Sums:	1308.02	1308.02	1.000			

Percentiles

	phi	*mm*
95%	-3.11	8.641
84%	-2.39	5.250
75%	-1.92	3.794
50%	-1.00	2.003
25%	-0.29	1.219
16%	-0.03	1.018
5%	0.47	0.724

Folks' Graphic Stats

	phi	*mm*
Mean (Mz)	-1.14	2.204
Sorting (SI)	1.13	
Skewness (SkI)	-0.18	
Kurtosis (KG)	0.90	

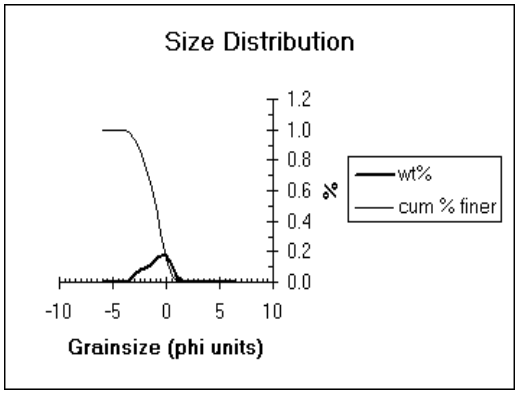

Sample: AG45

	mm	phi	Cum wt (g)	wt (g)	wt%	cum% finer	Modes	
1	64.00	-6	0.00	0.00	0.000	100.00		
2	45.25	-5.5	146.34	146.34	0.202	79.77	mode at	-5.8
3	32.00	-5	184.98	38.64	0.053	74.43		
4	22.63	-4.5	227.75	42.77	0.059	68.52		
5	16.00	-4	304.08	76.33	0.106	57.97	mode at	-4.3
6	11.31	-3.5	356.73	52.65	0.073	50.69		
7	8.00	-3	408.16	51.43	0.071	43.58		
8	5.66	-2.5	453.40	45.24	0.063	37.32		
9	4.00	-2	492.36	38.96	0.054	31.94		
10	2.83	-1.5	518.96	26.60	0.037	28.26		
11	2.00	-1	545.45	26.49	0.037	24.60		
12	1.41	-0.5	568.90	23.45	0.032	21.36		
13	1.00	0	590.04	21.14	0.029	18.44		
14	0.71	0.5	611.46	21.42	0.030	15.47		
15	0.50	1	634.29	22.83	0.032	12.32	mode at	0.75
16	0.35	1.5	655.86	21.57	0.030	9.34		
17	0.25	2	677.14	21.28	0.029	6.39		
18	0.18	2.5	694.26	17.12	0.024	4.03		
19	0.13	3	711.47	17.21	0.024	1.65	mode at	2.75
20	0.09	3.5	719.52	8.05	0.011	0.54		
21	0.06	4	723.40	3.88	0.005	0.00		
22	0.04	4.5	723.40	0.00	0.000	0.00		
23	0.03	5	723.40	0.00	0.000	0.00		
24	0.02	5.5	723.40	0.00	0.000	0.00		
25	0.02	6	723.40	0.00	0.000	0.00		
26	0.01	6.5	723.40	0.00	0.000	0.00		
27	0.01	7	723.40		0.000	0.00		
28	0.01	7.5	723.40		0.000	0.00		
29	0.00	8	723.40		0.000	0.00		
30	0.00	8.5	723.40		0.000	0.00		
		Sums:	723.4	723.4	1.000			

Percentiles

	phi	*mm*
95%	-5.88	58.746
84%	-5.60	48.656
75%	-5.05	33.208
50%	-3.45	10.941
25%	-1.05	2.077
16%	0.41	0.752
5%	2.29	0.204

Folks' Graphic Stats

	phi	*mm*
Mean (Mz)	-2.88	7.370
Sorting (SI)	2.74	
Skewness (SkI)	0.35	
Kurtosis (KG)	0.84	

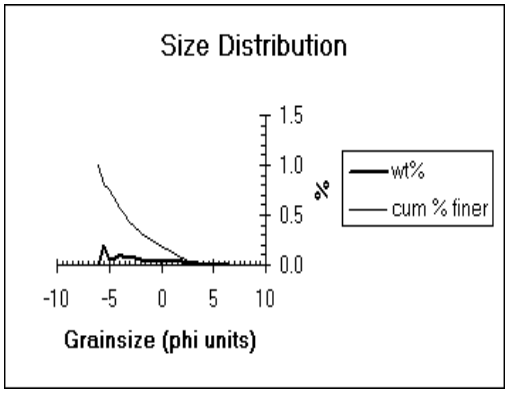

Sample: AG46

	mm	phi	Cum wt (g)	wt (g)	wt%	cum% finer	Modes	
1	181.01	-7.5	0.00	0.00	0.000	100.00		
2	128.00	-7	3051.00	3051.00	0.455	54.52	mode at	-7.3
3	90.50	-6.5	5426.40	2375.40	0.354	19.11		
4	64.00	-6	5426.40	0.00	0.000	19.11		
5	45.25	-5.5	5505.59	79.19	0.012	17.93		
6	32.00	-5	5794.13	288.54	0.043	13.63	mode at	-5.3
7	22.62	-4.5	6056.43	262.30	0.039	9.72		
8	16.00	-4	6266.33	209.90	0.031	6.59		
9	11.31	-3.5	6389.93	123.60	0.018	4.75		
10	8.00	-3	6468.73	78.80	0.012	3.57		
11	5.65	-2.5	6525.03	56.30	0.008	2.74		
12	4.00	-2	6557.73	32.70	0.005	2.25		
13	2.82	-1.5	6578.92	21.19	0.003	1.93		
14	2.00	-1	6595.68	16.76	0.002	1.68		
15	1.41	-0.5	6609.27	13.59	0.002	1.48		
16	1.00	0	6621.10	11.83	0.002	1.30		
17	0.70	0.5	6631.86	10.76	0.002	1.14		
18	0.50	1	6643.60	11.74	0.002	0.97	mode at	0.75
19	0.35	1.5	6654.66	11.06	0.002	0.80		
20	0.25	2	6666.44	11.78	0.002	0.63	mode at	1.75
21	0.17	2.5	6677.46	11.02	0.002	0.46		
22	0.12	3	6691.78	14.32	0.002	0.25		
23	0.08	3.5	6701.47	9.69	0.001	0.10		
24	0.06	4	6708.51	7.04	0.001	0.00		
25	0.04	4.5	6708.51	0.00	0.000	0.00		
26	0.03	5	6708.51	0.00	0.000	0.00		
27	0.02	5.5	6708.51		0.000	0.00		
28	0.01	6	6708.51		0.000	0.00		
29	0.01	6.5	6708.51		0.000	0.00		
30	0.00	7	6708.51		0.000	0.00		
		Sums:	6708.51	6708.51	0.995			

Percentiles

	phi	*mm*
95%	-7.45	174.252
84%	-7.32	160.241
75%	-7.23	149.619
50%	-6.94	122.460
25%	-6.58	95.879
16%	-5.28	38.733
5%	-3.57	11.861

Folks' Graphic Stats

	phi	*mm*
Mean (Mz)	-6.51	91.261
Sorting (SI)	1.10	
Skewness (SkI)	0.68	
Kurtosis (KG)	2.47	

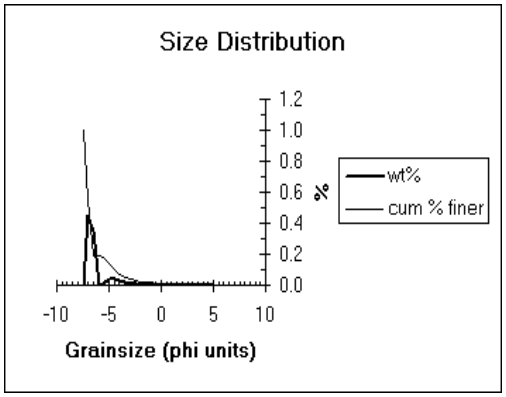

Sample: AG47

	mm	phi	Cum wt (g)	wt (g)	wt%	cum% finer	Modes	
1	64.00	-6	0.00	0.00	0.000	100.00		
2	45.25	-5.5	69.84	69.84	0.109	89.10		
3	32.00	-5	209.29	139.45	0.218	67.34		
4	22.63	-4.5	385.90	176.61	0.276	39.78	mode at	-4.8
5	16.00	-4	439.66	53.76	0.084	31.39		
6	11.31	-3.5	487.17	47.51	0.074	23.97		
7	8.00	-3	505.09	17.92	0.028	21.18		
8	5.66	-2.5	522.73	17.64	0.028	18.43		
9	4.00	-2	538.94	16.21	0.025	15.90		
10	2.83	-1.5	546.31	7.37	0.012	14.75		
11	2.00	-1	555.54	9.23	0.014	13.31		
12	1.41	-0.5	565.71	10.17	0.016	11.72	mode at	-0.8
13	1.00	0	575.85	10.14	0.016	10.14		
14	0.71	0.5	587.50	11.65	0.018	8.32		
15	0.50	1	603.62	16.12	0.025	5.80		
16	0.35	1.5	622.18	18.56	0.029	2.91		
17	0.25	2	640.80	18.62	0.029	0.00	mode at	1.75
18	0.18	2.5	640.80	0.00	0.000	0.00		
19	0.13	3	640.80	0.00	0.000	0.00		
20	0.09	3.5	640.80	0.00	0.000	0.00		
21	0.06	4	640.80	0.00	0.000	0.00		
22	0.04	4.5	640.80	0.00	0.000	0.00		
23	0.03	5	640.80	0.00	0.000	0.00		
24	0.02	5.5	640.80	0.00	0.000	0.00		
25	0.02	6	640.80	0.00	0.000	0.00		
26	0.01	6.5	640.80	0.00	0.000	0.00		
27	0.01	7	640.80		0.000	0.00		
28	0.01	7.5	640.80		0.000	0.00		
29	0.00	8	640.80		0.000	0.00		
30	0.00	8.5	640.80		0.000	0.00		
		Sums:	640.8	640.8	1.000			

Percentiles

	phi	*mm*
95%	-5.77	54.592
84%	-5.38	41.724
75%	-5.18	36.152
50%	-4.69	25.731
25%	-3.57	11.869
16%	-2.02	4.058
5%	1.14	0.454

Folks' Graphic Stats

	phi	*mm*
Mean (Mz)	-4.03	16.332
Sorting (SI)	1.89	
Skewness (SkI)	0.64	
Kurtosis (KG)	1.76	

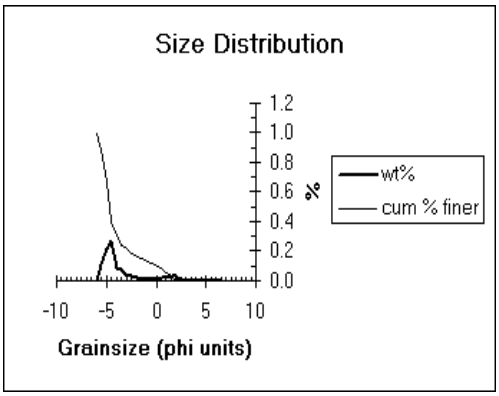

Sample: AG48 :

	mm	phi	Cum wt (g)	wt (g)	wt%	cum% finer	Modes	
1	64.00	-6	218.50	218.50	0.342	65.82		
2	45.25	-5.5	218.50	0.00	0.000	65.82		
3	32.00	-5	234.34	15.84	0.025	63.34		
4	22.63	-4.5	304.07	69.73	0.109	52.43		
5	16.00	-4	395.12	91.05	0.142	38.19	mode at	-4.3
6	11.31	-3.5	450.23	55.11	0.086	29.56		
7	8.00	-3	494.66	44.43	0.070	22.61		
8	5.66	-2.5	527.42	32.76	0.051	17.49		
9	4.00	-2	547.85	20.43	0.032	14.29		
10	2.83	-1.5	560.10	12.25	0.019	12.37		
11	2.00	-1	570.99	10.89	0.017	10.67		
12	1.41	-0.5	580.48	9.49	0.015	9.19		
13	1.00	0	589.67	9.19	0.014	7.75		
14	0.71	0.5	599.21	9.54	0.015	6.26		
15	0.50	1	609.35	10.14	0.016	4.67	mode at	0.8
16	0.35	1.5	618.34	8.99	0.014	3.26		
17	0.25	2	626.56	8.22	0.013	1.98		
18	0.18	2.5	639.20	12.64	0.020	0.00	mode at	2.3
19	0.13	3	639.20	0.00	0.000	0.00		
20	0.09	3.5	639.20	0.00	0.000	0.00		
21	0.06	4	639.20	0.00	0.000	0.00		
22	0.04	4.5	639.20	0.00	0.000	0.00		
23	0.03	5	639.20	0.00	0.000	0.00		
24	0.02	5.5	639.20	0.00	0.000	0.00		
25	0.02	6	639.20	0.00	0.000	0.00		
26	0.01	6.5	639.20	0.00	0.000	0.00		
27	0.01	7	639.20		0.000	0.00		
28	0.01	7.5	639.20		0.000	0.00		
29	0.00	8	639.20		0.000	0.00		
30	0.00	8.5	639.20		0.000	0.00		
		Sums:	639.2	639.2	1.000			

Percentiles

	phi	*mm*
95%	#N/A	#N/A
84%	#N/A	#N/A
75%	#N/A	#N/A
50%	-4.41	21.329
25%	-3.17	9.011
16%	-2.27	4.814
5%	0.90	0.537

Folks' Graphic Stats

	phi	*mm*
Mean (Mz)	#N/A	#N/A
Sorting (SI)	#N/A	
Skewness (SkI)	#N/A	
Kurtosis (KG)	#N/A	

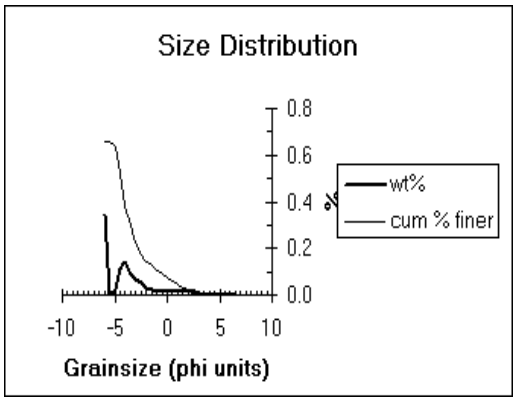

Sample: AG49

	mm	phi	Cum wt (g)	wt (g)	wt%	cum% finer	Modes	
1	64.00	-6	0.00	0.00	0.000	100.00		
2	45.25	-5.5	72.67	72.67	0.092	90.78	mode at	-5.8
3	32.00	-5	125.34	52.67	0.067	84.10		
4	22.63	-4.5	279.74	154.40	0.196	64.51	mode at	-4.8
5	16.00	-4	410.21	130.47	0.166	47.96		
6	11.31	-3.5	473.94	63.73	0.081	39.87		
7	8.00	-3	536.40	62.46	0.079	31.95		
8	5.66	-2.5	587.87	51.47	0.065	25.42		
9	4.00	-2	621.24	33.37	0.042	21.18		
10	2.83	-1.5	642.20	20.96	0.027	18.52		
11	2.00	-1	667.16	24.96	0.032	15.36	mode at	-1.3
12	1.41	-0.5	690.46	23.30	0.030	12.40		
13	1.00	0	713.11	22.65	0.029	9.53		
14	0.71	0.5	735.27	22.16	0.028	6.72		
15	0.50	1	757.37	22.10	0.028	3.91		
16	0.35	1.5	773.71	16.34	0.021	1.84		
17	0.25	2	788.21	14.50	0.018	0.00		
18	0.18	2.5	788.21	0.00	0.000	0.00		
19	0.13	3	788.21	0.00	0.000	0.00		
20	0.09	3.5	788.21	0.00	0.000	0.00		
21	0.06	4	788.21	0.00	0.000	0.00		
22	0.04	4.5	788.21	0.00	0.000	0.00		
23	0.03	5	788.21	0.00	0.000	0.00		
24	0.02	5.5	788.21	0.00	0.000	0.00		
25	0.02	6	788.21	0.00	0.000	0.00		
26	0.01	6.5	788.21	0.00	0.000	0.00		
27	0.01	7	788.21		0.000	0.00		
28	0.01	7.5	788.21		0.000	0.00		
29	0.00	8	788.21		0.000	0.00		
30	0.00	8.5	788.21		0.000	0.00		
		Sums:	788.21	788.21	1.000			

Percentiles

	phi	*mm*
95%	-5.73	53.034
84%	-5.00	31.944
75%	-4.77	27.242
50%	-4.06	16.699
25%	-2.45	5.467
16%	-1.10	2.146
5%	0.81	0.572

Folks' Graphic Stats

	phi	*mm*
Mean (Mz)	-3.39	10.461
Sorting (SI)	1.96	
Skewness (SkI)	0.50	
Kurtosis (KG)	1.16	

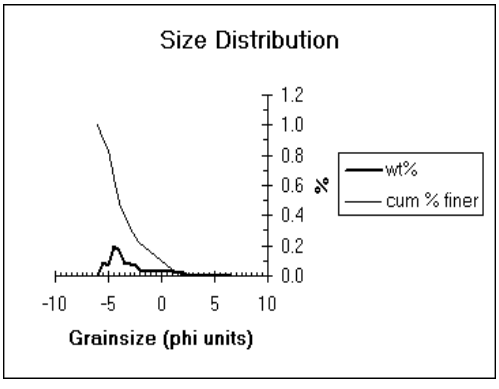

Sample: AG50

	mm	phi	Cum wt (g)	wt (g)	wt%	cum% finer	Modes	
1	64.00	-6	0.00	0.00	0.000	100.00		
2	45.25	-5.5	0.00	0.00	0.000	100.00		
3	32.00	-5	0.00	0.00	0.000	100.00		
4	22.63	-4.5	30.11	30.11	0.106	89.35		
5	16.00	-4	60.22	30.11	0.106	78.70	mode at	-4.3
6	11.31	-3.5	64.39	4.17	0.015	77.23		
7	8.00	-3	74.80	10.41	0.037	73.55		
8	5.66	-2.5	129.81	55.01	0.195	54.09	mode at	-2.8
9	4.00	-2	174.95	45.14	0.160	38.13		
10	2.83	-1.5	196.22	21.27	0.075	30.61		
11	2.00	-1	218.47	22.25	0.079	22.74	mode at	-1.3
12	1.41	-0.5	234.79	16.32	0.058	16.96		
13	1.00	0	246.98	12.19	0.043	12.65		
14	0.71	0.5	257.26	10.28	0.036	9.02		
15	0.50	1	267.38	10.12	0.036	5.44		
16	0.35	1.5	275.65	8.27	0.029	2.51		
17	0.25	2	282.76	7.11	0.025	0.00		
18	0.18	2.5	282.76	0.00	0.000	0.00		
19	0.13	3	282.76	0.00	0.000	0.00		
20	0.09	3.5	282.76	0.00	0.000	0.00		
21	0.06	4	282.76	0.00	0.000	0.00		
22	0.04	4.5	282.76	0.00	0.000	0.00		
23	0.03	5	282.76	0.00	0.000	0.00		
24	0.02	5.5	282.76	0.00	0.000	0.00		
25	0.02	6	282.76	0.00	0.000	0.00		
26	0.01	6.5	282.76	0.00	0.000	0.00		
27	0.01	7	282.76		0.000	0.00		
28	0.01	7.5	282.76		0.000	0.00		
29	0.00	8	282.76		0.000	0.00		
30	0.00	8.5	282.76		0.000	0.00		
		Sums:	282.76	282.76	1.000			

Percentiles

	phi	*mm*
95%	-4.77	27.194
84%	-4.25	19.011
75%	-3.20	9.173
50%	-2.37	5.176
25%	-1.14	2.210
16%	-0.39	1.309
5%	1.08	0.475

Folks' Graphic Stats

	phi	*mm*
Mean (Mz)	-2.34	5.050
Sorting (SI)	1.85	
Skewness (SkI)	0.10	
Kurtosis (KG)	1.17	

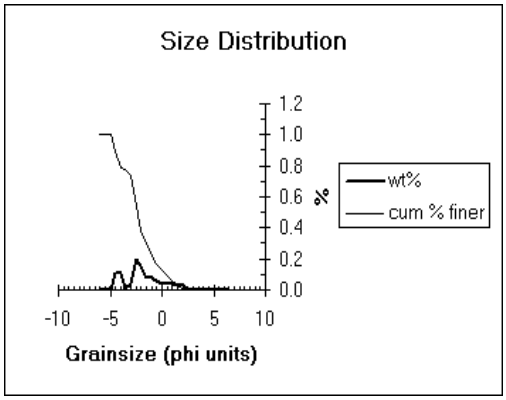

Sample: AG52

	mm	phi	Cum wt (g)	wt (g)	wt%	cum% finer	Modes	
1	181.02	-7.5	0.00	0.00	0.000	100.00		
2	128.00	-7	426.85	426.85	0.248	75.17	mode at	-7.3
3	90.51	-6.5	426.85	0.00	0.000	75.17		
4	64.00	-6	490.78	63.93	0.037	71.46	mode at	-6.3
5	45.25	-5.5	520.90	30.12	0.018	69.70		
6	32.00	-5	748.64	227.74	0.132	56.46		
7	22.63	-4.5	1059.74	311.10	0.181	38.36	mode at	-4.8
8	16.00	-4	1178.24	118.50	0.069	31.47		
9	11.31	-3.5	1270.24	92.00	0.054	26.12		
10	8.00	-3	1375.94	105.70	0.061	19.97	mode at	-3.3
11	5.66	-2.5	1441.79	65.85	0.038	16.14		
12	4.00	-2	1486.89	45.10	0.026	13.52		
13	2.83	-1.5	1519.82	32.93	0.019	11.60		
14	2.00	-1	1547.14	27.32	0.016	10.02		
15	1.41	-0.5	1570.88	23.74	0.014	8.64		
16	1.00	0	1591.01	20.13	0.012	7.46		
17	0.71	0.5	1611.33	20.32	0.012	6.28		
18	0.50	1	1634.49	23.16	0.013	4.94	mode at	0.75
19	0.35	1.5	1656.62	22.13	0.013	3.65		
20	0.25	2	1674.02	17.40	0.010	2.64		
21	0.18	2.5	1686.66	12.64	0.007	1.90		
22	0.13	3	1700.46	13.80	0.008	1.10		
23	0.09	3.5	1710.29	9.83	0.006	0.53		
24	0.06	4	1719.35	9.06	0.005	0.00		
25	0.04	4.5	1719.35	0.00	0.000	0.00		
26	0.03	5	1719.35	0.00	0.000	0.00		
27	0.02	5.5	1719.35		0.000	0.00		
28	0.02	6	1719.35		0.000	0.00		
29	0.01	6.5	1719.35		0.000	0.00		
30	0.01	7	1719.35		0.000	0.00		
		Sums:	1719.35	1719.35	0.981			

Percentiles

	phi	*mm*
95%	-7.40	168.815
84%	-7.18	144.784
75%	-6.48	89.056
50%	-4.82	28.277
25%	-3.41	10.621
16%	-2.47	5.551
5%	0.98	0.508

Folks' Graphic Stats

	phi	*mm*
Mean (Mz)	-4.82	28.325
Sorting (SI)	2.45	
Skewness (SkI)	0.19	
Kurtosis (KG)	1.12	

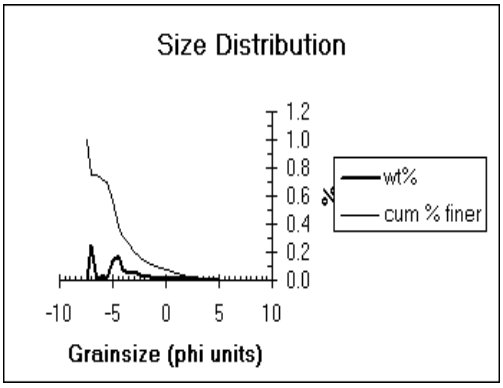

Sample: AG53

	mm	phi	Cum wt (g)	wt (g)	wt%	cum% finer	Modes	
1	64.00	-6	0.00	0.00	0.000	100.00		
2	45.25	-5.5	0.00	0.00	0.000	100.00		
3	32.00	-5	197.14	197.14	0.218	78.22	mode at	-5.3
4	22.63	-4.5	291.25	94.11	0.104	67.82		
5	16.00	-4	443.33	152.08	0.168	51.01	mode at	-4.3
6	11.31	-3.5	503.13	59.80	0.066	44.41		
7	8.00	-3	555.36	52.23	0.058	38.63		
8	5.66	-2.5	599.69	44.33	0.049	33.74		
9	4.00	-2	640.52	40.83	0.045	29.22		
10	2.83	-1.5	678.07	37.55	0.041	25.08		
11	2.00	-1	715.47	37.40	0.041	20.94		
12	1.41	-0.5	751.89	36.42	0.040	16.92		
13	1.00	0	783.94	32.05	0.035	13.38		
14	0.71	0.5	818.42	34.48	0.038	9.57		
15	0.50	1	854.13	35.71	0.039	5.62	mode at	0.75
16	0.35	1.5	882.89	28.76	0.032	2.44		
17	0.25	2	905.00	22.11	0.024	0.00		
18	0.18	2.5	905.00	0.00	0.000	0.00		
19	0.13	3	905.00	0.00	0.000	0.00		
20	0.09	3.5	905.00	0.00	0.000	0.00		
21	0.06	4	905.00	0.00	0.000	0.00		
22	0.04	4.5	905.00	0.00	0.000	0.00		
23	0.03	5	905.00	0.00	0.000	0.00		
24	0.02	5.5	905.00	0.00	0.000	0.00		
25	0.02	6	905.00	0.00	0.000	0.00		
26	0.01	6.5	905.00	0.00	0.000	0.00		
27	0.01	7	905.00		0.000	0.00		
28	0.01	7.5	905.00		0.000	0.00		
29	0.00	8	905.00		0.000	0.00		
30	0.00	8.5	905.00		0.000	0.00		
		Sums:	905	905	1.000			

Percentiles

	phi	*mm*
95%	-5.39	41.794
84%	-5.13	35.084
75%	-4.85	28.747
50%	-3.92	15.172
25%	-1.49	2.811
16%	-0.37	1.293
5%	1.10	0.467

Folks' Graphic Stats

	phi	*mm*
Mean (Mz)	-3.14	8.828
Sorting (SI)	2.17	
Skewness (SkI)	0.52	
Kurtosis (KG)	0.79	

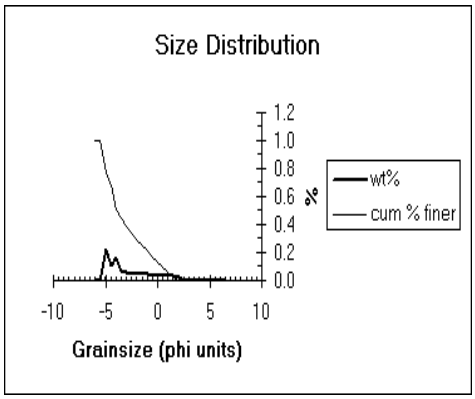

Sample: AG54

	mm	phi	Cum wt (g)	wt (g)	wt%	cum% finer	Modes	
1	64.00	-6	0.00	0	0.000	100.00		
2	45.25	-5.5	73.91	73.91	0.063	93.71		
3	32.00	-5	299.16	225.25	0.192	74.54	mode at	-5.3
4	22.63	-4.5	466.57	167.41	0.142	60.29		
5	16.00	-4	662.78	196.21	0.167	43.59	mode at	-4.3
6	11.31	-3.5	743.93	81.15	0.069	36.68		
7	8.00	-3	804.97	61.04	0.052	31.48		
8	5.66	-2.5	852.88	47.91	0.041	27.40		
9	4.00	-2	894.09	41.21	0.035	23.90		
10	2.83	-1.5	925.98	31.89	0.027	21.18		
11	2.00	-1	965.78	39.80	0.034	17.79	mode at	-1.3
12	1.41	-0.5	1004.46	38.68	0.033	14.50		
13	1.00	0	1042.75	38.29	0.033	11.24		
14	0.71	0.5	1081.10	38.35	0.033	7.98		
15	0.50	1	1120.37	39.27	0.033	4.64	mode at	0.75
16	0.35	1.5	1151.32	30.95	0.026	2.00		
17	0.25	2	1174.83	23.51	0.020	0.00		
18	0.18	2.5	1174.83	0.00	0.000	0.00		
19	0.13	3	1174.83	0.00	0.000	0.00		
20	0.09	3.5	1174.83	0.00	0.000	0.00		
21	0.06	4	1174.83	0.00	0.000	0.00		
22	0.04	4.5	1174.83	0.00	0.000	0.00		
23	0.03	5	1174.83	0.00	0.000	0.00		
24	0.02	5.5	1174.83	0.00	0.000	0.00		
25	0.02	6	1174.83	0.00	0.000	0.00		
26	0.01	6.5	1174.83	0.00	0.000	0.00		
27	0.01	7	1174.83		0.000	0.00		
28	0.01	7.5	1174.83		0.000	0.00		
29	0.00	8	1174.83		0.000	0.00		
30	0.00	8.5	1174.83		0.000	0.00		
		Sums:	1174.83	1174.83	1.000			

Percentiles

	phi	*mm*
95%	-5.60	48.591
84%	-5.25	37.971
75%	-5.01	32.270
50%	-4.19	18.278
25%	-2.16	4.461
16%	-0.73	1.656
5%	0.95	0.519

Folks' Graphic Stats

	phi	*mm*
Mean (Mz)	-3.39	10.474
Sorting (SI)	2.12	
Skewness (SkI)	0.55	
Kurtosis (KG)	0.94	

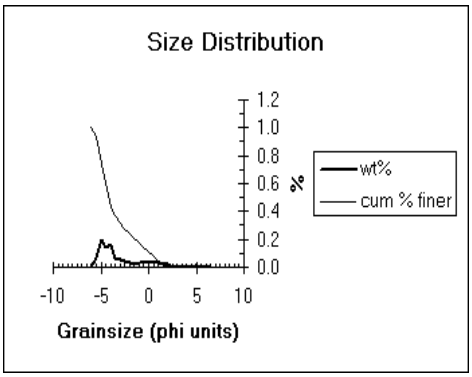

Sample: AG55

	mm	phi	Cum wt (g)	wt (g)	wt%	cum% finer	Modes	
1	64.00	-6	0.00	0.00	0.000	100.00		
2	45.25	-5.5	69.73	69.73	0.082	91.79		
3	32.00	-5	153.68	83.95	0.099	81.91		
4	22.63	-4.5	270.05	116.37	0.137	68.21		
5	16.00	-4	410.40	140.35	0.165	51.69	mode at	-4.3
6	11.31	-3.5	538.77	128.37	0.151	36.58		
7	8.00	-3	617.25	78.48	0.092	27.34		
8	5.66	-2.5	659.57	42.32	0.050	22.35		
9	4.00	-2	689.60	30.03	0.035	18.82		
10	2.83	-1.5	711.44	21.84	0.026	16.25		
11	2.00	-1	734.03	22.59	0.027	13.59		
12	1.41	-0.5	757.56	23.53	0.028	10.82	mode at	-0.8
13	1.00	0	778.42	20.86	0.025	8.36		
14	0.71	0.5	798.35	19.93	0.023	6.02		
15	0.50	1	818.68	20.33	0.024	3.62	mode at	0.75
16	0.35	1.5	835.33	16.65	0.020	1.66		
17	0.25	2	849.46	14.13	0.017	0.00		
18	0.18	2.5	849.46	0.00	0.000	0.00		
19	0.13	3	849.46	0.00	0.000	0.00		
20	0.09	3.5	849.46	0.00	0.000	0.00		
21	0.06	4	849.46	0.00	0.000	0.00		
22	0.04	4.5	849.46	0.00	0.000	0.00		
23	0.03	5	849.46	0.00	0.000	0.00		
24	0.02	5.5	849.46	0.00	0.000	0.00		
25	0.02	6	849.46	0.00	0.000	0.00		
26	0.01	6.5	849.46	0.00	0.000	0.00		
27	0.01	7	849.46		0.000	0.00		
28	0.01	7.5	849.46		0.000	0.00		
29	0.00	8	849.46		0.000	0.00		
30	0.00	8.5	849.46		0.000	0.00		
		Sums:	849.46	849.46	1.000			

Percentiles

	phi	*mm*
95%	-5.70	51.820
84%	-5.11	34.435
75%	-4.75	26.869
50%	-3.94	15.393
25%	-2.77	6.800
16%	-1.45	2.738
5%	0.71	0.610

Folks' Graphic Stats

	phi	*mm*
Mean (Mz)	-3.50	11.323
Sorting (SI)	1.88	
Skewness (SkI)	0.41	
Kurtosis (KG)	1.32	

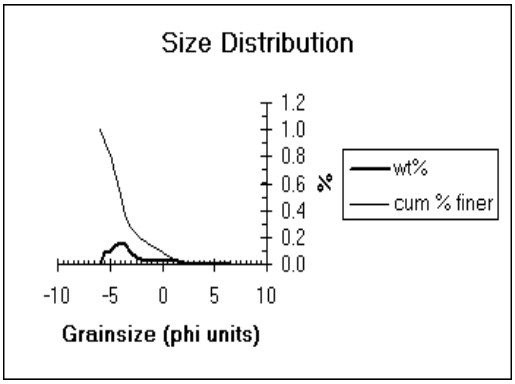

Sample: AG65

	mm	phi	Cum wt (g)	wt (g)	wt%	cum% finer	Modes	
1	64.00	-6	0.00	0.00	0.000	100.00		
2	45.25	-5.5	0.00	0.00	0.000	100.00		
3	32.00	-5	180.24	180.24	0.249	75.12	mode at	-5.3
4	22.63	-4.5	237.11	56.87	0.079	67.27		
5	16.00	-4	401.79	164.68	0.227	44.54	mode at	-4.3
6	11.31	-3.5	468.60	66.81	0.092	35.32		
7	8.00	-3	528.91	60.31	0.083	26.99		
8	5.66	-2.5	569.95	41.04	0.057	21.33		
9	4.00	-2	605.75	35.80	0.049	16.38		
10	2.83	-1.5	623.75	18.00	0.025	13.90		
11	2.00	-1	645.86	22.11	0.031	10.85	mode at	-1.3
12	1.41	-0.5	664.86	19.00	0.026	8.22		
13	1.00	0	680.34	15.48	0.021	6.09		
14	0.71	0.5	694.06	13.72	0.019	4.19		
15	0.50	1	706.19	12.13	0.017	2.52		
16	0.35	1.5	716.14	9.95	0.014	1.15		
17	0.25	2	724.44	8.30	0.011	0.00		
18	0.18	2.5	724.44	0.00	0.000	0.00		
19	0.13	3	724.44	0.00	0.000	0.00		
20	0.09	3.5	724.44	0.00	0.000	0.00		
21	0.06	4	724.44	0.00	0.000	0.00		
22	0.04	4.5	724.44	0.00	0.000	0.00		
23	0.03	5	724.44	0.00	0.000	0.00		
24	0.02	5.5	724.44	0.00	0.000	0.00		
25	0.02	6	724.44	0.00	0.000	0.00		
26	0.01	6.5	724.44	0.00	0.000	0.00		
27	0.01	7	724.44		0.000	0.00		
28	0.01	7.5	724.44		0.000	0.00		
29	0.00	8	724.44		0.000	0.00		
30	0.00	8.5	724.44		0.000	0.00		
		Sums:	724.44	724.44	1.000			

Percentiles

	phi	*mm*
95%	-5.40	42.210
84%	-5.18	36.213
75%	-4.99	31.831
50%	-4.12	17.389
25%	-2.82	7.083
16%	-1.92	3.792
5%	0.29	0.820

Folks' Graphic Stats

	phi	*mm*
Mean (Mz)	-3.74	13.366
Sorting (SI)	1.68	
Skewness (SkI)	0.45	
Kurtosis (KG)	1.07	

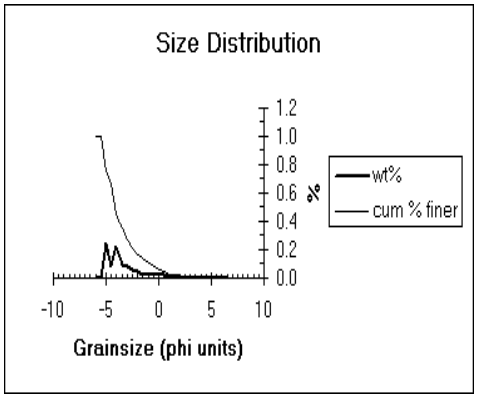

Sample: AG67

	mm	phi	Cum wt (g)	wt (g)	wt%	cum% finer	Modes	
1	128.00	-7	0.00	0.00	0.000	100.00		
2	90.51	-6.5	429.07	429.07	0.292	70.75	mode at	-6.8
3	64.00	-6	642.17	213.10	0.145	56.23		
4	45.25	-5.5	642.17	0.00	0.000	56.23		
5	32.00	-5	986.60	344.43	0.235	32.75	mode at	-5.3
6	22.63	-4.5	1092.61	106.01	0.072	25.53		
7	16.00	-4	1134.64	42.03	0.029	22.66		
8	11.31	-3.5	1186.26	51.62	0.035	19.14	mode at	-3.8
9	8.00	-3	1213.13	26.87	0.018	17.31		
10	5.66	-2.5	1238.37	25.24	0.017	15.59		
11	4.00	-2	1263.08	24.71	0.017	13.91		
12	2.83	-1.5	1280.41	17.33	0.012	12.73		
13	2.00	-1	1302.29	21.88	0.015	11.24		
14	1.41	-0.5	1326.47	24.18	0.016	9.59		
15	1.00	0	1352.54	26.07	0.018	7.81		
16	0.71	0.5	1382.18	29.64	0.020	5.79		
17	0.50	1	1414.76	32.58	0.022	3.57	mode at	0.75
18	0.35	1.5	1443.08	28.32	0.019	1.64		
19	0.25	2	1467.14	24.06	0.016	0.00		
20	0.18	2.5	1467.14	0.00	0.000	0.00		
21	0.13	3	1467.14	0.00	0.000	0.00		
22	0.09	3.5	1467.14	0.00	0.000	0.00		
23	0.06	4	1467.14	0.00	0.000	0.00		
24	0.04	4.5	1467.14	0.00	0.000	0.00		
25	0.03	5	1467.14	0.00	0.000	0.00		
26	0.02	5.5	1467.14	0.00	0.000	0.00		
27	0.02	6	1467.14		0.000	0.00		
28	0.01	6.5	1467.14		0.000	0.00		
29	0.01	7	1467.14		0.000	0.00		
30	0.01	7.5	1467.14		0.000	0.00		
		Sums:	1467.14	1467.14	1.000			

Percentiles

	phi	*mm*
95%	-6.91	120.636
84%	-6.73	105.892
75%	-6.57	95.180
50%	-5.37	41.278
25%	-4.41	21.227
16%	-2.62	6.140
5%	0.68	0.625

Folks' Graphic Stats

	phi	*mm*
Mean (Mz)	-4.90	29.940
Sorting (SI)	2.18	
Skewness (SkI)	0.47	
Kurtosis (KG)	1.44	

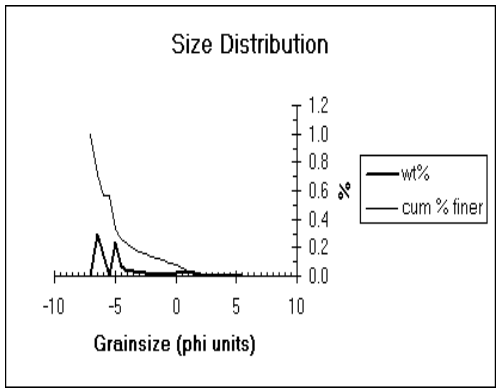

Sample: AG68

	mm	phi	Cum wt (g)	wt (g)	wt%	cum % finer	Modes	
1	256.00	-8	0.00	0.00	0.000	100.00		
2	181.02	-7.5	0.00	0.00	0.000	100.00		
3	128.00	-7	0.00	0.00	0.000	100.00		
4	90.51	-6.5	276.39	276.39	0.192	80.82	mode at	-6.8
5	64.00	-6	276.39	0.00	0.000	80.82		
6	45.25	-5.5	419.69	143.30	0.099	70.88		
7	32.00	-5	763.25	343.56	0.238	47.03	mode at	-5.3
8	22.63	-4.5	905.46	142.21	0.099	37.16		
9	16.00	-4	1066.55	161.09	0.112	25.99	mode at	-4.3
10	11.31	-3.5	1132.14	65.59	0.046	21.43		
11	8.00	-3	1178.22	46.08	0.032	18.24		
12	5.66	-2.5	1224.22	46.00	0.032	15.04		
13	4.00	-2	1255.33	31.11	0.022	12.88		
14	2.83	-1.5	1277.94	22.61	0.016	11.32		
15	2.00	-1	1302.23	24.29	0.017	9.63		
16	1.41	-0.5	1327.10	24.87	0.017	7.90	mode at	-0.8
17	1.00	0	1351.14	24.04	0.017	6.24		
18	0.71	0.5	1375.01	23.87	0.017	4.58		
19	0.50	1	1400.23	25.22	0.018	2.83	mode at	0.75
20	0.35	1.5	1422.33	22.10	0.015	1.30		
21	0.25	2	1441.00	18.67	0.013	0.00		
22	0.18	2.5	1441.00	0.00	0.000	0.00		
23	0.13	3	1441.00	0.00	0.000	0.00		
24	0.09	3.5	1441.00	0.00	0.000	0.00		
25	0.06	4	1441.00	0.00	0.000	0.00		
26	0.04	4.5	1441.00	0.00	0.000	0.00		
27	0.03	5	1441.00		0.000	0.00		
28	0.02	5.5	1441.00		0.000	0.00		
29	0.02	6	1441.00		0.000	0.00		
30	0.01	6.5	1441.00		0.000	0.00		
		Sums:	1441	1441	1.000			

Percentiles

	phi	*mm*
95%	-6.87	116.943
84%	-6.58	95.863
75%	-5.71	52.251
50%	-5.06	33.410
25%	-3.89	14.843
16%	-2.65	6.276
5%	0.37	0.772

Folks' Graphic Stats

	phi	*mm*
Mean (Mz)	-4.76	27.189
Sorting (SI)	2.08	
Skewness (SkI)	0.36	
Kurtosis (KG)	1.63	

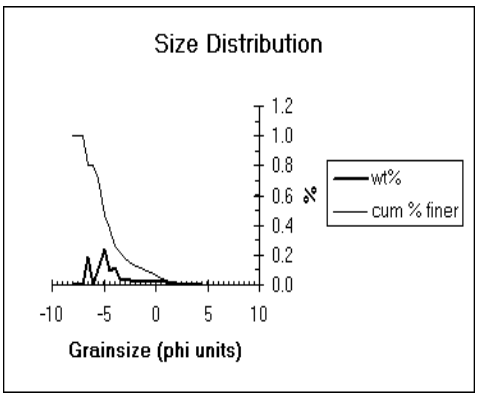

Sample: AG69

	mm	phi	Cum wt (g)	wt (g)	wt%	cum% finer	Modes	
1	256.00	-8	0.00	0.00	0.000	100.00		
2	181.02	-7.5	0.00	0.00	0.000	100.00		
3	128.00	-7	0.00	0.00	0.000	100.00		
4	90.51	-6.5	387.10	387.10	0.226	77.40	mode at	-6.8
5	64.00	-6	387.10	0.00	0.000	77.40		
6	45.25	-5.5	583.52	196.42	0.115	65.94		
7	32.00	-5	827.10	243.58	0.142	51.72	mode at	-5.3
8	22.63	-4.5	962.54	135.44	0.079	43.81		
9	16.00	-4	1066.58	104.04	0.061	37.74		
10	11.31	-3.5	1159.12	92.54	0.054	32.33		
11	8.00	-3	1243.10	83.98	0.049	27.43		
12	5.66	-2.5	1312.91	69.81	0.041	23.36		
13	4.00	-2	1370.07	57.16	0.033	20.02		
14	2.83	-1.5	1412.32	42.25	0.025	17.55		
15	2.00	-1	1465.06	52.74	0.031	14.47	mode at	-1.3
16	1.41	-0.5	1516.66	51.60	0.030	11.46		
17	1.00	0	1566.61	49.95	0.029	8.55		
18	0.71	0.5	1614.03	47.42	0.028	5.78		
19	0.50	1	1657.01	42.98	0.025	3.27		
20	0.35	1.5	1687.65	30.64	0.018	1.48		
21	0.25	2	1713.01	25.36	0.015	0.00		
22	0.18	2.5	1713.01	0.00	0.000	0.00		
23	0.13	3	1713.01	0.00	0.000	0.00		
24	0.09	3.5	1713.01	0.00	0.000	0.00		
25	0.06	4	1713.01	0.00	0.000	0.00		
26	0.04	4.5	1713.01	0.00	0.000	0.00		
27	0.03	5	1713.01		0.000	0.00		
28	0.02	5.5	1713.01		0.000	0.00		
29	0.02	6	1713.01		0.000	0.00		
30	0.01	6.5	1713.01		0.000	0.00		
		Sums:	1713.01	1713.01	1.000			

Percentiles

	phi	*mm*
95%	-6.89	118.551
84%	-6.65	100.147
75%	-5.90	59.518
50%	-4.89	29.681
25%	-2.70	6.505
16%	-1.25	2.375
5%	0.66	0.635

Folks' Graphic Stats

	phi	*mm*
Mean (Mz)	-4.26	19.183
Sorting (SI)	2.49	
Skewness (SkI)	0.41	
Kurtosis (KG)	0.97	

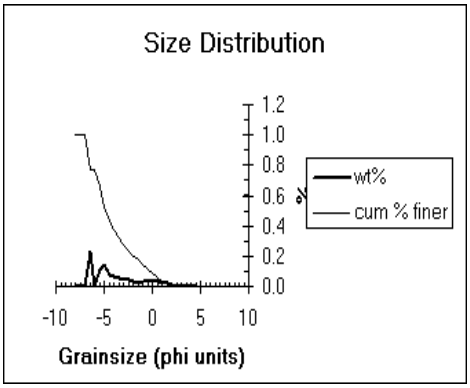

Sample: AG70

	mm	phi	Cum wt (g)	wt (g)	wt%	cum% finer	Modes	
1	256.00	-8	0.00	0.00	0.000	100.00		
2	181.02	-7.5	0.00	0.00	0.000	100.00		
3	128.00	-7	756.30	756.30	0.336	66.39	mode at	-7.3
4	90.51	-6.5	1040.90	284.60	0.126	53.75		
5	64.00	-6	1040.90	0.00	0.000	53.75		
6	45.25	-5.5	1423.08	382.18	0.170	36.76	mode at	-5.8
7	32.00	-5	1730.66	307.58	0.137	23.09		
8	22.63	-4.5	1944.26	213.60	0.095	13.60		
9	16.00	-4	2033.76	89.50	0.040	9.63		
10	11.31	-3.5	2068.64	34.88	0.015	8.08		
11	8.00	-3	2104.01	35.37	0.016	6.50	mode at	-3.3
12	5.66	-2.5	2127.93	23.92	0.011	5.44		
13	4.00	-2	2148.07	20.14	0.009	4.55		
14	2.83	-1.5	2162.92	14.85	0.007	3.89		
15	2.00	-1	2178.82	15.90	0.007	3.18	mode at	-1.3
16	1.41	-0.5	2193.18	14.36	0.006	2.54		
17	1.00	0	2205.41	12.23	0.005	2.00		
18	0.71	0.5	2217.50	12.09	0.005	1.46		
19	0.50	1	2230.34	12.84	0.006	0.89	mode at	0.75
20	0.35	1.5	2241.07	10.73	0.005	0.41		
21	0.25	2	2250.37	9.30	0.004	0.00		
22	0.18	2.5	2250.37	0.00	0.000	0.00		
23	0.13	3	2250.37	0.00	0.000	0.00		
24	0.09	3.5	2250.37	0.00	0.000	0.00		
25	0.06	4	2250.37	0.00	0.000	0.00		
26	0.04	4.5	2250.37	0.00	0.000	0.00		
27	0.03	5	2250.37		0.000	0.00		
28	0.02	5.5	2250.37		0.000	0.00		
29	0.02	6	2250.37		0.000	0.00		
30	0.01	6.5	2250.37		0.000	0.00		
		Sums:	2250.37	2250.37	1.000			

Percentiles

	phi	*mm*
95%	-7.43	171.922
84%	-7.26	153.486
75%	-7.13	139.882
50%	-5.89	59.291
25%	-5.07	33.584
16%	-4.63	24.697
5%	-2.25	4.769

Folks' Graphic Stats

	phi	*mm*
Mean (Mz)	-5.93	60.800
Sorting (SI)	1.44	
Skewness (SkI)	0.18	
Kurtosis (KG)	1.03	

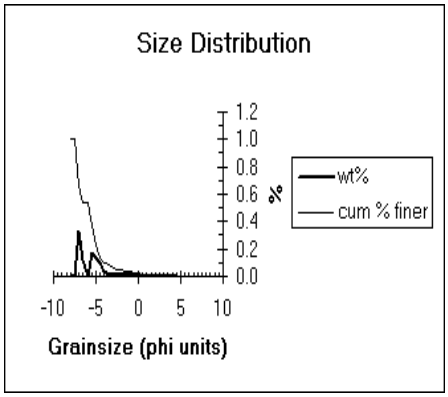

Sample: AG71

	mm	phi	Cum wt (g)	wt (g)	wt%	cum % finer	Modes	
1	64.00	-6	0.00	0.00	0.000	100.00		
2	45.25	-5.5	156.75	156.75	0.158	84.24		
3	32.00	-5	413.59	256.84	0.258	58.42	mode at	-5.3
4	22.63	-4.5	523.40	109.81	0.110	47.37		
5	16.00	-4	629.19	105.79	0.106	36.74		
6	11.31	-3.5	687.39	58.20	0.059	30.89		
7	8.00	-3	736.69	49.30	0.050	25.93		
8	5.66	-2.5	777.38	40.69	0.041	21.84		
9	4.00	-2	810.87	33.49	0.034	18.47		
10	2.83	-1.5	833.15	22.28	0.022	16.23		
11	2.00	-1	857.40	24.25	0.024	13.79	mode at	-1.3
12	1.41	-0.5	881.07	23.67	0.024	11.41		
13	1.00	0	904.21	23.14	0.023	9.09		
14	0.71	0.5	927.95	23.74	0.024	6.70		
15	0.50	1	953.09	25.14	0.025	4.17	mode at	0.8
16	0.35	1.5	976.42	23.33	0.023	1.82		
17	0.25	2	994.57	18.15	0.018	0.00		
18	0.18	2.5	994.57	0.00	0.000	0.00		
19	0.13	3	994.57	0.00	0.000	0.00		
20	0.09	3.5	994.57	0.00	0.000	0.00		
21	0.06	4	994.57	0.00	0.000	0.00		
22	0.04	4.5	994.57	0.00	0.000	0.00		
23	0.03	5	994.57	0.00	0.000	0.00		
24	0.02	5.5	994.57	0.00	0.000	0.00		
25	0.02	6	994.57	0.00	0.000	0.00		
26	0.01	6.5	994.57	0.00	0.000	0.00		
27	0.01	7	994.57		0.000	0.00		
28	0.01	7.5	994.57		0.000	0.00		
29	0.00	8	994.57		0.000	0.00		
30	0.00	8.5	994.57		0.000	0.00		
		Sums:	994.57	994.57	1.000			

Percentiles

	phi	*mm*
95%	-5.84	57.336
84%	-5.50	45.110
75%	-5.32	39.977
50%	-4.62	24.571
25%	-2.89	7.395
16%	-1.45	2.737
5%	0.84	0.560

Folks' Graphic Stats

	phi	*mm*
Mean (Mz)	-3.86	14.477
Sorting (SI)	2.02	
Skewness (SkI)	0.60	
Kurtosis (KG)	1.12	

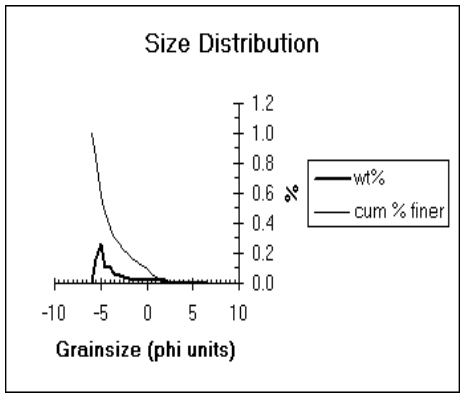

Appendix E
Petrographic Descriptions

List of Abbreviations

Alb	Albite
Aug	Augite
Hyp	Hypersthene
Oli	Olivine
Op	Opaque
Pl	Plagioclase
Pre	Prehnite
Pum	Pumpellyite
Qz	Quartz
Sp	Sphene
Xen	Xenolith

Sample #	Phenocrysts present	Proportion of crystals (%)	Shape and Size	Proportion of vesicles (%)	Proportion of lithics/xenoliths (%)	Groundmass	Comments
AG01	Qz>Alb>Pre>Pum >Sp	80 > 5 > 5 > 5 > 5	Very fine grained	0	0	N/A	Metamorphic xenolith, possibly prehnite-pumpellyite facies into greenschist facies
AG02	Pl > Aug > Hyp > Op > Oli	28 > 10 > 12 > 3 > 0.4	Subhedral, medium	5	2 (quartzofeldspathic xen)	40%, non-devitrified glass, hyalopilitic	Pl show heavy sieve and oscillatory zoning textures, twinned aug, glomeroporphyritic
AG03	Pl > Aug > Hyp > Op	24 > 8 > 7 > 5	Subhedral, Medium	12	5 (quartzofeldspathic xen)	39%, intersertal, partially crystalline, some trachytic	Pl shows sieve and oscill zoning, Aug in glomeroporphyritic clumps
AG04	Pl > Aug > Hyp > Op > Oli	30 > 9 > 4 > 1 > 0.2	Subhedral, medium	4	6 (lithics and qurtzofeldspathic xen)	46%, hyalopilitic, slightly devitrified glass in areas	Pl shows heavy sieve and oscill zoning, Aug twinned and in glomeroporphyritic clumps; poikilitic
AG05	Pl > Aug > Hyp > Op	32 > 8 > 7 > 5	Subhedral, medium	10	0	40% intersertal, some strongly devitrified glass, microlites trachytic	Less pyroxene than other samples. Pl shows sieve and zoning
AG06	Pl > Aug > Hyp > Op	30 > 7 > 5 > 1	Subhedral, medium to fine	8	4 (quartzofeldspathic xen)	45%, intergranular, some trachytic and minor felted	One Oli completely recryst to fine pyroxene. Glomeroporphyritic clumps; Pl shows heavy sieve and zoning. Poikilitic
AG07	Pl > Aug > Hyp > Op	27 > 6 > 5 > 5	Subhedral, medium to fine	8	15 (glassy clasts and quratzofeldspathic xen)	33%, intergranular, mostly felted, patchy areas with no microlites	One Oli recryst to fine pyroxene. Glomeroporphyritic; Pl shows sieve and oscill zoning; Aug twinned
AG08	Pl > Aug > Hyp > Op	32 > 7 > 5 > 5	Subhedral, medium	2	5 (quartzofeldspathic xen)	44%, intersertal, mainly felted with some patchy areas of trachytic	One Oli recryst to fine pyroxene. Pl shows sieve and zoning; poikilitic; glomeroporphyritic. Aug twinned
AG09	Pl > Aug > Hyp > Op	34 > 6 > 4 > 2	Subhedral, medium	8	6 (quartzofeldspathic xen)	43%, intergranular, some areas trachytic	One Oli recryst to fine pyrox. Glomeroporphyritic; Pl shows sieve and oscill zoning. Aug twinned
AG10	Pl > Aug > Hyp > Op	32 > 6 > 6 > 2	Subhedral, medium	10	1 (quartzofeldspathic xen)	43%, hyalopilitic, non-devitrified glass	Pl shows some sieve and zoning. Aug twinned
AG12	Pl > Aug > Hyp > Op	32 > 9 > 6 > 2	Subhedral, medium to fine	10	3 (quartzofeldspathic xen)	38%, intersertal, areas of partially devitrified glass	Pl shows some sieve and zoning, Aug twinned; glomeroporphyritic; poikilitic
AG14	Pl > Aug > Hyp > Op	30 > 7 > 6 > 4	Subhedral, medium to fine	10	0	42%, intersertal, some partially devitrified glass, most microlite trachytic	One Oli recryst to fine pyrox. Pl shows heavy sieve and oscill zoning
AG15	Pl > Aug > Hyp > Op > Oli	30 > 7 > 6 > 1 > 0.2	Subhedral, fine to medium	18	1 (quartzofeldspathic xen)	37%, hyalopilitic, minor partial devitrified glass	Glomeroporphyritic; Pl shows sieve and zoning, Aug twinned
AG16	Pl > Aug > Hyp > Op	28 > 8 > 7 > 3	Subhedral, fine to medium	7	5 (quartzofeldspathic xen)	40%, intergranular, devitrified glass, microlites in some areas felted	One Oli recryst to fine pyroxene; poikilitic; Pl show sieve and zoning
AG18	Pl > Aug > Hyp > Op	31 > 9 > 7 >1	Subhedral, medium	7	3 (quartzofeldspathic xen)	43%, intergranular some partially devitrified glass, microlites felted	Oli recryst to fine pyroxene. Pl shows sieve, quenching and zoning, Aug twinned, glomeroporphyritic
AG21	Pl > Aug > Hyp > Op > Oli	22 > 7 > 6 > 1 > 0.2	Subhedral, medium to fine	38	2 (quartzofeldspathic xen)	22%, hyalopilitic, non-devitrified glass	Pl shows heavy sieve and zoning. Glomeroporphyritic, poikilitic. Aug twinned

Sample #	Phenocrysts present	Proportion of crystals (%)	Shape and Size	Proportion of vesicles (%)	Proportion of lithics/xenoliths (%)	Groundmass	Comments
AG22	Pl > Aug > Hyp > Op	32 > 7 > 6 > 2	Subhedral, fine	7	4 (quartzofeldspathic xen)	43%, intergranular, some devitrified glass, microlite trachytic and some felted	Glomeroporphyritic; Pl shows sieve and oscill zoning, Aug twinned; poikilitic
AG23	Pl > Aug > Hyp > Op	25 > 7 > 6 > 2	Subhedral, fine	25	0	36%, hyalopilitic, non-devitrified glass	Pl shows large sieve and oscill zoning. Glomeroporphyritic, poikilitic
AG24	Pl > Aug > Hyp > Op	29 > 8 > 5 > 2	Subhedral, fine	10	0	46%, hyalopilitic, partially devitrified, some swirling patterns in glass	Pl shows heavy sieve and oscill zoning. Aug twinned. Glomeroporphyritic
AG25-12	Pl > Aug > Hyp > Op	21 > 9 > 6 > 1	Subhedral, medium	23	2	38%, hyalopilitic, partially devitrified glass	Mingled clast, glomeroporphyritic, Pl shows sieve and zoning, Aug twinned
AG26-29	Pl > Aug > Hyp > Op	26 > 8 > 5 > 1	Subhedral, medium	20	1 (quartzofeldspathic xen)	39%, intersertal, some partially devitrified glass, most microlite trachytic and felted	One Oli recryst to fine pyroxene. Pl shows heavy sieve and oscill zoning
AG29	Pl > Aug > Hyp > Op	15 > 3 > 3 > 0.5	Subhedral, fine to medium	43	0	37%, hyalopilitic, non-devitrified glass, mingled glass	Dark glass see some microlites, light glass no microlites, Pl shows sieve and zoning. Au poikilitic and twinned. Intensely mingled clast
AG35-1	Pl > Aug > Hyp > Op	21 > 6 > 4 > 1	Subhedral, fine	31	0	37%, hyalopilitic, non-devitrified glass	Rotoaira Lapilli, Pl shows sieve and oscill zoning, Aug twinned and poikilitic
AG36-6	Pl > Aug > Hyp > Op	22 > 7 > 5 > 3	Subhedral, fine	28	0	35%, hyalopilitic, non-devitrified glass	Rotoaira Lapilli, Pl shows sieve and zoning, Aug poikilitic and glomeroporphyritic
AG42-4	Pl > Aug > Hyp > Op	22 > 7 > 5 > 2	Subhedral, fine	29	0	35%, hyalopilitic, slightly devitrified glass, some microlites	Minor mingled pumice. Pl shows zoning and sieve. Aug glomeroporphyritic. Poikilitic
AG45-4	Pl > Aug > Hyp > Op	26 > 9 > 5 > 2	Subhedral, fine to medium	19	3 (quartzofeldspathic xen)	36%, intersertal, some partially devitrified glass, most microlite trachytic and felted	Pl shows heavy sieve and oscill zoning, Aug twinned. Glomeroporphyritic, poikilitic
AG46-1	Pl > Aug > Hyp > Op	24 > 7 > 5 > 1	Subhedral, fine	31	2 (quartzofeldspathic xen)	35%, hyalopilitic, non-devitrified glass	Glomeroporphyritic, Pl shows sieve and zoning, Aug partially dissolved also
AG48-2	Pl > Aug > Hyp > Op	29 > 9 > 7 > 3	Subhedral fine to medium	0	1 (quartzofeldspathic xen)	51% , intergranular, microlite trachytic and some felted	Dense wall rock lithic, Pl shows sieve and oscill zoning, Aug twinned
AG51	Pl > Aug > Hyp > Op	19 > 6 > 3 >1	Subhedral, fine to medium	32	0	39%, hyalopilitic, partially devitrified glass	Pl shows sieve and oscill zoning, Aug twinned and partially dissolved. Glomeroporphyritic and poikilitic
AG57	Pl > Aug > Hyp > Op	21 > 8 > 6 > 1	Subhedral, medium	27	3 (quartzofeldspathic xen)	34%, hyalopilitic, non- to slightly devitrified glass	Pl shows heavy sieve and oscill zoning, Aug partially dissolved edges. Some glomeroporphyritic
AG58	Pl > Aug > Hyp > Op	24 > 9 > 6 > 1	Subhedral, medium	1	3 (quartzofeldspathic xen)	56% , hyalopilitic, partially devitrified glass, some microlites felted	From dense lava lake. Pl shows sieve and zoning. Glomeroporphyritic

Sample #	Phenocrysts present	Proportion of crystals (%)	Shape and Size	Proportion of vesicles (%)	Proportion of lithics/xenoliths (%)	Groundmass	Comments
AG60	Pl > Aug > Hyp > Op > Oli	27 > 9 > 4 > 1 > 0.2	Subhedral, fine	16	2 (quartzofeldspathic xen)	41%, hyalopilitic, slightly devitrified glass, some crystallites	Pl shows sieve and oscill zoning, Aug twinned, Oli rimmed by fine pyroxene
AG61	Pl > Aug > Hyp > Op	24 > 8 > 5 > 1	Subhedral, fine	23	0	39%, hyalopilitic, non devitrified glass, rare crystallites	Pl shows sieve and zoning, Aug twinned. Glomeroporphyritic; poikilitic
AG62	Pl > Aug > Hyp > Op	25 > 9 > 4 > 1	Subhedral, fine	5	3 (quartzofeldspathic xen)	53%, intersertal, some partially devitrified glass, most microlite trachytic	One Oli recryst to fine pyroxene. Pl shows heavy sieve and oscill zoning, Aug glomeroporphyritic. Poikilitic
AG63	Pl > Aug > Hyp > Op	24 > 9 > 5 > 5	Subhedral medium to fine	2	5 (quartzofeldspathic xen and devitrified clasts)	54%, intersertal, minor partially devitrified glass, most microlite trachytic	Pl shows sieve and zoning, Aug glomeroporphyritic and twinned.
AG64	Pl > Aug > Hyp > Op	25 > 8 > 6 > 1	Subhedral, fine to medium	14	0	47%, intersertal, minor partially devitrified glass, most microlite trachytic	Pl shows heavy sieve and oscill zoning. Aug partially dissolved and twinned, glomeroporphyritic
AG65-4	Pl > Aug > Hyp > Op	27 > 9 > 6 > 1	Subhedral, fine to medium	0	0	57%, intergranular, microlite trachytic and some felted	Dense wall rock lithic. Pl shows sieve and oscill zoning, Aug twinned. Glomeroporphyritic; poikilitic
AG66	Pl > Aug > Hyp > Op	23 > 9 > 5 > 1	Subhedral, fine	27	0	35%, hyalopilitic, non- to slightly devitrified glass	Pl shows heavy sieve and zoning, Aug partially dissolved and twinned, glomeroporphyritic
AG68-29	Pl > Aug > Hyp > Op	21 > 9 > 6 > 1	Subhedral, fine	27	0	35%, hyalopilitic, slightly/partially devitrified glass	Mingled pumice clasts. Pl shows heavy sieve and oscill zoning. Phenocrysts fractured
AG70-2	Pl > Aug > Hyp > Op	22 > 6 > 4 > 1	Subhedral, fine	31	0	36%, hyalopilitic, non- to slightly devitrified glass	Glomeroporphyritic, Pl shows heavy sieve and zoning, Aug twinned
AG72	Pl > Aug > Hyp > Op	19 > 4 > 3 > 1	Subhedral fine to medium	34	0	39%, hyalopilitic, non- to slightly devitrified glass	Glomeroporphyritic, Pl shows sieve and oscill zoning, Aug twinned
AG74	Pl > Aug > Hyp > Op	21 > 6 > 4 > 1	Subhedral, medium to fine	22	3 (quartzofeldspathic xen)	43%, hyalopilitic, slightly devitrified glass	Pl shows heavy sieve and oscill zoning, Aug partially dissolved rims. Glomeroporphyritic and poikilitic

Appendix F
Geochemical Data

Glass Geochemistry – Electron Microprobe

	SiO_2	TiO_2	Al_2O_3	FeO	MnO	MgO	CaO	Na_2O	K_2O	P_2O_5	SO_3	Cl	Cr_2O_3	NiO	TOTAL
ID = 6655 AG68-29 glass light	69.95	0.65	13.05	3.32	0.00	0.54	2.43	3.40	3.39	0.51	-0.02	0.16	0.06	0.11	97.54
ID = 6656 AG68-29 glass light	69.17	0.71	12.88	3.15	0.11	0.52	2.43	3.43	3.31	0.33	0.07	0.19	0.05	0.12	96.44
ID = 6657 AG68-29 glass light	69.17	0.57	12.84	3.17	0.06	0.58	2.41	3.65	3.36	0.63	-0.03	0.18	0.01	0.26	96.84
ID = 6658 AG68-29 glass light	69.55	0.71	12.97	3.27	0.10	0.57	2.28	3.46	3.31	0.02	0.07	0.21	-0.08	0.15	96.58
ID = 6661 AG68-29 glass dark	67.73	0.73	14.04	3.96	0.10	0.70	3.29	3.63	2.96	0.24	-0.02	0.17	0.05	-0.07	97.50
ID = 6662 AG68-29 glass dark	67.91	0.84	13.47	4.56	0.10	0.59	3.11	2.46	3.15	0.25	-0.03	0.22	-0.02	0.13	96.72
ID = 6663 AG68-29 glass dark	67.30	0.81	13.75	4.43	0.08	1.01	3.51	3.64	3.01	0.31	0.01	0.11	0.01	0.16	98.14
ID = 6664 AG68-29 glass dark	67.92	0.81	13.36	3.99	0.09	0.82	2.82	3.46	3.24	0.38	-0.05	0.16	0.06	0.00	97.05
ID = 6665 AG68-29 glass dark	69.59	0.64	13.10	3.52	0.16	0.56	2.28	3.62	3.46	0.26	-0.03	0.17	0.08	-0.15	97.27
ID = 6685 AG36-6 glass light	62.75	0.82	15.28	4.68	0.19	1.17	3.98	3.82	2.51	0.21	-0.04	0.19	-0.02	0.11	95.64
ID = 6687 AG36-6 glass light	63.49	0.89	14.36	4.93	0.01	1.19	3.60	3.88	2.67	0.38	0.04	0.13	0.05	-0.04	95.59
ID = 6688 AG36-6 glass light	64.92	0.97	14.35	4.89	0.09	1.17	3.79	3.77	2.81	0.42	0.00	0.21	-0.07	0.00	97.32
ID = 6691 AG36-6 light	59.04	0.60	20.13	2.91	0.08	0.67	7.11	3.87	1.80	0.13	-0.03	0.12	0.00	-0.08	96.36
ID = 6694 AG62 glass dark	67.59	0.69	16.44	2.33	0.05	0.21	3.91	4.25	3.33	0.17	0.02	0.22	0.06	-0.07	99.22
ID = 6697 AG62 glass dark	68.96	0.46	16.72	0.96	0.03	-0.05	3.91	4.30	3.33	0.08	0.07	0.20	-0.05	0.09	99.01
ID = 6699 AG62 glass dark	71.76	0.58	13.54	0.81	0.04	-0.05	2.08	3.43	4.57	0.23	-0.07	0.13	0.01	0.09	97.15
ID = 6703 AG42-29 glass dark	68.84	0.57	13.00	3.17	0.12	0.33	2.15	3.85	3.33	0.32	-0.03	0.15	-0.02	0.09	95.87
ID = 6704 AG42-29 glass dark	66.94	0.59	13.06	2.95	0.01	0.49	2.15	3.76	3.38	0.06	0.05	0.23	0.02	-0.08	93.61
ID = 6711 AG42-29 glass light	70.55	0.56	13.01	3.31	0.11	0.42	2.20	3.94	3.41	0.12	-0.02	0.19	0.00	0.17	97.97
ID = 6712 AG42-29 glass light	70.01	0.66	13.03	3.11	0.09	0.56	2.27	3.60	3.48	0.36	0.10	0.22	-0.05	-0.05	97.40
ID = 6713 AG42-29 glass light	69.93	0.60	12.91	3.30	0.10	0.61	2.41	4.11	3.49	0.23	0.10	0.20	-0.09	0.04	97.94
ID = 6714 AG70-3 glass light	65.40	0.89	14.60	4.18	0.10	1.11	3.60	4.00	2.95	0.37	0.01	0.16	-0.08	0.10	97.39
ID = 6719 AG70-3 glass light	65.43	0.98	14.27	4.70	0.21	0.80	3.37	3.95	3.01	0.22	0.02	0.20	0.03	0.06	97.26
ID = 6720 AG70-3 glass light	65.53	0.99	14.12	4.87	0.09	1.06	3.47	4.04	2.95	0.38	-0.02	0.18	0.04	-0.05	97.65
ID = 6721 AG70-3 glass light	64.19	0.67	15.94	3.29	0.05	0.63	4.24	4.48	2.39	0.27	0.13	0.17	-0.01	0.03	96.47
ID = 6722 AG70-3 glass light	64.51	0.75	15.32	4.21	0.21	0.93	3.87	4.30	2.72	0.37	0.16	0.26	-0.01	0.04	97.63
ID = 6726 AG70-3 glass light	63.83	0.76	15.21	3.55	0.12	0.61	3.64	4.27	2.67	0.02	-0.02	0.13	0.06	0.00	94.86
ID = 6727 AG70-3 glass light	65.12	0.92	15.30	4.11	0.04	0.78	4.41	3.90	2.60	0.54	0.04	0.16	0.10	0.18	98.21
ID = 6573 AG29 glass dark	66.74	0.97	14.38	4.27	-0.11	0.57	3.77	2.86	2.75	0.18	-0.06	0.23	0.06	-0.11	96.50
ID = 6578 AG29 glass Light	71.67	0.67	13.01	3.28	0.07	0.55	1.90	3.15	3.54	0.33	-0.02	0.21	0.11	0.06	98.51
ID = 6584 AG29 glass	70.47	0.64	13.05	3.22	0.07	0.47	2.39	3.30	3.53	0.25	0.02	0.20	-0.06	0.02	97.58
ID = 6585 AG29 glass light	70.53	0.56	13.10	2.83	0.08	0.53	2.14	3.10	3.46	0.13	-0.06	0.12	-0.03	-0.22	96.28
ID = 6591 AG29 glass light	70.60	0.76	13.07	2.89	0.00	0.55	2.10	2.08	3.31	0.13	-0.13	0.14	0.01	-0.08	95.42
ID = 6592 AG29 glass dark	68.34	0.74	14.55	3.93	-0.01	0.49	3.77	3.72	3.02	0.28	0.00	0.23	0.05	0.11	99.21
ID = 6593 AG29 glass dark	69.31	0.71	13.22	3.78	0.01	0.66	2.78	3.58	3.47	0.25	0.00	0.18	-0.07	-0.02	97.86
ID = 6594 AG29 glass light	71.20	0.60	13.13	3.16	0.08	0.51	2.23	2.38	3.29	0.38	0.01	0.15	0.02	0.27	97.42

Glass Geochemistry Continued

	SiO_2	TiO_2	Al_2O_3	FeO	MnO	MgO	CaO	Na_2O	K_2O	P_2O_5	SO_3	Cl	Cr_2O_3	NiO	TOTAL
ID = 6595 AG29 glass light)	71.58	0.61	13.35	1.80	0.08	0.53	2.04	2.37	3.46	0.29	0.01	0.11	0.11	0.09	96.43
ID = 6596 AG42-4 dark glass	70.84	0.49	13.24	3.39	-0.06	0.55	2.42	3.63	3.51	0.26	-0.04	0.12	0.05	0.04	98.45
ID = 6597 AG42-4 dark glass	68.34	0.81	13.63	4.09	0.05	0.79	3.09	3.90	3.17	0.16	0.05	0.14	-0.02	-0.16	98.03
ID = 6608 AG42-4 glass light	65.68	0.81	14.20	5.09	-0.01	0.95	3.71	3.74	2.88	0.29	0.02	0.18	0.04	0.05	97.64
ID = 6609 AG42-4 glass light	66.30	1.01	14.18	5.25	0.08	1.14	3.96	3.96	2.82	0.37	-0.02	0.19	0.06	0.13	99.43
ID = 6611 AG42-4 glass dark	66.79	1.20	14.15	5.02	0.21	0.89	3.47	3.82	3.00	0.55	0.11	0.16	0.02	0.08	99.48
ID = 6612 AG42-4 glass dark	65.80	1.03	14.42	5.07	0.14	1.06	3.82	4.07	2.71	0.44	0.07	0.14	-0.05	0.04	98.73
ID = 6613 AG42-4 glass light	71.28	0.63	13.22	3.25	0.03	0.52	2.44	3.72	3.54	0.33	0.17	0.15	-0.03	0.10	99.34
ID = 6614 AG42-4 glass light	71.15	0.74	13.23	3.23	0.13	0.53	2.23	3.92	3.48	0.16	-0.13	0.12	0.00	0.05	98.84
ID = 6615 AG42-4 glass light	69.54	0.81	13.35	4.12	0.06	0.80	2.90	3.82	3.18	0.30	-0.02	0.16	-0.05	-0.01	98.95
ID = 6619 AG25-12 glass light	70.85	0.69	13.63	3.59	0.06	0.60	2.84	3.11	3.29	0.23	0.01	0.18	-0.08	0.11	99.11
ID = 6621 AG25-12 light glass	73.12	0.52	12.67	2.61	0.21	0.28	1.72	3.50	3.83	0.23	0.09	0.24	0.01	0.02	99.06
ID = 6622 AG25-12 light glass	69.36	0.63	14.25	3.84	0.10	0.79	3.37	3.80	2.99	0.39	0.08	0.21	-0.05	-0.05	99.71
ID = 6626 AG25-12 glass light	73.72	0.52	12.54	2.49	0.07	0.34	1.70	3.59	3.93	0.31	-0.02	0.20	-0.05	0.12	99.46
ID = 6632 AG25-12 dark glass	65.74	0.87	14.62	5.12	0.03	1.34	4.02	3.72	2.76	0.34	-0.08	0.12	0.03	0.00	98.62
ID = 6633 AG25-12 dark glass	64.71	0.81	15.35	4.02	0.01	1.08	3.87	3.81	2.78	0.29	0.04	0.13	-0.04	-0.07	96.79
ID = 6634 AG25-12 dark glass	65.29	0.97	14.24	5.58	0.16	1.21	4.19	3.55	2.74	0.43	-0.07	0.16	0.08	0.05	98.59
ID = 6635 AG25-12 dark glass	70.23	0.69	13.63	3.57	0.08	0.65	2.73	3.85	3.36	0.28	-0.10	0.22	-0.05	0.14	99.27

Phenocryst Mineralogy – Electron Microprobe

Pyroxene	SiO_2	TiO_2	Al_2O_3	FeO	MnO	MgO	CaO	Na_2O	K_2O	P_2O_5	SO_3	Cl	Cr_2O_3	NiO	TOTAL
Clinopyroxene															
ID = 6643 AG68-29	50.60	0.65	2.87	9.06	0.30	14.57	19.97	0.19	0.06	-0.01	0.13	0.00	0.18	-0.02	98.56
ID = 6682 BL01	51.61	0.60	2.38	9.24	0.30	15.52	19.56	0.06	0.08	0.04	0.08	0.03	0.33	0.00	99.82
ID = 6702 AG62 rim	52.37	0.24	2.81	5.69	0.10	17.77	19.34	0.13	0.10	-0.04	-0.02	-0.02	0.56	-0.06	98.98
ID = 6709 AG42-29	51.46	0.68	2.24	9.73	0.34	15.07	19.23	0.14	0.08	0.10	-0.07	0.02	0.05	0.08	99.15
ID = 6603 AG42-4	52.15	0.40	1.89	9.71	0.24	15.45	19.53	0.11	0.06	-0.08	-0.07	0.05	0.10	0.09	99.64
ID = 6620 AG25-12	51.71	0.59	1.85	11.22	0.15	14.50	19.43	0.16	0.06	0.02	0.02	0.02	0.12	0.10	99.95
Orthopyroxene															
ID = 6651 AG68-29	51.75	0.32	1.09	24.24	0.56	20.51	1.50	-0.02	0.04	-0.11	-0.09	0.06	-0.02	0.07	99.90
ID = 6652 AG68-29	52.38	0.22	0.41	24.67	0.76	19.62	1.50	-0.08	0.03	-0.03	-0.02	-0.07	0.01	-0.15	99.25
ID = 6667 BL01	53.57	0.32	1.10	17.11	0.54	25.14	1.55	-0.08	0.01	0.08	-0.01	0.00	0.06	-0.05	99.36
ID = 6683 BL01	54.02	0.29	1.18	18.83	0.42	24.26	1.54	-0.06	0.08	0.16	-0.05	0.02	0.04	-0.07	100.67
ID = 6684 AG36-6	51.56	0.18	1.00	22.57	0.34	20.75	1.46	-0.02	0.05	0.07	0.00	0.00	0.03	-0.19	97.81
ID = 6693 AG62 rim	54.08	0.26	1.02	16.83	0.23	25.41	1.56	-0.05	0.06	-0.01	-0.07	0.00	0.01	-0.01	99.31

orthopyroxene continued	SiO_2	TiO_2	Al_2O_3	FeO	MnO	MgO	CaO	Na_2O	K_2O	P_2O_5	SO_3	Cl	Cr_2O_3	NiO	TOTAL
ID = 6695 AG62	50.04	0.62	1.03	27.48	0.62	13.99	3.91	0.01	0.14	0.06	-0.01	0.12	0.00	0.03	98.04
ID = 6698 AG62	52.76	0.21	0.69	22.44	0.63	21.43	1.73	-0.02	0.02	0.07	0.05	0.05	-0.06	-0.05	99.96
ID = 6707 AG42-29	52.54	0.29	0.72	22.95	0.74	20.74	1.67	-0.03	0.07	0.02	0.02	0.12	0.03	-0.01	99.87
ID = 6580 AG29 centre	53.03	0.15	0.61	24.97	0.80	19.55	1.53	-0.02	0.05	0.09	-0.02	0.01	-0.01	-0.07	100.67
ID = 6581 AG29 rim	53.26	0.24	0.55	24.97	0.46	19.91	1.55	-0.07	0.04	0.10	0.02	0.04	-0.04	-0.05	101.00
ID = 6588 AG29	52.76	0.36	1.02	22.84	0.55	21.17	1.73	-0.07	0.07	-0.11	-0.09	0.05	0.09	0.16	100.52
ID = 6602 AG42-4	54.13	0.31	1.13	18.18	0.43	24.41	1.76	-0.05	0.10	-0.05	-0.01	0.12	-0.07	0.06	100.44
ID = 6618 AG25-12 centre	52.33	0.12	0.54	26.84	0.79	18.11	1.45	0.00	0.03	0.12	0.08	0.01	-0.02	-0.09	100.29
ID = 6625 AG25-12	52.46	0.25	0.49	25.60	0.77	19.07	1.63	-0.01	0.05	-0.01	0.06	0.03	0.03	-0.01	100.40

Olivine	SiO_2	TiO_2	Al2O3	FeO	MnO	MgO	CaO	Na_2O	K_2O	P_2O_5	SO_3	Cl	Cr_2O_3	NiO	TOTAL
ID = 6666 BL01	40.84	-0.04	0.09	11.91	0.22	47.10	0.20	-0.11	0.10	-0.11	0.00	0.06	0.11	0.22	100.60
ID = 6700 AG62	39.86	0.01	0.06	19.31	0.33	41.01	0.15	-0.16	0.06	-0.06	-0.09	0.03	0.02	0.21	100.76
ID = 6701 AG62	39.59	-0.02	0.05	21.21	0.22	39.53	0.11	-0.04	0.01	-0.05	0.02	0.00	-0.18	0.00	100.47

Plagioclase	SiO_2	TiO_2	Al_2O_3	FeO	MnO	MgO	CaO	Na_2O	K2O	P_2O_5	SO_3	Cl	Cr_2O_3	NiO	TOTAL
ID = 6641 AG68-29 centre	50.66	-0.01	30.85	0.53	0.05	0.01	14.53	3.30	0.24	0.00	0.05	0.00	0.07	0.17	100.44
ID = 6642 AG68-29 rim	52.60	0.15	29.30	0.46	0.00	0.05	12.80	4.22	0.31	-0.05	0.05	0.07	0.00	-0.14	99.82
ID = 6653 AG68-29 centre	51.28	0.03	30.04	0.65	-0.03	0.04	13.62	3.51	0.24	-0.11	0.00	-0.02	0.13	-0.10	99.29
ID = 6654 AG68-29 rim	49.40	0.11	30.76	0.78	-0.03	-0.01	14.60	2.86	0.16	-0.04	0.06	0.00	0.04	-0.05	98.66
ID = 6669 BL01	47.88	0.05	31.98	0.60	0.02	-0.04	15.58	2.32	0.20	0.00	-0.06	0.05	0.10	-0.18	98.51
ID = 6670 BL01	50.56	-0.02	30.53	0.48	0.06	0.03	14.31	3.31	0.22	-0.10	0.00	0.03	0.01	0.03	99.45
ID = 6689 AG36-6	48.75	0.02	29.05	0.42	-0.02	-0.02	13.66	3.48	0.31	0.05	-0.11	0.02	0.04	-0.10	95.56
ID = 6690 AG36-6	51.94	-0.05	29.10	0.60	-0.02	-0.05	12.89	3.98	0.22	0.00	0.04	0.03	0.07	0.01	98.76
ID = 6696 AG62	51.92	0.17	29.53	0.57	0.05	0.15	13.54	4.12	0.27	0.02	0.15	0.02	0.00	0.09	100.60
ID = 6723 AG70-3	50.88	0.05	30.64	0.42	-0.02	0.14	14.20	3.33	0.20	-0.07	0.01	0.03	-0.05	-0.06	99.71
ID = 6724 AG70-3	49.90	0.05	30.85	0.64	0.04	0.09	14.55	3.02	0.17	-0.05	0.04	-0.03	-0.02	0.05	99.28
ID = 6725 AG70-3	51.88	0.00	29.17	0.49	-0.02	0.06	12.71	4.05	0.29	-0.05	0.01	0.03	0.09	0.05	98.74
ID = 6582 AG29-	55.33	-0.02	27.48	0.46	0.05	0.11	10.55	5.26	0.40	0.04	0.07	-0.01	0.24	0.09	100.05
ID = 6583 AG29-	53.78	0.12	28.53	0.54	-0.03	-0.01	11.93	4.49	0.28	0.15	-0.05	0.03	0.01	-0.03	99.74
ID = 6604 AG42-4	53.88	0.13	28.70	0.59	0.10	0.08	11.88	4.60	0.33	0.16	0.00	0.01	-0.05	-0.07	100.34
ID = 6616 AG42-4 centre	53.52	0.10	28.95	0.57	-0.06	0.06	12.32	4.46	0.29	0.04	-0.03	0.05	0.11	0.05	100.43
ID = 6617 AG42-4 rim	54.13	0.10	28.12	0.59	0.01	0.15	11.29	4.84	0.38	-0.12	-0.09	0.05	0.03	-0.01	99.49
ID = 6627 AG25-12 centre	53.74	0.13	28.75	0.51	-0.06	0.03	12.01	4.65	0.27	-0.09	0.04	-0.02	0.02	-0.09	99.87
ID = 6628 AG25-12 rim	55.79	0.08	27.37	0.48	0.11	0.08	10.14	5.59	0.45	0.11	0.15	0.05	-0.08	0.18	100.48

ID = 6636 AG25-12 centre	51.41	-0.08	30.07	0.63	0.11	0.04	13.54	3.56	0.26	-0.18	-0.07	-0.01	0.04	-0.11	99.21
ID = 6637 AG25-12 rim	54.11	0.00	28.54	0.53	-0.01	0.04	11.79	4.78	0.37	0.04	-0.01	-0.01	0.04	0.10	100.30

Titanomagnetite/Ilmenite

		SiO_2	TiO_2	Al_2O_3	FeO	MnO	MgO	CaO	Na_2O	K_2O	P_2O_5	SO_3	Cl	Cr_2O_3	NiO	TOTAL
ID = 6645 AG68-29	Timt	0.18	15.77	2.41	70.34	0.37	2.07	0.04	0.01	0.04	0.07	0.01	0.04	0.25	0.02	91.62
ID = 6646 AG68-29	Timt	0.19	11.91	1.98	48.96	0.26	1.49	0.05	0.10	-0.04	-0.01	3.21	0.00	0.18	0.11	68.40
ID = 6648 AG68-29	Timt	0.19	12.40	3.01	71.10	0.30	2.27	0.13	0.00	-0.01	0.05	0.24	0.01	0.15	0.08	89.91
ID = 6649 AG68-29	Timt	1.12	0.19	0.89	75.19	0.11	-0.03	0.19	-0.01	0.07	0.07	0.68	-0.06	-0.13	0.04	78.32
ID = 6650 AG68-29	il	0.00	46.29	0.31	46.41	0.53	3.09	0.06	0.07	-0.01	0.01	-0.07	-0.01	0.06	0.06	96.81
ID = 6671 BL01	Timt	0.08	12.07	2.96	72.21	0.35	2.62	0.08	-0.05	0.03	0.11	-0.04	-0.02	0.75	0.11	91.24
ID = 6680 BL01	Timt	0.07	12.09	3.22	72.58	0.26	2.93	0.10	-0.05	-0.01	-0.07	0.01	-0.02	1.01	0.02	92.15
ID = 6681 BL01	Timt	0.22	12.41	3.35	73.20	0.24	2.85	-0.01	0.12	0.01	0.24	0.06	0.01	0.91	0.19	93.79
ID = 6705 AG42-29	Timt	0.22	15.98	2.22	70.47	0.42	1.98	0.06	-0.02	0.01	0.10	0.05	0.03	0.10	0.03	91.66
ID = 6706 AG42-29	Timt	0.14	16.03	2.22	71.50	0.41	1.87	0.03	0.00	0.04	-0.12	-0.07	0.06	0.05	0.30	92.46
ID = 6708 AG42-29	Timt	0.14	16.02	2.35	72.43	0.45	1.77	0.04	-0.03	-0.04	-0.03	-0.10	-0.03	0.36	-0.11	93.22
ID = 6716 AG70-3	Timt	0.02	2.78	2.44	81.84	0.30	1.74	0.07	0.00	-0.03	-0.03	-0.05	0.00	0.58	-0.06	89.58
ID = 6717 AG70-3	Timt	0.35	0.26	0.67	84.58	-0.04	0.14	0.07	0.07	0.02	0.02	0.05	0.05	-0.03	-0.01	86.21
ID = 6718 AG70-3	Timt	0.14	1.46	3.74	82.47	0.44	1.46	-0.02	0.00	0.06	-0.14	-0.03	-0.01	0.47	0.08	90.14
ID = 6579 AG29	Timt	0.22	9.54	2.71	76.39	0.32	1.29	0.01	0.07	0.01	0.10	-0.01	0.00	0.28	0.03	90.97
ID = 6586 AG29	Timt	0.89	17.14	2.47	66.92	0.37	1.40	0.11	0.09	0.08	0.13	0.16	0.01	0.32	0.07	90.15
ID = 6587 AG29	Timt	0.79	18.02	2.77	66.63	0.44	1.78	0.01	0.11	0.05	-0.05	0.09	0.10	0.35	0.30	91.40
ID = 6589 AG29	il	0.05	47.21	0.23	46.88	0.46	2.85	0.03	-0.04	-0.02	-0.13	-0.05	0.00	0.03	-0.04	97.45
ID = 6590 AG29	il	0.08	46.60	0.29	46.46	0.51	2.80	0.03	-0.08	-0.02	-0.11	-0.07	-0.01	-0.12	-0.02	96.36
ID = 6598 AG42-4	Timt	0.12	11.40	3.69	73.20	0.23	3.47	-0.04	0.01	-0.03	-0.04	0.04	0.03	0.51	0.06	92.64
ID = 6599 AG42-4	Timt	0.05	11.21	3.71	73.03	0.28	3.50	0.05	0.05	0.07	0.04	-0.04	-0.04	0.32	0.07	92.32
ID = 6600 AG42-4	Il	0.01	47.76	0.27	46.07	0.49	2.81	0.03	-0.02	-0.02	0.15	-0.05	0.02	0.02	-0.02	97.53
ID = 6601 AG42-4	il	0.01	48.55	0.19	46.34	0.64	2.85	0.04	0.06	0.01	-0.05	-0.04	0.05	0.03	0.07	98.74
ID = 6605 AG42-4	Timt	0.03	16.30	2.19	73.03	0.47	1.92	0.06	-0.02	0.00	-0.05	0.05	0.04	0.19	0.17	94.38
ID = 6606 AG42-4	il	0.15	47.61	0.39	46.60	0.45	3.00	0.09	-0.07	0.04	0.04	-0.06	0.01	0.20	0.07	98.53
ID = 6607 AG42-4	il	0.00	47.47	0.29	46.38	0.51	2.85	0.04	-0.03	0.06	-0.01	0.06	-0.01	-0.01	-0.19	97.40
ID = 6623 AG25-12	Timt	0.27	11.12	2.39	74.50	0.32	1.13	0.23	-0.01	0.07	-0.03	0.12	0.05	0.07	-0.14	90.08
ID = 6624 AG25-12	Timt	0.22	10.33	2.46	77.01	0.55	0.47	0.32	0.01	-0.01	-0.10	-0.12	0.00	0.10	-0.06	91.18
ID = 6629 AG25-12	Timt	0.13	18.33	1.90	70.76	0.41	1.62	0.03	-0.02	0.07	0.06	-0.13	-0.01	0.29	-0.14	93.31
ID = 6630 AG25-12	Timt	0.13	15.13	2.11	74.21	0.39	1.50	0.07	0.07	-0.04	-0.04	-0.10	0.03	0.34	-0.07	93.73
ID = 6631 AG25-12	Timt	0.29	15.93	2.25	70.87	0.45	1.56	0.26	-0.08	0.02	-0.04	-0.03	-0.05	0.43	0.11	91.97
ID = 6638 AG25-12	Timt	0.13	13.14	2.78	73.49	0.23	2.32	0.06	-0.03	0.01	-0.03	-0.09	-0.02	0.41	0.17	92.55

Whole Rock X-Ray Fluorescence Data – Normalised to

Major Oxides

Element	AG03	AG04	AG08	AG16	AG20	AG22	AG23	AG25-1	AG25-2	AG26-29	AG27-M	AG27	AG29	AG35	AG36
	Andesite	Andesite	Andesite	Andesite	Andesite	Andesite	Andesite	Andesite	Andesite	Andesite	Andesite	Andesite	Andesite	Andesite	Basaltic Andesite
SiO_2	57.96	59.41	58.80	59.06	58.82	60.21	58.51	61.46	57.77	58.36	58.43	60.84	59.98	57.02	52.52
TiO_2	0.72	0.72	0.78	0.75	0.73	0.77	0.78	0.72	0.73	0.75	0.75	0.71	0.76	0.80	0.99
Al_2O_3	16.24	16.71	17.27	16.35	16.01	16.73	17.42	16.78	15.93	16.35	16.53	16.77	16.62	18.18	21.26
Fe_2O_3	7.06	6.94	6.97	6.49	7.28	6.94	6.96	5.79	6.82	7.29	7.26	6.04	6.84	7.21	8.68
MnO	0.12	0.12	0.12	0.12	0.13	0.12	0.10	0.11	0.12	0.13	0.12	0.11	0.12	0.12	0.13
MgO	4.82	3.85	4.11	3.91	4.96	4.04	3.49	2.56	4.05	4.58	4.73	2.81	3.64	3.73	4.13
CaO	6.80	6.65	7.02	6.64	7.17	6.82	5.06	5.41	6.68	7.25	7.35	5.42	6.24	6.38	6.14
Na_2O	3.19	3.54	3.17	3.39	3.15	3.40	3.08	4.18	3.20	3.45	3.17	3.44	3.17	2.98	2.28
K_2O	1.56	1.65	1.40	1.70	1.53	1.70	1.67	2.09	1.63	1.54	1.52	2.04	1.78	1.43	0.98
P_2O_5	0.17	0.13	0.24	0.15	0.14	0.20	0.16	0.16	0.15	0.15	0.17	0.15	0.15	0.17	0.20
LOI	0.13	0.06	0.01	0.02	0.09	0.00	0.63	0.21	0.07	0.04	0.10	0.25	0.24	0.32	0.5
Total	98.76	99.77	99.90	98.56	100.00	100.92	97.85	99.47	97.15	99.87	100.13	98.57	99.54	98.34	97.81
Normalised															
Element	**AG03**	**AG04**	**AG08**	**AG16**	**AG20**	**AG22**	**AG23**	**AG25-1**	**AG25-2**	**AG26-29**	**AG27-M**	**AG27**	**AG29**	**AG35**	**AG36**
SiO_2	58.76	59.58	58.87	59.94	58.87	59.66	60.18	61.92	59.51	58.46	58.41	61.88	60.41	58.17	53.97
TiO_2	0.73	0.72	0.79	0.76	0.73	0.76	0.81	0.72	0.75	0.75	0.75	0.72	0.76	0.82	1.02
Al_2O_3	16.46	16.76	17.29	16.59	16.02	16.58	17.92	16.90	16.41	16.38	16.53	17.06	16.74	18.55	21.85
Fe_2O_3	7.16	6.96	6.98	6.59	7.29	6.87	7.16	5.84	7.02	7.30	7.26	6.14	6.89	7.36	8.92
MnO	0.12	0.12	0.12	0.12	0.13	0.12	0.10	0.11	0.12	0.13	0.12	0.11	0.12	0.12	0.13
MgO	4.89	3.86	4.12	3.96	4.96	4.00	3.59	2.58	4.17	4.58	4.73	2.86	3.66	3.80	4.24
CaO	6.89	6.67	7.03	6.73	7.18	6.76	5.20	5.45	6.88	7.26	7.34	5.52	6.29	6.51	6.31
Na_2O	3.23	3.55	3.18	3.44	3.15	3.37	3.17	4.21	3.29	3.46	3.17	3.50	3.19	3.04	2.34
K_2O	1.58	1.65	1.40	1.73	1.53	1.68	1.71	2.11	1.68	1.54	1.52	2.07	1.79	1.46	1.01
$P2O_5$	0.17	0.13	0.24	0.15	0.14	0.20	0.16	0.16	0.16	0.15	0.17	0.16	0.15	0.17	0.20
LOI															
Total	100.00	100.00	100.00	100.00	100.00	100.00	100.00	100.00	100.00	100.00	100.00	100.00	100.00	100.00	100.00

Major Oxide - Whole Rock XRF continued

Element	AG39_001	AG41	AG42-29	AG45	AG45-1	AG47	AG47-1r	AG47-2r	AG48-29	AG49	AG50	AG51	AG52	AG55
	Basalt	Andesite	Andesite	Basaltic Andesite	Basaltic Andesite	Andesite	Andesite	Andesite	Andesite	Andesite	Basaltic Andesite	Basaltic Andesite	Andesite	Andesite
SiO_2	48.02	57.45	58.42	55.97	55.21	60.51	60.56	60.14	57.19	58.77	55.81	56.30	58.44	58.77
TiO_2	1.00	0.77	0.77	0.81	0.79	0.77	0.74	0.80	0.81	0.74	0.83	0.80	0.76	0.75
Al_2O_3	21.93	18.46	17.68	18.18	17.45	17.57	17.25	17.21	18.33	16.19	16.86	16.23	17.30	16.75
Fe_2O_3	9.91	6.66	6.65	7.59	7.79	6.57	6.22	6.97	6.96	6.81	8.02	7.84	7.00	6.54
MnO	0.12	0.11	0.12	0.13	0.13	0.11	0.11	0.12	0.13	0.12	0.13	0.13	0.12	0.12
MgO	5.11	3.17	3.13	4.41	4.95	3.10	2.96	3.64	3.32	4.35	4.89	5.47	3.96	3.42
CaO	6.09	5.85	5.83	6.87	7.35	5.92	5.69	6.77	5.90	7.03	7.94	7.83	6.53	5.98
Na_2O	1.72	3.16	3.31	2.91	2.79	3.50	3.55	3.43	3.13	3.20	3.00	3.04	3.30	3.35
K_2O	0.55	1.55	1.72	1.37	1.26	1.84	1.88	1.71	1.59	1.58	1.28	1.42	1.61	1.84
P_2O_5	0.19	0.17	0.17	0.15	0.16	0.16	0.19	0.17	0.21	0.15	0.15	0.14	0.16	0.22
LOI	0.47	0.34	0.33	0.43	0.33	0.27	0.24	0.02	0.45	0.08	0.11	0.16	0.26	0.32
Total	95.10	97.69	98.13	98.81	98.20	100.33	99.39	100.98	98.01	99.02	99.02	99.35	99.46	98.05
Normalised														
Element	AG39_001	AG41	AG42-29	AG45	AG45-1	AG47	AG47-1r	AG47-2r	AG48-29	AG49	AG50	AG51	AG52	AG55
SiO_2	50.74	59.02	59.74	56.89	56.41	60.47	61.08	59.57	58.62	59.40	56.42	56.76	58.91	60.13
TiO_2	1.05	0.79	0.79	0.82	0.80	0.77	0.74	0.79	0.83	0.74	0.84	0.80	0.77	0.77
Al_2O_3	23.17	18.96	18.08	18.48	17.83	17.56	17.40	17.05	18.79	16.36	17.05	16.36	17.44	17.14
Fe_2O_3	10.47	6.84	6.80	7.71	7.96	6.56	6.28	6.90	7.13	6.89	8.11	7.91	7.05	6.69
MnO	0.12	0.11	0.12	0.13	0.14	0.11	0.11	0.12	0.13	0.12	0.13	0.13	0.12	0.12
MgO	5.40	3.26	3.20	4.49	5.06	3.10	2.98	3.60	3.41	4.40	4.94	5.51	4.00	3.50
CaO	6.44	6.01	5.96	6.98	7.51	5.91	5.74	6.70	6.04	7.11	8.03	7.89	6.59	6.12
Na_2O	1.81	3.24	3.38	2.96	2.85	3.50	3.58	3.39	3.20	3.23	3.03	3.07	3.33	3.42
K_2O	0.58	1.59	1.76	1.39	1.28	1.84	1.90	1.70	1.63	1.60	1.30	1.43	1.63	1.89
P_2O_5	0.20	0.17	0.18	0.15	0.16	0.16	0.19	0.17	0.21	0.15	0.15	0.14	0.16	0.23
LOI														
Total	100.00	100.00	100.00	100.00	100.00	100.00	100.00	100.00	100.00	100.00	100.00	100.00	100.00	100.00

Major Oxide - Whole Rock XRF continued

Element	AG57	AG58	AG60	AG61	AG62	AG63	AG65-4	AG67	AG68	AG68/2	AG69	AG70-3	AG74	BL01
	Andesite	Andesite	Andesite	Andesite	Andesite	Andesite	Andesite	Andesite	Andesite	Andesite	Andesite	Andesite	Andesite	Andesite
SiO_2	59.32	59.73	57.98	57.95	57.94	59.01	59.69	58.25	59.59	59.16	60.08	58.31	58.19	59.26
TiO_2	0.73	0.76	0.72	0.72	0.72	0.73	0.74	0.78	0.77	0.77	0.78	0.78	0.73	0.74
Al_2O_3	16.19	16.35	15.98	15.67	15.81	16.15	16.42	17.37	17.79	17.73	16.70	16.81	16.26	16.27
Fe_2O_3	7.15	6.87	7.20	7.17	7.14	7.06	7.00	7.15	6.69	6.80	6.91	7.08	7.26	7.26
MnO	0.12	0.12	0.12	0.12	0.12	0.12	0.12	0.12	0.11	0.12	0.12	0.12	0.13	0.13
MgO	4.97	3.99	4.96	4.89	4.99	4.88	4.28	3.99	3.65	3.44	3.93	4.02	4.85	4.98
CaO	7.23	6.84	6.72	7.10	7.33	7.15	7.12	6.57	6.24	6.22	6.44	6.73	7.38	7.40
Na_2O	3.17	3.37	3.06	3.12	3.15	3.11	3.32	3.75	3.22	3.21	3.36	3.24	3.17	3.34
K_2O	1.58	1.70	1.54	1.55	1.53	1.56	1.63	1.63	1.63	1.64	1.75	1.66	1.47	1.54
P_2O_5	0.15	0.16	0.13	0.15	0.16	0.14	0.17	0.16	0.16	0.15	0.15	0.18	0.17	0.14
LOI	0.09	0.01	0.17	0.11	0.02	0.04	0.04	0.30	0.33	0.28	0.19	0.15	0.06	0.06
Total	100.71	99.89	98.59	98.56	98.91	99.95	100.53	100.07	100.19	99.52	100.39	99.09	99.66	101.10
Normalised														
Element	**AG57**	**AG58**	**AG60**	**AG61**	**AG62**	**AG63**	**AG65-4**	**AG67**	**AG68**	**AG68/2**	**AG69**	**AG70-3**	**AG74**	**BL01**
SiO_2	58.95	59.80	58.91	58.86	58.59	59.06	59.40	58.38	59.68	59.62	59.96	58.94	58.42	58.65
TiO_2	0.73	0.76	0.74	0.73	0.73	0.73	0.74	0.78	0.77	0.78	0.77	0.79	0.73	0.73
Al_2O_3	16.09	16.37	16.24	15.92	15.99	16.16	16.34	17.41	17.82	17.87	16.67	16.99	16.33	16.10
Fe_2O_3	7.10	6.88	7.32	7.28	7.22	7.06	6.97	7.16	6.70	6.85	6.89	7.16	7.29	7.18
MnO	0.12	0.12	0.13	0.12	0.13	0.12	0.12	0.12	0.11	0.12	0.12	0.12	0.13	0.12
MgO	4.94	4.00	5.04	4.97	5.04	4.89	4.26	4.00	3.65	3.47	3.92	4.07	4.87	4.92
CaO	7.19	6.85	6.82	7.22	7.41	7.15	7.09	6.58	6.25	6.27	6.42	6.80	7.40	7.33
Na_2O	3.15	3.38	3.11	3.17	3.18	3.11	3.30	3.76	3.22	3.23	3.35	3.28	3.18	3.30
K_2O	1.57	1.70	1.57	1.57	1.54	1.56	1.62	1.63	1.64	1.65	1.74	1.67	1.48	1.53
P_2O_5	0.15	0.16	0.14	0.16	0.16	0.14	0.17	0.16	0.16	0.15	0.14	0.18	0.17	0.13
LOI														
Total	100.00	100.00	100.00	100.00	100.00	100.00	100.00	100.00	100.00	100.00	100.00	100.00	100.00	100.00

Trace Element Whole Rock XRF Data

Element (ppm)	AG01	AG03	AG04	AG08	AG16	AG20	AG22	AG23	AG25-1	AG25-2	AG26-29	AG27	AG27-M	AG29	AG35	AG36	AG39
S	41	194	57	75	223	144	45	5544	143	115	111	201	187	137	216	782	959
Cl	< 2.0	23	13	77	365	501	129	252	632	589	357	608	579	478	554	498	429
V	97	168	163	182	153	168	156	176	86	145	176	109	174	122	162	184	216
Cr	32	115	62	36	53	126	52	56	18	72	106	34	122	38	67	60	141
Co	27	30	22	31	30	42	30	24	24	36	40	49	44	25	41	43	55
Ni	13.3	27	21	10.1	11.8	25	12.5	13.6	7.3	20	24	9.9	27	11.1	15.2	13.7	26
Cu	17.2	42	33	15.6	17.6	34	21	15.6	24	34	35	22	33	18.2	25	23	33
Zn	118	70	67	70	66	71	63	69	59	69	73	69	75	66	66	63	54
Ga	13.6	17.1	16.8	18.1	17.2	17.2	17.6	18.5	16.9	17.9	17.0	18.8	17.6	18.4	18.8	22	22
As	4.2	1.5	2.4	1.3	2.6	2.9	2.2	5.6	5.2	3.1	3.3	6.2	3.4	4.4	4.3	4.0	3.8
Rb	1.2	54	53	48	59	50	58	62	71	55	52	73	50	60	49	33	18.2
Sr	408	280	257	273	252	281	258	257	241	259	266	245	265	245	237	219	179
Y	26	16.3	20	21	23	21	22	21	23	23	22	24	23	22	23	22	16.6
Zr	212	125	129	122	134	123	134	142	161	131	125	165	128	137	153	177	162
Nb	8.9	6.0	6.0	6.2	6.1	5.9	6.5	6.3	6.9	6.1	6.1	7.4	5.9	6.5	7.1	7.9	7.2
Ba	14.3	295	309	303	326	295	326	364	368	302	293	355	287	315	272	200	135
La	27	5.0	9.9	7.5	12.1	8.9	9.4	11.6	15.1	8.8	10.9	15.7	11.2	7.7	10.0	10.7	7.2
Ce	51	14.2	30	24	26	27	29	29	35	25	25	32	25	27	29	35	25
Nd	17.1	9.7	14.8	11.1	< 10	10.3	10.3	19.4	13.7	10.8	< 10	11.7	13.9	13.3	15.1	14.1	10.1
Hf	5.5	4.0	4.3	3.5	5.5	3.6	2.9	3.3	4.7	3.2	3.2	4.6	3.1	3.1	4.5	5.0	4.6
Pb	5.0	8.2	9.0	8.5	10.1	9.4	9.5	7.0	12.1	10.5	8.6	13.2	9.6	11.8	12.2	14.0	12.2
Th	12.3	7.5	7.9	8.1	8.4	7.4	8.2	8.8	10.0	7.9	7.3	10.4	7.9	8.4	8.9	10.1	7.9
U	4.4	3.5	3.7	3.2	4.2	3.5	4.4	3.8	3.8	3.8	3.6	4.1	4.2	3.5	4.1	3.8	3.4

Trace Element – Whole Rock XRF continued

Element (ppm)	AG41	AG42-29	AG45	AG45-1	AG47	AG47-1	AG47-2	AG48-29	AG49	AG50	AG51	AG52	AG55	AG55-1	AG57	AG58	AG60	AG61	AG62
S	203	512	435	387	396	418	113	494	129	263	166	524	328	168	87	93	323	161	84
Cl	554	542	612	617	567	563	365	678	446	396	200	643	254	546	131	382	183	54	331
V	138	140	173	199	126	109	160	147	172	230	211	135	134	177	178	170	168	159	170
Cr	36	32	87	107	28	26	39	41	107	89	151	62	46	118	142	54	132	116	127
Co	43	48	34	32	30	37	29	30	36	34	40	29	35	45	33	34	30	35	35
Ni	12.4	12.4	22	24	9.7	8.3	12.3	16.1	26	21	36	16.2	14.2	25	30	11.4	29	29	30
Cu	17.0	16.2	42	43	13.4	12.3	17.9	30	33	37	31	25	30	43	43	17.7	33	40	39
Zn	69	71	70	73	68	67	68	70	73	80	76	68	71	77	72	69	72	68	72
Ga	20	18.8	19.1	17.8	19.1	18.6	18.1	18.6	17.6	18.5	18.0	17.8	18.4	18.4	17.1	17.8	16.6	16.3	17.8
As	5.5	5.0	4.6	3.6	4.6	5.1	3.5	5.4	3.5	1.8	1.8	4.0	4.6	3.2	1.8	2.6	3.7	2.4	1.9
Rb	55	61	44	42	62	66	59	56	54	43	46	54	63	49	52	60	53	52	51
Sr	244	246	239	251	250	249	260	243	254	263	258	254	249	266	284	257	277	281	297
Y	22	24	24	24	24	24	23	22	22	24	22	23	22	22	21	23	19.4	20	21
Zr	158	162	140	130	154	161	137	165	129	120	120	142	153	126	125	135	125	124	125
Nb	7.4	7.5	6.5	6.3	7.2	7.1	6.2	7.6	6.2	5.6	5.8	6.5	6.9	6.0	6.0	6.2	6.0	6.0	6.0
Ba	288	300	256	250	318	330	325	290	304	265	309	294	320	301	300	320	282	302	295
La	11.6	11.9	11.7	8.4	11.4	11.1	10.5	7.3	10.1	6.4	9.7	10.2	11.0	10.8	8.7	9.4	8.2	10.0	8.4
Ce	29	30	29	28	32	31	29	29	27	22	24	29	29	25	24	26	23	23	23
Nd	11.8	12.5	15.5	14.1	17.5	10.9	11.3	14.0	13.6	13.1	13.6	10.0	13.4	12.7	11.7	13.8	11.3	13.2	13.9
Hf	5.5	5.1	2.9	4.9	4.7	5.4	4.5	5.6	3.4	2.6	3.2	4.7	3.9	3.3	3.2	3.7	3.5	3.9	2.9
Pb	11.8	12.8	11.4	10.6	12.9	13.5	11.0	13.1	9.2	8.9	7.1	12.0	10.6	10.0	9.2	10.4	10.6	7.8	8.9
Th	9.7	9.2	7.5	7.4	9.9	10.1	8.1	9.6	8.3	7.2	7.3	8.9	9.6	7.6	8.1	8.6	8.1	7.4	7.7
U	3.8	4.9	4.2	3.8	4.0	4.2	3.5	4.2	3.5	4.1	3.9	3.9	4.0	3.8	3.9	4.3	3.9	3.8	4.6

Trace Element – Whole Rock XRF continued

Element (ppm)	AG63	AG65-4	AG67	AG68	AG68-2	AG69	AG70-3	AG74	BL01
S	36	243	174	207	149	94	145	33	137
Cl	149	472	661	638	614	788	932	324	202
V	175	170	148	149	146	147	164	185	165
Cr	128	88	55	55	47	70	55	131	125
Co	34	30	33	45	42	31	31	32	44
Ni	29	17.1	15.5	18.3	15.5	20	14.5	34	31
Cu	36	24	29	21	21	17.0	21	43	39
Zn	77	71	73	73	75	70	86	76	73
Ga	17.4	17.3	18.1	19.0	19.0	17.2	19.1	16.8	16.7
As	1.9	3.1	5.2	6.2	6.1	4.3	2.5	1.8	2.5
Rb	50	55	54	57	57	59	59	50	51
Sr	297	266	253	250	248	247	276	268	295
Y	25	22	23	24	23	23	25	25	22
Zr	127	130	140	152	155	140	145	124	125
Nb	6.0	6.3	6.5	7.0	7.2	6.5	6.8	5.9	5.9
Ba	312	313	281	309	307	318	347	304	305
La	12.2	8.5	8.3	12.7	12.5	11.3	11.3	9.5	10.1
Ce	34	28	27	29	32	27	33	27	23
Nd	15.3	14.3	< 10	16.7	12.4	< 10	18.5	13.2	11.2
Hf	4.0	2.7	5.0	4.9	4.0	5.0	4.7	3.7	3.9
Pb	9.2	10.3	11.5	11.8	12.6	10.6	16.7	9.2	7.1
Th	8.0	7.5	9.1	10.0	9.7	8.0	8.8	7.3	8.1
U	4.2	4.0	4.2	4.6	3.9	3.3	4.2	4.1	3.9

MAGMA (Kware) Results
Whole Rock - Viscosity, Bulk Density, Liquidus Temperature

Sample	Magma Viscosity Pa-s	Liquidus Temperature °C	Magma Bulk Density kg m^{-3}
AG03	2.06E+04	1139	2,694
AG04	2.58E+04	1135	2,664
AG08	2.25E+04	1149	2,678
AG16	2.83E+04	1137	2,657
AG20	1.33E+04	1143	2,701
AG22	2.51E+04	1137	2,666
AG23	4.75E+04	1134	2,642
AG25-1	8.38E+04	1112	2,588
AG25-2	2.20E+04	1137	2,675
AG26-29	1.34E+04	1142	2,699
AG27-m	1.36E+04	1147	2,703
AG27	8.58E+04	1120	2,602
Ag29	3.79E+04	1132	2,650
AG35	2.61E+04	1153	2,680
AG36	1.20E+04	1192	2,749
AG39	3.95E+03	1222	2,831
AG41	4.54E+04	1147	2,647
AG42-29	4.65E+04	1136	2,640
Ag45	1.37E+04	1162	2,714
AG45-1	8.77E+03	1165	2,738
AG47	5.48E+04	1130	2,627
AG47-1	6.78E+04	1126	2,613
Ag47-2	3.05E+04	1136	2,659
AG48-29	3.61E+04	1147	2,658
AG49	1.99E+04	1142	2,680
AG50	7.52E+03	1158	2,743
Ag51	6.27E+03	1155	2,746
AG52	2.40E+04	1144	2,672
AG55	3.89E+04	1132	2,641
AG55-1	1.40E+04	1147	2,701
AG57	1.41E+04	1144	2,697
AG58	2.51E+04	1136	2,665
AG60	1.38E+04	1144	2,699
AG61	1.29E+04	1143	2,701
AG62	2.88E+00	797	2,246
AG63	1.51E+04	1145	2,695
AG65-4	2.03E+04	1139	2,678
AG67	1.88E+04	1141	2,677
Ag68	3.86E+04	1143	2,652
Ag68-2	3.99E+04	1141	2,652
AG69	2.94E+04	1135	2,658
AG70-3	2.14E+04	1142	2,677
AG74	1.25E+04	1147	2,706
Average	*2.69E+04*	*1136.163*	*2,669*
Minimum	*2.88E+00*	*797*	*2,246*
Maximum	*8.58E+04*	*1222*	*2,831*